THÈSE

En vue de l'obtention du

DOCTORAT DE L'UNIVERSITÉ DE TOULOUSE

Délivré par l'Université Toulouse III - Paul Sabatier
Discipline ou spécialité : Physico-Chimie Théorique

Présentée et soutenue par Wissam Helal
Le 18 Mai 2009

Titre : Utilisation des méthodes de localisation multi-référence pour les systèmes quasi-dégénérés

---

JURY
Prof. Gian Luigi Bendazzoli, Professeur à l'Université de Bologna
Prof. Isabelle Baraille, Professeur à l'Université de Pau
Dr. Jacques Bonvoisin, Chargé de Recherche àu CEMES, Toulouse
Prof. Thierry Leininger, Professeur à l'Université Paul Sabatier

---

École doctorale : *Sciences de la Matière*
Unité de recherche : *Laboratoire de Chimie et Physique Quantiques (UMR 5256)*
Directeurs de Thèse : *Prof. Stefano Evangelisti*
Prof. Thierry Leininger

To my family:
Mother, Father, Brother, & Manal

With love and respect...

Acknowledgement

I would like to express my deep appreciation to my advisors Prof. Stefano Evangelisti and Prof. Thierry Leininger for their guidance, fruitful discussions, continuous support and encouragement through the course of this work.

Special thanks go to Daniel Maynau and Nadia Ben Amor for the collaboration and for being very patience while explaining to me the arcanes of CASDI program code.

I was deeply touched by the friendship and assistance of all the members of the "Laboratoire de Chimie et Physique Quantiques" at Paul Sabatier University.

I would also like to express my gratitude to the members of the defence committe: Prof. Gian Luigi Bendazzoli, Prof. Isabelle Baraille, Prof. Jacques Bonvoisin, and Prof. Thierry Leininger.

The financial support of the Institute of Research on Complex Atomic and Molecular Systems (IRSAMC) during some periods through the course of this work is profoundly acknowledged.

I would also like to thank my professors in Yarmouk University and Applied Science University in Jordan, for encouraging me to pursue my postgraduate study.

Contents

List of Figures

List of Tables

Chapter 1

Introduction

Le théme principal de cette thèse est l'étude de la structure électronique et des propriétés physico-chimiques d'un certain nombre de composés à valence mixte en utilisant des méthodes de chimiqie quantique *ab-initio* multi-référence fortement corrélées.

Les composés à valence mixte étudiés dans cet ouvrage sont: un cation de "spiro" moléculaire, une série de chaînes linéaires cationiques de béryllium, et deux molécules cationiques de la famille "*bis*-triarylamines" (voir la section §6.1 pour la nomenclature IUPAC de ces deux molécules). Les méthodes de chimie quantique utilisées dans cette étude sont les méthodes *ab-initio* multi-référence utilisant à la fois des orbitales moléculaires canoniques et localisées. La méthode *ab-initio* multi-référence variationnelle et locale (CASDI), développée récemment dans notre laboratoire "Laboratoire de Chimie Physique et quantiques" à l'Université de Toulouse III, a reçu une particularité spécifique dans ce travail pour l'étude des propriétés électroniques des composés à valence mixte.

Considérant le caractère quasi-dégénéré des composés à valence mixte, la méthode *ab-initio* multi-reference locale semble être adéquate pour traiter tels composés chimiques. Cette hypothèse a été testée dans le cadre des travaux de cette thèse, en comparant les résultats de la méthode *ab-initio* multi-référence locale à d'autres méthodes bien établies.

Le cation moléculaire à valence mixte de type spiro étudié dans ce travail, 5,5'(4H,4H')-spirobi[cyclopenta[c]pyrrole]2,2',6,6'tetrahydro cation, est un composé chimique modèle avec une taille moléculaire relativement petite. Ce dernier point a pu ouvrir la possibilité d'avoir des nombreux résultats des calculs quantique *ab-initio* multi-référence sur cette molécule. Plusieurs résultats ont été obtenus pour la molécule "spiro" par le fait de calculer sa structure électronique : les bas états électroniques à travers une coor-

donnée de réaction du transfert d'électron intramoléculaire, et quelques paramètres spectroscopiques à valence mixte. Malheureusement, dans la littérature scientifique, aucun des résultats expérimentaux de la molécule "spiro" ne sont disponibles pour valider nos modèles théoriques et procédures de calculs. Néanmoins, considérant le caractère "modèle" de l'étude sur cette molécule particulière, les résultats des calculs obtenus ont été comparés avec d'autres méthodes bien établies de chimie quantique.

En outre, notre objectif était d'étendre cette enquête au-delà des systèmes modèles et à inclure quelques autres systèmes moléculaires à valence mixte pour être traités à l'aide des méthodes *ab-initio* locale multi-référence fortement corrélées. Gardant cela à l'esprit, une série de chaînes cationiques linéaires atomiques de béryllium, avec le nombre d'atomes de béryllium dans les chaînes varie de 6 à 12, a été étudiée. Les résultats obtenus pour ces systèmes sont très prometteurs et peuvent ouvrir de nombreuses nouvelles perspectives pour des futures recherches et investigations.

Enfin, notre objectif était aussi de pousser les limites de la méthode *ab-initio* multi-référence pour inclure des molécules relativement importantes en taille qui ne sont pas généralement traitées par un tel niveau de la théorie, tout en gardant en même temps une grande précision quantitative. Les molécules candidates sont deux *bis*-triarylamines, à savoir, le N,N,N',N'-tetra(4-méthoxyphényl)-1,4-phénylènediamine et le *bis*{4-[N,N-di(4-méthoxyphényl)amino]phényl}butadiyne. Nous avons choisi en particulier cette classe de molécules puisque leur modélisation théorique et exigences de calculs présentent un véritable défi en raison de leur grande taille moléculaire et de leur propre nature chimique en tant que des composés à valence mixte. En outre, et contrairement à la molécule cationique du "spiro" étudié dans ce projet, les *bis*-triarylamines sont des composés "réelles" où de nombreux résultats expérimentaux, concernant leur caractéristiques de valence mixte, peuvent être trouvées dans la littérature scientifique. En raison de leur taille inhabituelle, et donc du temps important de calculs nécessaires, le projet sur ces deux molécules n'a pas été terminé durant le délai de mon projet de doctorat. Cependant, les résultats préliminaires de calculs établis pour ces deux molécules sont présentés et discutés.

La thèse est organisée comme suite: chapitre 2 se penche aux méthodes *ab initio* de chimie quantique basées sur les fonctions d'ondes. En fait, la plupart des méthodes décrites dans ce chapitre ne sont pas utilisés pendant le cours de la thèse. Cependant, les méthodes *ab-initio* corrélées et les méthodes multi-référence localisés, qui sont largement utilisés dans ce travail, et qui sont expliqués plus en détail à la fin du chapitre 2, ne pouvait pas

être correctement discutées sans présenter les caractéristiques principales et les limites des méthodes *ab-initio* "traditionnelles". Chapitre 3 est entièrement consacré à la chimie et la physique générale des composés moléculaires chimiques à valence mixte. Dans ce chapitre, j'ai brièvement examiné les principaux modèles pour conceptualiser correctement le transfert de charge intramoléculaire, ou le transfert d'électrons, dans des systèmes moléculaires à valence mixte. Une enquête sélectionnée, mais pas complète, de certains composés organiques et inorganiques à valence mixte est également discutée dans ce chapitre. Les chapitres 4, 5 et 6 constituent le noyau de cette thèse, dans laquelle les résultats de la modèlisation théorique et les procédures de calcul effectué sur la les systèmes moléculaires chimiques sélectionnés sont présentés et discutés. Dans ces chapitres, les résultats et les discussions sont signalés par les articles publiés au cours de mon projet de doctorat. Les résultats non publiés sont présentés et discutés séparémet dans les chapitres correspondants. Chapitre 4 présente les résultats de la molécule cationique du "spiro". Le chapitre suivant présente des résultats montrant un caractère à vlence mixte dans une série de chaînes linéaires d'atomes de béryllium. Le chapitre 6 est consacré aux deux molécules cationiques de la famille *bis*-triarylamine, étudié dans un niveau préliminaire dans ce travail. Dans le dernier chapitre, des conclusions des résultats obtenus dans ce travail et quelques remarques sur les perspectifs des travaux futurs possibles sont fait remarquer.

Chapter 2

Theoretical methods of calculations: *ab-initio* methods

2.1 Introduction

In the present chapter, quantum chemical *ab-initio* methods are briefly described. In particular, the localized Multi-Reference method that is used extensively in this work, recently developed in our laboratory, is presented with some details. This section will serve as a very short historical review and an explanation of the notation used.

2.1.1 Quantum mechanics and quantum chemistry

Quantum mechanics was formulated during the first half of the twentieth century, after the failure of classical mechanics to explain some physical phenomena. The new theory, which generalizes all classical theories, successfully explained black-body radiation [1], the photoelectric effect [2], and other phenomena at the microscopic level, like the hydrogen atom electronic orbitals [3] and the Compton effect [4]. The correspondence principle, which describes the cases in which classical mechanics approaches quantum mechanics, was introduced by Niels Bohr in 1923 [5], and in 1924 de Broglie proposed the wave-particle duality of matter [6,7]. The new quantum theory was formulated with many mathematical representations, the most famous are: *matrix mechanics*, developed by Heisenberg, Born, and Jordan in 1925 [8–10]; *wave mechanics*, developed by Schrödinger in 1926 [11–16]; *second quantization*, sometimes known as "transformation theory", developed by Dirac in

1927 for photons [17], then extended by Jordan and Klein to massive bosons [18], and by Jordan and Wigner to fermions [19]; and the formulation known as *path integral* developed by Feynman in 1948 [20, 21]. Schrödinger proved that Heisenberg matrix mechanics is equivalent to Schrödinger wave mechanics [13]. The very basic principles of quantum mechanics are postulated rather than derived. A complete integration of general relativity with quantum mechanics is still not very well established, nevertheless, the results of quantum theory when applied to micro-physical structures and mechanisms are spectacular.

Quantum chemistry, sometimes called molecular quantum mechanics, a branch of theoretical chemistry, may be defined as the application of quantum mechanics to predict phenomena and solve problems in chemistry. An early generation of theoretical chemists build powerful theoretical models, that apply explicitly the new concepts of quantum theory to atoms and molecules, in order to understand and explain their electronic structure, properties, and chemical reactivity. Two significant models were introduced: the first is the Valence Bond (VB) model, sometimes called the homo-polar method or the directed electron pairs, developed by Heitler, London, Pauling, and Slater [22–25], which is mainly characterized by the "localization" of bonds; the second is the Molecular Orbital (MO) model developed by Lennard-Jones, Hund, and Mulliken [26–32], in which an electron is not assigned to a particular valence but is allowed to move in a field of the same symmetry as that of the molecule. The two procedures represents different approximations, and "philosophies", to the solution of a complicated secular equation, but their final results are equivalent [33], as long as qualitative pictures and representations are concerned.

The computational revolution in quantum chemistry, that started in the early 1950's, made it possible to solve the Schrödinger equation approximately with different approaches and accuracies: *ab-initio* (from first principles) methods [34–46], see the following references [47–52] for bibliographic compilations on *ab-initio* methods and applications; semiempirical methods [53–56]; Density Functional Theory (DFT) methods [57–63]; and Quantum Monte Carlo (QMC) methods [64–67]. DFT methods are sometimes classified by some authors as *ab-initio* methods. Since this "revolution", many theoretical models and computational techniques within the *ab-initio* family have been developed. Hartree-Fock (HF), Configuration Interaction (CI), Many-Body Perturbation Theories (MBPT), Coupled Cluster (CC), Complete Active Space Self Consistent Field (CASSCF), Generalized Valence Bond (GVB), Multi-Reference Configuration Interaction (MRCI) and Multi-Reference Perturbation Theories (MRPT) are among the most famous and well-established *ab-initio* methods.

The next sections in this chapter will consider briefly and review these methods with a special emphasis on the methods used in this work.

2.1.2 Notation used in the present work

2.1.2.1 Bracket notation

A physical state is represented by a *state vector* in a complex vector space. Following Dirac [68], such a vector is called a *ket* and is denoted by $|\Psi\rangle$. This state ket is postulated to contain complete information about the physical state. An *observable*, such as energy, can be represented by an *operator*, such as $\hat{A}$, in the vector space in question. Generally, an operator acts on a ket from the left $\hat{A}|\Psi\rangle$. To every ket $|\Psi\rangle$, there exist a *bra*, denoted by $\langle\Psi|$ in the bra space dual to the ket space. The bra dual to $c|\Psi\rangle$ is postulated to be $c^*\langle\Psi|$, where c is a complex number.

An *inner product* of a bra and a ket for an N-particle vector state, representing two square integrable functions $\Psi_1(\mathbf{r}_1, \ldots, \mathbf{r}_N)$ and $\Psi_2(\mathbf{r}_1, \ldots, \mathbf{r}_N)$ is defined as,

$$\langle\Psi_1|\Psi_2\rangle \equiv \int \Psi_1^*(\mathbf{r}_1, \ldots, \mathbf{r}_N)\Psi_2(\mathbf{r}_1, \ldots, \mathbf{r}_N)d(\mathbf{r}_1, \ldots, \mathbf{r}_N) \tag{2.1}$$

from the definition (2.1), we have, $\langle\Psi_1|\Psi_2\rangle = \langle\Psi_2|\Psi_1\rangle^*$. Moreover,

$$\langle\Psi_1|c\Psi_2\rangle = c\,\langle\Psi_1|\Psi_2\rangle \tag{2.2}$$

$$\langle c\Psi_1|\Psi_2\rangle = c^*\,\langle\Psi_1|\Psi_2\rangle \tag{2.3}$$

$$\langle\Psi_3|\Psi_1 + \Psi_2\rangle = \langle\Psi_3|\Psi_1\rangle + \langle\Psi_3|\Psi_2\rangle\,. \tag{2.4}$$

where $|\Psi_3\rangle$ is a third function.

2.1.2.2 Second quantization

The notation build for second quantization representation of quantum mechanics for fermions [19], is widely adopted in modern quantum chemical methods [46, 69–71]. In this representation, all operators and states can be constructed from a set of elementary creation and annihilation operators. If ϕ_i is a one-electron state and $|0\rangle$ is the vacuum state (no particle), the creation operator a_i^+ will create a particle in the state ϕ_i if applied to the

vacuum state $|0\rangle$,

$$a_i^+|0\rangle = |\phi_i\rangle \tag{2.5}$$

The annihilation operator a_i will give the vacuum state if applied to ϕ_i,

$$a_i|\phi_i\rangle = |0\rangle \tag{2.6}$$

The following anti-commutation relations hold:

$$[a_i^+, a_j^+]_+ = a_i^+ a_j^+ + a_j^+ a_i^+ = 0 \tag{2.7}$$

$$[a_i, a_j]_+ = 0 \tag{2.8}$$

$$[a_i^+, a_j]_+ = \delta_{i,j} \tag{2.9}$$

where δ_{ij} is the Kronecker delta (equals 1 for $i = j$ and 0 otherwise). From equations (2.7) – (2.9), all the algebric properties of the second quantization formalism follow.

The Slater determinant describing a wavefunction of N electrons (see section §2.2.3) is represented by an occupation number vector $|\mathbf{k}\rangle$,

$$|\mathbf{k}\rangle = |k_1, k_2, \ldots, k_N\rangle, k_p = \begin{cases} 1, & \phi \text{ occupied;} \\ 0, & \phi \text{ unoccupied.} \end{cases} \tag{2.10}$$

thus, k_p is the occupation number corresponding to the spin-orbital ϕ_p.

2.2 Basic approximations in *ab-initio* methods

2.2.1 Schrödinger equation

One major deal in quantum chemistry is trying to solve the time-independent non-relativistic Schrödinger eigenvalue equation [11] for chemical systems,

$$\hat{\mathcal{H}}|\Psi\rangle = E|\Psi\rangle \tag{2.11}$$

In equation (2.11), $\hat{\mathcal{H}}$ is the non-relativistic Hermitian and linear energy operator, the Hamiltonian operator; Ψ, the eigenvector of an Hilbert space, is the time-independent

wave function, or state function, of the system, which is a function of the space and spin coordinates of the elementary particles composing the system, and which contains all the information about the system; and E, the eigenvalue constant, is the total energy of the system.

The Hamiltonian operator $\hat{\mathcal{H}}$ for a particular chemical system of interest is constructed in order to find, by means of solution of (2.11), the energy E and the wave function Ψ of the system. Once Ψ is found, it can be used to find some other properties. In practice, the Schrödinger equation could be solved exactly only for systems with one electron. Many approximations are inevitable to treat real chemical systems. Nevertheless, many of these approximations are reliable and lead to accurate results, in the limit of the available computational resources.

2.2.2 The Hamiltonian operator and the Born-Oppenheimer approximation

The non-relativistic Hamiltonian operator, $\hat{\mathcal{H}}$, of a system composed of N electrons, with the corresponding $\mathbf{r}_i$ space position vector for the ith electron; and M nuclei, with the corresponding $\mathbf{R}_A$ space position vector for the Ath nucleus, is defined in atomic units as:

$$\hat{\mathcal{H}} = -\sum_{i=1}^{N}\frac{1}{2}\nabla_i^2 - \sum_{A=1}^{M}\frac{1}{2M_A}\nabla_A^2 - \sum_{i=1}^{N}\sum_{A=1}^{M}\frac{Z_A}{r_{iA}} + \sum_{i=1}^{N}\sum_{j>i}^{N}\frac{1}{r_{ij}} + \sum_{A=1}^{M}\sum_{B>A}^{M}\frac{Z_A Z_B}{R_{AB}} \qquad (2.12)$$

where M_A is the ratio of the mass of nucleus A to the mass of an electron, Z_A is the atomic number of nucleus A, $r_{iA} = |\mathbf{r}_{iA}| = |\mathbf{r}_i - \mathbf{R}_A|$, $r_{ij} = |\mathbf{r}_i - \mathbf{r}_j|$, $R_{AB} = |\mathbf{R}_A - \mathbf{R}_B|$, and ∇^2 is the Laplacian operator for the ith electron and the Ath nucleus expressed in any suitable coordinates system. In equation (2.12), the first term is the kinetic energy operator of the electrons; the second term is the kinetic energy operator of the nuclei; the last three terms are the potential energy operators of the system particles, the third term represents the Coulomb attraction between electrons and nuclei, the fourth and fifth terms represent the repulsion between electrons and between nuclei, respectively.

Small magnetic terms, like spin-orbit coupling and spin-spin interaction, which are usually of minor significance to the chemical energies, are neglected in the Hamiltonian operator (2.12). In cases where the velocities of the electrons approach the velocity of light, like the inner-shell electrons of heavy atoms, the Hamiltonian operator (2.12) ceases

to be appropriate and relativistic effects should be considered [72–74].

To simplify the Hamiltonian operator, Born-Oppenheimer (BO) approximation [75, 76] is used. Taking the fact that the nuclei move much slower than the electrons, since $m_{p^+}/m_{e^-} = 1836$, one can consider the electrons in a molecule to be moving in a field of fixed nuclei. By treating the nuclei as stationary sources of electrostatic fields, the second term of the Hamiltonian operator (2.12), *i.e.* the kinetic energy of the nuclei, can be neglected, and the last term of equation (2.12), *i.e.* the repulsion between the nuclei, can be considered to be constant which is usually added at the end of a calculation (any constant added to an operator has no effect on the operator eigenfunctions and only adds to the operator eigenvalues).

The remaining terms in equation (2.12) are together called the electronic Hamiltonian operator $\hat{\mathcal{H}}_{el}$ which describes the motion of N electrons in the field of M point charges,

$$\hat{\mathcal{H}}_{el} = -\sum_{i=1}^{N} \frac{1}{2}\nabla_i^2 - \sum_{i=1}^{N}\sum_{A=1}^{M} \frac{Z_A}{r_{iA}} + \sum_{i=1}^{N}\sum_{j>i}^{N} \frac{1}{r_{ij}} \tag{2.13}$$

Using the electronic Hamiltonian operator $\hat{\mathcal{H}}_{el}$ would yield the electronic wave function Ψ_{el} and the electronic energy E_{el}, as the eigenfunction and eigenvalue of the Schrödinger equation (2.11), respectively. Ψ_{el} and E_{el} depends parametrically on the nuclear coordinates, Ψ_{el} is a function of the electrons only ($\Psi_{el} = \Psi_{el}(\mathbf{r}_i)$).

Within the adiabatic approximation [77–79], the nuclei move on a Potential Energy Surface (PES) obtained by calculating Ψ_{el} and E_{el} using the BO approximation at each nuclear configuration on the PES [80, 81].

The Born-Oppenheimer and the adiabatic approximations are extensively used in quantum chemical methods. However, non-adiabatic processes are present in many important chemical systems [82]. In such cases, the Born-Oppenheimer approximation breaks down. This is particularly true in some charge transfer reactions and non-crossing regions (see the next chapter) where the electronic coupling between the two (or more, see section §3.2.4) electronic states is relatively high [83, 84].

2.2.3 The wave function and its relevant basic approximations

First, spatial orbitals and spin-orbitals are defined. A spatial orbital, $\psi_i(\mathbf{r})$, is a one-electron wave function, where $\mathbf{r}$ is a coordinate vector in the ordinary 3-dimensional space.

In order to satisfy Pauli exclusion principle [85], two one-electron spin functions $\alpha(\sigma)$ and $\beta(\sigma)$, corresponding to spin up $(1/2)$ and spin down $(-1/2)$ respectively, are introduced. The spin functions are orthonormal, i. e., $\langle\alpha|\alpha\rangle = 1$, $\langle\beta|\beta\rangle = 1$, and $\langle\alpha|\beta\rangle = \langle\beta|\alpha\rangle = 0$. A spin-orbital, $\phi_i(\mathbf{x})$, where $\mathbf{x} = \{\mathbf{r}, \sigma\}$, is a one-electron wave function, which is a product of one-electron spatial orbital and a one-electron spin function.

In order to overcome the incapability to solve the so called r_{12} terms (the third term of equation (2.13)), quantum chemical *ab-initio* wave function based methods reduce the N-body problem to N one-body problems. In MO theory, this corresponds to approximate the electronic wave function $\Psi_{el}(\mathbf{x}_1, \ldots, \mathbf{x}_N)$ of a molecule containing N electrons as the product of N spin orbitals $\phi_i(\mathbf{x})$. This is the orbital approximation. The many-electron wave function should, however, be antisymmetric with respect to the interchange of the coordinate $\mathbf{x}$ of any two electrons, a condition needed to satisfy Pauli exclusion principle. In addition, the many-electron wave function should take into consideration the indistinguishability of the electrons that are assigned to particular spin-orbitals. One way to satisfy these criteria, within the orbital approximation context, is writing the total wave function of a system containing N electrons and N spin-orbitals as an antisymmetrized product of N one-electron spin-orbitals. This product is usually referred to as a Slater determinant [86, 87],

$$\Psi_{el}(\mathbf{x}_1, \mathbf{x}_2, \ldots, \mathbf{x}_N) \approx \Psi_{\mathrm{SD}}(\mathbf{x}_1, \mathbf{x}_2, \ldots, \mathbf{x}_N) = \frac{1}{\sqrt{N!}} \begin{vmatrix} \phi_1(\mathbf{x}_1) & \phi_2(\mathbf{x}_1) & \ldots & \phi_N(\mathbf{x}_1) \\ \phi_1(\mathbf{x}_2) & \phi_2(\mathbf{x}_2) & \ldots & \phi_N(\mathbf{x}_2) \\ \ldots & \ldots & \ldots & \ldots \\ \phi_1(\mathbf{x}_N) & \phi_2(\mathbf{x}_N) & \ldots & \phi_N(\mathbf{x}_N) \end{vmatrix} \tag{2.14}$$

where $1/\sqrt{N!}$ is a normalization factor. A short hand of writing the Slater determinant (2.14) using a ket space is,

$$|\Psi_{\mathrm{SD}}\rangle = |\phi_1 \phi_2 \ldots \phi_N\rangle \tag{2.15}$$

where only the diagonal elements of the determinant are written, and the normalization factor is omitted.

Configuration State Function (CSF) is defined as the set of all the Slater determinants with the same orbital occupation but different spin-orbital occupation numbers.

The molecular orbitals of a Slater determinant are expressed as a superposition of Atomic Orbitals (AO). The method is known as Molecular Orbitals-Linear Combination of

Atomic Orbitals (MO-LCAO). In this method, the spatial molecular orbitals $\psi_i(\mathbf{r})$ are expanded as a linear combination of known one-electron basis functions $\chi_\mu(\mathbf{r})$, conventionally called atomic orbitals (although in general they are not solutions to atomic Schrödinger equation), centered on the atoms that constitute the molecule,

$$\psi_i(\mathbf{r}) = \sum_{\mu=1}^{K} C_{\mu,i}\chi_\mu(\mathbf{r}) \tag{2.16}$$

where $C_{\mu,i}$ are the expansion coefficients of the set of basis functions $(1, \ldots, \mu, \ldots, K)$ used for each molecular orbital i. Clearly, the coefficients $C_{\mu,i}$ are the elements of the matrix $\mathbf{C}$. The MO-LCAO procedure, proposed by Roothaan [88] for HF *ab-initio* calculations, made it possible to compute the Hartree-Fock equations (see section §2.2.4) by transforming them from differential eigenvalue equations, that are difficult to solve by machine algorithms, to algebric eigenvalue equations that could be solved numerically using efficient matrix algorithms. These algebric equations are known as Roothaan-Hall equations. [88, 89]

To exactly represent the molecular orbitals $\psi_i(\mathbf{r})$, within Born-Oppenheimer approximation, the basis functions $\chi_\mu(\mathbf{r})$ should form a complete set. This requires an infinite number of basis functions ($K = \infty$) in equation (2.16). In practice, one must use a finite number K of basis functions. This is called the basis set approximation. However, if K is large enough and the functions $\chi_\mu(\mathbf{r})$ are well chosen, one can represent the molecular orbitals with an acceptable error.

The molecular orbitals $\psi_i(\mathbf{r})$ of a given molecular wave function show the same kinds of possible symmetry behavior as the overall electronic wave function does [88]. The molecular orbitals are therefore classified according to the irreducible representations (symmetry species) of the molecular point group. Hence, in MO-LCAO method, the atomic orbitals are chosen to construct molecular orbitals so that upon application of the molecular symmetry operators each molecular orbital transforms according to one of the irreducible representations of the molecular point group. The atomic orbitals (basis functions) chosen in this way are called symmetry-adapted basis functions, and thus the method is known as Symmetry-Adapted Linear Combination of atomic orbitals (SALC). This constraint imposed by using the SALC's is, indeed, a source of a significant reduction in the computational time of calculations, particularly for molecules belonging to high symmetry point groups.

Basis functions and basis sets, particularly those used in this work, are briefly treated in section §2.6.

An N-electron wave function can exactly be expanded in a linear combination of all the Slater determinants obtained from N one-electron functions:

$$\Psi_{exact} = \sum_I C_I \Psi_I \tag{2.17}$$

As far as the the one-electron basis set is complete, the expansion is exact within Born-Oppenheimer approximation.

2.2.4 Hartree-Fock Self-Consistent Field

In the Hartree-Fock (HF) method [90, 91], the expansion of the wave function in a linear combination of Slater determinants (2.17) is truncated to a single term:

$$\Psi_{exact} \approx \Psi_0 \tag{2.18}$$

HF method is, thus, a *single reference method*. Replacing the true N-electron wave function Ψ_{exact} by a single Slater determinant Ψ_0 (Ψ_{HF} in the following) is, indeed, a fairly drastic approximation. The variational principle is used to find the "best" Slater determinant (that one particular Ψ_{SD} which gives the lowest energy):

$$E^{el}_{\mathrm{HF}} = \min_{\Psi_{\mathrm{HF}}} \left\langle \Psi_{\mathrm{HF}} | \hat{\mathcal{H}}_{el} | \Psi_{\mathrm{HF}} \right\rangle \tag{2.19}$$

where the E^{el}_{HF} is the Hartree-Fock electronic energy and will be denoted by E_{HF} in the following. The variational freedom in this expression is in the choice of molecular orbitals. For computational convenience, the spin-orbitals are usually chosen to be orthonormal: $\langle \phi_i | \phi_j \rangle = \delta_{ij}$.

Given orbital orthogonality, the energy of a single determinant wavefunction (excluding nuclear repulsion) is

$$E_{\mathrm{HF}} = \sum_i^N \left\langle i | \hat{h} | i \right\rangle + \frac{1}{2} \sum_{ij}^N ([ii|jj] - [ij|ji]) \tag{2.20}$$

where $\langle i|h|i\rangle$ are one-electron integrals defined as,

$$\left\langle i|\hat{h}|i\right\rangle = \int \phi_i^*(\mathbf{x}_1)\hat{h}(\mathbf{r}_1)\phi_j(\mathbf{x}_1)d\mathbf{x}_1 \tag{2.21}$$

where the one-electron operator $\hat{h}$ is defined as,

$$\hat{h}(i) = -\frac{1}{2}\nabla_i^2 - \sum_A \frac{Z_A}{r_{iA}} \tag{2.22}$$

the two-electron integrals of the type $[ii|jj]$ are generally called Coulomb integrals, while those of type $[ij|ji]$ are called exchange integrals. A two-electron integral is defined as,

$$[ij|kl] = \int \phi_i^*(\mathbf{x}_1)\phi_j(\mathbf{x}_1)\frac{1}{r_{12}}\phi_k^*(\mathbf{x}_2)\phi_l(\mathbf{x}_2)d\mathbf{x}_1 d\mathbf{x}_2 \tag{2.23}$$

In the derivation of the HF equations, Lagrange multipliers ε_{ij} are introduced to guarantee that all pairs of HF orbitals i and j will be orthogonal. Upon solution of the HF equations only the diagonal elements ε_{ii}, which are called orbital energies, have non-zero values. Koopmans' theorem [92] states that these orbital energies ε_{ii}, or simply ε_i, may be associated with the ionization potentials of the closed-shell atom or molecule for which the SCF wave function has been obtained. More precisely,

$$\varepsilon_i = \left\langle i|\hat{h}|i\right\rangle + \sum_j [ii|jj] - [ij|ji] \tag{2.24}$$

where the sum of Coulomb minus exchange integrals goes over all spin-orbitals. Koopmans showed that the energy difference between the SCF energy calculated for a neutral molecule using equation (2.20) and the energy of a single determinant resulting from removing one spin-orbital ϕ_i from this wavefunction is the ionization potential of the molecule for the corresponding spin-orbital and is just the orbital energy ε_i given by equation (2.24).

HF equations are solved using a self consistent procedure. An SCF wave function is the single determinant of lowest energy within a finite basis set.

Hartree-Fock self-consistent field theory accounts for the bulk ($\approx 99\%$) of the total energy of the molecule. However, the component of the energy left out in such a model, which results from the neglect of instantaneous interactions (correlations) between electrons, is crucial for the description of chemical bond formation. Moreover, HF theory does

not behave correctly at regions far from the equilibrium. HF-SCF wavefunctions actually provides an excellent starting point for subsequent calculations of electron correlation (section §2.3) that enhances the accuracy deficiency encountered by HF-SCF calculations.

2.2.4.1 RHF, UHF and ROHF methods

For closed shell systems with singlet configurations, HF wave functions are characterized by having doubly occupied spatial orbitals, that is to say, two spin orbitals: ϕ_i with a spin function α and ϕ_j with a spin function β, that share the same spatial orbital ψ_i and have the same orbital energy. If this restriction was imposed from the beginning in a calculation, an approximated wave function that is known as "Restricted Hartree-Fock" (RHF) wave function [88] well be generated. RHF approximation is inappropriate for open shell chemical systems (like the Spiro molecular cation studied in chapter 4 and all other -mixed-valence systems ions). There are two possibilities for the computational treatment of open shell systems within the HF-SCF approximation: The first method is the "Unrestricted Hartree-Fock" (UHF) [93, 94]. The second method is the "Restricted Open-shell Hartree-Fock" (ROHF) [95].

In the UHF approximation, the notion of doubly occupied spatial orbitals is completely ignored and each spin-orbital is allowed to have its own spatial part and orbital energy. However, using the spin-orbitals in the UHF calculations may introduce serious problems. Actually, the obtained wave function is mono-determinantal and is not an eigenfunction of the spin operator.

ROHF approximation, on the other hand, permits to obtain spin-orbitals, by a self-consistent way, that minimize the energy of a multi-determinantal state that is formed from one spin configuration and that take into consideration the symmetries of the system. ROHF method differentiates two types of orbitals, according to their occupation: Doubly occupied orbitals; and active orbitals, where the occupation is determined by the spin and space symmetries of the system. ROHF wave function $|\Psi_{HF}\rangle$ is thus can be written as,

$$|\Psi_{ROHF}\rangle = \left|\psi_1^2 \ldots \psi_n^2\right\rangle \otimes |\Psi\rangle \tag{2.25}$$

where the orbitals $\psi_1 \ldots \psi_n$ are the doubly occupied orbitals; and $|\Psi\rangle$, based on p active

orbitals $\psi_{n+1}, \ldots, \psi_{n+p}$, can be defined as,

$$|\Psi\rangle = \sum_I C_I \left| \psi_{n+1}^{\alpha_{n+1}^I} \ldots \psi_{n+p}^{\alpha_{n+p}^I} \right\rangle \tag{2.26}$$

where I span the determinants that form $|\Psi\rangle$; C_I is the coefficient of the determinant I; and the exponent α_{n+i}^I corresponds to the occupation of the ith active orbital in the I determinant (it has the value 0 in the case of an empty orbital, 1 if the orbital is occupied by an α electron, -1 if the orbital is occupied by a β electron, and 2 in the case of doubly occupied orbital.)

2.3 Correlated *ab-initio* methods

2.3.1 Definitions

In order to discuss properly the different correlated *ab-initio* methods, it is necessary to define first some fundamental concepts.

1. *Size extensivity* [96], is the property of a method that scales correctly with the number of particles.

2. *Size consistency* [97], is a method that leads during a molecular fragmentation to a wave function which is multiplicatively separable and an energy which is additively separable.

   Size consistency is only defined if the two fragments are non-interacting, while size extensivity implies that fragments can be interacting.

3. *Coulomb hole* is a region surrounding each electron, in an atom or a molecule, in which the probability of finding another electron of the opposite spin is small. This is due to the fact that electrons try to repel each others (r_{12} effect).

4. *Fermi hole* is a region surrounding each electron, in an atom or a molecule, in which the probability of finding another electron of the same spin is small. This is due to Pauli exclusion principle.

5. *Excited determinants* are defined, for a system of N electrons and $2K$ spin-orbitals, as the set of single determinants that could be formed from the combination of $2K$

spin-orbitals with N electrons when $2K > N$. The number of which is defined by the binomial coefficient,

$$\binom{2K}{N} = \frac{(2K)!}{N!(2K-N)!} \tag{2.27}$$

where the HF ground state determinant is one of these.

A singly excited determinant is one which differs by a single spin-orbital from the HF determinant, etc.

6. *Brillouin theorem* (BT) [98, 99] states that matrix elements of the electronic Hamiltonian operator between the HF determinant for a closed-shell atom or molecule and all singly excited determinants, that differs by a single spin-orbital of the same symmetry, are zero,

$$\langle \Psi_{HF} | \hat{\mathcal{H}}_{el} | \Psi_S \rangle = 0 \tag{2.28}$$

where Ψ_S is a singly excited determinant wave function. For SCF wave functions $|\Psi_{SCF}\rangle$, Brillouin's theorem states that

$$\langle \Psi_{SCF} | \hat{\mathcal{H}}_{el} | \Psi_S \rangle = 0 \tag{2.29}$$

only if the single spin-orbital in $|\Psi_S\rangle$ not in $|\Psi_{SCF}\rangle$ can be constructed from the finite basis set in which the SCF calculation was carried out.

2.3.2 Electron correlation energy

HF theory is an approximation to the Schrödinger equation of molecules. The results of HF energy are not *exact*. In order to improve these results, electron correlation must be considered in the subsequent methods that still use HF wave function as a start. It should be reminded that the neglect of electron correlation is not the only source of error in HF method. Basis set truncation error (incompleteness of the basis set), deviations from Born-Oppenheimer approximation, and the neglect of relativistic effects are all important sources of error in *ab initio* molecular electronic calculations. Löwdin has defined the correlation energy as: "The correlation energy for a certain state with respect to a specified Hamiltonian is the difference between the exact eigenvalue of the Hamiltonian and its expectation value in the Hartree-Fock approximation for the state under consideration" [100]. Electron correlation energy E_{corr} for a system is thus calculated, for a given basis

set, as:

$$E_{corr} = E_{exact} - E_{HF} \tag{2.30}$$

where E_{exact} is the exact non-relativistic energy of the system and E_{HF} is the corresponding energy calculated by HF method. As guaranteed by the variational principle, the electron correlation energy E_{corr} is always negative. Typically, the correlation energy is defined within the finite basis set used, and the convergence with respect to increasing the basis set size is then considered separately. It should be noted that E_{corr} is not a constant through the whole PES, it becomes greater at points far from the equilibrium. One more point is that Fermi correlation, arises from the Pauli antisymmetry principle, is not part of the of electron correlation energy as defined above, since it is already taken into account in the HF level.

Correlation energy for an open-shell molecule is usually defined with respect to unrestricted Hartree-Fock (UHF) theory, while some authors prefer to define it with respect to restricted Hartree-Fock theory. This may lead to some ambiguities. In addition, Goddard has suggested to replace the HF approximation with a reference wave function that corresponds to all configurations that are necessary for the qualitatively correct description of the system under consideration, and suggested an alternative definition of the correlation energy for large R in the dissociation process [101]. This reference wave function could be a multiconfiguration reference function §(2.3.4) or a Generalized Valence Bond (GVB) wave function [102–105]. Electron correlation effects, as defined above, are clearly not directly observable. In fact, E_{corr} in equation (2.30) is a measure of the errors that are inherent in HF theory.

Criteria for a theoretical model to be suitable as a method for the solution of the correlation problem in molecules have been formulated by Pople *et al.* [96], extended by Bartlett and Purvis [97], and summarized by Bartlett [106] and Wilson [107]. The method should be as follows:

1. Size-extensive;

2. Generally applicable to a wide range class of problems and a wide variety of molecules within one framework;

3. Invariant to classes of transformations, particularly unitary transformations among degenerate orbitals;

4. Efficient and cost effective, with the amount of computer time not increasing too rapidly with the size of the system;

5. Applicable to excited states and open-shells;

6. Able to dissociate a molecule correctly into its fragments.

No single method satisfies all the criteria mentioned.

More details on electron correlation energy are discussed elsewhere in the literature [37, 39, 42, 43, 96, 106, 108–112]

2.3.2.1 Dynamical and non-dynamical correlation

While the definition of the correlation energy defined in equation 2.30 is satisfactory near equilibrium, it becomes less satisfactory as molecular bonds are stretched. It is usual to recognize that the correlation energy so defined may be split into two parts, which Sinanoğlu is generally acknowledged to be the first to recognize [113]: "Correlation effects may be divided into 'dynamical' and 'nondynamical' ones. Dynamical correlation occurs with a 'tight pair' of electrons as in He or in the $(2p_z)^2$ in Ne, etc. There is no one configuration in the Configuration Interaction wavefunction which mixes strongly with the Hartree Fock configuration and CI is slowly convergent. 'Non-dynamical' correlations, on the other hand, arise from degeneracies or near-degeneracies (first order CI)."

Dynamical correlation energy (DCE) is associated with the lowering of the energy as a result of correlating the motion of the electrons due to Coulomb repulsion. DCE is not considered in HF mean field (independent particle model) approximation. DCE is a short range phenomena. *Non-dynamical correlation energy* (NDCE) is associated with the lowering of the energy through interaction of the HF configuration with low-lying excited states. It is a near-degeneracy effect and a long range phenomena. It is difficult, and in most cases impossible, to calculate exactly the values of each of the dynamical and the non-dynamical correlation energies separately [114].

2.3.3 Dynamical correlation: Single-Reference Methods

2.3.3.1 Configuration interaction

Configuration interaction (CI), sometimes called superposition of configurations or configuration mixing, is one of the oldest correlation methods [115–122]. CI requires one to

build a set of n-electron configuration state functions (CSFs or spin-adapted Slater determinants) by replacing occupied molecular orbitals (MOs) in some SCF reference function with virtual (unoccupied) orbitals. The Hamiltonian is then diagonalized in the resulting basis of n-electron configurations. In the CI method, the wave function is constructed as a linear combination of determinants or CSF's,

$$|\mathbf{C}\rangle = \sum_i C_i |i\rangle \tag{2.31}$$

where $\mathbf{C}$ is a vector containing the expansion coefficients C_i. The coefficients C_i are determined by a variational optimization of the expectation value of the electronic energy. This means minimization of the ground state,

$$E_{CI} = \min_{\mathbf{C}} \left\langle \mathbf{C}|\hat{\mathcal{H}}_{el}|\mathbf{C} \right\rangle \tag{2.32}$$

The MO's used for building the excited Slater determinants are taken from HF calculation and held fixed. Subscripts S, D, T, Q, etc. indicate singly, doubly, triply, quantuply etc. excited relative to the HF configuration.

Full CI (FCI) method for an n-electron system is defined as the wave function that includes all possible excitations through order n. With a complete basis set, FCI method would become the exact solution of the non-relativistic electronic Schrödinger equation. It is the FCI method to which all approximate methods are compared. Therefore, FCI energies are used as benchmarks tests for other methods [123–135]. The number of configurations in a FCI expansion grows exponentially with the size of the system. FCI methods are intractable for all but very small molecules, *e.g.* diatomic molecules of the first-raw elements. Novel algorithmic developments have contributed toward increasing the number of configurations which can be included in a practical FCI calculation [136–144].

Truncated CI is the term used whenever a limited number of excitations in the CI expansion is used. CI with Singles (CIS) does not give any improvement over the HF results for the ground state energies as all matrix elements between the HF wave function and singly excited determinants are zero (Brillouin theorem).The lowest CI level that gives improvements over HF energy is CI with Doubles (CID) model. The singly excited determinants have non-zero matrix elements with the doubly excited determinants. CI with Singles and Doubles (CISD) was for a long time a "standard" method for the treatment of

electron correlation. Better improvements to the CISD method are CISDT and CISDTQ models which scales rapidly with the number of particles of the system ($> N^8$).

The following concepts have a great impact in the development of CI calculations: The formulation of Direct Configuration Interaction (DCI) approach [145]; the introduction to electronic structure theory of the Unitary Group Approach (UGA) by Paldus [146]; the introduction of a Graphical representation of the UGA-based CI expansion by Shavitt, leading to the Graphical Unitary Group Approach (GUGA) [147, 148]; and the separation of the GUGA graph into two parts, the complex internal part and the simple external part, by Siegbahn [149].

The CI approach to the many-electron problem suffers from two main disadvantages. First, all truncated CI methods are not size extensive. For instance, as the molecule gets larger, CISD method recovers less and less of the correlation energy. Second, the CI description of the electronic energy is not particularly compact. Thus, even though higher excitations are less important than those of lower orders, their number is very large. As a result, the CI wave function converges slowly with the number of the variational parameters.

CI was the dominant and preferred electron correlation technique until the early 1980s when it was superseded by size-consistent techniques such as perturbation theory or coupled cluster methods [150].

2.3.3.2 Many-Body Perturbation Theory

In perturbation methods, the Hamiltonian operator consists of two parts, a reference $\hat{\mathcal{H}}_0$ part and a perturbation $\hat{\mathcal{H}}'$ part, where $\hat{\mathcal{H}}'$ is relatively "small" compared to $\hat{\mathcal{H}}_0$. The theoretical framework of Many-Body Perturbation Theory (MBPT) is defined by adding corrections to solutions which employ an independent particle model using perturbational methods.

Møller Plesset theorem [151] is a corollary of Brillouin's theorem. It adds electron correlation effects by means of Rayleigh-Schrödinger perturbation theory usually to second (MP2), third (MP3) or fourth (MP4) order. For open shell molecules, MPn theory can directly be applied only to unrestricted Hartree-Fock reference functions (since ROHF states are not in general eigenvectors of the Fock operator). However, the resulting energies often suffer from severe spin contamination, leading to very wrong results. A much better alternative is to use MP methods based on restricted Hartree-Fock references.

Unlike variational methods, as CI, in which the energy is an upper bound to the exact energy, perturbation methods offer no such guarantee. Nevertheless, the size extensivity of MP methods combined with the low cost relative to CI methods make MP calculations a good choice for including electron correlation.

2.3.3.3 Coupled-cluster methods

Coupled-cluster theory [152–154] expresses the exact wave function within the basis set approximation as,

$$\Psi = e^{\hat{T}}\Psi_{\mathrm{HF}} \tag{2.33}$$

where Ψ_{HF} is a single CSF HF determinant that is used in the SCF process to generate a set of spin-orbitals. The operator $\hat{T}$, called the cluster operator, generates, when acting on Ψ_{HF}, single, double, etc., excitations and is defined as,

$$\hat{T} = \hat{T}_1 + \hat{T}_2 + \hat{T}_3 + \ldots + \hat{T}_n \tag{2.34}$$

where n is the total number of electrons and the various $\hat{T}_i$ operators generate all possible determinants having i excitations from the reference. As in CI method, and using the same notation, one can compute CCD, where $\hat{T} = \hat{T}_2$; CCSD, where $\hat{T} = \hat{T}_1 + \hat{T}_2$; etc. The CCSDT calculations gives very accurate results for correlation energy but are very demanding computationally and are only feasible for small molecules with small basis sets. Several approximate forms of CCSDT have been developed, for instance, in the CCSD(T) method, triple excitations are calculated based on perturbation theory.

2.3.4 Non-dynamical correlation: Multi-Configuration SCF

Multi-configurational self-consistent field (MCSCF) method uses a linear combination of configuration state functions (CSF) or configuration determinants to approximate the exact molecular electronic wavefunction. In a MCSCF calculation, the set of coefficients of both the CSFs or determinants and the basis functions in the molecular orbitals are varied to obtain the total electronic wavefunction with the lowest possible energy. The non-dynamical correlation included in the MCSCF method is particularly useful in the quasi-degenerate cases like in molecular ground states with low-lying excited states or in bond breaking situations.

2.3.4.1 CASSCF

One of the most used forms of MCSCF is Complete Active Space Self-Consistent Field (CASSCF) [155–158], in which the MCSCF procedure is applied to some molecular orbitals called the active orbitals. In CASSCF, the orbitals are divided into three classes:

1. Occupied orbitals, (O) that are doubly occupied in all the reference determinants;
2. Active orbitals, (A) that have a variable occupation number in the reference determinants;
3. Virtual orbitals, (V) that are unoccupied in all reference determinants.

The CASSCF wave function corresponds to a FCI wave function in the active space, while the occupied and virtual orbitals are optimized through an SCF-like procedure.

2.3.5 Dynamical corrections on non-dynamical wave-functions: Multi-Reference Methods

The calculation of dynamical and non-dynamical correlation energies is obtained by using multi-reference methods where dynamical correlation is calculated over a multi-reference wave function. Three methods are explained below: a multi-reference method that uses variational CI dynamical correlation, MRCI; and two multi-reference methods that use perturbational corrections, CASPT and NEVPT methods.

2.3.5.1 Multireference configuration interaction

In a Multi-Reference Configuration interaction (MRCI) [159, 160], a CI calculation is performed with an MCSCF wave function as the reference function instead of a single reference CSF as in CI method. CASSCF wave functions are often used as the starting point for MRCI calculations. Typically, MRCI is a useful method to study a large section of a PES, where significant changes in bonding, and thus in correlation energy, are taking place so a proper method is needed to predict dynamical and non-dynamical correlation energies. The MRCI method has been shown to reproduce FCI results very closely for a wide range of spectroscopic problems [161]. As with single-reference CI, most MRCI calculations truncate the CI expansion to include only singles and doubles (MRCISD). If a CASSCF wave function is used as reference, MRCISD could be also designated as CAS+SD.

2.3.5.2 Multireference perturbation theory

The generalization of MPn theory to the multireference case involves using an MCSCF wave function for Ψ_0 instead of a single-determinant RHF or UHF one. However, it is less obvious what should be chosen for $\hat{\mathcal{H}}_0$, as the MCSCF MOs do not diagonalize any particular set of one-electron operators.

Several different implementations of MP2 type expansions based on a CASSCF reference (CASPT2) were developed [162] in the 1990's and a wide range of applications was tested. Another method of doing multireference perturbation theory calculations is the the n-electron valence perturbation theory (NEVPT) method [163–166].

2.3.6 Some practical aspects and limitations of non-dynamical correlation methods

For large molecular systems, one strategy to approximate non-dynamical correlation is to perform CASSCF calculations in small active spaces. In that case, non-dynamical correlation is not completely described in the zero-order wave function. Practically, this approximation introduces arbitrariness into the theoretical descriptions because the active space is not uniquely defined and must be chosen based on physical considerations for each particular process. Often, small active orbital spaces lead to significant errors, which cannot be completely recovered by subsequent calculations of dynamical correlation. It has been shown by Davidson that CASSCF calculations for the Cope rearrangement (that involves a sigmatropic rearrangement of hydrocarbon dienes) performed in a π-orbitals active space is qualitatively incorrect, and inclusion of $\sigma - \pi$ correlation by subsequent second order perturbation theory (CASMP2) calculations changes the energetics along the reaction coordinate significantly [167]. There are other cases also where large active spaces are necessary and can be close to the computational limit for CASSCF method [168].

2.4 Localized multi-reference methods

2.4.1 Localization in chemistry and quantum chemistry

Traditional chemistry is based on local concepts. Lewis representation of molecules [169] and the Valence Bond (VB) method [22–25, 170, 171] are two examples on early molecular

models based on locality in terms of bonds and lone-electron pairs. On the other hand, locality is not reflected in standard electronic structure calculations in which the molecular orbital theory presumes molecular orbitals extended over the whole molecule with various coefficients on each atom. However, Fock observed that a one determinant many-electron wave function is invariant with respect to unitary transformations among its molecular orbitals [91]. One thus has freedom in the choice of the orbitals that describes a given system. Based on this observation, many authors pointed out the interest of using Localized Molecular Orbitals (LMO) [172–175].

2.4.2 Linear Scaling

One of the most important advantages of using LMO's is their use in linear scaling procedures [176]. In order to perform molecular electronic-structure calculations in which computational time scales linearly with the number N of atoms, one could take the advantage of the fact that interaction between different fragments goes to zero with increasing distance. In this way, a large amount of unnecessary bi-electronic integrals, between distant atomic orbitals, can be neglected during a calculation. This effect can be obtained by using local orbitals.

Not only can localization methods be of great interest in the computational level, but on the theoretical level as well. Localized molecular orbitals provide the link between Hartree-Fock theory and the concept of chemical bonds formed between two atoms. Moreover, they are indispensable for exploiting the nature of dynamical, short-range, electron correlation.

Localization methods were applied to to Single-Reference (SR) methods like HF-SCF [176,177], and methods based on dynamical correlation such as second-order Møller-Plesset (MP2) perturbation theory [178], single and double configuration interaction CI(SD) [179], and single and double coupled cluster CC(SD) [180]. However, many important chemical processes and systems, like chemical bond breaking and formation, transition states, electronically excited states, magnetic systems, and mixed valence systems, are degenerate or quasi-degenerate in nature. Only multi-reference methods, in which non-dynamical correlation procedures such as CAS-SCF and FCI are applied, could treat successfully quasi-degenerate systems. Unfortunately, linear scaling for non-dynamical correlation is an open problem, but it should be noticed that orbital localization is a necessary condition toward linear scaling multi-reference electronic structure calculations.

2.4.3 CASDI program

A formalism for obtaining *a priori* local orbitals of CAS-SCF type was recently developed in our laboratory [181–185]. *A priori*, in this context, means that the final localized orbitals are directly obtained and optimized from guess localized orbitals [186, 187]. On the other hand, if the localized orbitals were obtained from canonical optimized orbitals, the method is designated as *a posteriori* [172, 174, 177]. An advantage of using *a priori* localized molecular orbitals is that one can choose, among the large number of possible CAS spaces, the particular set of active orbitals that are relevant for the study of a particular phenomenon.

At the moment, two versions, variational [182] and perturbative [183], of the developed algorithm exist. The variational method is briefly described in the following. The algorithm consists of a two step procedure: in the first step, a set of orthogonal atomic orbitals is generated through a symmetric orthonormalization of the non-orthogonal atomic orbitals, these orthogonal atomic orbitals are then combined to form a set of guess localized molecular orthogonal orbitals through a hierarchic combination of symmetric and Schmidt orthogonalization, in order to avoid core/valence mixing. The generated localized molecular orthogonal orbitals at the end of the first step can be centered on a bond or an atom (e.g., for lone pairs and core orbitals), they can also be distributed on a molecular fragment. In the second step, the localized orthogonalized molecular orbitals are optimized using a super-CI-like procedure, equivalent to that proposed by Ruedenberg and coworkers [188]. Starting from a CAS-CI wavefunction $|\Psi_{\mathrm{CAS}}\rangle$, the CAS+S set of internally contracted single excitations is produced, where the single excitation operators $a_i^+ a_j$ act on the wavefunction $|\Psi_{\mathrm{CAS}}\rangle$ as a whole. A new wavefunction in the CAS+S space $|\Psi_{\mathrm{CAS+S}}\rangle$ is produced. By diagonalizing the one-body density matrix Γ_1 associated to $|\Psi_{\mathrm{CAS+S}}\rangle$, a new set of orbitals is obtained, which can be used to build a new $|\Psi_{\mathrm{CAS}}\rangle$ wavefunction. The procedure is iterated until wavefunction invariance is achieved and optimized natural orbitals of CAS-SCF type are obtained through satisfying the generalized Brillouin theorem (GBT) [189]. The diagonalization of Γ_1 completely mixes the orbitals within each class and the original locality of the guess orbitals would be lost. Taking advantage of the invariance of the CAS-SCF wavefunction with respect to orbital rotations within each orbital class, a block diagonalization of Γ_1 would minimize the mixing between the orbitals at each iteration. As a result, the orbitals at convergence maintain as far as possible the

same nature as the initial guess orbitals.

The new method has been implemented and successfully tested for the ground and the excited states of different organic conjugated systems [190–193], magnetic metal containing systems [194, 195], fullerenes [196, 197], and other chemical systems [198–201]. Geometry optimization within a localized CAS-SCF approach was also investigated [202]. In this work, we have used the variational version to optimize CAS+S and CAS+SD wavefunction starting from localized guess orbitals.

2.5 DFT methods used

Density Functional Theory (DFT) was developed by Hohenberg and Kohn in 1964 [203, 204]. In DFT method, the electron density ρ is regarded as the central variational quantity of interest. Despite the fact that the knowledge of exact DFT functionals is incomplete, DFT still enjoys widespread popularity because it provides a good balance between computational effort and accuracy. However, there are a number of well-known situations where DFT is inadequate: strongly correlated systems, excited states, and open-shell systems, just to name a few. In this work, the DFT method was used to optimize the geometries of the *bis*-triarylamine molecules studied in chapter 6.

2.6 Basis sets used

The most common and practical method to construct molecular orbitals is the many-center expansion (equation (2.16)) of MO's from known basis functions (atomic orbitals). Two main types of basis functions are used in quantum chemical calculations: Slater Type Orbitals (STO) [205], in which multi-center molecular integrals (resulted from the expansion (2.16)) are difficult to compute; and Gaussian Type Orbitals (GTO) [206], which do not properly represent the nuclear cusp and the tail as STO's does, but have the advantage of being faster than STO's in calculating multi-center molecular integrals.

To overcome the inaccuracies caused by the zero slopes of GTO's at and near the nuclear cusp regions and the fast decay of the tails far from the nucleus, several GTO's, called Primitive GTOs (PGTO) could be used to approximate one GTO, called Contracted GTO (CGTO). Clearly, more PGTO's are needed if high accuracy is desired, but this will generate another problem which is the computational cost. A compromise is the linear

combination of primitive GTO's with a fixed expansion coefficients,

$$\chi_r = \sum_i^k a_{r,i} g_u \tag{2.35}$$

where $\chi_{r,i}$ are the contracted GTO's that will be used in the expansion (2.16); g_u are the primitives GTO's; and $a_{r,i}$ are the contraction coefficients which are not parameters to be determined by variation principle, but are held fixed during the calculation after finding their proper values by some suitable method before the orbital optimization. This contraction saves computational time with little loss in accuracy if the contraction coefficients $a_{r,i}$ are well chosen.

There are two ways commonly used in modern quantum chemical packages for contracting a set of primitive GTO's to a set of contracted GTO's:

1. Segmented contraction, where each primitive GTO is only used in one contracted function. The contraction coefficients, fixed during a calculations, can be determined by a variational uncorrelated optimization method, like an atomic HF calculation. For this reason, those basis sets are appropriate for ground-state HF calculations. Examples on this kind of contraction are:

   (a) Pople style basis sets (STO-nG, k-nlmG),

   (b) Dunning-Huzinga Basis sets.

2. General contraction, where all the primitive GTO's, on a given atom and of a given angular momentum, enter all the contracted functions having that angular momentum, but with different contraction coefficients. Moreover, correlated atomic calculations are used to find the contraction coefficients, and thus, they are usually suitable for molecular calculations with different correlation levels. Examples on this kind of contraction are:

   (a) Atomic Natural Orbitals (ANO) [207], where a large primitive GTO's set is contracted to a small number of contracted GTO's by using natural orbitals, from a correlated calculation on the free atom, typically at the CISD level [208, 209].

   (b) Correlation consistent basis sets.

All the calculations in this work were done using ANO basis set for first row atoms [207].

Chapter 3

Mixed valence systems

3.1 Introduction

In this chapter, mixed-valency and mixed-valence molecules are surveyed. The next section will present the theoretical background underlying electron, or charge, transfer reactions and mixed-valence systems. A discussion of the quantum mechanical computational capabilities and limitations to treat these kind of molecules and their physicochemical properties is then presented before a literature survey of organic and inorganic mixed-valence systems is briefly given. In the last section, the issue of computing a reaction coordinates that corresponds to the intramolecular charge transfer reaction is discussed.

3.2 Electron-transfer reactions and mixed-valency

3.2.1 Introduction

Electron-transfer (ET) reactions are fundamental processes in chemistry and biology [210–212]. As a result of major advances in experimental and computational techniques, great progress has been achieved in the understanding and control of ET processes [213, 214]. Numerous investigations were devoted to the study of ET processes in real biological systems [215], in biomimetic model compounds [216, 217], and in structurally simple and completely artificial low molecular weight systems [218, 219]. The aims range from the desire to understand ET processes in nature to the design of molecular wires for electronic communication and other electronic devices [220–229].

3.2.2 Mixed-valence systems and their classification

Mixed-valence compounds are characterized by inter-valence charge transfer (CT) between two or more redox sites existing in different oxidation states. Since the seminal work of Creutz and Taube on mixed-valence compounds [230], these simple inorganic derivatives, compared to natural ET systems, were used as test cases in order to study basic aspects of ET theories [231, 232], that is, to check the applicability of Marcus ET theory and its extension, the Hush theory for interpreting intervalence charge-transfer (IV-CT) absorption spectra [233–237].

Robin and Day classified mixed-valence compounds, with two (or more) redox centers, according to the size of the electronic interaction between these centers [238]. There are three categories in Robin and Day classification:

1. class I: there is *no* coupling between the centers, that is to say, the redox centers are completely localized, and behave as separate entities,

2. class II: intermediate coupling between the mixed valence centers exists, and therefore the charge is partly localized,

3. class III: coupling is so strong that the system is completely delocalized and intermediate redox states have to be attributed to the redox centers.

An important feature of class II and class III mixed-valence complexes is the appearance in the visible or near-infrared region of the IV-CT band, associated with the optical excitation from the minimum of the ground electronic state to the lowest excited electronic state, which cannot be attributed to the system subunits.

It should be noted that cases in which there is a transition between two adjacent classes are frequent. For instance, the transition between class II and class III systems has recently attracted considerable attention [239–242].

3.2.3 Electron transfer theory and potential energy surfaces

In ET reactions, the transfer of electron is accompanied by nuclear rearrangements. Therefore, it is convenient to consider the potential energy of the system as a function of nuclear coordinates Q, i.e., Potential Energy Surfaces (PES). According to Marcus [243–245] the potential energy surface of a degenerate mixed-valence system can be constructed from

parabolic functions each representing a diabatic, or zero-order, non-interacting state (denoted by $a, b, c, \ldots$). In this picture, solvent and counterion effects are obviously neglected, and therefore molecules are treated in a gas phase model. The discussion below also assumes that the intramolecular ET reaction in the corresponding system is dominated by two electronic states and that these two states are related to each other by a symmetry plane between them (this assures that the system is symmetric). The total wave function Ψ_0 of the non-interacting system is

$$\Psi_0 = \psi_a \psi_b \tag{3.1}$$

where ψ_a and ψ_a are the wave functions of the diabatic states a and b respectively. If there is an electronic interaction (coupling) between the states a and b, their corresponding wave functions will mix with each other, to an extent that depends on the magnitude of the interaction. This leads to an effective removing of the degeneracy at the crossing of the diabatic wave functions, i.e., the formation of the avoided crossing, which gives rise to two new and separate adiabatic (first-order) states of energies E^1 and E^2, (defined below). A typical symmetric PES showing two adiabatic states resulted from a coupling of two diabatic states is sketched in Figure 3.1.

The associated wave functions of these new adiabatic states, Ψ_1 and Ψ_2, are linear combinations of ψ_a and ψ_b,

$$\Psi_1 = c_a \psi_a + c_b \psi_b, \tag{3.2a}$$

$$\Psi_2 = c_a \psi_b - c_b \psi_a \tag{3.2b}$$

The electronic coupling V_{ab}, known as coupling matrix element, tunneling matrix element, or resonance exchange integral, is defined as half the splitting between the adiabatic potential energy surfaces E^1 and E^2 at the crossing seam (see Figure 3.1),

$$2V_{ab} = E^2 - E^1 \tag{3.3}$$

Where E^2 is the higher and E^1 is the lower root (solution) of the secular equation:

$$\begin{vmatrix} H_{aa} - E & H_{ab} - ES_{ab} \\ H_{ba} - ES_{ba} & H_{bb} - E \end{vmatrix} = 0 \tag{3.4}$$

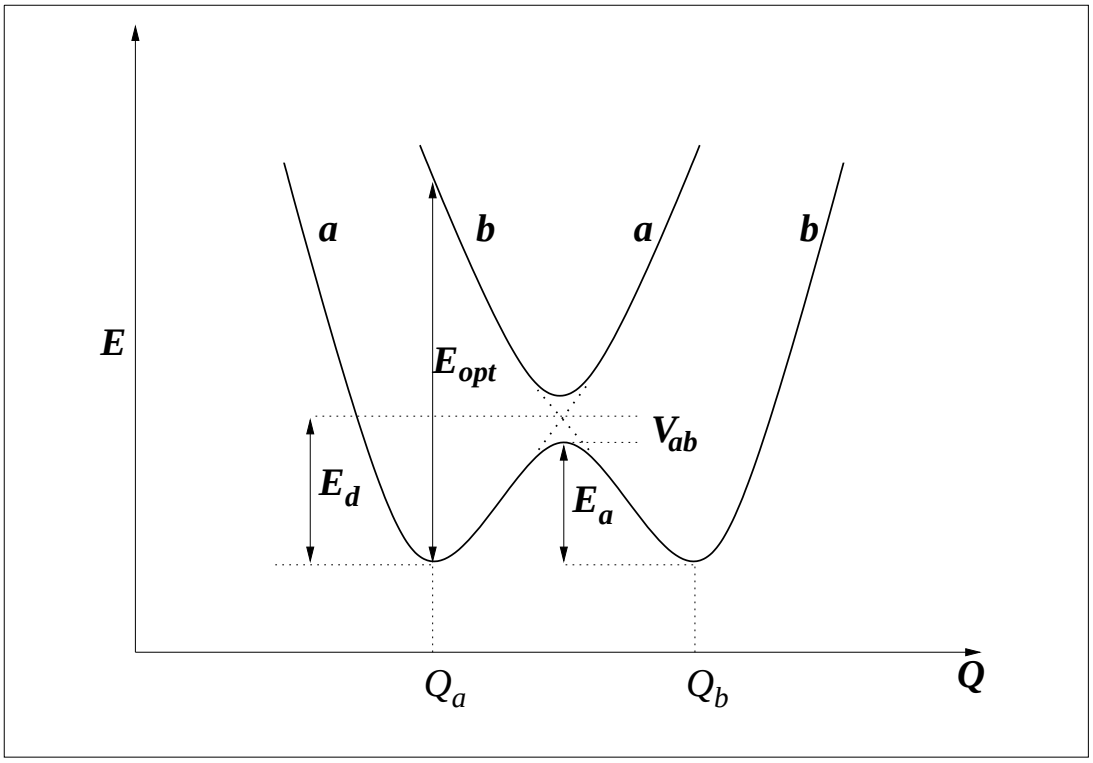

Figure 3.1: *A cross section of an energy profile for initial state a and final state b in a typical symmetric (exothermicity or $\Delta E = 0$) ET reaction.The solid curves are the adiabatic surfaces, the dashed lines refer to diabatic surfaces. Q_a and Q_b are equilibrium nuclear coordinates of a and b respectively. Electron transfer matrix V_{ab}, diabatic activation energy E_d, adiabatic activation energy E_a, and the intramolecular reorganizing energy E_{opt}, are indicated.*

where $H_{aa} = \langle\psi_a|H|\psi_a\rangle$, $H_{bb} = \langle\psi_b|H|\psi_b\rangle$, $H_{ab} = \langle\psi_a|H|\psi_b\rangle$, $S_{ab} = \langle\psi_a|\psi_b\rangle$, and H is the electronic Hamiltonian operator $\hat{\mathcal{H}}_{el}$ defined in equation (2.13). At the crossing seam $H_{aa} = H_{bb}$, therefore V_{ab} becomes:

$$V_{ab} = \frac{H_{ab} - S_{ab}(H_{aa})}{1 - S_{ab}^2} \tag{3.5}$$

In the limit of small S_{ab}, $V_{ab} \approx H_{ab}$. The electronic coupling integral, V_{ab}, is a key quantity in ET models, in which its role is both mixing the two diabatic states and mixing the electronic ground state with that of the excited state. These two "mixings" are explained next.

For class II systems, two intramolecular electron-transfer pathways are conceivable

[237]: (1) the thermal process where the system moves from one minimum of the lower adiabatic surface over a transition state, along the electron-transfer coordinate to the other minimum, where the energy of this transition is the adiabatic energy barrier separating the two equilibrium points, called E_a; and (2) the optical way where the system is photo-excited from one minimum of the lower adiabatic surface to the Franck-Condon state of the upper adiabatic surface. The energy of this IV-CT excitation is the Marcus reorganization energy λ and it is equal to the optical transition energy E_{opt} in the cases of symmetric PES's (see Figure 3.1).

It is important to mention that a charge transfer processes can be sometimes classified as: through-bond and through-space CT. In a through-bond CT, the transfer of electrons between the redox units proceeds by way of an intermediate electronic state that uses wave functions localized on the bridge-unit between the redox sites. In contrast, a through-space CT is the result of the direct spatial overlap of the two redox units wave functions while the bridge is used only to bring the two units together.

In addition to the classical two-state model described so far (sometimes called Marcus two-state model), there are other theoretical approaches to describe ET reactions. Quantum mechanical treatments account for the integral role of vibronic coupling which becomes increasingly important with stronger electronic coupling due to the dynamic interaction between the vibrational and electronic motions (i.e. the failure to meet the Born Oppenheimer approximation) [246,247]. The PKS model proposed by Piepho, Krausz and Schatz was originally formulated as a two-state, one-dimensional model along an anti-symmetric vibrational coordinate, q [248, 249].

Some other models includes, semi-classical [250], molecular orbital (e.g., the Ondrechen model) [251], and three-state models. The latter are briefly described in the next subsection. These and other models were reviewed and described in greater detail by many authors [242, 244, 252, 253].

3.2.4 Three-state classical models

The classical two-state model is based on Born-Oppenheimer approximation and is strictly valid only in the strongly localized and delocalized limits. In the bridged mixed-valence systems in which the electron transfer is mediated by a third state, the inclusion of an additional electronic state is often necessary. For instance, systems that are transitions

between localized and delocalized regimes (i.g., transition between class II and class III) are not properly described by a two-state model and the so called three-state models [241, 254–256] are indeed more adequate to treat such systems.

The three-state model proposed by Brunschwig, Creutz and Sutin [241] provides an extension to the two-state classical model by explicitly including a third electronic state (c) formed by charge transfer to or from the bridging ligand. The influence of this additional state depends on its energy relative to the other two diabatic states (a and b). When the mediating state is of high energy, the electron transfer can be treated analytically by invoking perturbative (superexchange) mixing of the reactant, product and mediating states: the wave functions for the former diabatic states are modified by including perturbative contributions from the higher electronic states. On the other hand, if the mediating state is sufficiently low lying, charge transfer can take place by a sequential electron or hole transfer reaction (chemical mechanism) in which the bridging group becomes reduced or oxidized [241]. In general, a 3×3 Hamiltonian must be solved to obtain the adiabatic surfaces of the three states. The electron transfer process involves superexchange coupling of the three states, where states a and b couple to state c through the electronic coupling parameter V_{ac} ($= V_{bc}$), and the direct V_{ab} coupling is zero.

The same authors had also proposed a four-state ET model for systems with several d electrons in which the treatment of electrons other than the transferring one is necessary [241]. An example of the latter case is symmetric D_{2h} Ru_{II}–Bridge–Ru_{III} complexes such as the pyrazine-bridged dimer $[(NH_3)_5Ru]_2pz^{5+}$ where at least three electrons need to be considered.

Potential energy surfaces and reaction pathways for bridged mediated electron transfer molecular ionic systems were also recently reported [257–260]. The subject of PES and the reaction coordinates of mixed valence systems will be treated in the last section in this chapter.

3.3 Computational quantum mechanical methods of mixed-valence molecules

Semiempirical computational methods such as INDO, AM1 and PM3, and *ab initio* methods such as Hartree-Fock Self-Consistent Field method (HF-SCF), post Hartree-Fock cor-

related methods, and Density Functional Theory (DFT) (see the previous chapter for a detailed treatment of *ab initio* methods) have been extensively employed to provide rapid calculations of the structural and electronic properties of mixed-valence systems [83,261,262]. These calculations could be compared with the experimental values of V_{ab} and E_{opt} which in turn can be estimated from IV-CT band structure, intensity, and position.

Among the many measurable quantities of mixed-valence ET reactions, the numerical calculation of V_{ab} had received a great interest. The semiempirical CNDO/S, INDO, and related methods have been exploited by several groups in estimating V_{ab} [83], while Nelsen and Newton had shown recently an estimation of V_{ab} from AM1 calculations [263].

Extensive application of *ab initio* methods has been made to study electron transfer in many systems. Most studies have used HF wave functions and thus have been limited to reactions involving the lowest state of a given symmetry, but some studies have used correlated wave functions [264,265]. In the ab initio determination of V_{ab}, several different strategies can in principle be employed. For instance, the diabatic way involves explicit determination of the matrix elements of equation (3.4), which is usually accomplished by exploiting the properties of symmetry-broken SCF solutions for weakly coupled systems and therefore is limited to uncorrelated wave functions [266, 267]. A second possibility is to compute the adiabatic energies and to obtain V_{ab}, making use of equation (3.3). This approach allows for a wide variety of technical solutions making use, for instance, of orbital energies (by using Koopmans' theorem) or sophisticated correlated eigenstates. However, such an approach is not free of difficulties since the calculation of E^1 and E^2 (say from a multireference configuration interaction (MRCI) expansion) should ensure that the same degree of electron correlation is incorporated into the two adiabatic states.

To overcome these difficulties, Sanz and Malrieu reported [268] on an alternative method to compute V_{ab} at the correlated level in which the determination of adiabatic energies or diabatic wave functions was not compulsory. In this procedure, only electron correlation contributions to the off-diagonal term H_{ab} were explicitly computed. The method allows for a variational calculation by means of the CI matrix built up from the minimal set of determinants contributing to the energy difference between the adiabatic states a and b (Difference-Dedicated CI, DDCI).

Density functional theory (DFT) has been extensively applied in modern theoretical approaches to a wide variety of chemical problems. However, its application to the computation of the ET matrix element is limited by the fact that such a theory was originally

developed for the ground state, while equation (3.3) also needs the energy for the first excited state. DFT computations of excited-state energies is quite an involved task, and a large effort in this direction is currently made [269].

Theoretical and computational framework for quantitatively modeling the electronic characteristics of mixed-valence systems between the localized and delocalized regimes has been also proposed [270]. The formalism accounts for the key features of the shift, including the central role of both anti-symmetric and symmetric modes within the full treatment of the vibronic coupling problem. The Generalized Mulliken-Hush (GMH) method [271, 272] can be successfully used for calculating the electronic matrix coupling elements in which three and more states are present in an electron transfer process.

3.4 Mixed-valence molecules

Mixed-valence compounds were extensively studied since the 1960's. In contrast to inorganic and organometallic mixed-valence compounds, much less is known about purely organic mixed-valence systems, although a great number of derivatives have been synthesized that might have mixed-valence character in one possible oxidation state.

3.4.1 Inorganic mixed-valence molecules

A typical inorganic mixed-valence compounds are composed of symmetrical complexes in which two metal atoms are connected by a bridging ligand. One famous example is $[(NH_3)_5Ru - pyz - Ru(NH_3)_5]^{5+}$, where pyz = pyrazine, synthesized and studied by Cruetz and Taube in 1969 [230]. This initiated the synthesis of a great variety of molecular mixed-valence compounds [231, 273–276]. The synthesis of new mixed-valence compounds including bridged dimers of ruthenium is still an active field of research [277–283]. Their properties, in particular the electronic coupling between the metal centers through the bridge, are investigated using electrochemistry, spectroelectrochemistry, absorption spectroscopies, EPR (electronic paramagnetic resonance), and DFT (density functional theory) calculations, while the analysis of the intervalence band in this type of complexes, the effect of solvent, the effect of localization, and dynamics have been the subject of recent theoretical works [241, 284–288].

Theoretical calculations on mixed-valence complexes containing other transition metals

are also very frequent in the literature [289].

3.4.2 Organic mixed-valence molecules

The study of pure organic mixed-valence compounds appeared relatively later than their inorganic counterparts. Organic mixed-valence molecules tend to exhibit stronger inter-site coupling than their transition-metal-based analogues [290]. Moreover, the Inter-Valence Charge Transfer (IV-CT) band of organic mixed-valence systems are not affected by the overlap with other low-lying transition, contrary to what may occur for inorganic compounds due to appearance of the $d \rightarrow d$ metal to ligand (MLCT) or ligand to metal (LMCT) charge transfer excitations.

Many different pure organic redox centers have been investigated, including quinones and imides [291, 292], dioxaborines [293], nitro groups [294, 295], and perchlorotriphenylmethyl centers [296, 297] in anionic organic mixed-valence systems, and hydrazines [298, 299], 1,4-dialkoxybenzenes [300,301], and various alkylamines [287,302] in cationic systems.

Triarylamine mixed-valence species have been the focus of a number of studies [259,260, 303–318]; triarylamines may be readily combined with a wide range of bridging groups and, with appropriate substitution patterns, can be converted to rather stable radical cations at only moderate oxidizing potentials [319]. The importance of these molecules comes from their use as hole-transport agents in organic electronics applications [320,321], in which the intermolecular charge-transfer process involves electron hopping between neutral molecules and the corresponding mixed-valence radical cation.

Lambert and Nöll have studied the mixed-valence properties of a variety of *bis*-triarylamine systems in which the terminal aryl groups have methoxy groups in the 4-position, including those with phenylene, biphenyl, and phenylene-ethynylene bridging groups [259, 260, 307]; (see Figure 3.2 for typical molecular structures of this class). Additionally, several theoretical and computational works have been published on these compounds. Coropceanu *et al.* performed a time dependent DFT calculations on molecule 1 cation (1^+) shown in Figure 3.2, their measurement of the lowest optical transitions were close to experimental data and it was suggested that molecule 1^+ is a class II/III borderline system [309]. The latter work was extended to include all the molecules shown in Figure 3.2, where the electronic coupling parameter were also evaluated [311], and some general conclusions have been drawn about the classification of the molecular cations studied. For instance, according

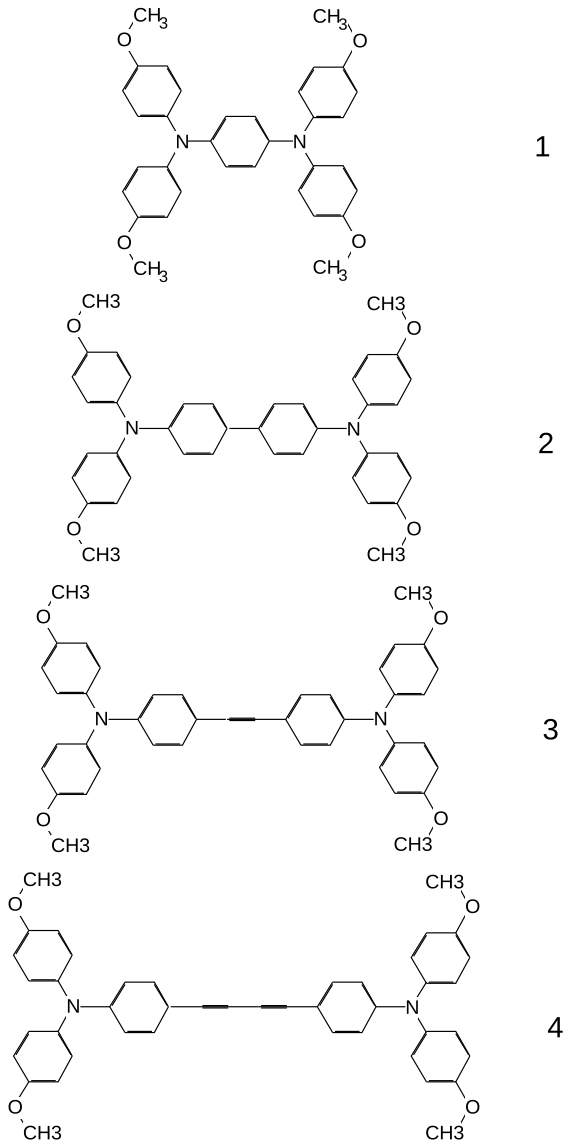

Figure 3.2: *Typical molecular structures of bis-triarylamines. (The IUPAC names of molecules* 1 *and* 4 *are given in chapter 6).*

to these calculations, it was suggested that molecules 3^+ and 4^+ can be classified as class II mixed-valence systems, while the IV-CT profiles of molecules 1^+ and 2^+ was found to be consistent with class III systems exhibiting strong coupling of the electron transfer to symmetrical vibrations [311]. The effect of temperature on the charge transfer transitions on these molecules were also investigated theoretically by the same group [313].

Molecules 1^+ and 4^+ shown in Figure 3.2 were investigated at a preliminary level during

the course of this thesis, see chapter 6.

3.5 Reaction coordinates

A reaction coordinate, or a reaction path, is defined as the steepest-descent pathway, in the many-dimensional nuclear coordinate space, connecting the two equivalent minima and passing through the saddle point (the transition state) on the crossing seam surface [322].

In this work, we have replaced the exact reaction path by an approximated one, in which the geometries are obtained by averaging the geometries of two points on the reaction coordinate according to a mixing parameter ξ. The mixing parameter is plotted on the abscissa of a reaction coordinate, it could be chosen to have different ranges, typically from -0.5 to $+0.5$, and different increments. An averaged geometry can be obtained by two different methods:

1. mixing linearly the optimized equilibrium, or minimum, geometry with the optimized transition state, or saddle point, geometry at the crossing seam;

2. mixing linearly the geometries of the two optimized minima.

The first choice would produce a transition state structure in which the first derivative of energy, $dE/d\xi$, is non zero. The second choice seems to be preferable, since it produces a smooth curve on the whole ξ range, including the crossing seam at $\xi = 0.00$. Another advantage of mixing the two optimized equilibrium geometries is the possibility to test the geometry of the transition state point on the reaction coordinate with respect to the truly optimized transition state geometry. For these two reasons, we have chosen the second method. Using such a method is justified in the framework of the two-state model used for the molecular cations investigated.

Therefore, for all the systems studied in this work, the reaction coordinate was obtained by mixing linearly the optimized coordinates of the two equilibrium geometries:

$$Q(\xi) = \left(\frac{1}{2} - \xi\right) Q_A + \left(\frac{1}{2} + \xi\right) Q_B \tag{3.6}$$

where $Q(\xi)$ is the nuclear configuration at the point ξ on the reaction path, while Q_A and Q_B represent the nuclear coordinates of the two optimized equilibrium geometries.

The mixing parameter ξ was varied from -1.00 to $+1.00$ (-1.50 to $+1.50$ in the case of Spiro) in steps of 0.05. In such a way, Q_A is the geometry of the first minimum, this geometry corresponding to the point $\xi = -0.50$, where the positive charge is localized on one redox site of the molecular cation. Q_B is the geometry of second minimum, this geometry corresponding to the point $\xi = +0.50$, where the positive charge is localized on the other site of the molecule. The internal coordinates of the systems at the crossing seam, $\xi = 0.00$, are calculated as the average of the internal coordinates, of the two equilibrium points. The Born-Oppenheimer potential energy surfaces were then obtained by calculating the energies of the different electronic states that are most engaged for the corresponding ET reaction, at each step value of the parameter ξ.

In order to test the quality of the averaged transition state geometry and energy for the different molecules used in this work, geometry optimization at the crossing seam was carried on. The optimized geometries were then compared with the corresponding geometries of the obtained by mixing geometries of the two optimized minima. For all systems studied in this work, the differences between the optimized and the average geometries of the crossing seam states were very close, see chapters 4 and 5. This was also true for the energy differences between the electronic states of the averaged and the optimized geometry at the crossing seam. For these reasons, we believe that the geometry path obtained through equation (3.6) is very close to the optimal one.

Chapter 4

The "Spiro" molecular cation

4.1 Introduction

The Spiro π-σ-π molecular cation, 5,5'(4H,4H')-spirobi[cyclopenta[c]pyrrole]2,2',6,6'tetrahydro cation (the "Spiro" molecule in the following), shown in Figure 4.1, was thoroughly and extensively investigated as a model system during the course of this thesis. The Spiro system consists of two equivalent π moieties, lying onto two orthogonal planes, and separated by a spirocycloalkane rigid σ bridge. The spiro group is an sp^3 central carbon atom connected to four other adjacent carbon atoms forming together a tetrahedral shape. At the end of each π moiety, the two highly conjugated pyrrole groups, each with an sp^2 nitrogen atom bearing an electron pair of electrons, are the nominal donor/acceptor, or redox, centers in the Spiro molecule. If an electron is extracted from the neutral Spiro molecule, the resulting hole tends to localize either on the left or the right π system, inducing a deformation of the molecular geometry and an equilibrium state for each case. Therefore, two equivalent minima, separated by an energy barrier which represents the transition state between the two equilibrium states, exist for the cation, and the ground state presents the double-well potential energy surface which is typical for mixed-valence systems of class II (Figure 3.1). In this work, a classical (or Marcus-like) two-state model (see section §3.2.3) is adopted for the study of the electronic structure and spectroscopic states of mixed-valence Spiro molecular cation. It is important to remind that a three-state model for some special cases of mixed valence systems (see section §3.2.4) are sometimes more adequate than the simplified classical two-state model. The justification of using such a simplified two-state model in this study of Spiro is discussed in this chapter.

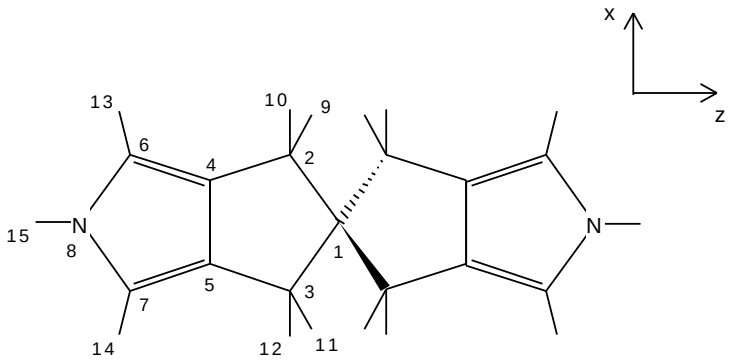

Figure 4.1: *The Spiro π-σ-π system 5,5'(4H,4H')-spirobi[cyclopenta[c]-pyrrole]2,2',6,6'tetrahydro molecule.*

Since the mid 1970's, Spiro, and the broader class of of molecules with π-σ-π composition, have been proposed as molecular electronic devices, since their electronic molecular structure allows them to be considered as strong candidates to be used as molecular switches or molecular memory devices [323–329]. In order for such a molecule to function as a device, each π moiety should be effectively insulated from the the other π moiety. This is achieved by having the spirocycloalkane as the σ bridge, making the plane of each π moiety perpendicular to that of the other one. Molecules of this type can be looked upon as a double-well potential for an electron that can hop back and forth between the two wells at some characteristic frequency, which depends on the height and the shape of the potential energy barrier. Such a two-state molecule can serve as a binary system in which one state represents "on" and the other represents "off" [324]. In this case, the two minima should be separated by a sufficiently high barrier, so that neither tunneling nor thermal fluctuations can intentionally switch one state to the other. Only by external control, e.g., an electric field or light, should one be able to switch. The height of the barrier can be controlled by chemical and structural modifications. However, the latter point is possible if the chemical bonds of the σ bridge are mostly responsible for the transfer of electrons, that is, through-bond ET.

The purpose of the study performed on Spiro in this project, was not to extract some conclusions about the potentiality of Spiro as a successful molecular device. Rather, and as a first step, a comprehensive understanding of the electronic structure and the low-lying spectroscopic states through the whole intramolecular charge transfer reaction coordinate

was thought to be necessary, and, therefore, an extensive investigation using highly correlated *ab-initio* multi-reference methods, using both canonical and localized molecular orbitals, was carried on Spiro molecular cation.

Spiro has been previously studied as a model system [325, 330, 331], since its relatively small size permits high level *ab-initio* investigations. Aviram *et al.* proposed a method and an algorithm based on symmetry broken SCF solutions of the diabatic states, by using RHF/STO-3G and RHF/3-21G to calculate V_{ab} and other ET mixed-valence parameters of the Spiro cation [325]. Their study showed that Spiro cation is a double-well-potential molecule with a significant energy barrier against the transfer of electrons from one end of the molecule to the other end, and that this barrier is sufficiently high so the stored bit of information is not inadvertently lost. The effect of an external electric field, treated as an external perturbation, on the values of computed V_{ab}, λ, E_d, and E_a was also observed. Through these calculations, they have found that the energy of the barrier decreases rapidly as the external field strength is increased. On the other hand, they have reported that V_{ab} and λ are not affected by the strength of the applied electric field.

They have also estimated the through-space contribution to the total V_{ab} value. This was done by calculating V_{ab} at zero field for a super-molecule consisting of a pyrrole and a pyrrole cation located at the same distance and angle 90° as the corresponding structure at the seam of crossing in Spiro. Moreover, the basis set of all carbons have been extensively augmented to assure the flexibility needed for the two fragments to overlap through space. They have found that through-space contribution to the total value of V_{ab} is less than 9%. Hence, one of their main conclusions was that Spiro does exhibit characteristics that are appropriate for molecular device applications.

Calzado *et al.* have measured the electronic coupling matrix element V_{ab} for Spiro, and other two mixed-valence systems, using UHF, DFT/B3-LYP, and the *ab-initio* variational Difference-Dedicated Configuration Interaction (DDCI) method [331]. They have concluded that DFT results of V_{ab} were underestimated by $15 - 20\%$ than that of DDCI. Nevertheless, they have pointed out some advantages of measuring such mixed-valence characteristics using DFT, such as the price and the simplicity of the DFT method used as compared to DDCI. Moreover, they have noticed that DFT provides more reliable results than UHF method at only a reasonable increment of computational effort.

Finally, Dehareng *et al.* have reported a more extensive study of Spiro, and other 5 pure organic mixed cation molecules, at *ab-initio* HF, CIS, CISD, MP2 and CASSCF

levels [330]. They have concluded that: 1) CIS level is quite misleading, 2) minimal basis sets should not be used except for geometry guesses for higher calculation levels, 3) the CASSCF level is certainly very appealing to determine excited states energies, but the appropriate choice of the active space remains a very delicate task, 4) the UHF level is subject to instabilities that makes the determination of V_{ab}, λ, E_d, and E_a only qualitative, 5) the inclusion of some electronic correlation to the UHF method (like UMP2, UMP4, UCISD) has a great influence on E_d and E_a but not as large on λ values.

4.2 Spiro symmetry and orbitals

The ideal symmetry of the neutral system is D_{2d}, where the principal axis of rotation, the C_2 axis, is the z-axis that passes through the two nitrogen atoms, see Figure 4.1. The ground electronic state geometry of the distorted cation shows two equivalent minima having a lower symmetry, C_{2v}. The two minima are separated by a saddle point at the crossing seam with a symmetric D_{2d} geometry. The σ/π separation is an approximated one, since σ and π orbitals belong to the same irreducible representations in both D_{2d} and C_{2v}. In Figure 4.2, the ten valence "π" orbitals for the symmetric D_{2d} neutral Spiro are shown together with their symmetry assignments. Notice that the symmetries reported in Figure 4.2 and the rest of this chapter are those of the C_{2v} point group. This is due to the fact that all the calculations performed on D_{2d} Spiro were done in the reduced C_{2v} subgroup, since the computer codes used in are not able to carry out calculations on non-Abelian groups, as D_{2d} point group. The D_{2d} symmetry is then imposed by setting the necessary constraints on the coordinates.

The orbitals in Figure 4.2 have been obtained at SCF level and by using a minimal basis set. The neutral "π" system contains twelve electrons, so the six lowest orbitals in Figure 4.2 are occupied, while the remaining four are empty (only the valence "π" orbitals of Spiro are considered here). The electronic configuration of the Spiro valence π orbitals, at the single determinant level, in the C_{2v} point group, is given by: (σ-core) $(1b_1)^2$ $(1b_2)^2$ $(2b_1)^2$ $(2b_2)^2$ $(1a_2)^2$ $(2a_2)^1$. The Highest Occupied Molecular Orbital (HOMO) of the system is the $2a_2$ orbital. By removing an electron from the HOMO, the ground state of the cation is obtained, which is therefore the $^2A_2$ state. Since the HOMO-1 $1a_2$ orbital is very close in energy to that of $2a_2$ orbital, one can expect a strong participation of this orbital to the low-lying states of the cation. Two more orbitals play an important role in the low-energy

spectrum: these are the two degenerated $2b_1$ and $2b_2$ orbitals (they actually belong to the degenerated E irreducible representation of D_{2d}, see Table 4.1). For this reason, our minimal CAS calculations have been performed by using these four orbitals as the active space, see section §4.3.5 below.

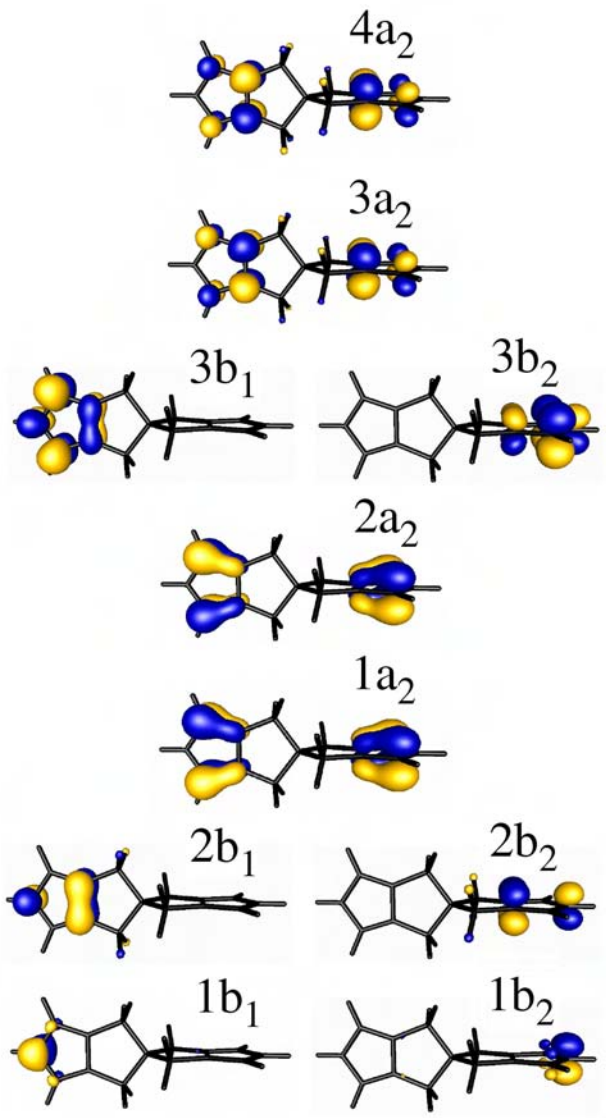

Figure 4.2: *Valence "π" molecular orbitals of the neutral Spiro molecule computed at RHF-SCF/SZ for D_{2d} geometry using C_{2v} irreducible representations. (See Table 4.1).*

In Table 4.1, the orbitals are classified accordingly to both D_{2d} and C_{2v} groups. It can be seen that the degenerated e orbitals in the D_{2d} group correspond to a pair b_1-b_2 in C_{2v}.

Table 4.1: *The designation of the valence "π" molecular orbitals of the Spiro neutral molecule shown in Figure 4.2 for the D_{2d} geometry using C_{2v} irreducible representations and the corresponding MO's in D_{2d} symmetry together with their orbital energies (in a.u.). Orbitals 1 to 6 are doubly occupied, while orbitals 7 to 10 are empty.*

MO number	C_{2v} sym.	D_{2d} sym.	orbital energy
1,2	$1b_1$ $1b_2$	$1e$	−0.6456
3,4	$2b_1$ $2b_2$	$2e$	−0.4221
5	$1a_2$	$1b_1$	−0.3990
6	$2a_2$	$1a_2$	−0.3947
7,8	$3b_1$ $3b_2$	$3e$	+0.1280
9	$3a_2$	$2b_1$	+0.2128
10	$4a_2$	$2a_2$	+0.2179

In a similar way, the a_2 orbitals in C_{2v} are classified either b_1 or a_2 in D_{2d}. For this reason, the two lowest states of the cation *have different symmetry* in D_{2d}: the lowest one has A_2 symmetry, while the first excited state has B_1 symmetry (while they are both A_2 in C_{2v}). In D_{2d}, the reaction coordinate has the same symmetry as the z axes, hence B_2. Since in this group $B_1 \otimes B_2 = A_2$, the two lowest states are indeed mixed by an antisymmetric deformation of the coordinates in the z direction.

In some previous reports, the Spiro cation was studied in the C_{2v} point group, if the charge is localized on either one of the two aromatic moieties in the molecule, while a D_{2d} geometry was taken for the totally delocalized state [325]. Other recent studies at CAS-SCF level, suggested C_2 and C_1 point groups for the two situations, respectively [330]. However, according to these calculations, the distortion from exact C_{2v} and D_{2d} symmetries are extremely small. Moreover, CAS-SCF tends to enhance symmetry-breaking distortions (see the computational details section and Figure 3 in reference [332] reported in section §4.4.3), so it is not clear whether these slight departures from higher symmetries are real or artefactual. Therefore, in view of the model character of the present investigation, we decided to use the high symmetry groups in this study.

4.3 Calculations and computational procedures

4.3.1 Electronic states computed

In the calculations performed on Spiro, only the valence "π" orbitals of the cation were given attention, since these orbitals are responsible for the intramolecular charge transfer process in the Spiro mixed-valence molecular system. It should be also reminded that the electronic states computed for Spiro at every point on the reaction coordinate are that of C_{2v} point group.

The electronic, or spectroscopic, states that are considered along all or some points on the reaction path of intramolecular charge transfer in Spiro are: two state-averaged $^2A_2$, which will be denoted as 1^2A_2 and 2^2A_2 in the the following; one $^2B_1$; and one $^2B_2$ state. Indeed, all our CAS-SCF calculations were performed by averaging the two lowest $^2A_2$ electronic states with equal weight, since if only one electronic state is optimized, a CAS-SCF instability [333] appears (see Figure 3 in the article published on Spiro [332] and reported in section §4.4.3)), and the energy surface is discontinuous at the crossing seam (D_{2d}) point geometry.

No $^2A_1$ electronic state was considered in this study since $^2A_1$ state does not exist in the π orbitals set as the π orbitals do not transform as the irreducible representation A_1.

4.3.2 Basis sets used

Four contraction schemes of basis sets of Atomic Natural Orbitals (ANO) type [207] were used: SZ ((1s) for each H and (2s1p) for each C and N), DZ ((2s) for each H and (3s2p) for each C and N), DZP ((2s1p) for each H and (3s2p1d) for each C and N) and TZP ((3s1p) for each H and (4s3p1d) for each C and N).

The number of contracted orbitals of the minimal basis set (SZ) is 89, while that of the largest basis set used (TZP) is 354 orbitals. The number of contracted orbitals of DZ and DZP basis sets are 163 and 280 respectively.

4.3.3 Geometry optimization

Geometry optimization of the neutral Spiro molecule, were calculated using Restricted Open shell Hartree Fock (ROHF) with TZP basis set. The same method and basis set were used to optimize the geometry of the $^2A_2$ electronic state of the cation at both C_{2v}

and D_{2d} geometries. The geometry of the Spiro di-cation $^3A_1$ was also optimized at this level. Some of these optimized geometries were used to calculate the reaction coordinate of the intramolecular charge transfer process in Spiro. The details of these calculations are discussed in section §4.4.3.

4.3.4 The reaction coordinates

The details of producing the reaction coordinates of the intramolecular charge transfer in Spiro are found in the subsection entitled "reaction coordinates" in the article shown in section §4.4.3. Here, only the notation necessary to follow the discussion below is mentioned. The reaction coordinate was obtained by mixing linearly the optimized coordinates of the two equilibrium C_{2v} geometries by using the equation (see also section 3.5:

$$Q(\xi) = \left(\frac{1}{2} - \xi\right) Q_A + \left(\frac{1}{2} + \xi\right) Q_B \tag{4.1}$$

where $Q(\xi)$ is the nuclear configuration at the point ξ on the reaction path, while Q_A and Q_B represent the nuclear coordinates of the two optimized C_{2v} geometries. The mixing parameter ξ was varied from -1.50 to $+1.50$ in steps of 0.05. In such a way, Q_A is the geometry of the first C_{2v} minimum, this geometry corresponds to the point $\xi = -0.50$, where the positive charge is localized on one moiety of the molecule. Q_B is the geometry of second C_{2v} minimum, which will, this geometry corresponds to the point $\xi = +0.50$, where the positive charge is localized on the other moiety of the molecule. The internal coordinates of Spiro cation at the crossing seam, which has a D_{2d} symmetry, are calculated as the average of the two C_{2v} internal coordinates, and it is obtained at the crossing seam point $\xi = 0.00$. The Born-Oppenheimer potential energy surfaces were obtained by calculating the energies of 1^2A_2, 2^2A_2, $^2B_1$ and $^2B_2$ electronic states at each step value of the parameter ξ.

4.3.5 The choice of the active space

Given the Spiro electronic configuration of the π valence orbitals as presented in the previous section §4.2, it would be reasonable to choose our minimal active space of Spiro to include the two, near degenerate, HOMO ($1a_2$) and HOMO-1 ($1a_2$) orbitals in addition to the two degenerate $2b_1$ and $2b_2$ orbitals, which are close in energy to that of the HOMO

and HOMO-1 orbitals, see Figure 4.2 and Table 4.1. For a monocation Spiro, this active space is designated as CAS(7/4), i.e., 7 active electrons in 4 active orbitals. In order to improve the description of the Spiro valence π orbitals, and to see the effect of including more valence π orbitals in the active space on the results of the spectroscopic states and the different mixed-valence ET parameters, two other larger active spaces were also used in computing CASSCF, and other MRCI methods, using canonical and localized orbitals. One is CAS(11/10) active space, which include all the 6 valence π orbitals and the lowest four virtual π orbitals shown in Figure 4.2, that is: $(1b_1)^2$ $(1b_2)^2$ $(2b_1)^2$ $(2b_2)^2$ $(1a_2)^2$ $(2a_2)^1$ $(3b_1)^0$ $(3b_2)^0$ $(3a_2)^0$ $(4a_2)^0$. The other active space used in this study is CAS(7/8) which excludes the lowest two occupied valence π orbitals, namely $(1b_1)^2$ and $(1b_2)^2$ from the CAS(11/10) active space. Hence, the orbitals included in the latter CAS(7/8) active space are: $(2b_1)^2$ $(2b_2)^2$ $(1a_2)^2$ $(2a_2)^1$ $(3b_1)^0$ $(3b_2)^0$ $(3a_2)^0$ $(4a_2)^0$, which corresponds to the valence π system of the eight carbon atoms located on the two external pyrrole cycles.

The exclusion of $(1b_1)^2$ and $(1b_2)^2$ orbitals, which corresponds to the two nitrogen atoms valence π orbitals, from the complete valence π system in CAS(7/8) is justified by the fact that C_6-N distance, see Figure 4.1 for atom numbering of Spiro, has a small dependence on the reaction path during an intramolecular charge transfer compared to the significant change of C_4-C_5 and C_4-C_6 bond distances during such a process (for more details on this point, see Table 2 and Figure 5 in the article published on Spiro [332] and reported in section §4.4.3).

4.3.6 Methods of calculations used

In this subsection, the calculations performed on Spiro are mentioned together with their corresponding notation used. The methods of calculations performed on Spiro are: CAS-SCF, denoted as CAS; CAS-CI, denoted as CAS_{guess}; single excitation CI on CAS-SCF reference wave function, denoted as CAS+S; and single and double excitations CI on CAS-SCF reference wave function, denoted as CAS+SD. Two techniques of CAS+SD were used: contracted CAS+SD [159,160], denoted as C-CAS+SD; and uncontracted CAS+SD, which keeps the same notation without any prefix. In the following, and when it is appropriate, any of these calculation methods used will be denoted as X. Two types of guess orbitals were used in performing any of the above mentioned calculation methods X: canonical orbitals, labeled with the subscript X_{can}; and localized orbitals, of *a priori* type, labeled

with the subscript X_{loc}. Localized orbitals were not used for C-CAS+SD calculations. In addition, CAS-CI (CAS_{guess}) calculations were only performed by using localized orbitals. Finally, If all the σ orbitals were kept frozen during an orbital optimization, a subscript X_{frz} is added.

Its worthwhile to mention that, due to hardware limitations, some calculations were not feasible. For instance, CAS+SD were not calculated using the smallest active space CAS(7/4) with DZP and TZP basis sets, and the two largest active spaces CAS(7/8) and CAS(11/10) with any basis set. The less demanding CAS+S calculations were carried out using the active space CAS(7/4) with the four basis set, CAS(7/8) active space with SZ and DZ basis sets, and CAS(11/10) active space with only the minimal SZ basis set contraction.

4.4 Results of the theoretical modeling and calculations on Spiro

4.4.1 Introduction

In this section, the results of the calculations done on Spiro are presented and discussed. A published article on Spiro is reported in subsection §4.4.3. The unpublished results are then reported and discussed in separate subsections. Many of the unpublished results are tabulated in the Appendix chapter (chapter 8), but are, when necessary, commented and discussed in the present chapter.

4.4.2 A preliminary publication on Spiro

An introductory article that report the preliminary results of the calculations performed on Spiro was published in "Lecture Notes in Computational Sciences" in 2006 [334]. In this article, the notation used is somewhat different from that explained above and presented elsewhere in this chapter. Moreover, the results presented in this paper are included in the far comprehensive publication reported in the next subsection. For these reasons, this publication, entitled "Ab-Initio Multi-reference Study of a Bistable Spiro Molecule", is reported in section §8.1 in the appendix.

4.4.3 Results of CAS(7/4) active space using SZ and DZ basis sets

The following article was published in 2008 in the "Journal of Computational Chemistry" [332]. This article will be named "article I" in the following. In this publication, the results of CAS-SCF, CAS+S, CAS+SD, and C-CAS+SD calculations, using both canonical and localized orbitals, are reported (only canonical orbitals were used for C-CAS+SD). These levels of theory were used to compute, numerically, ET characteristics and the energetics of the spectroscopic electronic states through the intramolecular charge transfer reaction coordinate. In particular, two points in the reaction coordinate were given a special attention: the equilibrium point, or minimum, having C_{2v} point group geometry; and the D_{2d} transition state, or saddle point. In this contribution, only the results of the calculations using the smallest active space (CAS(7/4)), with SZ and DZ basis sets were reported. This particular active space and these two basis sets were chosen to be presented since, as mentioned above, CAS+SD$_{can}$, CAS+SD$_{loc}$, and C-CAS+SD$_{can}$ were only feasible using CAS(7/4) active space with the two smallest basis sets. In this article, the aim was the possibility to compare CAS+SD$_{can}$ and, to a more extent, CAS+SD$_{loc}$ with the well-established C-CAS+SD method. The same comparison was also made at CAS-SCF and CAS+S levels to see the effect of, both, using canonical orbitals, on one hand; and the dynamical correlation, on the other hand.

The article also presented and discussed the theoretical model used to produce the reaction coordinates and the PES curves of the low-lying adiabatic electronic states. Moreover, the geometry changes, i.e., the bond length changes, of the particular bonds of Spiro were followed during ET reaction coordinate and the results were discussed.

Ab-initio Multireference Study of an Organic Mixed-Valence Spiro Molecular System

WISSAM HELAL, STEFANO EVANGELISTI, THIERRY LEININGER, DANIEL MAYNAU
Laboratoire de Chimie et Physique Quantiques, Université de Toulouse et CNRS, 118, Route de Narbonne, F-31062 Toulouse Cedex, France

Received 5 June 2007; Accepted 11 February 2008
DOI 10.1002/jcc.20982
Published online 30 May 2008 in Wiley InterScience (www.interscience.wiley.com).

Abstract: The electronic structure and some electron transfer properties of a model mixed-valence Spiro molecular cation have been investigated at CAS-SCF, CAS+S, and CAS+SD levels starting from canonical and localized orbitals, using SZ, DZ, and TZP basis sets. The potential energy surfaces of the adiabatic ground and the lowest three excited electronic states have been computed, within a two-state model, and a double-well potential has been obtained for the ground electronic state. We have demonstrated the low coupling interaction between the two redox moieties of this molecular cation by following the charge localization/delocalization in the valence π system through the reaction coordinate of the intramolecular charge transfer. The effect of dynamical correlation, using either localized or canonical orbitals, was found to be crucial for a quantitative description of the electronic structure and some important electron transfer parameters of this mixed-valence system.

 J Comput Chem 30: 83–92, 2009

Key words: spiro; nondynamical correlation; CAS-SCF; CAS+S; CAS+SD; localization; organic mixed-valence systems

Introduction

Mixed-valence compounds are characterized by inter-valence charge transfer (CT) between two or more redox sites existing in different oxidation states. These systems are classified, according to Robin and Day,[1] into three classes: class I, the redox centers are completely localized and behave as separate entities, class II, the system is partially delocalized due to the intermediate coupling between the mixed-valence centers, and class III, where the system is completely delocalized due to a strong coupling between the redox centers and thus a single minimum is observed for the electronic ground state. Mixed-valence compounds have been widely studied in recent times, particularly for their interest in molecular electronics.[2–7] These molecules are also important for the fundamental study of the electron transfer process.[8–12]

Although many of the considered systems contain transition-metal atoms as mixed-valence centers,[9–11,13–17] purely organic compounds have also been investigated theoretically.[18–28] Among these types of molecules, the spiro π-σ-π system 5,5′(4H,4H′)-spirobi[cyclopenta[c]pyrrole]2,2′,6,6′tetrahydro cation (the "Spiro" molecule in the following), shown in Figure 1, has been often studied as a model system,[2,20,29,30] since its relatively small size, permits high-level *ab initio* investigations.

In this contribution, we present the results of Complete Active Space Self-Consistent Field (CAS-SCF), and subsequent multi-configurational wavefunctions corrected with single excitation (CAS+S) and single and double excitations (CAS+SD) using both canonical and localized orbitals for the CAS space calculations on the Spiro molecular cation. To assess the validity of an internally contracted Multi-Reference Configuration Interaction (MRCI) approach,[31] uncontracted MRCI calculations were also performed. It is shown that the contribution of the nondynamical correlation is crucial in order to obtain reliable quantitative results.

In the following Section the Spiro molecule is described. Then we briefly review the localization method used in this study. After a computational details Section, the geometry of the Spiro molecule and the reaction coordinate are discussed in a separate Section. We then report and analyze the results of the calculations in the "results and discussions" Section showing the usefulness of the localization methods at CAS+SD level when applied to mixed-valence systems,

Correspondence to: W. Helal; e-mail: helal@irsamc.ups-tlse.fr

Contract/grant sponsors: Centre National de la Recherche Scientifique (CNRS); Paul Sabatier University of Toulouse; European Community (Cost in Chemistry–D37).

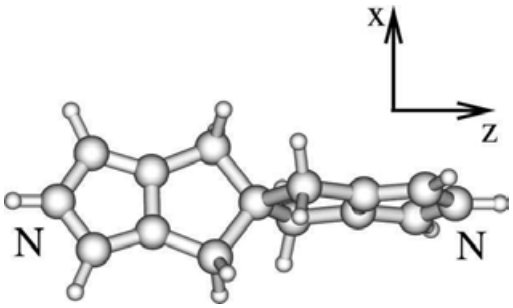

Figure 1. The spiro π-σ-π system 5,5′(4H,4H′)-spirobi[cyclopenta[c]-pyrrole]2,2′,6,6′tetrahydro molecule.

the issue of the nature of the active space is also addressed in this Section. In the last Section we draw some conclusions and point out some perspectives for future work.

The Spiro Molecule

The geometry of the Spiro molecular system, which is the object of the present study, is shown in Figure 1. The system consists of two equivalent π moieties, lying onto two orthogonal planes, and separated by a σ bridge. If an electron is extracted from this molecule, the resulting hole tends to localize either on the left or the right π system, inducing a deformation of the molecular geometry. Therefore two equivalent minima exist for the cation, and the ground state presents the double-well surface which is typical for mixed-valence systems of class II. A classical two-state model[32–35] is adopted in this study for the intramolecular charge transfer between the two moieties in the Spiro cation. It is important to mention that a three-state model for the general case of mixed valence systems is more adequate than the simplified two-state model in some cases,[36,37] the justification of using such a simplified two-state model is discussed in the subsection on the reaction coordinate.

The ideal symmetry of the neutral system is D_{2d}, where the principal axis of rotation, the C_2 axis, is the z-axis that passes through the two nitrogen atoms, see Figure 1. The ground electronic state geometry of the distorted cation shows two equivalent minima having a lower symmetry, C_{2v}. The two minima are separated by a saddle point at the crossing seam with a symmetric D_{2d} geometry. The σ/π separation is an approximated one, since σ and π orbitals belong to the same irreducible representations in both D_{2d} and C_{2v}. In Figure 2, the ten valence "π" orbitals for the symmetric D_{2d} neutral Spiro are shown together with their symmetry assignments (notice that the symmetries reported in Figure 2 and the rest of this article are those of the C_{2v} point group, see Table 1).

The orbitals have been obtained at SCF level and by using a minimal basis set. The neutral "π" system contains twelve electrons, so the six lowest orbitals are occupied, while the remaining four are empty. The Highest Occupied Molecular Orbital (HOMO) of the system is the $2a_2$ orbital (only the "π" orbitals are considered here). By removing an electron from the HOMO, the ground state of the cation is obtained, which is therefore the $^2A_2$ state. Since the HOMO-1 $1a_2$ orbital is very close in energy to that of $2a_2$ orbital, one can

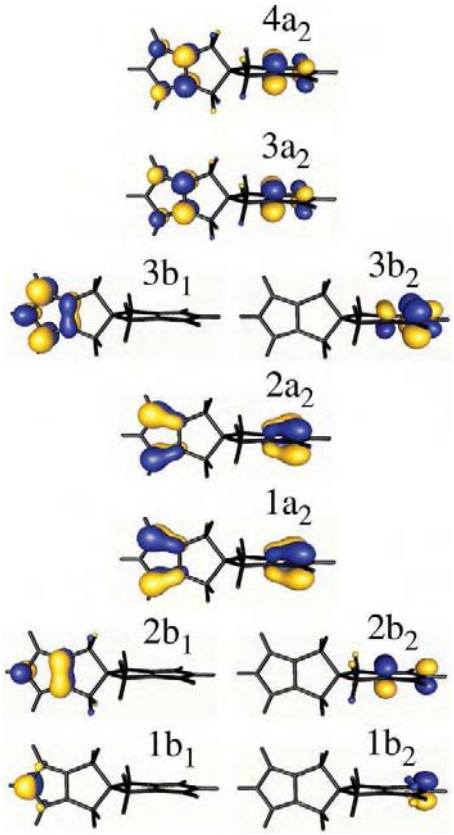

Figure 2. Valence "π" molecular orbitals of the neutral Spiro molecule computed at RHF-SCF/SZ for D_{2d} geometry using C_{2v} irreducible representations. See Table 1.

expect a strong participation of this orbital to the low-lying states of the cation. Two more orbitals play an important role in the low-energy spectrum: these are the two degenerated $2b_1$ and $2b_2$ orbitals

Table 1. The Designation of the Valence "π" MO's of the Spiro Neutral Molecule Shown in Figure 2 for the D_{2d} Geometry Using C_{2v} Irreducible Representations and the Corresponding MO's in D_{2d} Symmetry Together with Their Orbital Energies (in a.u.).

MO number	C_{2v} sym.		D_{2d} sym.	Orbital energy
1,2	$1b_1$	$1b_2$	$1e$	−0.6456
3,4	$2b_1$	$2b_2$	$2e$	−0.4221
5	$1a_2$		$1b_1$	−0.3990
6	$2a_2$		$1a_2$	−0.3947
7,8	$3b_1$	$3b_2$	$3e$	+0.1280
9	$3a_2$		$2b_1$	+0.2128
10	$4a_2$		$2a_2$	+0.2179

Orbitals 1 to 6 are doubly occupied, while orbitals 7–10 are empty.

(they actually belong to the degenerated E irreducible representation of D_{2d}, see Table 1). For this reason, our CAS calculations have been performed by using this four-orbital active space (see also the sections on computational details and results and discussion).

In Table 1, the orbitals are classified accordingly to both D_{2d} and C_{2v} groups. It can be seen that the degenerated e orbitals in the D_{2d} group correspond to a pair b_1-b_2 in C_{2v}. In a similar way, the a_2 orbitals in C_{2v} are classified either b_1 or a_2 in D_{2d}. For this reason, the two lowest states of the cation have different symmetry in D_{2d}: the lowest one has A_2 symmetry, while the first excited state has B_1 symmetry (while they are both A_2 in C_{2v}). In D_{2d}, the reaction coordinate has the same symmetry as the z axes, hence B_2. Since in this group $B_1 \otimes B_2 = A_2$, the two lowest states are indeed mixed by an antisymmetric deformation of the coordinates in the z direction.

In some previous reports, the Spiro cation was studied in the C_{2v} point group, if the charge is localized on either one of the two aromatic moieties in the molecule, while a D_{2d} geometry was taken for the totally delocalized state.[2,30] Other recent studies at CAS-SCF level, suggested C_2 and C_1 point groups for the two situations, respectively.[20] However, according to these calculations, the difference from exact C_{2v} and D_{2d} symmetries are extremely small. Moreover, CAS-SCF tends to enhance symmetry-breaking distortions (see the computational details section), so it is not clear whether these slight departures from higher symmetries are real or artifactual. Therefore, in view of the model character of the present investigation, we decided to use the high symmetry groups in this study.

Localized Multireference Method

Locality is not reflected in standard electronic structure calculations. However, Fock observed that a one determinant many-electron wave function is invariant with respect to unitary transformations among its molecular orbitals.[38] On the basis of this observation, many authors pointed out the interest of using localized molecular orbitals.[39–41] One of the most important advantages of using localized molecular orbitals is their use in linear scaling procedures.[42] The existing linear scaling methods have been successfully applied to different levels of theory that use single-reference determinants.[42–45] However, many important chemical processes and systems, like chemical bond breaking and formation, transition states, electronically excited states, magnetic systems, and mixed-valence systems, are degenerate or quasi-degenerate in nature. Only multireference methods, that recover the nondynamical correlation energy, could treat successfully quasi-degenerate systems. Unfortunately, linear scaling for nondynamical correlation is an open problem, but it should be noticed that orbital localization is a necessary condition toward linear scaling multi-reference electronic structure calculations.

Recently, a formalism for obtaining *a priori* local orbitals of CAS-SCF type was developed by our group.[46–50] *A priori*, in this context, means that the final localized orbitals are directly obtained and optimized from guess localized orbitals.[51,52] On the other hand, if the localized orbitals were obtained from canonical optimized orbitals, the method is designated as *a posteriori*.[39,40,53] An advantage of using *a priori* localized molecular orbitals is that one can choose, among the large number of possible CAS spaces, the particular set of active orbitals that are relevant for the study of a particular phenomenon.

At the moment, two versions, variational,[47] and perturbative,[48] of the developed algorithm exist. The variational method is briefly described in the following (the method is described in detail in ref. 47). The algorithm consists of a two step procedure: in the first step, a set of orthogonal atomic orbitals is generated through a symmetric orthonormalization of the non-orthogonal atomic orbitals, these orthogonal atomic orbitals are then combined to form a set of guess localized molecular orthogonal orbitals through a hierarchic combination of symmetric and Schmidt orthogonalization, in order to avoid core/valence mixing. The generated localized molecular orthogonal orbitals at the end of the first step can be centered on a bond or an atom (e.g., for lone pairs and core orbitals), they can also be distributed on a molecular fragment. In the second step, the localized orthogonalized molecular orbitals are optimized using a super-CI-like procedure, equivalent to that proposed by Ruedenberg et al..[54] Starting from a CAS-CI wavefunction $|\Psi_{CAS}\rangle$, the CAS+S set of internally contracted single excitations is produced, where the single excitation operators $a_i^+ a_j$ act on the wavefunction $|\Psi_{CAS}\rangle$ as a whole. A new wavefunction in the CAS+S space $|\Psi_{CAS+S}\rangle$ is produced. By diagonalizing the one-body density matrix Γ_1 associated to $|\Psi_{CAS+S}\rangle$, a new set of orbitals is obtained, which can be used to build a new $|\Psi_{CAS}\rangle$ wavefunction. The procedure is iterated until wavefunction invariance is achieved and optimized natural orbitals of CAS-SCF type are obtained through satisfying the generalized Brillouin theorem (GBT).[55] The diagonalization of Γ_1 completely mixes the orbitals within each class and the original locality of the guess orbitals would be lost. Taking advantage of the invariance of the CAS-SCF wavefunction with respect to orbital rotations within each orbital class, a block diagonalization of Γ_1 would minimize the mixing between the orbitals at each iteration. As a result, the orbitals at convergence maintain as far as possible the same nature as the initial guess orbitals.

The new method has been implemented and successfully tested for the ground and the excited states of different organic conjugated systems,[56–59] magnetic metal containing systems,[60,61] fullerenes,[62,63] and other chemical systems.[64–67] Geometry optimization within a localized CAS-SCF approach was also investigated.[68] In our study we have used the variational version to optimize CAS+S and CAS+SD wavefunction starting from localized guess orbitals.

Computational Details

In all our calculations, we were only interested in the valence "π" electrons of the cation, since these are the electrons engaged in the charge transfer process in the Spiro cation mixed-valence system.

We performed CAS-SCF calculations for several geometries along the reaction path (see next section). At CAS-SCF level, if only one electronic state is optimized, a CAS-SCF instability[69] appears (see Fig. 3), and the energy surface is discontinuous at the D_{2d} geometry. Therefore, all our CAS-SCF calculations were performed by averaging the two lowest $^2A_2$ electronic states with equal weight.

Two state-averaged $^2A_2$, which will be designated as 1^2A_2 and 2^2A_2 in the present article, one $^2B_1$ and one $^2B_2$ state were calculated

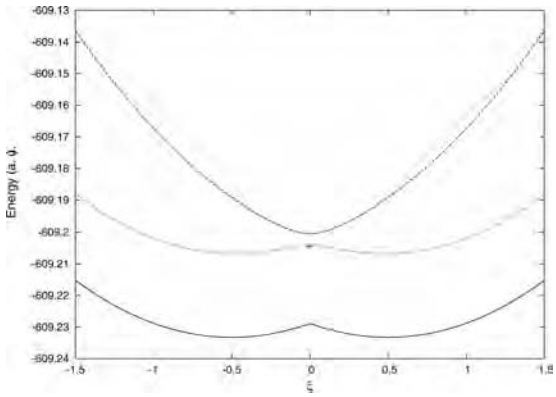

Figure 3. Potential energy surfaces of Spiro cation Showing the CAS-SCF instability of the state-specific $^2A_2$. Energy in a.u. as a function of the mixing parameter ξ at CAS(7/4)/TZP level: State-specific $^2A_2$ (solid curve), two $^2A_2$ state-averaged (1^2A_2 (dots) and 2^2A_2 (dashed curve)), and one point at $\xi = 0.00$ (D_{2d} geometry) computed with RHF/TZP (+).

for the two C_{2v} and D_{2d} geometries. No $^2A_1$ electronic state was considered in this study since $^2A_1$ state does not exist as the π orbitals do not transform as the irreducible representation A_1.

Atomic natural orbitals (ANO-L) basis sets[70] were used in all calculations, by using different contraction levels: SZ ((1s) for H and (2s1p) for C and N), DZ ((2s) for H and (3s2p) for C and N) and TZP ((3s1p) for H and (4s3p1d) for C and N).

Geometry optimization of the neutral Spiro molecule, were calculated using Restricted Open shell Hartree Fock (ROHF) with TZP basis set. The same method and basis set were used to optimize the geometry of the $^2A_2$ electronic state of the cation at both C_{2v} and D_{2d} geometries. The geometry of the Spiro di-cation $^3A_1$ was also optimized at this level. These optimized geometries were used to calculate the reaction coordinate of the charge transfer process in Spiro cation. The details of these calculations are discussed in the next section.

The energies of the electronic states using different levels of Multiconfigurational methods and basis sets were calculated for two points on the reaction coordinate, namely, the C_{2v} geometry at the minimum of the potential energy surface and the D_{2d} geometry at the crossing seam. CAS(7/4), 7 active electrons in four occupied active orbitals ($2b_1$, $2b_2$, $1a_2$, and $2a_2$) were used in the active space.

CAS-SCF, CAS+S, and CAS+SD, using canonical and localized orbitals, denoted by can and loc subscripts respectively in the following, were calculated using SZ and DZ basis set. In the case of CAS+SD$_{can}$ level, both internally contracted[31] and uncontracted MRCI approaches were used, denoted by C-CAS+SD$_{can}$ and CAS+SD$_{can}$ respectively. In all CAS+S and CAS+SD calculations, the 1*s* orbitals of C and N were kept frozen.

The orbital pictures were made with gOpenMol version 2.3.[71] Geometry optimization and single point calculations using RHF-SCF, ROHF, CAS-SCF and C-CAS+SD$_{can}$ were done using the MOLPRO computer code version 2002.6[72] and MOLCAS code version 6.0.[73] Both MOLPRO and MOLCAS codes can only treat Abelian point groups, therefore, since D_{2d} is a non-Abelian group, D_{2d} calculations were performed by using the C_{2v} symmetry, and imposing the D_{2d} symmetry by setting the necessary constraints on the coordinates. CAS$_{loc}$, CAS+S$_{loc}$, CAS+SD$_{loc}$, CAS+S$_{can}$, and CAS+SD$_{can}$ calculations were done using the Toulouse program CASDI.[74]

Geometry and Reaction Coordinate

Reaction Coordinate

The optimized symmetric neutral Spiro system will be denoted as $D_{2d}[AA]$. The optimized symmetric mono-cation, at D_{2d} symmetry in $^2A_2$ state, will be denoted as $D_{2d}[AA]^+_{opt}$, while $D_{2d}[AA]^{+2}$ is the optimized di-cation $^3A_1$ state. On the other hand, we indicate by [*A*] each one of the two moieties of the Spiro cation in the C_{2v} symmetry. In this way, $C_{2v}[A]$ indicates the geometry of the neutral moiety of the cation optimized at C_{2v} symmetry, while $C_{2v}[A^+]$ indicates the charged moiety.

The reaction coordinate, defined as the steepest-descent pathway, in the many-dimensional nuclear coordinate space, connecting the two equivalent minima and passing through the saddle point (the transition state) on the crossing seam surface,[75] cannot be obtained at MRCI level with our algorithm. We replaced the exact reaction path by an approximated one, in which the geometries are obtained by averaging the geometries of two points on the reaction coordinate. An averaged geometry can be obtained by two different methods:

1. mixing linearly the optimized C_{2v} geometry with the optimized D_{2d} geometry at the crossing seam;
2. mixing linearly the geometries of the two optimized C_{2v} minima.

The first choice would produce a D_{2d} structure in which the first derivative of energy, $dE/d\xi$, is non zero. The second choice seems to be preferable, since it produces a smooth curve on the whole ξ range, including the crossing seam at $\xi = 0.00$. Another advantage of mixing the two optimized C_{2v} geometries is the possibility to test the D_{2d} point on the reaction coordinate with respect to the truly optimized D_{2d} for the cation. For these two reasons, we have chosen the second method. Using such a method is justified in the framework of the two-state model used in this study.

Therefore, the reaction coordinate was obtained by mixing linearly the optimized coordinates of the two equilibrium C_{2v} geometries:

$$Q(\xi) = \left(\frac{1}{2} - \xi\right) Q_A + \left(\frac{1}{2} + \xi\right) Q_B \qquad (1)$$

where $Q(\xi)$ is the nuclear configuration at the point ξ on the reaction path, while Q_A and Q_B represent the nuclear coordinates of the two optimized C_{2v} geometries. The mixing parameter ξ was varied from -1.50 to $+1.50$ in steps of 0.05. In such a way, Q_A is the geometry of the first C_{2v} minimum, which will be denoted $C_{2v}[A^+]$, this geometry corresponding to the point $\xi = -0.50$, where the positive charge is localized on one moiety of the molecule. Q_B is the geometry of second C_{2v} minimum, which will be denoted $C_{2v}[A]$, this geometry corresponding to the point $\xi = +0.50$, where the positive charge is localized on the other moiety of the molecule.

Table 2. Bond Lengths, in Å, of the Spiro Molecule Calculated at the CAS(7/4)/TZP Level for Six Different Moieties: Two C_{2v} Geometries; $C_{2v}[A^+]$ ($\xi = -0.50$) and $C_{2v}[A]$ ($\xi = +0.50$) an Four D_{2d} Geometries ($\xi = 0.00$); the Dication $D_{2d}[AA]^{+2}$ Triplet, the Neutral $D_{2d}[AA]$, the Averaged $D_{2d}[AA]^{+}_{avr}$ and the Optimized $D_{2d}[AA]^{+}_{opt}$.

	Bond length					
Bond	$C_{2v}[A^+]$	$C_{2v}[A]$	$D_{2d}[AA]^{+2}$	$D_{2d}[AA]$	$D_{2d}[AA]^{+}_{avr}$	$D_{2d}[AA]^{+}_{opt}$
C_1–C_2	1.579	1.581	1.582	1.580	1.580	1.578
C_2–C_4	1.495	1.497	1.496	1.499	1.496	1.493
C_2–H_9	1.083	1.084	1.083	1.084	1.083	1.084
C_4–C_5	1.355	1.409	1.351	1.411	1.382	1.382
C_4–C_6	1.416	1.357	1.420	1.357	1.387	1.385
C_6–N_8	1.352	1.365	1.349	1.369	1.359	1.360
C_6–H_{13}	1.070	1.068	1.070	1.068	1.069	1.068
N_8–H_{15}	0.995	0.991	0.989	0.989	0.993	0.992

The internal coordinates of Spiro cation at the crossing seam, which has a D_{2d} symmetry, is calculated as the average of the two C_{2v} internal coordinates, $C_{2v}[A^+]$ and $C_{2v}[A]$. This averaged geometry will be denoted as $D_{2d}[AA]^{+}_{avr}$, and it is obtained at the crossing seam point $\xi = 0.00$. The Born-Oppenheimer potential energy surfaces were obtained by calculating the energies of 1^2A_2, 2^2A_2, $^2B_1$, and $^2B_2$ electronic states at each step value of the parameter ξ, using CAS_{can} and C-CAS+SD_{can} both with TZP basis.

To test the quality of the averaged D_{2d} geometry, the electronic state energies of the latter were compared with the corresponding state energies of the optimized D_{2d} geometry. The results show a very small difference between the averaged and the optimized D_{2d} geometries (see next section). In addition, a comparison of the corresponding bond lengths of the Spiro cation at the averaged and optimized D_{2d} geometries also shows an extremely small difference between the two structures (see next subsection). For these reasons, we believe that the geometry path obtained through eq. (1) is very close to the optimal one.

Spiro Geometry

The bond lengths of Spiro in different geometries computed at CAS(7/4)/TZP level are shown in Table 2 (See Fig. 4 for the atomic numbering). It can bee seen that the geometries of the averaged $D_{2d}[AA]^{+}_{avr}$ molecular cation, obtained using eq. (1) is very close to that of the optimized, $D_{2d}[AA]^{+}_{opt}$. Differences between the corresponding bond lengths of the two geometries are extremely small: 3×10^{-3} Å at most.

A closer look at Table 2 also reveals that the geometry of the moiety of the Spiro cation holding the charge, $C_{2v}[A^+]$, is very close to that of the Spiro di-cation, $C_{2v}[AA]^{+2}$. On the other hand, the geometry of the neutral moiety of the Spiro cation $C_{2v}[A]$, is very close to the geometry of the neutral Spiro $C_{2v}[AA]$. This confirms that the charge, in the case of a C_{2v} minima, is localized in one moiety of the molecule ground stater. This could lead to the conclusion that our model system is a low interacting system between the two redox nonadiabatic states of the molecule which means that the Spiro cation is a valence trapped class II mixed-valence system.

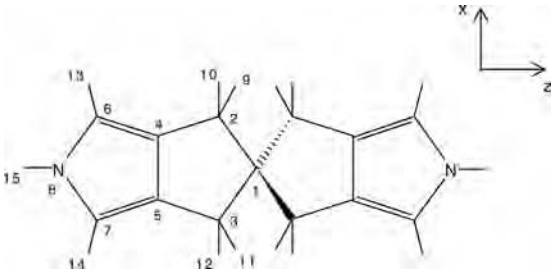

Figure 4. The Spiro molecule atomic numbering.

Although there are some bonds that are almost unchanged with respect to the reaction coordinate during a charge transfer process, the pyrrole unit bonds of the Spiro cation are very sensitive for such a process. In particular, C_4–C_5 bond length increases significantly while C_4–C_6 bond is reduced during a CT process, this is clearly seen in Figure 5, where the bond lengths of the Spiro cation are plotted against the reaction coordinate parameter ξ. We also observed, see Table 2 and Figure 5, that C_6–N_8 bond is less affected than C_4–C_5 and C_4–C_6 with respect to CT reaction, and this could be explained by the fact that a CT on the ground state involves the a_2 orbitals which have a node on the two nitrogen atoms.

Results and Discussion

Figure 6 shows the potential energy surfaces of the ground and the next lower three excited electronic states of the Spiro cation computed with CAS_{can}/TZP (Fig. 6 top) and C-CAS+SD_{can}/TZP (Fig. 6 bottom). A continuous adiabatic double-well surface was obtained for the ground electronic state, while a parabolic adiabatic surface was obtained for the first excited state. These two lower

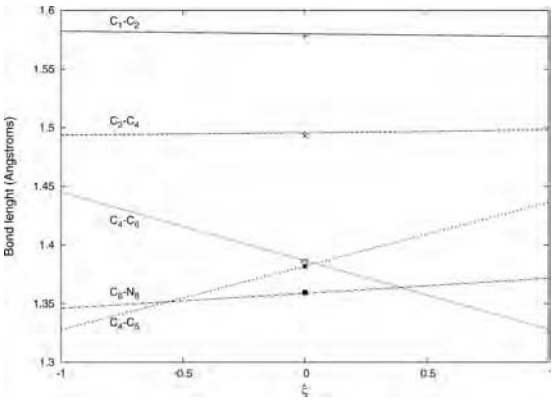

Figure 5. Bond lengths of Spiro cation, in Å, as a function of the mixing parameter ξ. Where the point $\xi = -0.50$ corresponds to the geometry distances of $C_{2v}[A^+]$, $\xi = 0.50$ to the geometry distances of $C_{2v}[A]$, and $\xi = 0.00$ to the geometry distances of $D_{2d}[AA]^{+}_{avr}$. The isolated points are the corresponding bond lengths of the optimized $D_{2d}[AA]^{+}_{opt}$ geometry.

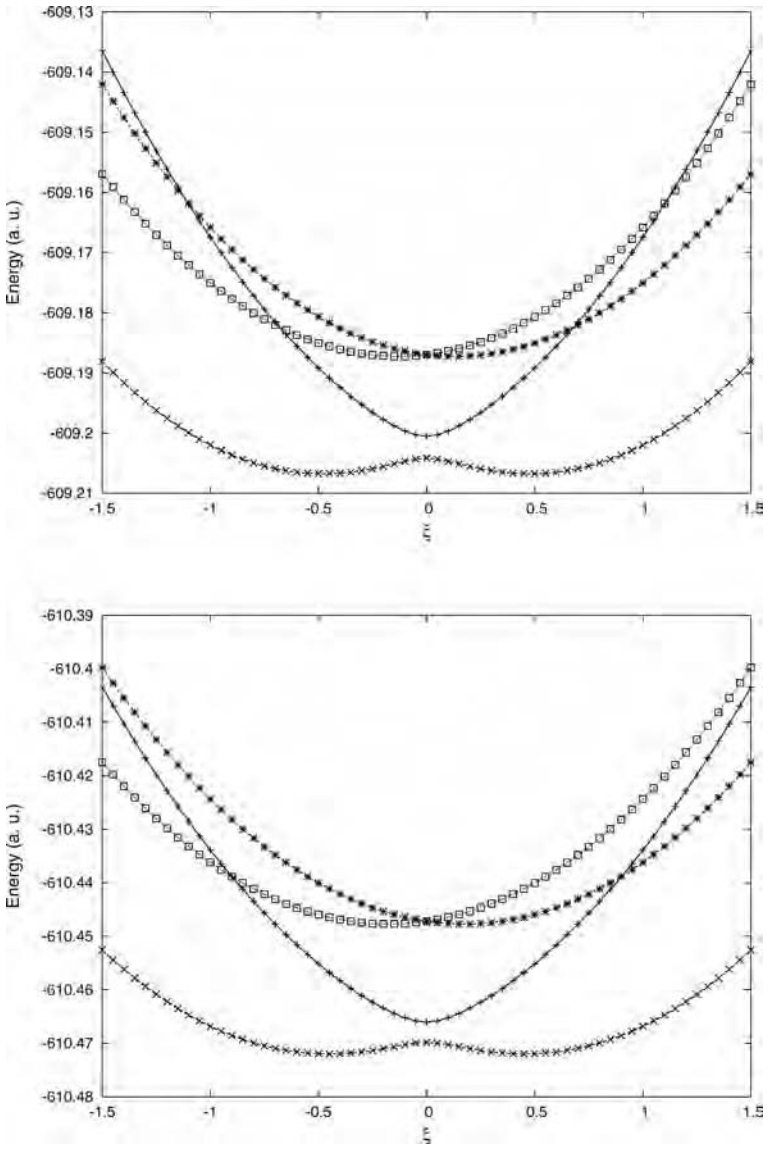

Figure 6. Potential energy surfaces of Spiro cation for the ground and the lower three excited states. Energy in a.u. as a function of the mixing parameter ξ: CAS(7/4)$_{can}$/TZP (top), C-CAS+SD(SD)$_{can}$/TZP (bottom). 1^2A_2 (×), 2^2A_2 (+), $^2B_1$ (∗), and $^2B_2$ (□).

states have an $^2A_2$ symmetry and correspond actually to the state-averaged $^2A_2$ (1^2A_2 and 2^2A_2 respectively). The second and third excited states are degenerate at the D_{2d} geometry ($\xi = 0.00$) and correspond to the $^2B_1$ and $^2B_2$ symmetries. The global behavior of CAS-SCF and C-CAS+SD is similar, although the well depth is lower at C-CAS+SD level. On the other hand, the energy of the excited states of *B* symmetry tends to be higher at C-CAS+SD level.

The absolute energies and energy differences between the different electronic states at both D_{2d} geometry ($\xi = 0.00$) and C_{2v} geometry ($\xi = 0.50$) with CAS(7/4) computed by using different methods are reported in Tables 3 and 4 using SZ basis set and Tables 5 and 6 using DZ basis set. For each method, in Tables 4 and 6, the reference energy has been taken as the energy of the ground state 1^2A_2 at the point $\xi = 0.00$, (D_{2d} geometry). In such a way, the

Table 3. Energy (a.u.) of the Different States of Spiro Cation, at D_{2d} Geometry ($\xi = 0.00$) and C_{2v} Geometry ($\xi = 0.50$), for Different Methods Using SZ Basis Set and CAS(7/4): CAS-SCF, CAS+S_{can}, C-CAS+SD_{can}, CAS_{loc}, CAS+S_{loc}, and CAS+SD_{loc}.

Geometry	State	CAS_{can}	CAS+S_{can}	CAS+SD_{can}	C-CAS+SD_{can}	CAS_{loc}	CAS+S_{loc}	CAS+SD_{loc}
D_{2d}	1^2A_2	−607.818761	−607.867010	−608.497404	−608.393342	−607.818309	−607.869516	−608.497676
	2^2A_2	−607.815317	−607.863868	−608.493882	−608.389791	−607.814868	−607.866445	−608.494212
	$^2B_1$	−607.801717	−607.832468	−608.477641	−608.372785	−607.800878	−607.836126	−608.477425
	$^2B_2$	−607.801717	−607.832468	−608.477641	−608.372785	−607.800878	−607.836126	−608.477425
C_{2v}	1^2A_2	−607.821933	−607.868712	−608.499870	−608.395887	−607.821582	−607.871438	−608.500290
	2^2A_2	−607.800341	−607.848894	−608.479379	−608.375411	−607.799783	−607.852817	−608.479630
	$^2B_1$	−607.798706	−607.831784	−608.475244	−608.370591	−607.797982	−607.837476	−608.474939
	$^2B_2$	−607.793353	−607.821732	−608.468252	−608.363373	−607.792019	−607.825980	−608.467912

Table 4. Energy (kJ/mol) of the Different States of Spiro Cation, at D_{2d} Geometry ($\xi = 0.00$) and C_{2v} Geometry ($\xi = 0.50$), for Different Methods Using SZ Basis Set and CAS(7/4): CAS-SCF, CAS+S_{can}, C-CAS+SD_{can}, CAS_{loc}, CAS+S_{loc}, and CAS+SD_{loc}.

Geometry	State	CAS_{can}	CAS+S_{can}	CAS+SD_{can}	C-CAS+SD_{can}	CAS_{loc}	CAS+S_{loc}	CAS+SD_{loc}
D_{2d}	1^2A_2	0.000	0.000	0.000	0.000	0.000	0.000	0.000
	2^2A_2	9.043	8.249	9.246	9.323	9.035	8.063	9.096
	$^2B_1$	44.748	90.691	51.888	53.972	45.766	87.666	53.170
	$^2B_2$	44.748	90.691	51.888	53.972	45.766	87.666	53.170
C_{2v}	1^2A_2	−8.328	−4.468	−6.476	−6.684	−8.593	−5.048	−6.862
	2^2A_2	48.362	47.563	47.325	47.076	48.638	43.842	47.380
	$^2B_1$	52.655	92.485	58.181	59.732	53.369	84.120	59.698
	$^2B_2$	66.710	118.879	76.537	78.682	69.024	114.303	78.146

For each method, the reference energy has been taken as the energy of the ground state 1^2A_2 in the D_{2d} geometry.

Table 5. Energy (a.u.) of the Different States of Spiro Cation, at D_{2d} Geometry ($\xi = 0.00$) and C_{2v} Geometry ($\xi = 0.50$), for Different Methods Using DZ Basis Set and CAS(7/4): CAS-SCF, CAS+S_{can}, C-CAS+SD_{can}, CAS_{loc}, CAS+S_{loc}, and CAS+SD_{loc}.

Geometry	State	CAS_{can}	CAS+S_{can}	CAS+SD_{can}	C-CAS+SD_{can}	CAS_{loc}	CAS+S_{loc}	CAS+SD_{loc}
D_{2d}	1^2A_2	−608.847468	−608.903594	−609.831554	−609.677281	−608.846770	−608.908804	−609.831383
	2^2A_2	−608.843664	−608.900125	−609.827674	−609.673361	−608.842997	−608.905484	−609.827600
	$^2B_1$	−608.827797	−608.861137	−609.808242	−609.653514	−608.826895	−608.864884	−609.808070
	$^2B_2$	−608.827797	−608.861137	−609.808242	−609.653514	−608.826895	−608.864884	−609.808070
C_{2v}	1^2A_2	−608.849617	−608.904694	−609.833234	−609.679059	−608.849094	−608.910002	−609.831383
	2^2A_2	−608.832163	−608.888706	−609.816527	−609.662305	−608.831314	−608.895001	−609.827600
	$^2B_1$	−608.825787	−608.861247	−609.806799	−609.652346	−608.825116	−608.864240	−609.806682
	$^2B_2$	−608.820946	−608.852125	−609.800532	−609.645710	−608.819818	−608.856267	−609.800375

Table 6. Energy (kJ/mol) of the Different States of Spiro Cation, at D_{2d} Geometry ($\xi = 0.00$) and C_{2v} Geometry ($\xi = 0.50$), for Different Methods Using DZ Basis Set and CAS(7/4): CAS-SCF, CAS+S_{can}, C-CAS+SD_{can}, CAS_{loc}, CAS+S_{loc}, and CAS+SD_{loc}.

Geometry	State	CAS_{can}	CAS+S_{can}	CAS+SD_{can}	C-CAS+SD_{can}	CAS_{loc}	CAS+S_{loc}	CAS+SD_{loc}
D_{2d}	1^2A_2	0.000	0.000	0.000	0.000	0.000	0.000	0.000
	2^2A_2	9.987	9.108	10.187	10.290	9.908	8.717	9.933
	$^2B_1$	51.646	111.473	61.207	62.400	52.182	115.312	61.209
	$^2B_2$	51.646	111.473	61.207	62.400	52.182	115.312	61.209
C_{2v}	1^2A_2	−5.640	−2.887	−4.410	−4.669	−6.102	−3.148	−4.914
	2^2A_2	40.185	39.091	39.455	39.319	40.581	36.239	39.546
	$^2B_1$	56.923	111.184	64.995	65.467	56.854	117.002	63.289
	$^2B_2$	69.636	135.134	81.448	82.888	70.764	137.934	79.849

For each method, the reference energy has been taken as the energy of the ground state 1^2A_2 in the D_{2d} geometry.

Table 7. Energy Differences (kJ/mol) Between the States of Spiro Cation, Computed at the Optimized D_{2d} Geometry and the Energy of the Ground State 1^2A_2 in the Averaged D_{2d} Geometry Using CAS(7/4)/TZP.

State	D_{2d}(opt)	D_{2d}(opt) - D_{2d}(avr)
1^2A_2	−0.112	−0.112
2^2A_2	9.697	0.071
$^2B_1$	44.378	−0.803
$^2B_2$	44.378	−0.803

The third column in the table shows the energy differences (kJ/mol) of the corresponding states between the optimized and the averaged D_{2d} geometries.

energy values of 2^2A_2 electronic state at D_{2d} geometry represent $2V_{ab}$, which is defined as the splitting between the adiabatic potential energy surfaces at the crossing seam in a two-state model, where V_{ab} is the electronic coupling matrix element. The energy values of 2^2A_2 electronic state at C_{2v} geometry represent the ET barrier.

In Table 7 the difference between the electronic state energies of the averaged and optimized D_{2d} geometry, at CAS(7/4)/TZP level, are reported. From a comparison with the corresponding results of Table 2, it is clear that the effect of replacing the optimized D_{2d} geometry by the averaged one obtained by eq. (1) is extremely small, particularly for the 1^2A_2 and 2^2A_2 states where the energy differences are −0.112 and 0.071 kJ/mol respectively.

The total energy values at the SZ and DZ basis set reported in Tables 3 and 5, respectively, are considered first. The CAS_{can} total energy values for the electronic states of both basis sets were found to be lower than CAS_{loc} by around $4 - 9 \times 10^{-4}$ a.u. This was to be expected since canonical CAS-SCF energy is converged variationally which is not the case for the corresponding localized CAS energy. Although CAS+S_{loc} energy is not variational at convergence, it was found that CAS+S_{loc} total energies were lower than that of CAS+S_{can} by around $3 - 4 \times 10^{-3}$ a.u. Finally, we have found that CAS+SD_{can} state energies were much lower than the corresponding C-CAS+SD_{can} values by 1×10^{-1} a.u. for SZ and 1.5×10^{-1} a.u. for DZ basis set though the molecular orbitals that were used in the contracted and uncontracted MRCI were the same. On the other hand, there was no clear trend between CAS+SD_{can} and CAS+SD_{loc} since the *A* states using the localized orbitals were 3×10^{-4} a.u. lower than that of the canonical orbitals while the opposite is true for the *B* states for SZ basis set in both geometries. In the case of DZ basis, the total energies of CAS+SD_{loc} were lower than that of CAS+SD_{can} values for all the electronic states except for the 2^2A_2 electronic state at C_{2v} geometry. It is worthwhile to mention that we have not performed contracted CAS+S_{can} calculations since this level is actually equivalent to canonical CAS-SCF level.

When the energy differences of the electronic states in kJ/mol are considered, Tables 4 and 6, the most striking observation is that the trend in CAS, CAS+S, and CAS+SD is not monotonic. Indeed, CAS+S level overcorrelates the CAS results with respect to CAS+SD results. This is true for both canonical and localized orbitals and for both SZ and DZ basis sets. Moreover, CAS+SD_{loc} results are very similar to both CAS+SD_{can} and C-CAS+SD_{can} results for all the electronic states considered in this study in both geometries. For instance, $2V_{ab}$ values for CAS+SD_{can}, C-CAS+SD_{can} and CAS+SD_{loc} with DZ basis set are 10.187, 10.290, and 9.933 kJ/mol respectively.

Our CAS+SD results for the $2V_{ab}$ values are in good agreement with the B3-LYP calculations of Sanz et al., 9.52 kJ/mol, and to a lesser extent with their UHF and DDCI results, 10.98 and 11.89 kJ/mol respectively, on the Spiro cation.[29] Dehareng et al.[20] found a value of 4.13 kJ/mol for the 1^2A_2 state in C_{2v} geometry using CAS(3/4).[29] This is similar to our CAS+SD result with DZ basis set though the geometry proposed by the authors was C_1 for the C_{2v} geometry (See the section on the Spiro molecule for more details).

It is worthwhile to mention that our calculations on the Spiro molecule confirm the low effect of the basis set on the coupling matrix element V_{ab},[13,29] see Tables 4 and 6. However, the other states were found to be more dependent on the basis set. For instance, the energy barrier, or the energy of the 1^2A_2 state in C_{2v} geometry, was found to be ~30–40% lower in DZ than the minimal basis set. A systematic study of the effect of basis set and the size of the active space on the potential curves of the Spiro molecule is under investigation.

Conclusions

In the treatment of mixed valence systems, accurate quantitative results are crucially important, particularly for the cases where the potential energy barriers are relatively small, even less than 4.2 kJ/mol. To reach such an accuracy, the inclusion of dynamical correlation is important. For this reason, even though the CAS-SCF results are qualitatively acceptable, the CAS+SD level of description was found to be desirable. In the case of the CAS+S results, on the other hand, a strong overcorrelation was observed. Although more numerical experience is required, this level of description do not seem to be particularly suited for the treatment of these systems.

The computed electronic states at CAS-SCF and CAS+SD levels along the reaction coordinate of the charge transition between the two redox sites of the mixed valence Spiro cation produced an adiabatic double-well potential energy surface for the electronic ground state and single minimum PES for the other low-lying excited states. The comparison of the computed geometries of the neutral, dication, and the two moieties of the C_{2v} geometry of the cation predicts a strong valence trapping of the charge for this bistable molecular system. Moreover, the reaction coordinate path obtained by mixing linearly the two localized (asymmetric) geometries using a two-state model was proved to be a very good approximation for the charge transfer reaction coordinate of Spiro molecular system.

In the treatment of larger multireference systems, the use of large active spaces is often necessary for an accurate description of the energy differences found in these types of molecules. Notwithstanding, the control of the nature of the active space is an extremely difficult task in canonical CAS-SCF, and the use of large active space is often problematic. For this reason, we believe that the use of local orbitals in a CAS+SD context can be a very powerful tool for the treatment of mixed-valence systems. It is interesting to see the effect of including the complete valence "π" system in the spiro molecular cation. The use of two recently developed multi-reference variational and perturbative methods is very appealing: the selected excitation for CAS+SD method using localized orbitals developed

by our group[76] devoted to CAS and CI calculations on large systems, and the *n*-electron valence perturbation theory (NEVPT) method,[77–80] and work in this direction for the Spiro cation and other larger molecular mixed valence systems is ongoing in our group.

References

1. Robin, M.; Day, P. Adv Inorg Radiochem 1967, 10, 247.
2. Farazdel, A.; Dupuis, M.; Clementi, E.; Aviram, A. J Am Chem Soc 1990, 112, 4206.
3. Joachim, C.; Gimzewski, J. K.; Aviram, A. Nature 2000, 408, 541.
4. Fraysse, S.; Coudret, C.; Launay, J.-P. Eur J Inorg Chem 2000, 2000, 1581.
5. Barigelletti, F.; Flamigni, L. Chem Soc Rev 2000, 29, 1.
6. Lukas, A. S.; Bushard, P. J.; Wasielewski, M. R. J Am Chem Soc 2001, 123, 2440.
7. Braun-Sand, S. B.; Wiest, O. J Phys Chem B 2003, 107, 9624.
8. Barbara, P. F.; Meyer, T. J.; Ratner, M. A. J Phys Chem 1996, 100, 13148.
9. Demadis, K. D.; Hartshorn, C. M.; Meyer, T. J. Chem Rev 2001, 101, 2655.
10. Launay, J.-P. Chem Soc Rev 2001, 30, 386.
11. Brunschwig, B. S.; Creutz, C.; Sutin, N. Chem Soc Rev 2002, 31, 168.
12. Lambert, C.; Nöll, G.; Schelter, J. Nat Mater 2002, 1, 69.
13. Calzado, C. J.; Sanz, J. F. J Am Chem Soc 1998, 120, 1051.
14. Nelsen, S. F. Chem Eur J 2000, 6, 581.
15. Carissan, Y.; Heully, J.-L.; Alary, F.; Daudey, J.-P. Inorg Chem 2004, 43, 1411.
16. D'Alessandro, D. M.; Keene, R. Chem Soc Rev 2006, 35, 424.
17. Chisholm, M. H.; Patmore, N. J. Acc Chem Res 2007, 40, 19.
18. Lahlil, K.; Moradpour, A.; Bowlas, C.; Menou, F.; Cassoux, P.; Bonvoisin, J.; Launay, J.-P.; Dive, G.; Dehareng, D. J Am Chem Soc 1995, 117, 9995.
19. Lambert, C.; Gaschler, W.; Schmälzlin, E.; Meerholz, K.; Bräuchle, C. J Chem Soc Perkin Trans 2 1999, 577.
20. Dehareng, D.; Dive, G.; Moradpour, A. Int J Quantum Chem 2000, 76, 552.
21. Malagoli, M.; Brédas, J. L. Chem Phys Lett 2000, 327, 13.
22. Johnson, R. C.; Hupp, J. P. J Am Chem Soc 2001, 123, 2053.
23. Coropceanu, V.; Malagoli, M.; André, J. M.; Brédas, J. L. J Chem Phys 2001, 115, 10409.
24. Coropceanu, V.; Malagoli, M.; André, J. M.; Brédas, J. L. J Am Chem Soc 2002, 124, 10519.
25. Lambert, C.; Nöll, G. Chem Eur J 2002, 8, 3467.
26. Lambert, C.; Amthor, S.; Schelter, J. J Phys Chem A 2004, 108, 6474.
27. Szeghalmi, A. V.; Erdmann, M.; Engel, V.; Schmitt, M.; Amthor, S.; Kriegisch, V.; Nöll, G.; Stahl, R.; Lambert, C.; Leusser, D.; Stalke, D.; Zabel, M.; Popp, J. J Am Chem Soc 2004, 126, 7834.
28. Nelsen, S. F.; Kondradsson, A. E.; Telo, J. P. J Am Chem Soc 2005, 127, 920.
29. Sanz, J. F.; Calzado, C. J.; Marquez, A. Int J Quantum Chem 2000, 76, 458.
30. Helal, W.; Bories, B.; Evangelisti, S.; Leininger, T.; Maynau, D. in Lecture Notes in Computer Science (LNCS 3980); Gavrilova, M. et al. Eds.; Springer-Verlag: New York, 2006; I-744.
31. Werner, H.-J.; Knowles, P. J. J Chem Phys 1988, 89, 5803.
32. Marcus, R. A. J Chem Phys 1956, 24, 979.
33. Marcus, R. A. J Chem Phys 1965, 43, 679.
34. Hush, N. S. Trans Faraday Soc 1961, 57, 155.
35. Hush, N. S. Elecrochim Acta 1968, 13, 1005.
36. Fernández, E.; Blancafort, L.; Olivucci, M.; Robb, M. J Am Chem Soc 2000, 122, 7528.
37. Blancafort, L.; Fernández, E.; Olivucci, M.; Robb, M. J Am Chem Soc 2001, 123, 722.
38. Fock, V. Z Phys 1930, 61, 126.
39. Boys, S. F. Rev Mod Phys 1960, 32, 296.
40. Edmiston, C.; Ruendenberg, K. Rev Mod Phys 1963, 35, 457.
41. Weinstein, H.; Paunez, R. Adv At Mol Phys 1971, 7, 97.
42. Goedecker, S. Rev Mod Phys 1999, 71, 1085.
43. Ayala, P. Y.; Scuseria, G. E. J Chem Phys 1999, 110, 3660.
44. Hampel, C.; Werner, H. J. J Chem Phys 1996, 104, 6286.
45. Scuseria, G. E.; Ayala, P. Y. J Chem Phys 1999, 111, 8330.
46. Guihéry, N.; Malrieu, J.-P.; Evangelisti, S.; Maynau, D. Chem Phys Lett 2001, 349, 555.
47. Maynau, D.; Evangelisti, S.; Guihéry, N.; Calzado, C. J.; Malrieu, J.-P. J Chem Phys 2002, 116, 10060.
48. Angeli, C.; Evangelisti, S.; Cimiraglia, R.; Maynau, D. J Chem Phys 2002, 117, 10525.
49. Angeli, C.; Calzado, C. J.; Cimiraglia, R.; Evangelisti, S.; Guihéry, N.; Malrieu, J.-P.; Maynau, D. J Comput Method Sci Eng 2002, 3, 1.
50. Angeli, C.; Calzado, C. J.; Cimiraglia, R.; Evangelisti, S.; Guihéry, N.; Malrieu, J.-P.; Maynau, D.; Pitarch-Ruiz, J. V.; Sparta, M. Mol Phys 2003, 101, 1389.
51. Daudey, J. P. Chem Phys Lett 1974, 24, 574.
52. Rubio, J.; Povill, A.; Malrieu, J.-P.; Reinhardt, P. J Chem Phys 1997, 107, 10044.
53. Pipek, J.; Mezey, P. G. J Chem Phys 1989, 90, 4916.
54. Ruedenberg, K.; Cheung, L. M.; Elbert, S. T. Int J Quantum Chem 1979, 16, 1069.
55. Levy, B.; Berthier, G. Int J Quantum Chem 1968, 2, 307.
56. Pitarch-Ruiz, J.; Evangelisti, S.; Maynau, D. Chem Phys Lett 2003, 372, 22.
57. Pitarch-Ruiz, J.; Evangelisti, S.; Maynau, D. Int J Quantum Chem 2004, 97, 688.
58. Pitarch-Ruiz, J.; Evangelisti, S.; Maynau, D. Int J Quantum Chem 2005, 101, 325.
59. Pitarch-Ruiz, J.; Calzado, C. J.; Evangelisti, S.; Maynau, D. Int J Quantum Chem 2006, 106, 609.
60. Calzado, C. J.; Evangelisti, S.; Maynau, D. J Phys Chem 2003, 107, 7581.
61. Suaud, N.; Pastor, G. M.; Evangelisti, S.; Maynau, D. Chem Phys Lett 2003, 378, 503.
62. Pitarch-Ruiz, J.; Evangelisti, S.; Maynau, D. J Mol Struct (Theochem) 2004, 681, 203.
63. Pitarch-Ruiz, J.; Evangelisti, S.; Maynau, D. J Chem Theory Comput 2005, 1, 1079.
64. Calzado, C. J.; Evangelisti, S.; Maynau, D. J Mol Struct (Theochem) 2003, 621, 51.
65. Evangelisti, S.; Guihéry, N.; Leininger, T.; Malrieu, J.-P.; Maynau, D.; Pitarch-Ruiz, J. V.; Suaud, N.; Angeli, C.; Cimiraglia, R.; Calzado, C. J. J Mol Struct (Theochem) 2004, 709, 1.
66. Borini, S.; Maynau, D.; Evangelisti, S. J Comput Chem 2005, 26, 1042.
67. Junquera-Hernández, J. M.; Pitarch-Ruiz, J.; Sánchez-Marín, J.; Maynau, D.; Evangelisti, S. J Comput Chem 2005, 26, 1254.
68. Leininger, T.; Angeli, C.; Evangelisti, S.; Cimiraglia, R.; Maynau, D. Chem Phys Lett 2003, 371, 49.
69. Bauschlicher, C. W.; Langhoff, S. R. J Chem Phys 1988, 89, 4246.
70. Widmark, P.-O.; Malmqvist, P.-A.; Roos, B. Theor Chim Acta 1991, 77, 291.
71. Laaksonen, L.; Anderson, S.; Boyd, K.; Häkkinen, E.; Varis, M. gOpenMol, Center for Scientific Computing, Espoo: Finland, 2003.
72. Amos, R. D.; Bernhardsson, A.; Berning, A.; Celani, P.; Cooper, D. L.; Deegan, M. J. O.; Dobbyn, A. J.; Eckert, F.; Hampel, C.; Hertzer, G.; Knowels, P. J.; Korona, T.; Lindh, R.; Lloyd, A. W.; McNicholas, S. J.; Manby, F. R.; Meyer, W.; Mura, M. E.; Nicklass, A.; Palmieri, P.; Pitzer, R.; Raunhut, G.; Schütz, M.; Schumann, U.; Stoll, H.; Stone, A. J.; Tarroni, R.; Thorsteinsson, T.; Werner, H.-J. MOLPRO Version 2002.6.

73. Andersson, K.; Barysz, M.; Bernhardsson, A.; Blomberg, M. R. A.; Carissan, Y.; Cooper, D. L.; Fülscher, M. P.; Gagliardi, L.; de Graaf, C.; Hess, B. A.; Hagberg, D.; Karlström, G.; Lindh, R.; Malmqvist, P.-Å.; Nakajima, T.; Neogrády P.; Olsen, J.; Raab, J.; Roos, B. O.; Ryde, U.; Schimmelpfennig, B.; Schütz, M.; Seijo, L.; Serrano-Andrés, L.; Siegbahn, P. E. M.; Stålring, J.; Thorsteinsson, T.; Veryazov, V.; Widmark, P.-O. MOLCAS Version 6.0, Lund Universiy, Sweeden, 2004.
74. Maynau, D.; Ben-Amor, N.; Pitarch-Ruiz, J. CASDI Program; University of Toulouse: France, 1999.
75. Kato, S.; Jaffe, R. L.; Komornicki, A.; Morokuma, K. J Chem Phys 1983, 78, 4567.
76. Bories, B.; Maynau, D.; Bonnet, M.-L. J Comput Chem 2007, 28, 632.
77. Angeli, C.; Cimiraglia, R.; Evangelisti, S.; Leininger, T.; Malrieu, J.-P. J Chem Phys 2001, 114, 10252.
78. Angeli, C.; Cimiraglia, R.; Malrieu, J.-P. J Chem Phys 2002, 117, 9138.
79. Angeli, C.; Borini, S.; Cestari, M.; Cimiraglia, R. J Chem Phys 2004, 121, 4043.
80. Angeli, C.; Bories, B.; Cavallini, A.; Cimiraglia, R. J Chem Phys 2006, 124, 054108.

4.4.4 Results of CAS(7/4) active space with the augmented basis sets

In this and the following two subsections, all the calculations that were performed on Spiro and were not reported in article I are presented. All the results presented in these three subsections were, at the best, limited at CAS+S level (see section §4.3.6). For that reason, and in order to have some reference values of the methods used for the larger active spaces and basis sets, the results of C-CAS+SD$_{can}$ method using CAS(7/4) with DZ basis set (reported in tables 5 and 6 in article I) will be considered as the benchmark values. It should not be deduced from this choice that C-CAS+SD$_{can}$ is more accurate than CAS+SD$_{can}$ or CAS+SD$_{loc}$ methods. In fact, C-CAS+SD$_{can}$ method is a well known and a largely tested and accepted method. Moreover, it has been shown that CAS+SD$_{can}$ and CAS+SD$_{loc}$ give very similar results to C-CAS+SD$_{can}$ method, at least, as long as the mixed-valence Spiro is concerned (see article I).

The energies, in kJ/mol, of the different electronic states at two points on the reaction coordinate of Spiro using CAS(7/4) with DZP basis set are tabulated in Table 4.2. In this and the following tables that consider the electronic state energies of Spiro, for each method, the reference energy has been taken as the energy of the ground state 1^2A_2 at the point the saddle point ($\xi = 0.00$), (D_{2d} geometry). In such a way, the energy values of 2^2A_2 electronic state at D_{2d} geometry represent $2V_{ab}$ (see section 3.2.3). While the energy values of 2^2A_2 electronic state at C_{2v} geometry represent the energy of the ET barrier (E_a). The results of CAS-CI (denoted as CAS$_{loc-guess}$) are added in this table.

The general trends of both CAS-SCF using canonical orbitals (CAS$_{can}$) and CAS-SCF using localized orbitals CAS$_{loc-opt}$ (where the subscript X$_{opt}$ is added to the latter to remind that the orbitals are optimized contrary to that of CAS$_{loc-guess}$ method) are similar to that of SZ and DZ basis sets using the same active space (Tables 4 and 6 in article I). This is also true for the same calculations using TZP basis set contraction, see Table 4.3. However, the anomaly of the results of CAS+S level for $^2B_1$ and $^2B_2$ electronic states in both C_{2v} and D_{2d} geometries, that were observed and reported in article I, was not removed or even systematically enhanced by using extended basis sets like that used for the results shown in Tables 4.2 and 4.3. Therefore, it is fair to conclude that the general trends that were observed in SZ and DZ basis sets using CAS(7/4) active space are generally consistent when using more extended basis sets contractions. On the other hand, the results of CAS-CI are,

Table 4.2: *Energies (kJ/mol) of the different states of Spiro cation, at D_{2d} geometry ($\xi = 0.00$) and C_{2v} geometry ($\xi = 0.50$), for different methods using DZP basis set and CAS(7/4): CAS_{can}, C-$CAS+SD_{can}$, $CAS_{loc-guess}$, $CAS_{loc-opt}$ and $CAS+S_{loc}$. For each method, the reference energy has been taken as the energy of the ground state 1^2A_2 in the D_{2d} geometry.*

Geometry	State	CAS_{can}	C-$CAS+SD_{can}$	$CAS_{loc-guess}$	$CAS_{loc-opt}$	$CAS+S_{loc}$
D_{2d}	1^2A_2	0.000	0.000	0.000	0.000	0.000
	2^2A_2	9.664	10.077	2.180	9.639	8.455
	$^2B_1$	46.521	61.379	381.999	47.320	117.357
	$^2B_2$	46.521	61.379	381.999	47.320	117.357
C_{2v}	1^2A_2	-6.528	-5.196	-11.541	-6.939	-4.185
	2^2A_2	39.852	39.042	37.575	40.253	36.271
	$^2B_1$	51.802	64.937	399.894	51.969	118.619
	$^2B_2$	63.421	80.668	388.335	64.974	139.422

in general, very far to be consistent with those of CAS, CAS+S and CAS+SD results, and this behavior is generally independent of the size of the basis set (see below), although the qualitative trend of CAS-CI results are quite consistent with that of the highly correlated methods.

The absolute energies, in hartree (or a.u.), of the results of the calculations using CAS(7/4) with DZP and TZP basis sets are tabulated in section §8.2 in the Appendix. In addition, and to report the CAS-CI results of the two smallest basis sets, tables of the results of SZ and DZ basis sets of the same active space in both kJ/mol and in atomic units are also included in the same section in the appendix chapter. It can be shown that there is no quantitative enhancement of CAS-CI results when augmented basis sets are considered, although the values of $^2A_2$ electronic state are relatively enhanced when passing from the minimal basis set (0.76 kJ/mol) to the other extended basis sets (around 2.1 kJ/mol). These latter values should be compared with that of, for instance, C-CAS+SD (10.3 kJ/mol) or $CAS+SD_{loc}$ (9.9 kJ/mol) at DZ basis set.

At this point, we can conclude that both dynamical and nondynamical correlations are

Table 4.3: *Energies, in kJ/mol, of the different states of Spiro cation, at D_{2d} geometry ($\xi = 0.00$) and C_{2v} geometry ($\xi = 0.50$), for different methods using TZP basis set and CAS(7/4): CAS_{can}, C-$CAS+SD_{can}$, $CAS_{loc-guess}$, $CAS_{loc-opt}$ and $CAS+S_{loc}$. For each method, the reference energy has been taken as the energy of the ground state 1^2A_2 in the D_{2d} geometry.*

Geometry	State	CAS_{can}	C-$CAS+SD_{can}$	$CAS_{loc-guess}$	$CAS_{loc-opt}$	$CAS+S_{loc}$
D_{2d}	1^2A_2	0.000	0.000	0.000	0.000	0.000
	2^2A_2	9.626	9.999	2.139	9.607	8.392
	$^2B_1$	45.181	59.461	381.441	45.985	116.820
	$^2B_2$	45.181	59.461	381.441	45.985	116.820
C_{2v}	1^2A_2	-6.753	-5.580	-11.708	-7.164	-3.333
	2^2A_2	39.390	38.523	37.052	39.814	36.068
	$^2B_1$	50.231	62.704	398.870	50.446	117.813
	$^2B_2$	61.731	78.246	387.602	63.325	138.023

necessary to reproduce the quantitative accuracy needed to describe properly the electronic states of Spiro. However the inclusion of the mono-excitation dynamical corrections on the CAS-SCF wave functions were found to be deficient, in term of accuracy, and the highly expensive CAS+SD level is needed if one seeks a good quantitative description. In addition, using localized orbitals, for this particular active space, did not change significantly the trend of the results of any of the levels of theory considered for the CAS (7/4) active space.

The following two subsections will try to ask the following question: Is a quantitative accuracy achieved at CAS+S level when a larger the active space is used? In particular, the role of using localized orbitals will also be addressed in the context of this question. The interest of this question is relevant if one seeks obtaining, relatively, reliable theoretical results on mixed-valence systems by using only the cheapest possible methods.

4.4.5 Results of CAS(7/8) active space with all the basis sets

The results of CAS_{can}, $CAS_{loc-guess}$, $CAS_{loc-opt}$, and $CAS+S_{loc}$ methods used to compute the energies of the Spiro electronic states, in kJ/mol, using CAS(7/8) active space are

Table 4.4: *Energies, in kJ/mol, of the different states of Spiro cation, at D_{2d} geometry ($\xi = 0.00$) and C_{2v} geometry ($\xi = 0.50$), for different methods using SZ basis set and CAS(7/8): CAS_{can}, $CAS_{loc-guess}$, $CAS_{loc-opt}$ and CAS+S_{loc}. For each method, the reference energy has been taken as the energy of the ground state 1^2A_2 in the D_{2d} geometry.*

Geometry	State	CAS_{can}	$CAS_{loc-guess}$	$CAS_{loc-opt}$	CAS+S_{loc}
D_{2d}	1^2A_2	0.000	0.000	0.000	0.000
	2^2A_2	8.003	0.759	8.367	8.148
	$^2B_1$	41.133	272.175	45.067	69.772
	$^2B_2$	41.133	272.175	45.067	69.772
C_{2v}	1^2A_2	-5.882	-11.504	-5.894	-4.017
	2^2A_2	45.717	44.011	46.141	44.767
	$^2B_1$	51.707	298.730	55.157	75.441
	$^2B_2$	61.811	278.073	65.732	96.332

presented in Table 4.4 with SZ basis set and Table 4.5 with DZ basis set. The absolute energy results of the same calculations are reported in section §8.2 in the Appendix together with other results using the two larger basis sets.

At CAS_{can} level, the ET energy barrier (E_a) and the energy splitting at the crossing seam ($2V_{ab}$) values are lowered using CAS(7/8) active space by $\sim$ 30% and $\sim$ 12% respectively as compared to that of CAS(7/4). This is true for both SZ and DZ basis sets.

Again, electronic energy states calculated with CAS-SCF using localized orbitals are close to that of canonical orbitals with any basis set of the same active space. When CAS+S results are considered, a significant lowering of E_a values using DZ basis is observed. For instance, CAS+S(7/8)/DZ value of E_a is -2.12 kJ/mol; that means, the energy of the ET barrier is lowered around 35% and 50% with that of CAS(7/4)/DZ and CAS(7/8)/DZ respectively, and more than 50% when compared with that of CAS+SD using CAS(7/4) active space and DZ basis set. In addition, the energy results of B states are not compatible with that of CAS+SD results found in article I, since CAS+S results predicts a lower mixing (or higher separation) between the ground and first excited state with the B states (the higher excited states) with the larger active space than CAS-SCF or CAS+SD methods

Table 4.5: *Energies, in kJ/mol, of the different states of Spiro cation, at D_{2d} geometry ($\xi = 0.00$) and C_{2v} geometry ($\xi = 0.50$), for different methods using DZ basis set and CAS(7/8): CAS_{can}, $CAS_{loc-guess}$, $CAS_{loc-opt}$ and CAS+S_{loc}. For each method, the reference energy has been taken as the energy of the ground state 1^2A_2 in the D_{2d} geometry.*

Geometry	State	CAS_{can}	$CAS_{loc-guess}$	$CAS_{loc-opt}$	CAS+S_{loc}
D_{2d}	1^2A_2	0.000	0.000	0.000	0.000
	2^2A_2	9.066	2.149	9.288	8.751
	$^2B_1$	46.564	323.555	52.284	90.281
	$^2B_2$	46.564	323.555	52.284	90.281
C_{2v}	1^2A_2	-4.471	-11.127	-4.762	-2.1191
	2^2A_2	38.603	38.410	39.147	36.392
	$^2B_1$	54.820	347.412	60.544	93.687
	$^2B_2$	62.529	325.186	67.824	112.003

using any active space with any basis set. The computational values of $2V_{ab}$ using CAS+S are merely affected by the size of the active space: 8.717 kJ/mol with the CAS(7/4)+S and 8.750 kJ/mol with the CAS(7/8)+S using DZ basis, that means an energy difference less than 0.4% between the two active spaces. A difference of 1% is obtained for the case of SZ basis set. It is worth noting that the computed value of $2V_{ab}$ was found to be dependent on the size of the active space using CAS-SCF, it was lower in the case of CAS(7/8) by $11\% - 13\%$ depending on the basis set than that of CAS(7/4) as mentioned above. The computed value $2V_{ab}$ was also found to be dependent on the nature of the active space as reported by Dehareng *et al.* [330].

4.4.6 Results of CAS(11/10) active space with all the basis sets

The results of the electronic states relative energy values, in kJ/mol at CAS(11/10) using SZ and TZP basis sets are reported in Tables 4.6 and 4.7 respectively. The results of this active space for other basis sets (DZ and DZP) both in a.u. (absolute energies) and in kJ/mol, and that of SZ and TZP basis sets in a.u. are reported in section §8.2 in

Table 4.6: *Energies (kJ/mol) of the different states of Spiro cation, at D_{2d} geometry ($\xi = 0.00$) and C_{2v} geometry ($\xi = 0.50$), for different methods using SZ basis set and CAS(11/10): CAS_{can}, $CAS_{loc-guess}$, $CAS_{loc-opt}$ and $CAS{+}S_{loc}$. For each method, the reference energy has been taken as the energy of the ground state 1^2A_2 in the D_{2d} geometry.*

Geometry	State	CAS_{can}	$CAS_{loc-guess}$	$CAS_{loc-opt}$	$CAS{+}S_{loc}$
D_{2d}	1^2A_2	0.000	0.000	0.000	0.000
	2^2A_2	7.409	0.602	7.661	7.810
	$^2B_1$	14.182	95.864	4.746	62.696
	$^2B_2$	14.182	95.864	4.746	62.696
C_{2v}	1^2A_2	-7.991	-12.213	8.022	-4.503
	2^2A_2	47.524	44.942	7.832	45.090
	$^2B_1$	19.025	101.968	9.596	68.278
	$^2B_2$	41.175	122.355	1.756	89.682

the Appendix. In these tables, the calculations limits were further restricted by the large number of configuration state functions and thus, for instance, CAS+S method was only feasible for the minimal (SZ) basis set. Therefore, the results of CAS-SCF and CAS+S methods for the different basis sets using complete freezing of all the sigma orbitals in Spiro are added in these tables.

The results of CAS-SCF calculations using CAS(10/11) suffers serious problems and misrepresentations on the quantitative as well as the qualitative levels of describing the Spiro ground and excited states PES shapes and energies. First, in the case of SZ, DZ, and DZP basis sets, at the C_{2v} minimum geometry, the two B symmetry states, which represent the second and third excited states, are lower in energy than that of 2^2A_2 first excited state. While at the D_{2d} geometry, the quantitative energy results of the $^2B_1$ and $^2B_2$ states are far to be compatible with that of CAS(7/4) or CAS(7/8) with any level of theory and using any basis set. At D_{2d} geometry, the two degenerate B states are separated from the first excited state by the same value as that between the ground state and the first excited state. For the sake of comparison with CAS+SD results at DZ basis set, these two higher excited states were separated from the first excited state by five folds as that for

Table 4.7: *Energies (kJ/mol) of the different states of Spiro cation, at D_{2d} geometry ($\xi = 0.00$) and C_{2v} geometry ($\xi = 0.50$), for different methods using TZP basis set and CAS(11/10): CAS_{can}, $CAS_{loc-guess}$, $CAS_{loc-opt-frz}$ and $CAS{+}S_{loc-frz}$. For each method, the reference energy has been taken as the energy of the ground state 1^2A_2 in the D_{2d} geometry.*

Geometry	State	CAS_{can}	$CAS_{loc-guess}$	$CAS_{loc-opt-frz}$	$CAS{+}S_{loc-frz}$
D_{2d}	1^2A_2	0.000	0.000	0.000	0.000
	2^2A_2	8.449	1.937	2.816	2.685
	$^2B_1$	9.706	116.057	87.291	116.733
	$^2B_2$	9.706	116.057	87.291	116.733
C_{2v}	1^2A_2	37.053	-12.482	-11.679	-10.033
	2^2A_2	86.341	38.220	38.519	36.922
	$^2B_1$	114.867	117.633	88.354	117.870
	$^2B_2$	134.302	138.584	110.142	139.841

$2V_{ab}$ values. Second, in the case of TZP basis set, the energy of the ground state, having 1^2A_2 symmetry, at the minimum C_{2v} geometry is higher than that of D_{2d} geometry (the energy of 1^2A_2 electronic state at C_{2v} geometry is positive), thus, a parabola is obtained for the electronic ground state in Spiro which implies that the energy barrier separating the two minima disappeared for this bistable system.

Actually, the valence π isosurface orbitals obtained using this large "complete" active space at CAS-SCF/TZP level at the C_{2v} minimum geometry of the $^2B_1$ state shows a different physical content, since, some of the π orbitals are replaced by orbitals having σ character, see Figure 4.3.

As mentioned above, it was not possible to perform a CAS-SCF and CAS+S calculations using localized molecular orbitals with TZP, nevertheless, the valence π isosurface orbitals of CAS(11/10) and CAS+S(11/10) at SZ basis set level starting with using localized guess orbitals are very interesting to compare with that of CAS(11/10)/TZP. Isosurface orbitals of CAS(11/10)/SZ and CAS+S(11/10)/S using localized molecular orbitals are shown in Figures 4.4 and 4.5 respectively. It is clear from these two figures that the using localized

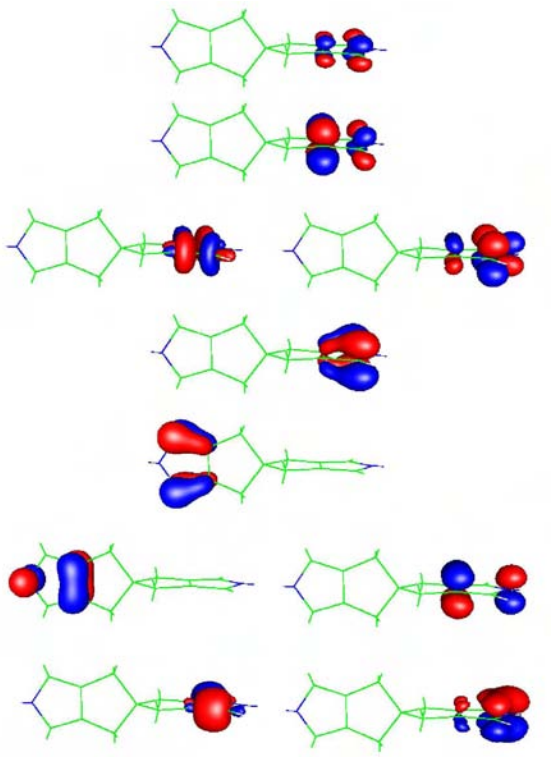

Figure 4.3: *Canonical MO's of CAS(11/10)/TZP for Spiro$^+$ in C_{2v} geometry for B_1 state.*

guess orbitals for optimizing a CAS space orbitals removes all the anomalies that were found with canonical CAS-SCF orbitals. However, in order to obtain more general conclusions about this point, the comparison should be made with the corresponding basis set, i.e., with TZP basis set.

4.4.7 NEVPT calculations

The results of NEVPT calculations performed on Spiro for the different active spaces and basis sets were reported in two published articles [335, 336] that are reported in section §8.1 of the appendix. The first publication, entitled "Can the second order multireference perturbation theory be considered a reliable tool to study mixed-valence compounds?" that was published in *Journal of Chemical Physics* [335], considers the minimal active space possible CAS(1/2) and the minimal basis set. The second publication on Spiro using NEVPT, entitled "Application of a "charge-averaged" second order Multireference

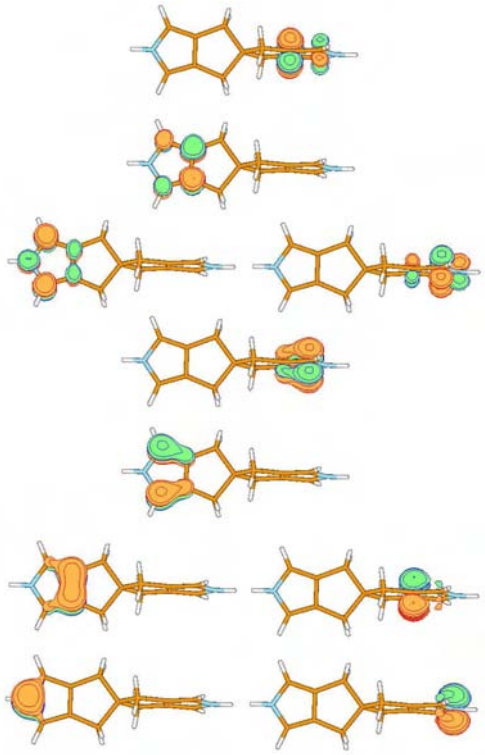

Figure 4.4: *Localized guess MO's of CAS(11/10)/SZ for Spiro$^+$ in C_{2v} geometry for B_1 state.*

Perturbation Theory strategy to the study of a model Mixed-Valence compound" was published in *Journal of Molecular Structure: Theochem* [336], it considers larger active spaces and more extended basis sets.

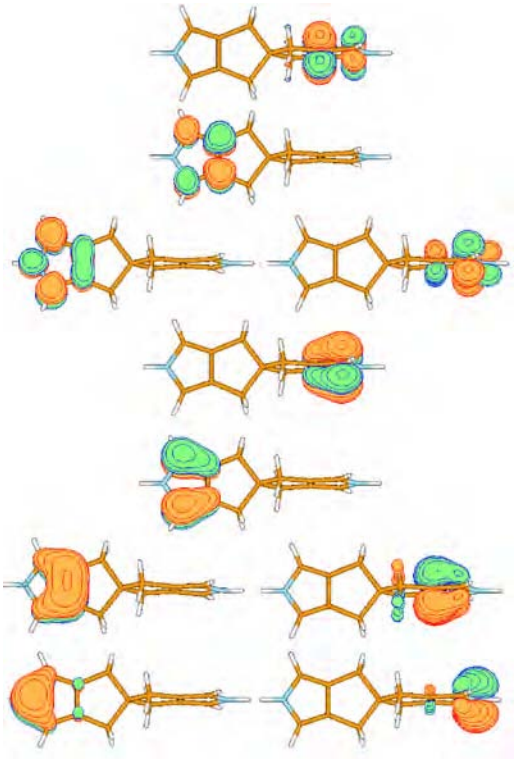

Figure 4.5: *Localized optimized MO's of CAS+S(11/10)/SZ for Spiro$^+$ in C_{2v} geometry for B_1 state.*

Chapter 5

Linear beryllium chains

The second step of this work is the theoretical study of the bistability for a series of linear beryllium chains. The experimental application of this system was not addressed, since its beyond the scope of this study. However, the methods of deposing single atomic metals on different kinds of surfaces are getting more and more attention recently. Actually, this kind of system was found to be very promising and the results found may clarify some points for further future investigation.

The results obtained so far are reported in the following article that is published in *Journal of Physical Chemistry A* [337].

Page 1 of 37 Submitted to Journal of Chemical Theory and Computation

Electronic Bistability in Linear Beryllium Chains

Wissam Helal [a], Antonio Monari [b],
Stefano Evangelisti [a], and Thierry Leininger [a]

[a] Laboratoire de Chimie et Physique Quantiques, UMR 5626,
Université de Toulouse et CNRS
118, Route de Narbonne, F-31062 Toulouse Cedex - France

[b] Dipartimento di Chimica Fisica e Inorganica,
Università di Bologna
Viale Risorgimento 4, I-40136 Bologna - Italy

* E-mail: stefano@irsamc.ups-tlse.fr

October 27, 2008

Abstract

A theoretical investigation on the electronic bistability of a series of cationic linear chains composed of beryllium atoms, Be_N^+, (with $N = 6, ..., 12$), is presented. The calculations were performed at CAS-SCF and MR-CI levels by using an ANO basis set containing $6s4p3d2f$ orbitals for each atom. Our results show a consistent gradual shift between different classes of mixed-valence compounds as the number of beryllium atoms increases, from class-III strong coupling toward class-II valence trapped. Indeed, in the largest cases ($N > 10$), the cationic chains were found to be closer to class I, where the coupling vanishes. The intramolecular electron transfer parameters V_{ab}, E_a, and E_{opt} were calculated for each atomic chain. It is shown that the decrease of V_{ab} with increasing N follows an exponential pattern.

Keywords:
cationic beryllium chains, mixed-valence systems, CAS-SCF, MR-CI

1 Introduction

Mixed-valence compounds are characterized by inter-valence charge transfer (CT) between two or more redox sites existing in different oxidation states. The great interest in mixed-valence compounds lays primarly in their use as model systems for the study of the ubiquitous electron transfer (ET) phenomena.[1–3] In addition, these molecules are extensively investigated for their molecular electronic applications.[4–8] Robin and Day classified mixed-valence compounds into three categories:[9] (a) the redox centers are completely localized where there is no electronic coupling between the redox centers (class I), (b) intermediate electronic coupling between the mixed valence centers exists and the charge is partly localized in one redox center (class II), and finally, (c) class III derivatives where coupling is so strong that the system is completely delocalized and intermediate redox states have to be attributed to the redox centers. The transition between class II and class III systems has recently attracted considerable attention.[10–13]

According to Marcus[14–16] the Potential Energy Surface (PES) of a degenerate mixed-valence system can be constructed from parabolic functions, each representing a diabatic, non-interacting, state, see Figure 1. In the case of two interacting states a and b, the electronic interaction (coupling) between these states will mix their wave functions with each other, to an extent that depend on the magnitude of the interaction. This leads to an effective removing of the degeneracy at the crossing of the diabatic wave functions, i.e., the formation of the avoided crossing, which gives rise to two new and separate adiabatic states of energies E^1 and E^2, (defined below).

A typical symmetric PES showing two adiabatic states resulted from a coupling of two diabatic states is sketched in Figure 1. The electronic coupling V_{ab}, known as the coupling matrix element, is defined as half the splitting between the adiabatic potential energy surfaces E^1 and E^2 at the crossing seam (see Figure 1),

$$2V_{ab} = E^2 - E^1 \tag{1}$$

where E^1 and E^2 in the most simple model (a two-state model) can be represented as the solutions of a 2×2 secular equation.[15,17] For class II systems, two intramolecular electron-transfer pathways are conceivable:[18]

1. A thermal process where the system moves from one minimum of the lower adiabatic surface over a transition state along the electron-transfer coordinate to the other minimum. The activation energy of this transition is the adiabatic energy barrier separating the two equilibrium points, E_a.

2. An optical process where the system is photoexcited from one minimum of the lower adiabatic surface to the Franck-Condon state of the upper adiabatic surface. The energy of this excitation is the Marcus reorganization energy λ and is equal to the optical transition energy: E_{opt} in the case of symmetric PES's.

It is worthwhile to mention that for more complex systems, this simple model may not correctly represents the mixed-valence and ET parameters, and other more complicated models are required for a proper modelling of these systems.[19,20]

In this Article, we investigate the possible presence of electron bistability in atomic linear chains. For the sake of simplicity, isolated chains only will be considered here, although we plan in the future to investigated surface-deposed chains and more complex systems. The construction of individual atomic metal chains precisely deposed on nanosurfaces was experimentaly made possible by the advent of new nanotechnological techniques such as the Scanning Tunneling Microscopy (STM)[21–25] and other combined techniques.[26,27] While gold atomic chains have received a considerable attention,[26–28] other metallic chains have also been investigated.[29,30] These atomic metal chains present interesting one-dimensional electronic properties.[28,31–33] As an example, atomic metallic chains are characterized by edge orbitals that can be considered as the analogues of surface states.[34]

In previous studies, we investigated the electronic structure of neutral Beryllium chains.[35–37] It was found that, close to the equilibrium geometry, these systems present two singly occupied equivalent edge orbitals, located at the chain extremities. Because of their very weak interaction, these orbitals give rise to two quasi-degenerate states, a singlet and a triplet. If an electron is extracted from the system, and the chain length is sufficiently long, the resulting hole will localize in one of the two edge orbitals. This induces an asymmetric distortion of the geometric framework of the chain, and the formation of a mixed-valence system.

In the present contribution, the structure of a series of cationic beryllium chains, Be_N^+ (with $N = 6, ..., 12$), has been computed at Complete Active Space Self-Consistent Field (CAS-SCF) and Multi-Reference Configuration Interaction (MR-CI) levels. In particular, it was found that the extent of

the charge localization, and thus the bistability, of a beryllium chain cation depends exclusively on the number of the atoms constituting the chain. The nature of this dependency is addressed in this work. CAS-SCF and MR-CI calculations, were applied to the beryllium cationic chains in order to compute the intramolecular charge transfer parameters, namely $2V_{ab}$, E_a, and E_{opt}, of the systems under investigation. It should be mentioned that, to the best of our knowledge, this is the first study that explicitly considers the mixed-valence nature of atomic-chain cations.

2 Linear beryllium chains

Beryllium and other atomic linear chains have been recently investigated by our group.[35–39] Here, we briefly recall the structure of neutral beryllium chains. At large distances, the beryllium atoms are essentially isolated atoms in their ground state, and the system is weakly bounded by dispersion (van der Waals) interactions. This fact is confirmed by the structure of the valence orbitals, which are essentially symmetry-combinations of the $2s$ orbitals of the beryllium atoms. At a distance of about 5.5 bohr, the wavefunction experiences a rapid change toward a totally different structure. Two singly occupied edge orbitals are present at the chain extremities. This is the result of the formation, in the direction of the chain axes (say, z), of two sp_z hybrid orbitals on each Be atom. By combining these hybrid orbitals, Be-Be single σ bonds are formed between adjacent atoms. Globally, there are $N-1$ of these σ bonds, and they host $2N-2$ out of the $2N$ valence electrons of the system. The two remaining valence electrons are placed into the two terminal (edge) hybrid orbitals that do not combine themselves with any other valence orbital. Being equivalent and located in different regions of the molecule, they are quasi-degenerate. Hence they give rise to two quasi-degenerated low-lying states, a singlet and a triplet.

The extraction of an electron from a neutral chain will leave the cation charge localized in one of the two edges of the linear chain, thus potentially inducing a deformation of the chain geometry. As previously stated this will be reflected by the possible formation of a bistable (a double-well) electronic ground state PES, or, in other words, the formation of a mixed-valence sys-

tem of class II. The symmetry of a neutral linear Be_N chain is $D_{\infty h}$, where the principal axis of rotation, C_∞, passes through all the beryllium atoms. The ground electronic state geometry of the distorted cations shows two equivalent minima having $C_{\infty v}$ symmetry. The two minima are separated by a saddle point at the crossing seam with a symmetric $D_{\infty h}$ geometry. In the following, the orbitals designation and the symmetry states of $D_{\infty h}$ and $C_{\infty v}$ point groups will be discussed in terms of D_{2h} and C_{2v} symmetry elements and point groups respectively (see Section 3, Computational Details). The occupied valence orbitals of Be_7^+ at D_{2h} and C_{2v} geometries are shown in Figures 2 and 3 respectively. Contrary to the D_{2h} case, the highest two occupied Molecular Orbitals (MO's) of the C_{2v} systems are completely localized, each one at one of the borders of the Be_7^+ chain. The Highest Occupied Molecular Orbital (HOMO) and the Lowest Unoccupied Molecular Orbital (LUMO) are chosen as the active space orbitals for all the beryllium chain cations in the CAS-SCF and MR-CI calculations.

3 Computational Details

ROHF, CAS-SCF, and contracted MR-CI (C-MR-CI)[40,41] were obtained for the system of Be_N^+ ($N = 6-12$) using MOLPRO code version 2002.6.[42] Since the MOLPRO code can only treat Abelian point groups, all calculations were performed using C_{2v} or D_{2h} symmetry point group instead of $C_{\infty v}$ and $D_{\infty h}$, respectively. However, for convenience, the geometry of the saddle point (of D_{2h} symmetry) was performed by MOLPRO using C_{2v} subgroup. The orbital density isosurfaces plots were obtained by using gOpenMol version 2.3.[43] Geometry optimization, single point calculations and Potential Energy Surfaces for the whole series of Be_N^+ were computed using Atomic Natural Orbitals (ANO)[44] basis set with $6s$, $4p$, $3d$, and $2f$ for each beryllium atom. The active space was choosen in such a way to include the HOMO (see Figure 3) and the LUMO for each chain, both for D_{2h} and C_{2v} geometries. For all the cationic chains, the two active orbitals would be occupied by a single active electron, hence the designation CAS(1/2). The same active orbitals were used for C-MR-CI calculations.

In order to avoid PES discontinuity at the saddle point, state-averaged CASSSF were computed for the $^2A_1$ states of Be_N^+ chains. Two state-averaged $^2A_1$ state were computed, namely 1^2A_1 and 2^2A_1. As a first step, geometry optimizations of Be_N^+ chains at the equilibrium, C_{2v} geometries, and at transition states, D_{2h} geometries, were performed at ROHF level. These geometries were used to construct the reaction coordinates of all the series of Be_N^+ chains.

The reaction paths were obtained by averaging the geometries of two

points on the reaction coordinates according to a mixing parameter ξ.[45] The simplest choice is to mix linearly the geometries of the two (equivalent) optimized minima. This choice will produce smooth curves on the whole ξ range, including the crossing seam, and it will make possible to test the geometries of the transition states on the reaction coordinates with respect to the truly optimized transition state geometries. The geometries along the reaction coordinate has been calculated using the formula:[45]

$$Q(\xi) = \left(\frac{1}{2} - \xi\right) Q_A + \left(\frac{1}{2} + \xi\right) Q_B \tag{2}$$

where $Q(\xi)$ is the nuclear configuration at the point ξ on the reaction path, while Q_A and Q_B represent the nuclear coordinates of the two optimized (equivalent) C_{2v} geometries. The mixing parameter ξ was varied from -1.00 to $+1.00$ in steps of 0.05. For large values of N, the crossing is waekly avoided. Therefore. for $N = 10-12$, smaller steps of 0.01 were used in the range -0.05 to $+0.05$ in order to obtained smooth curves. In this model, Q_A (the geometry of the first C_{2v} minimum) corresponds to the point $\xi = -0.50$, Q_B (the geometry of second C_{2v} minimum) corresponds to the point $\xi = +0.50$, and the averaged D_{2h} geometry corresponds to the crossing seam at $\xi = 0.00$. The Born-Oppenheimer potential energy surfaces were obtained by calculating the energies of 1^2A_1 and 2^2A_2 electronic states for each step value of the parameter ξ, using CAS-SCF and C-MR-CI methods.

In order to test the quality of the reaction coordinate, the energy of the optimized D_{2h} geometry was compared with the corresponding energy computed at $\xi = 0.00$. The results show a very small energy difference

between the averaged and the optimized D_{2h} geometries. As an example, for the beryllium chain where $N = 7$, the optimized D_{2h} geometry was 0.504 kJ/mol lower than that of the averaged D_{2h} Be_7^+ geometry at $\xi = 0.00$. In addition, a comparison of the corresponding bond lengths of the chains at the averaged and optimized D_{2h} geometries also shows an extremely small difference between the two structures. Considering the same chain (i.e., Be_7^+), the bond length values of bond 1 are 4.228 and 4.186 bohr for averaged and optimized D_{2h} geometries respectively. The difference between bond lengths of the other bonds of averaged and optimized D_{2h} Be_7^+ geometries were even smaller than that of bond 1, and the same is true for the other atomic beryllium chains. For these reasons, we believe that the geometry path obtained through equation (2) is very close to the optimal one. This is not surprising, if one consider the relatively small distortion of the chain geometry when the hole moves from one extremity to the opposite one. More complex systems are likely to present a very different behavior.

The $2V_{ab}$ values were computed by using equation (1), as the difference between the energies of 1^2A_1 and 2^2A_2 adiabatic states at the crossing seam, $\xi = 0.00$. The E_a values were computed by subtracting the adiabatic state energies of 1^2A_1 state at the crossing seam, $\xi = 0.00$, and the equilibrium geometry, $\xi = 0.50$. Finally, the E_{opt} values were computed by subtracting the adiabatic state energies of 1^2A_1 and 2^2A_2 states at the equilibrium geometry, $\xi = 0.50$.

4 Results and Discussion

The bond lengths of the optimized Be_N^+ chain equilibrium geometries are presented in Table 1. Bond numbering scheme can be summarized as follows: bond number 1 is the terminal bond on the "cationic" side, that is, the side where the charge is localized. Bond 2 is the bond adjacent to bond 1, etc. In this way, the last bond for each chain (bond $N-1$) is the terminal bond on the "neutral" side. When looking at the bond lengths of Be_N^+ collected in Table 1, one can immediately notice the strong geometry deformation of all the beryllium chains and, therefore, the strong localization of the cation charge in a terminal bond of a chain. For instance, the terminal "cationic" bond (bond 1) of Be_6^+ has a length of 4.359 bohr, while the bonds $3-5$, are very close in value, ranging from 4.076 to 4.088 bohr. This is also shown in Figure 4, where bond lengths of Be_N^+ are plotted as a function of bond numbers, using the same bond numbering scheme as in Table 1. Figure 4 shows clearly that, for a single chain, bond length changes for bond numbers >2 are very small, while a significant change is observed for bonds 1. It is worthwhile to note that bonds number 2 are slightly more "cationic", i.e. longer, than bonds number 3 to $N-1$, but significantly less than bond 1. It is also interesting to note that the deformation of bond 1 is almost constant with N. As an example we can see that for bond number 1 the lenght is 4.359 bohr for $N=6$ and 4.369 bohr for $N=12$. Similar behaviors can be found for the other bonds.

CAS-SCF and MR-CI Potential Energy Surfaces as a function of ξ for Be_N^+, are shown in Figures 5 and 6 respectively. The figures show PES for

$N = 6 - 10$. These plots represent the adiabatic surfaces of the Be_N^+ chains where, for each chain, the lower electronic ground state is the 1^2A_1 state, by using the corresponding C_{2v} symmetry elements, and the higher first excited electronic state is the 2^2A_2 state. The absolute atomic units energies of all the electronic states were scaled in such a way to set the zero of energy scale to the middle point of the splitting between the ground and first excited states at the crossing seam, $\xi = 0$. The values of $2V_{ab}$, E_a, and E_{opt} for Be_N^+ chains using CAS-SCF and MR-CI are presented in Table 2.

A consistent gradual shift toward valence trapping, or bistability, from $N = 6 - 12$ is observed. The Be_N^+ chains tend to move from class III to class I, passing by class II, mixed-valence systems, while increasing the number of beryllium atom N in a chain. This is true for both CAS-SCF and MR-CI calculations, as shown in Figures 5 and 6, although the bistability is more pronounced at CAS-SCF level. For instance, for $N = 6$, a very weak valence trapping, or charge localization, is observed, since the values of $2V_{ab}$ are relatively large and that of E_a are very small (the energy barrier actually disappear in the case of $N = 6$ using an MR-CI calculation). On the other hand, beryllium chains with far higher N, say $10 - 12$, have relatively high energy barrier E_a values, and relatively low electronic coupling $2V_{ab}$ values, see Table 2.

The MR-CI results, when compared with that of CAS-SCF, tend to slightly decrease the energy separation between the adiabatic ground state, 1^2A_1, and the first excited electronic state 2^2A_2 ($2V_{ab}$) for each N, as shown in Table 2. As far as the activation energy E_a is concerned, on the contrary, the inclusion of dynamic correlation seems to decrease the barrier at the crossing

seam.

The relationship between the coupling V_{ab} and the number of beryllium atoms N in a chain has been considered. The two quantities obey to an exponential relationship

$$V_{ab}(N) = V_{ab}^{0} e^{-\alpha N} \tag{3}$$

where V_{ab}^{0} is a constant. A plot of $\log 2V_{ab}$ as a function of N is shown in Figure 7. An overall linear behavior is observed, confirming the previous relationship. However, slight deviations from linearity appear for the highest N values. By plotting $\log 2V_{ab}$ as a function of even and odd N values separately, one obtains a far better linear behavior even for high N values, this is demonstrated in Figure 8 where plots of $\log 2V_{ab}$ as a function of even and odd N plots at CAS-SCF level are shown. The same behavior was also obtained at MR-CI level. Table 3 reports the values of α obtained by a least-square fitting of $\log V_{ab}$ as a function of N for CAS-SCF and MR-CI methods and for even and odd values of N. It is important to mention that the general exponential behaviour of $2V_{ab}$ may be attributed to the absence of chemical substituents. This situation is in contrast with the case of most organic and inorganic mixed valence systems, where substituent could contribute directly to the thermal ET process (through bond ET). A complete investigation of this point is anyway beyond the scope of this work.

Finally, the vertical electron affinity of the cation, was considered. It is defined as $E(\mathrm{Be}_N^+) - E(\mathrm{Be}_N)$, computed at the optimized cation geometry, and it is, in this way, a positive quantity. In Table 4 the dependence of the electron affinity with N is reported. It appears that, by augmenting the

number of atoms in the chain, the electronic affinity becomes smaller. The weak dependence on N, however, confirms the very localized nature of the hole. The values are illustrated in Figure 9. The MR-CI values are larger (about 5%) than the corresponding CAS-SCF results. This is consistent with the presence of a larger dynamical correlation energy in the neutral species than in the ions, a common fact in CI calculations. There is also a tiny increase of the EA by going from the symmetric $D_{2\infty}$ geometry to the distorted $C_{2\infty}$ one, probably due to the less diffuse character of the singly occupied edge orbital in the distorted geometry with respect to the symmetric one.

The present results suggest the possibility of using cationic linear chains of beryllium atoms as electronic "charge transfer" devices, in which intramolecular charge transfer parameters, e.g., V_{ab}, could be directly controlled, or "designed", by varying the number of atoms of the chain.

5 Conclusions

It has been shown that linear beryllium chains behave like mixed-valence systems when one electron is removed from the system. An increase of electronic bistability (valence trapping or charge localization) with increasing the number of beryllium atoms N in a cationic chain has been evidenced. As expected in the case of extended mixed-valence systems, there is a decraesing V_{ab} with increasing N. In particular, a linear relationship between $\log 2V_{ab}$ and the number of beryllium atoms (N) has been found. Indeed, at the equilibrium geometry the chain length is, to a very good extent, directly proportional to the number of atoms. This fact justifies the exponential relationship between $2V_{ab}$ and the chain length, consistent with the fact that in the cation the hole is located in one of the two edge orbitals.

These results are particularly interesting for at least two reasons. First of all, mixed-valence systems could be used in order to design interesting devices, particularly in the field of Molecular Electronics. A promising possibility would be to deposit beryllium chains on nanodevices (on top of graphene surfaces and nanorods or inside nanotubes) in order to exploit the mixed valence nature of the cation. The possibility of going from class I to class III in a tunable way, by simply changing the number of atoms in the chain, makes these system particularly atracting. Moreover, as isolated objects, beryllium chains are relatively simple systems. For this reason, they are particularly adapted to assess the quality of the theoretical methods used to perform these studies.

Finally, it is worth mentioning that preliminary investigations on neutral

atomic chains containing atoms of the Groups 2 and 12 seem to indicate that the presence of edge orbitals is not restricted to beryllium alone. If these results will be confirmed by subsequent investigations, the number of possibilities for mixed-valence atomic chains would be extremely large. Although the stability of isolated chains toward collapse into more-stable compact clusters is still to be investigated, linear structures could perhaps be stabilized by deposition on inert surfaces. This possibility, combined with the remarkable predicted properties of the neutral chains, could open interesting perspectives in the fast growing field of nanodevices.

Acknowledgements

This work was supported by the French "Centre National de la Recherche Scientifique" (CNRS), the Italian Ministry of University and Research (MUR), and the University of Bologna under the project "PRIN 2006. Molecular Quantum Mechanics: Computational Methods and Analysis of Novel Phenomena". Support from the European Community under the COST D37 action (GRIDCHEM) is also gratefully acknowledged.

References

[1] Creutz, C. *Prog. Inorg. Chem.* **1983**, *30*, 1.

[2] Richardson, D. E.; Taube, H. *Coord. Chem. Rev.* **1984**, *60*, 107.

[3] Barbara, P. F.; Meyer, T. J.; Ratner, M. A. *J. Phys. Chem.* **1996**, *100*, 13148.

[4] Joachim, C.; Gimzewski, J. K.; Aviram, A. *Nature* **2000**, *408*, 541.

[5] Fraysse, S.; Coudret, C.; Launay, J.-P. *Eur. J. Inorg. Chem.* **2000**, *1* 1581.

[6] Barigelletti, F.; Flamigni, L. *Chem. Soc. Rev.* **2000**, *29*, 1.

[7] Lukas, A. S.; Bushard, P. J.; Wasielewski, M. R. *J. Am. Chem. Soc.* **2001**, *123*, 2440.

[8] Braun-Sand, S. B.; Wiest, O. *J. Phys. Chem. B* **2003**, *107*, 9624.

[9] Robin, M.; Day, P. *Adv. Inorg. Radiochem.* **1967**, *10*, 247.

[10] Nelsen, S. F. *Chem. Eur. J.* **2000**, *6*, 581.

[11] Demadis, K. D.; Hartshorn, C. M.; Meyer, T. J. *Chem. Rev.* **2001**, *101*, 2655.

[12] Brunschwig, B. S.; Creutz, C.; Sutin, N. *Chem. Soc. Rev.* **2002**, *31*, 168.

[13] D'Alessandro, D. M.; Keene, R. *Chem. Soc. Rev.* **2006**, *35*, 424.

[14] Marcus, R. A.; Sutin, N. *Biochim. Biophys. Acta* **1985**, *811*, 265.

[15] Sutin, N. *Prog. Inorg. Chem.* **1983**, *30*, 441.

[16] Creutz, C.; Newton, M. D.; Sutin, N. *J. Photochem. Photobiol. A* **1994**, *82*, 47.

[17] Newton, M. D.; Sutin, N. *Annu. Rev. Phys. Chem.* **1984**, *35*, 437.

[18] Hush, N. S. *Coord. Chem. Rev.* **1985**, *64*, 135.

[19] Fernández, E.; Blancafort, L.; Olivucci, M.; Robb, M., *J. Am. Chem. Soc.*, 2000, **122**, 7528.

[20] Blancafort, L.; Fernández, E.; Olivucci, M.; Robb, M., *J. Am. Chem. Soc.*, 2001, **123**, 722.

[21] Stipe, B. C.; Resaei, M. A.; Ho, W. *Science* **1998**, *280*, 1732.

[22] Weiss, P. S.; Yokota, H.; Allara, D. L. *J. Phys.: Condens. Matter* **1998**, *10*, 7703.

[23] Gimzewski, J. *Phys. World* **1998**, *11*, 29.

[24] Andres, R. P.; Bielefeld, J. D.; Henderson, J. I.; Janes, D. B.; Kolagunta, V. R.; Kubiak, C. P.; Mahoney, W. J.; Osifchin, R. G. *Science* **1996**, *273*, 1690.

[25] Bumm, L. A.; Arnold, J. J.; Cygan, M. T.; Dunbar, T. D.; Burgin, T. P.; Jones II, L.; Allara, D. L.; Tour, J. M.; Weiss, P. S. *Science* **1996**, *271*, 1705.

[26] Ohnishi, H.; Kondo, Y.; Takayanagi, K. *Nature* **1998**, *395*, 780.

[27] Rubio-Bollinger, G.; Bahn, S. R.; Agraït, N.; Jacobsen, K. W.; Vieira, S. *Phys. Rev. Lett.* **2001**, *87*, 026101.

[28] Crain, J. N.; Pierce, D. T. *Science* **2005**, *307*, 703.

[29] Bahn, S. R.; Jacobsen, K. W. *Phys. Rev. Lett.* **2001**, *87*, 266101.

[30] Amorim, E. P; da Silva, A. J. R.; Fazzio, A.; da Silva, E. Z. *Nanotechnology* **2007**, *18*, 145701.

[31] Emberly, E. G.; Kirczenow, G. *Phys. Rev. B* **1999**, *60*, 6028.

[32] Himpsel, F. J.; Altmann, K. N.; Bennewitz, R.; Crain, J. N.; Kirakosian, A.; Lin, J.-L.; McChesney, J. L. *J.Phys.: Condens. Matter* **2001**, *13*, 11097.

[33] Nilius, N.; Wallis, T. M.; Ho, W. *Science* **2002**, *297*, 1853.

[34] Davidson, S. G.; Stęślicka, M. Basic Theory of Surface States, Clarendon, Oxford, 1992.

[35] Monari, A.; Vetere, V.; Bendazzoli, G.; Evangelisti, S.; Paulus, B. *Chem. Phys. Lett.* **2008**, *465*, 102.

[36] Vetere, V.; Monari, A.; Scemama, A.; Bendazzoli, G.; Evangelisti, S. *J. Chem. Phys.*, submitted.

[37] Pastore, M .; Monari, A.; Vetere, V.; Bendazzoli, G.; Evangelisti, S. *J. Chem. Phys.*, submitted.

[38] Vetere, V.; Monari, A.; Bendazzoli, G. L.; Evangelisti, S.; Paulus, B. *J. Chem. Phys.* **2008**, *128*, 024701.

[39] Bendazzoli, G. L.; Evangelisti, S.; Monari, A.; Paulus, B.; Vetere, V. *J. Phys. Conf. Series* **2008**, *117* 012005.

[40] Knowles, P. J.; Werner, H.-J. *Chem. Phys. Lett.* **1988**, *145*, 514.

[41] Werner, H.-J.; Knowles, P. J. *J. Chem. Phys.* **1988**, *89*, 5803.

[42] Amos, R. D.; Bernhardsson, A.; Berning, A.; Celani, P.; Cooper, D. L.; Deegan, M. J. O.; Dobbyn, A. J.; Eckert, F.; Hampel, C.; Hertzer, G.; Knowels, P. J.; Korona, T.; Lindh, R.; Lloyd, A. W.; McNicholas, S. J.; Manby, F. R.; Meyer, W.; Mura, M. E.; Nicklass, A.; Palmieri, P.; Pitzer, R.; Raunhut, G.; Schütz, M.; Schumann, U.; Stoll, H.; Stone, A. J.; Tarroni, R.; Thorsteinsson, T.; and Werner. H.-J. MOLPRO Version 2002.6.

[43] Laaksonen, L.; Anderson, S.; Boyd, K.; Häkkinen, E.; Varis, M. gOpenMol, Center for Scientific Computing, Espoo, Finland, 2003.

[44] Widmark, P.-O.; Malmqvist, P.-Å.; Roos, B. *Theor. Chim. Acta* **1990**, *77*, 291.

[45] Helal, W.; Evangelisti, S.; Leininger, T.; Maynau, D. *J. Comput. Chem.* **2008**, in press, DOI: 10.1002/jcc.20982.

Figure Captions

Figure 1: A cross section of an energy profile for initial state a and final state b in a typical symmetric (exothermicity or $\Delta E = 0$) ET reaction.The solid curves are the adiabatic surfaces, the dashed lines refer to diabatic surfaces. Q_a and Q_b are equilibrium nuclear coordinates of a and b respectively. Electron transfer matrix V_{ab}, diabatic activation energy E_d, adiabatic activation energy E_a, and E_{opt} are indicated.

Figure 2: The occupied valence and active orbitals of Be_7^+ at D_{2h} (symmetric) geometry, produced at CAS-SCF(1/2) level using ANO basis set $(6s, 4p, 3d, 2f)$.

Figure 3: The occupied valence and active orbitals of Be_7^+ at C_{2v} (unsymmetric) geometry, produced at CAS-SCF(1/2) level using ANO basis set $(6s, 4p, 3d, 2f)$. The electron hole is localized in the terminal bond at the left side of the chain.

Figure 4: The optimized bond lengths of Be_N^+, in bohr, at C_{2v} geometry as a function of bond number for different N values ($N = 6, ..., 12$).

Figure 5: Adiabatic potential energy surfaces of Be_N^+ ($N = 6 - 10$) for the ground electronic states 1^2A_1 and the first excited states 2^2A_1. Energies in au (see the text), produced at CAS-SCF, as a function of ξ. Solid and red curves $N = 6$; long-dashed ($- - -$) and green curves $N = 7$; short-dashed (- - -) and blue curves $N = 8$; dots ($\cdots$) and dark pink curves $N = 9$; doted-dashed ($- \cdot - \cdot -$) and turquoise curves $N = 10$.

Figure 6: Adiabatic potential energy surfaces of Be_N^+ ($N = 6 - 10$) for the ground electronic states 1^2A_1 and the first excited states 2^2A_1. Energies in au

(see the text), produced at C-MR-CI, as a function of ξ. Solid and red curves $N = 6$; long-dashed $(- - -)$ and green curves $N = 7$; short-dashed (- - -) and blue curves $N = 8$; dots $(\cdots)$ and dark pink curves $N = 9$; doted-dashed $(- \cdot - \cdot -)$ and turquoise curves $N = 10$.

Figure 7: $\log 2V_{ab}$, calculated at CAS-SCF and C-MR-CI, as a function of the number of beryllium atoms N.

Figure 8: $\log 2V_{ab}$, calculated at CAS-SCF as a function of even and odd N.

Figure 9: Electronic affinites, in kJ/mol, of the cationic Be_N^+ as a function of the number of atoms N in a chain.

Table 1: Bond lengths, in bohr, of optimized Be_N^+.

	Bond length of Be_N^+						
Bond no.	N=6	N=7	N=8	N=9	N=10	N=11	N=12
1	4.359	4.364	4.366	4.368	4.368	4.369	4.369
2	4.139	4.143	4.146	4.147	4.147	4.147	4.148
3	4.088	4.094	4.097	4.098	4.099	4.099	4.100
4	4.076	4.087	4.092	4.094	4.095	4.095	4.096
5	4.086	4.083	4.093	4.097	4.099	4.100	4.101
6		4.093	4.089	4.098	4.103	4.105	4.106
7			4.105	4.093	4.102	4.106	4.108
8				4.102	4.096	4.105	4.109
9					4.105	4.097	4.106
10						4.106	4.098
11							4.108

Table 2: $2V_{ab}$, E_a, and E_{opt} energy values, in kJ/mol, of Be_N^+.

Method	N	$2V_{ab}$	E_a	E_{opt}
CAS-SCF	6	10.356	-0.577	16.567
	7	4.813	-1.741	13.174
	8	2.340	-2.466	11.980
	9	1.066	-2.899	11.452
	10	0.548	-3.066	11.190
	11	0.226	-3.172	11.018
	12	0.137	-3.182	10.919
MR-CI	6	13.276	0.441	17.181
	7	6.299	-0.628	12.202
	8	3.040	-1.487	10.527
	9	1.398	-2.061	9.936
	10	0.694	-2.336	9.721
	11	0.296	-2.503	9.613

Table 3: Least-square fitted values of α (see text for details). The correlation coefficient ρ is reported too.

	CAS-SCF	MR-CI	CAS-SCF even N	CAS-SCF odd N	MR-CI even N	MR-CI odd N
α	-0.734	-0.755	-0.721	-0.765	-0.738	-0.764
ρ	0.9989	0.9997	0.9998	0.9999	0.9999	0.9999

Table 4: Electronic affinites, in kJ/mol, of Be_N^+, optimized at the cation geometries, for D_{2h} and C_{2v} geometries both at CASSCF and MRCI.

	Electronic Affinites			
	CASSCF		MRCI	
N	D_{2h}	C_{2v}	D_{2h}	C_{2v}
6	556.397	551.612	588.426	585.297
7	555.306	549.337	585.807	581.540
8	553.952	547.318	583.151	578.022
9	552.808	545.801	580.839	575.143
10	551.827	544.696	578.824	572.855
11	551.109	543.909	577.178	571.043
12	550.516	543.324		

Figure 1:

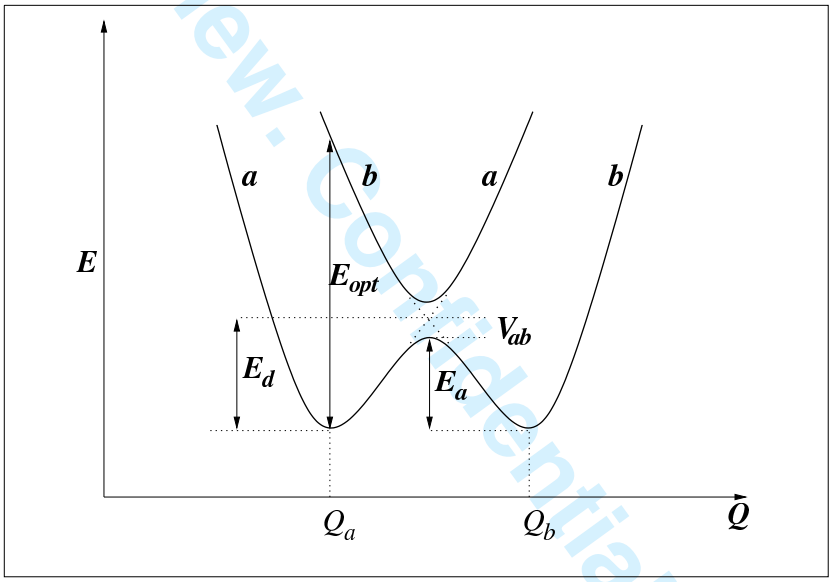

Figure 2:

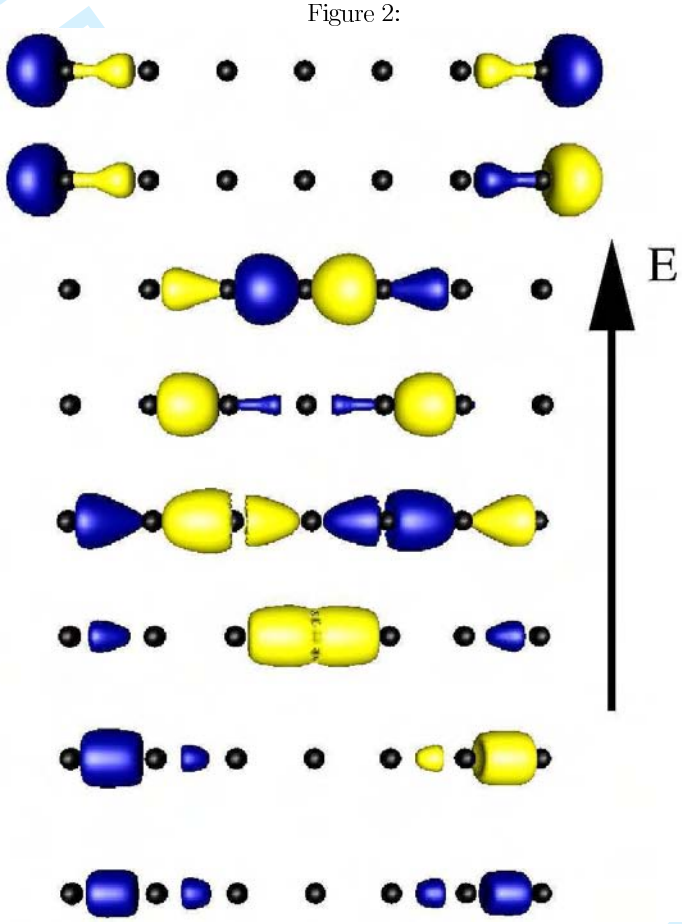

Figure 3:

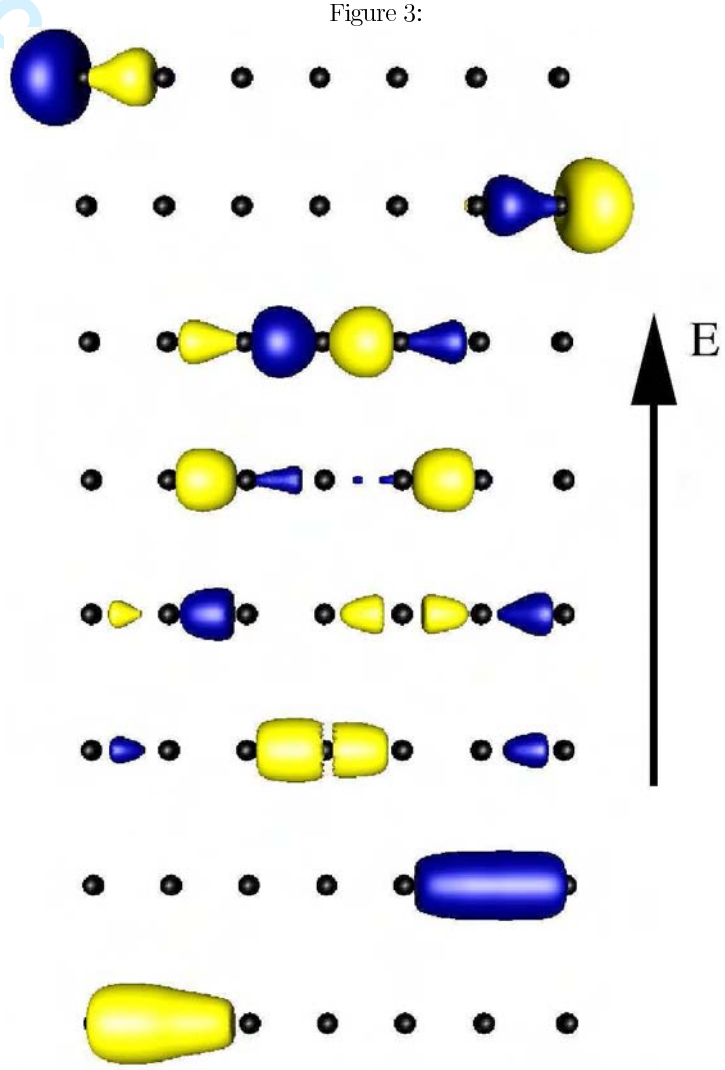

Figure 4:

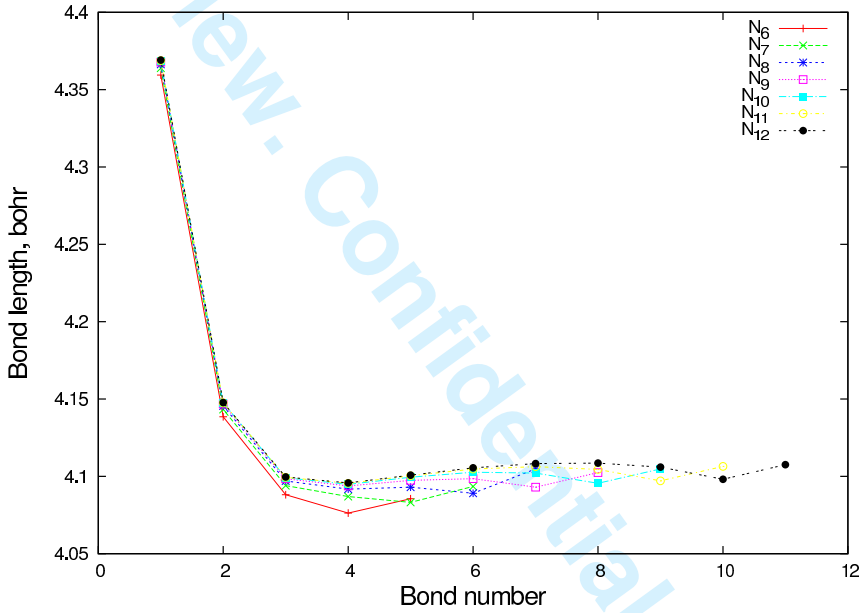

Figure 5:

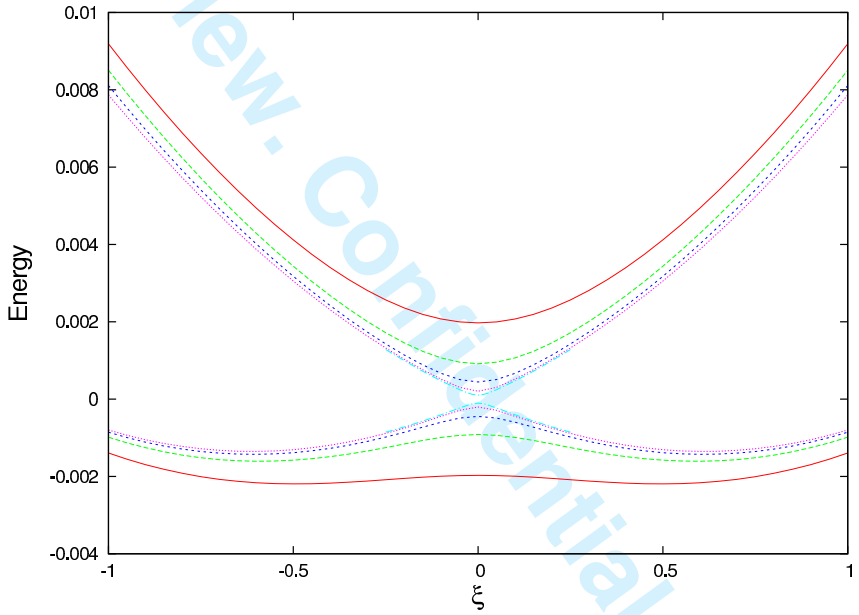

Figure 6:

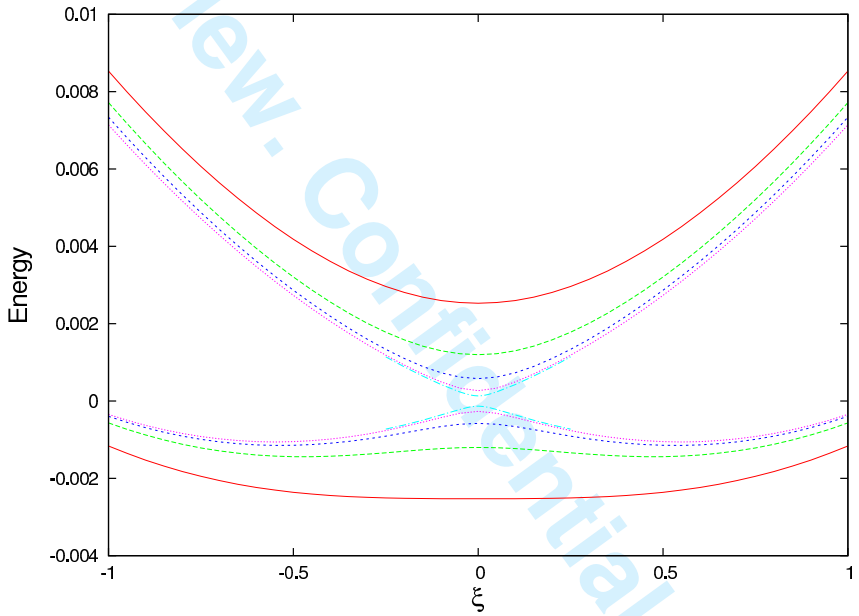

Figure 7:

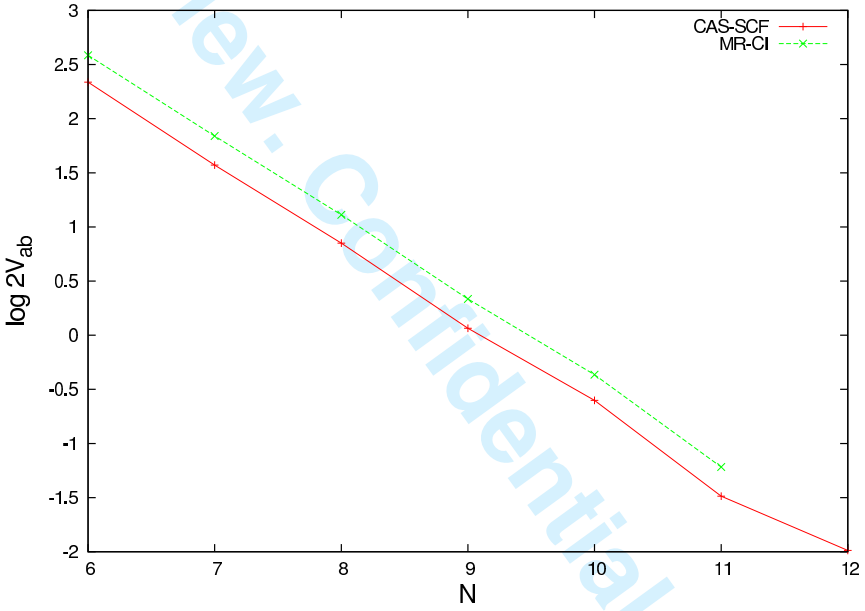

Figure 8:

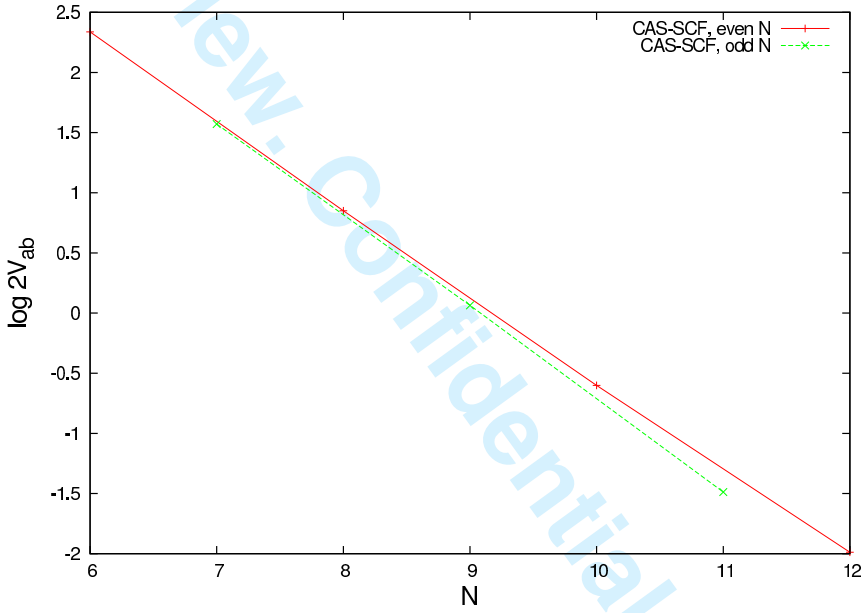

Figure 9:

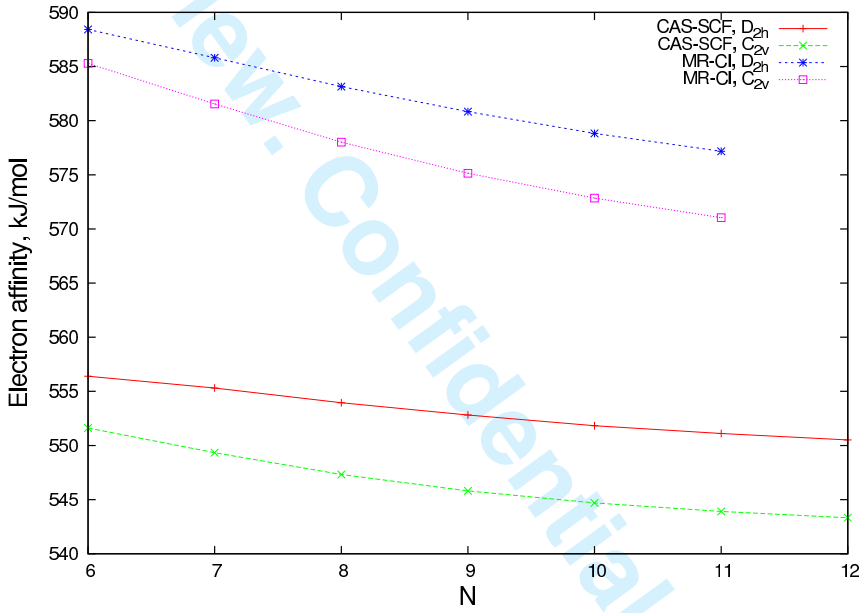

Chapter 6

The *bis*-Triarylamines

6.1 Introduction

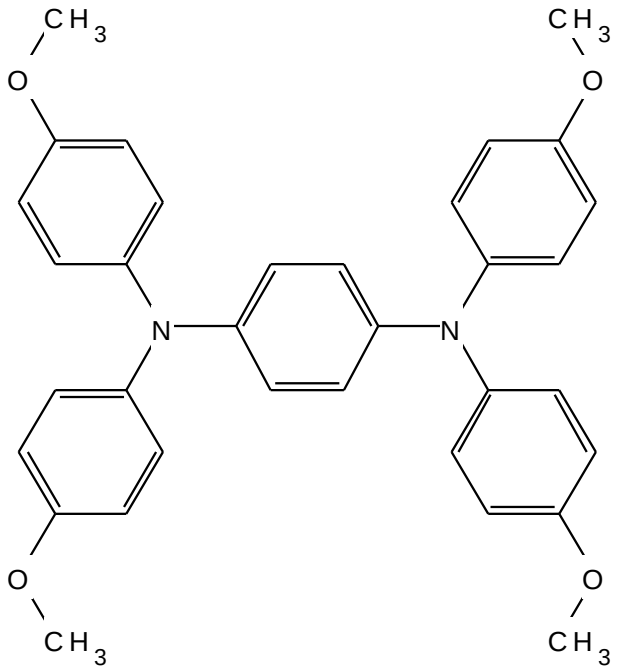

Figure 6.1: *bis-Triarylamine (1): N,N,N',N'-Tetra(4-methoxyphenyl)-1,4-phenylenediamine.*

The two *bis*-Triarylamines molecules investigated, at a preliminary level, in this work are the cations of: N,N,N',N'-Tetra(4-methoxyphenyl)-1,4-phenylenediamine, labeled tri-

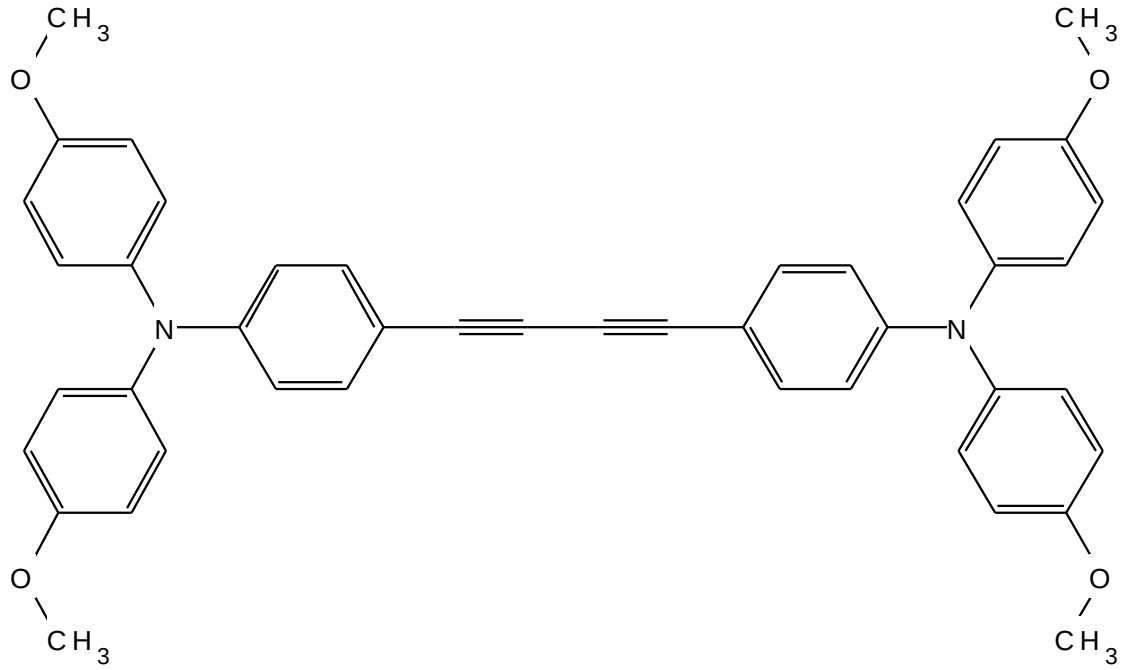

Figure 6.2: *bis-Triarylamine (4): Bis{4-[N,N-di(4-methoxyphenyl)amino]phenyl}butadiyne.*

arylamine 1, shown in Figure 6.1; and bis{4-[N,N-di(4-methoxyphenyl)amino]phenyl}butadiyne, labeled triarylamine 4, shown in Figure 6.2. These two molecules (and the other *bis*-Triarylamines shown in Figure 3.2) are composed of two symmetric triphenylamine groups that are connected by a hydrocarbon conjugated bridge. The terminal aryl groups having methoxy groups in 4-position. The bridge in triarylamine 1 is a simple benzene ring connected, at positions 1 and 4, to the two nitrogen atoms of each triphenylamine group; while that of triarylamine 4 is a Bis-phenyl butadiene. The main characteristic of these molecules is the high conjugation and, therefore, the strong π character of the bridge unit. It should be also noted that the geometries of both the neutral and cation Triarylamines 1 and 4 are not planar, since there are dihedral angles between the two triphenylamine groups on each molecule and between the aryls of each triphenylamine group in each molecule.

In principle, the two nitrogen atoms in these two systems serve as a charge donor/acceptor in the cation state while the bridge serves as a charge mediator. Taking the last point in consideration, a two state model, like that used for Spiro, may not properly describe these kind of systems where a third state, that correspond to the bridge, my actively participate

in the charge transport during an ET reaction. Therefore, the inclusion of a third state is most likely necessary.

The point group of both neutral Triarylamines 1 and 4 is D_2, with the principal axis of rotation, the C_2 axis, is the z axis that passes through the two nitrogen atoms (see Figures 6.1 and 6.2). If an electron is extracted from the system of these two molecules, the charge, will not be distributed equivalently on both sides of the system. Either a strong localization of the charge in one equilibrium geometry or a very weak charge localization will distort the molecular geometry of the ground state, leaving the cation with a lower symmetry C_2 point group through the whole range of the reaction coordinate, except at the point where the charge is totally delocalized (the saddle point in the case of a class II bistable compound), where the point group is D_2.

The classification of Triarylamines 1 and 4 cations, and other *bis*-triarylamine molecules, into class II valence trapped and class III charge delocalized systems is not always straightforward and clear. Though it is generally accepted that this family is a class II/III transition [259, 260, 307, 311], some studies had shown that triarylamine 4^+ is a class II localized mixed-valence system [307, 311], while triarylamine 1^+ is a class III system [311]. Earlier works had suggested that molecule 1^+ is a class II/III borderline system [239–241, 307, 309].

Practically, these two molecules are relatively very large in size to perform correlated *ab-initio* geometry optimizations and highly correlated *ab-initio* single point calculations. This is specially true for triarylamine 4 where there are 346 electrons distributed in 50 second-row atoms and 36 hydrogen. This was one of the main difficulties on performing calculations on Triarylamines 1^+ and 4^+.

6.2 Triarylamine 1 cation

The energies of the Triarylamine 1^+ molecule calculations using CASDI code using SZ basis set, where the guess MO's were localized, for the two geometries C_2 and D_2 shows no bistability of this molecule. The absolute energy of the geometry at D_2 was around 10^{-5} hartree lower than that of C_2 ($\xi = 0.5$) structure. This indicates that PES of the ET in Triarylamine 1^+ is almost flat through the reaction path between the supposed two minima points. However, the orbitals of the HOMO and LUMO of this molecule conducted at CASSCF(2/1) active space at SZ basis set, where the two active space orbitals are HOMO and LUMO MO's, using the localization of the guess orbitals shows that these orbitals are

localized each on a nitrogen atom, see Figure 6.3.

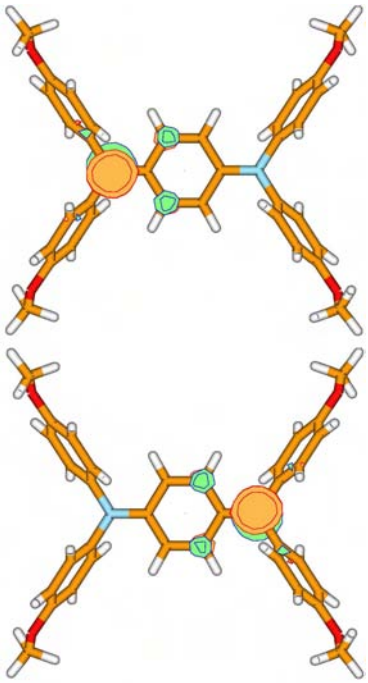

Figure 6.3: *bis-triarylamine* 1*: Molecular orbitals (HOMO up and LUMO bottom) of Bis{4-[N,N-di(4-methoxyphenyl)amino]phenyl}butadiyne obtained by localizing the guess orbitals at CASSCF(1/2) level.*

6.3 Triarylamine 4 cation

6.3.1 HF and DFT energies of the optimized geometries

Table 6.1 below, reports the energies of two points, namely D_2 and C_2 of the neutral, bication, and the cation of triarylamine 4^+ using HF and DFT methods to optimize the geometry, with DZP basis set. From Table 6.1, we can conclude that DFT methods predict a two-well PES for the ground state, whereas it is not the case for the geometries obtained at HF level of optimization. The LUMO, HOMO and SOMO orbitals of the neutral Triarylamine 4 optimized at HF/DZP level are shown in Figure 6.5. While that of the C_2 geometry optimized at HF/DPZ and starting by a guess geometry where the two halves of the molecules are connected together by attaching a neutral half molecule to a

Table 6.1: *Energy (a.u.) of triarylamine* 4 *(indicated as T4 in this table), neutral, cation ($^+$) and bication ($^{++}$) using ROHF/ANO-DZP and DFT-B3LYP/ANO-DZP methods.*

T4 geom/opt	DFT/DZP	HF/DZP*
$T4$ D_2/HF		-2095.88456718
$T4^{++}$ D_2/HF		-2095.40573826
$T4^+$ D_2/HF		-2095.66930134
$T4^+$ C_2/HF		-2095.66930087
ΔE (kJ/mol)		0.001
$T4^+$ D_2/HF		-2095.66930134
$T4^+$ C_2/HF(mix)**		-2095.66847332
ΔE (kJ/mol)		2.174
$T4^+$ D_2/DFT	-2107.66894878	-2095.64529745
$T4^+$ C_2/DFT	-2107.66924111	-2095.64657110
ΔE (kJ/mol)	-0.768	-3.344
$T4^+$ D_2/DFT	-2107.66894878	-2095.64529745
$T4^+$ C_2/DFT(mix)**	-2107.66922682	-2095.64639050
ΔE (kJ/mol)	-0.730	-2.870

* HF energies are calculated after the geom. opt. in DFT for each structure.
** (mix) indicates an input starting geometry half-mixed dication/neutral optimized geometries.

bication other half, are shown in Figure 6.6 where we can clearly see the localization of the orbitals of SOMO and HOMO on each side of the molecule, though this localization is not symmetric. This was not found in the other geometries obtained by other methods shown in Table 6.1.

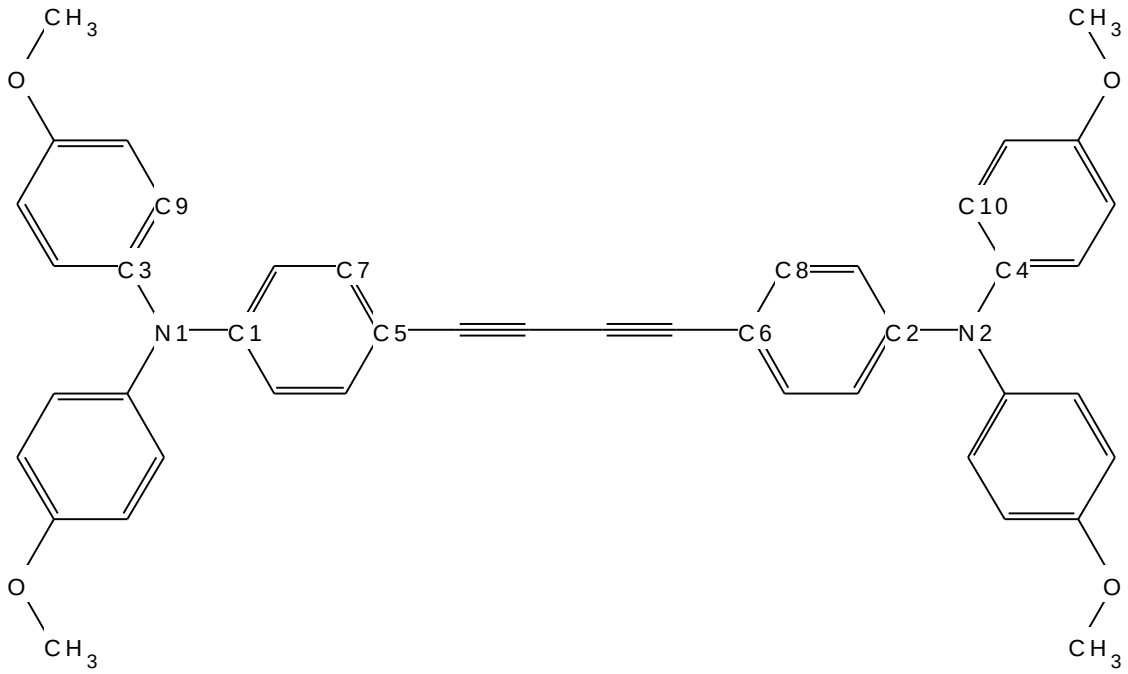

Figure 6.4: *Molecule triarylamine* 4 *with atom numbering*

6.3.2 Geometries of the optimized structures

The bond lengths and the bond angles of triarylamine 4 found by the methods used in Table 6.1 are reported in Table 6.2 together with the results previously published by Bredas *et al.* [311]. Figure 6.4 should be consulted for bond lengths and bond angles numbering. Generally speaking, the geometrical differences between the "active" sites of the two sides of the molecule are small, for example, much less than that found in Spiro, see Chapter 4. However the CN bond lengths of the two sides are found to be asymmetric when geometry was optimized by both HF and DFT in the case of mixing the two half bication and half neutral structures. The comparison with the results found by Bredas *et al.* could be misleading since they have supposed a totally symmetric geometry for the ground and excited state cation equilibrium geometry.

Table 6.2: *Geometry of Triarylamine* 4 *(indicated as T*4 *in the Table), neutral, cation and bication. Distances are in Angstroms. (Br) stands for the geometries of T*4 *found by Bredas et al. in JACS 2002, vol. 124, pp. 10519 - 10530 using DFT B3LYP method and* $6-31G^{**}$ *basis. CN1: bond distance between C1 and N1, CN2: bond distance between C2 and N2, CN3: bond distance between C3 and N1, CN4: bond distance between C4 and N2, DH1: dihedral angle between C7, C5, C6, and C8, DH2: dihedral angle between C4, N2, N1, and C3, DH3: dihedral angle between C1, N1, C3, and C9, and DH4: dihedral angle between C2, N2, C4, and C10. See Figure 6.4 for atom numbering.*

	CN1	CN2	CN3	CN4	DH1	DH2	DH3	DH4
$T4$ (Br)	1.408				4	65	48	
$T4^{+}$ (Br)	1.390				1	54	48	
$T4^{+*}$ (Br)	1.418				1	80	40	
$T4$ D_2/HF	1.397	1.397	1.421	1.421	23.911	30.213	59.678	59.678
$T4^{++}$ D_2/HF	1.423	1.423	1.394	1.394	61.363	37.918	37.436	37.436
$T4^{+}$ D_2/HF	1.347	1.347	1.436	1.436	4.190	24.981	75.104	75.104
$T4^{+}$ C_2/HF	1.347	1.347	1.436	1.436	4.234	24.968	75.156	75.132
$T4^{+}$ C_2/HF(mix)	1.382	1.413	1.427	1.400	26.089	31.884	71.652	39.099
$T4^{+}$ D_2/DFT	1.384	1.384	1.429	1.429	13.957	32.602	50.531	50.531
$T4^{+}$ C_2/DFT	1.385	1.385	1.429	1.429	12.570	32.282	51.976	52.017
$T4^{+}$ C_2/DFT(mix)	1.385	1.785	1.429	1.429	12.761	32.401	52.004	51.509

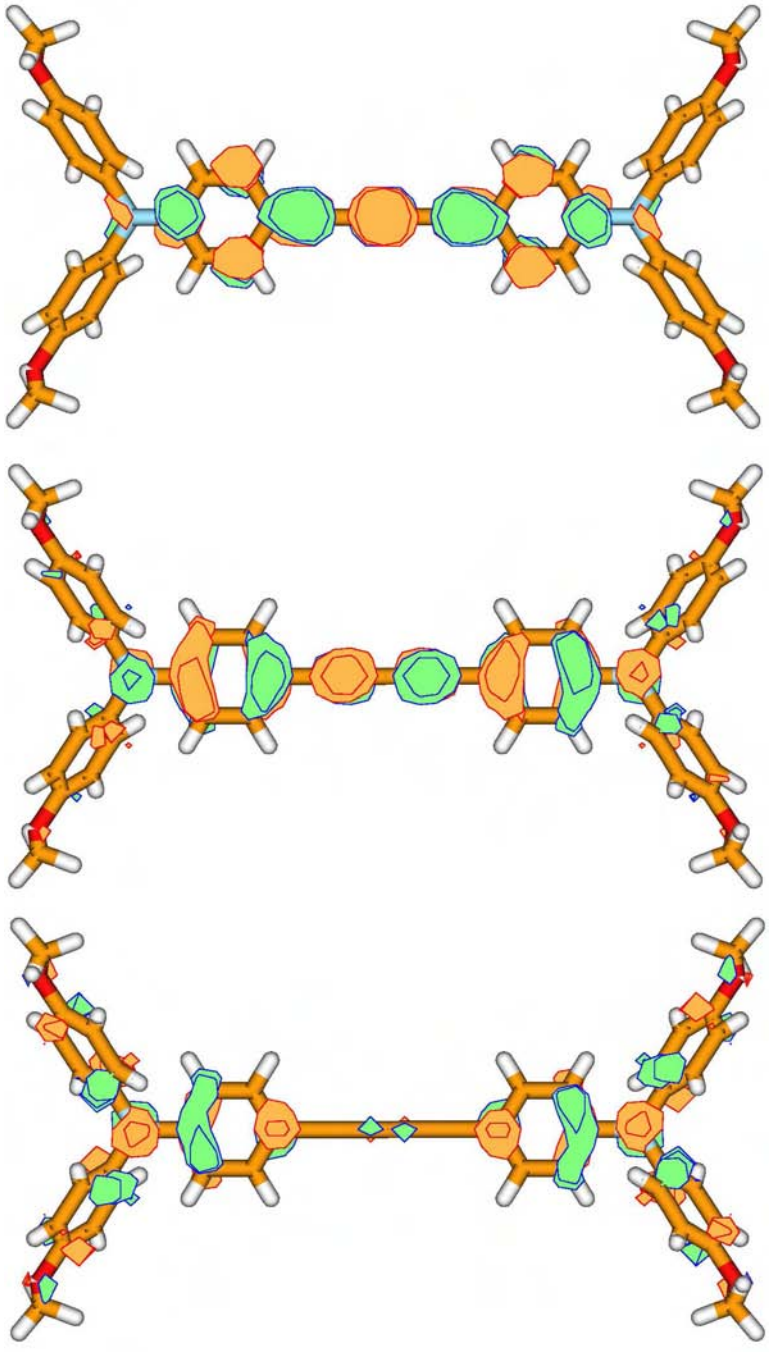

Figure 6.5: *ROHF/ANO-DZP MO's of Triarylamine* 4 D_2*/HF: bottom, SOMO; middle, HOMO; top, LUMO*

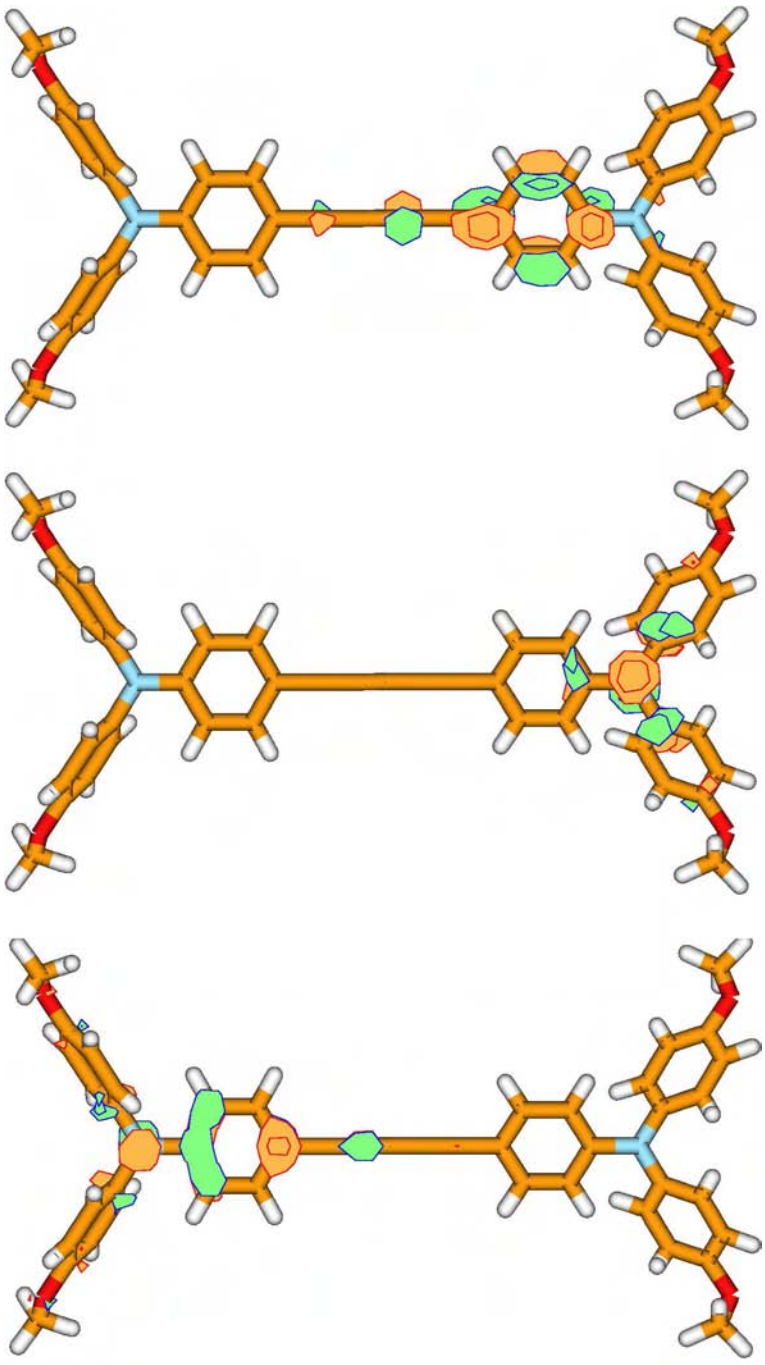

Figure 6.6: *ROHF/ANO-DZP MO's of Triarylamine* 4^{+} *C_2/HF(mix): bottom, SOMO; middle, HOMO; top, LUMO*

Chapter 7

Conclusion

Dans ce travail, une enquête théorique et computationnelle de la structure électronique et des coordonnées de réaction du transfert de charge de certains composés à valence mixte a été réalisée. Les composés à valence mixte utilisés dans cet étude allaient d'un système moléculaire modèle, relativement petit, comme le cation du Spiro, aux molécules relativement grandes et "réelles" comme les cations des composés à valence mixte, comme les *bis*-triarylamines. Un nouveau genre de système moléculaire, les chaînes linéaires atomiques de béryllium, étudiées pour la première fois en tant que composés à valence mixte, a été également montré.

Les outils théoriques et informatiques utilisés dans ce travail ont été appliqués différemment selon les limites de calculs confrontés à cause de la taille de la molécule, les jeux de base, et la taille de l'espace actif utilisé pour le composé à valence mixte correspondant. L'utilisation des méthodes *ab-initio* multi-référence pour l'étude des composés à valence mixte est pertinente, car ces méthodes peuvent décrire correctement ces systèmes moléculaires avec des fonctions d'onde de plusieurs configurations électroniques dans leurs états fondamentaux. Les avantages de l'utilisation des orbitales localisées dans les méthodes *ab-initio* multi-référence utilisées pour certains de ces composés à valence mixte ont été décrites.

Par ailleurs, la bistabilité du cation de Spiro et des chaînes liéaires atomiques de béryllium (Be_n) a été démontrée par nos calculs. La bistabilité des deux molécules cationiques *bis*-triarylamines étudiées dans ce travail n'a pas été clairement montrée a cause des limites de calculs.

Dans le cadre de ce travail, il a été montré que, pour le cas du Spiro, l'inclusion de la corrélation dynamique (CAS+SD) aux fonctions d'onde de corrélation non-dynamique

(CAS-SCF) est nécessaire pour obtenir des résultats quantitatifs précis pour le calcul de la structure électronique des composés à vlence mixte et ses propriétés moléculaires. Les problèmes liés au orbitales CAS-SCF canoniques avec une grande taille d'espace actif dans les composés à valence mixte peuvent être surmontés efficacement en utilisant des orbitales multi-référence localisées. La corrélation "exagérée" trouvée en utilisant le niveau (CAS+S) dans le cas de Spiro ne peut pas nécessairement être généralisés à d'autres composés à valence mixtes. Cependant, plusieurs expériences sont nécessaires pour comprendre les raisons d'un tel comportement et pour conclure si ce phénomène se reproduit dans d'autres systèmes à valence mixte.

L'avantage principale d'utiliser des chaînes linéaires atomiques de béryllium (Be_N) en tant que composés à valence mixte est la possibilité d'un réglage fin des caractéristiques propres au composés à valence mixtes, comme $2V_{ab}$, E_a et E_{opt}, et la possibilité d'introduire d'autres unités atomiques a la chaîne, ou même la possibilité d'utiliser des chaines "ramifiées", au lieu de linéaires, afin d'avoir plus de deux centres d'oxydoréduction, et donc, des composés avec des nouvelles caractéristiques. Cette étude montre que les recherches futures de chaînes qui contiennent des clusters de béryllium sont très attrayantes. En outre, la possibilité de faire un "design" moléculaire d'un grand nombre de structures chimiques de ces composés à valence mixte qui ne sont pas coûteuses au niveau de calcul, même au niveaux CAS-SCF et CAS+SD, est une avantage important de l'étude des chaînes de béryllium. Il est également suggéré que l'étude expérimentale de ces composés à valence mixte intéressante est une étape importante pour étudier d'avantage la possibilité d'utiliser ce genre de composés dans les dispositifs moléculaires.

Chapter 8

Appendix

8.1 Other results in published articles: CASSCF, MRCI, and NEVPT calculations on Spiro

The following three published articles on Spiro molecular cation were mentioned and cited in sections §4.4.2 and 4.4.7.

Ab-Initio Multi-reference Study of a Bistable Spiro Molecule

Wissam Helal, Benoît Bories, Stefano Evangelisti,
Thierry Leininger, and Daniel Maynau

Laboratoire de Physique Quantique UMR 5626 du CNRS, IRSAMC,
Université Paul Sabatier,
118, Route de Narbonne, 31062 Toulouse, Cedex, France
stefano.evangelisti@irsamc.ups-tlse.fr

Abstract. CAS-SCF and MRCI calculations are presented, in order to investigate the electronic states involved in the intramolecular charge-transfer process of a bistable spiro cation. The potential energy curves of the ground and the first three excited states have been calculated, and a double well potential has been obtained for the ground state. The effect of dynamical correlation was found to be crucial for a quantitative description of this system. Our results also indicate the usefulnes of a local-orbital description of bistable systems.

1 Introduction

Mixed-Valence compounds have been widely studied in recent times, particularly for their interest in molecular electronics [1]. Although many of the considered systems contain transition-metal atoms as mixed-valence centers [2], purely organic compounds have also been investigated theoritically [3]. Among these types of molecules, the spiro $\pi - \sigma - \pi$ system $C_{13}N_2H_{14}$ has been often studied as a model system [3]-[7], since its relatively small size, permits high-level *ab initio* investigations.

The geometry of the spiro molecule, which is the object of the present study, is shown in Figure 1. The system consists of two π moities, placed on two orthogonal planes, and separated by a σ bridge. If an electron is extracted from this molecule, the resulting hole tends to localize either on the left or the right π system, inducing a deformation of the molecular geometry. Therefore two equivalent minima exist for the cation, and the ground state presents the double well curve which is typical for mixed-valence systems.

In this contribution, we present the results of Complete-Active-Space Self-Consistent-Field (CAS-SCF) and subsequent Multi-Reference Configuration-Interaction (MRCI) investigations on the spiro molecular cation of Figure 1. The ground-state geometry of this system shows two equivalent minima having C_{2v} symmetry, separated by a D_{2d} saddle point, at any level of calculation. It is shown that the contribution of the dynamical correlation is crucial in order to obtain quantitative results.

M. Gavrilova et al. (Eds.): ICCSA 2006, LNCS 3980, pp. 744–751, 2006.

Fig. 1. The spiro molecular system

Spiro cation was studied in the C_{2v} point group (if the charge is localized on either one of the two aromatic moities in the molecule), while a D_{2d} geometry was taken for the totally delocalized state [6]. More recent studies, suggested C_1 and C_2 point groups for the two situations, respectively [3]. However, according to these calculations, the difference from exact C_{2v} and D_{2d} symmetries are extremely small. Therefore, in view of the preliminary character of the present investigation, we decided to use the high symmetry groups in this study.

2 Computational Details

The principal axis of rotation, the C_2 axis, is the straight line connecting the two nitrogen atoms. B_1, B_2 and two averaged states of A_2 symmetry (which will be designated as $A_2(1)$ and $A_2(2)$ in the present article) were calculated for the two geometries. No A_1 symmetry states were considered in this study since their energies are much higher than that for the other states. In all our CAS-SCF calculations, we were only interested in the π electrons of the cation, since these are the electrons engaged in the electron transfer process in conjugated systems.

Restricted Hartree Fock (RHF), CAS-SCF and Contracted MR-CI (C_MRCI) calculations were done using the MOLPRO computer code version 2002.6 [8] and MOLCAS code version 6.0 [9]. Both MOLPRO and MOLCAS codes can only treat abelian point groups. Therefore, since D_{2d} is a non-abelian group, D_{2d} symmetry orbitals calculations were performed using the C_{2v} symmetry generators.

Atomic Natural Orbitals (ANO) basis sets [10] were used in all calculations, by using different contraction levels: SZ ((1s) for H and (2s1p) for C and N), DZ ((2s) for H and (3s2p) for C and N), DZP ((2s1p) for H and (3s2p1d) for C and N) and TZP ((3s1p) for H and (4s3p1d) for C and N). Geometry optimizaton of the A_2 state for both C_{2v} and D_{2d} geometries were calculated for the cation at the RHF level, by using the TZP basis set.

The Born-Oppenheimer potential surfaces were obtained by calculating the corresponding states energies of each piont on the reaction geometry coordinate, which in turn was obtained by mixing linearly the optimized coordinates of the two equilibrium C_{2v} geometries [6]:

$$Q(\xi) = \xi Q_B + (1 - \xi) Q_A \tag{1}$$

Table 1. Energy differences (KJ/mol) between the different states of the spiro cation, computed at (7/4) CAS-SCF level and by using different basis sets. For each method, the energy zero has been taken as the energy of the ground state $A_2(1)$ in the D_{2d} geometry.

CAS-SCF:	SZ	DZ	DZP	TZP
D_{2d}				
$A_2(1)$	0.000	0.000	0.000	0.000
$A_2(2)$	9.043	9.987	9.664	9.626
B_1	44.748	51.646	46.521	45.181
B_2	44.748	51.646	46.521	45.181
C_{2v}				
$A_2(1)$	-8.328	-5.640	-6.528	-6.753
$A_2(2)$	48.362	40.185	39.852	39.390
B_1	52.655	56.923	51.802	50.231
B_2	66.710	69.636	63.421	61.731

where $Q(\xi)$ is the nuclear configuration at any point on the reaction path, while Q_A and Q_B represent the nuclear coordinates of the two C_{2v} geometries. The mixing parameter ξ was varied from -1.00 to 2.00 in steps of 0.05. In such a way, Q_A (the first C_{2v} minimum), corresponds to the point $\xi = 0.00$, where the positive charge is localized on one moity of the molecule; Q_B (the second C_{2v} minimum) corresponds to the point $\xi = 1.00$, where the positive charge is localized on the second moity; the D_{2d} geometry, being the average of the two C_{2v} geometries, is represented by the point $\xi = 0.50$ on the reaction coordinate. In order to test the quality of this averaged D_{2d} geometry, the corresponding state energies of the later were compared with those of the optimized D_{2d} geometry. The results show a very small difference between the averaged and the optimized D_{2d} geometries (see next section). For this reason, we believe that the geometry path obtained through equation (1) is very close to the optimal one.

The energy of the A_2, B_1 and B_2 states of the potential surface were calculated, for different values of the parameter ξ, with a TZP basis using CAS-SCF method with 7 active electrons and 4 active space π orbitals (one b_1, one b_2 and two a_2). Contracted MRCI(SD) were also performed using the same active space, with the $1s$ orbitals of the carbon and nitrogen atoms being freezed.

In order to assess the validity of a Contracted approach, uncontracted MRCI(SD) were also performed for the two key points on the reaction coordinate,

Table 2. Energy differences (KJ/mol) between the different states of the spiro cation, computed at Contracted MRCI (C_MRCI) and Uncontracted MRCI (MRCI) by using different basis sets. For each method, the energy zero has been taken as the energy of the ground state $A_2(1)$ in the D_{2d} geometry.

C_MRCI:	SZ	DZ	DZP	TZP	*MRCI:*	SZ	DZ
D_{2d}							
$A_2(1)$	0.000	0.000	0.000	0.000		0.000	0.000
$A_2(2)$	9.323	10.290	10.077	9.999		9.246	10.187
B_1	53.972	62.400	61.379	59.461		51.888	61.207
B_2	53.972	62.400	61.379	59.461		51.888	61.207
C_{2v}							
$A_2(1)$	-6.684	-4.669	-5.196	-5.580		-6.476	-4.410
$A_2(2)$	47.076	39.319	39.042	38.523		47.325	39.455
B_1	59.732	65.467	64.937	62.704		58.181	64.810
B_2	78.682	82.888	80.668	78.246		76.537	81.448

namely, the C_{2v} minimum ($\xi = 0.00$) and the D_{2d} saddle point ($\xi = 0.50$). This was done by using the Toulouse program CASDI [11], and for the two smallest basis sets only.

These two points, were also chosen to perform a CAS-SCF/TZP calculation, using the MOLPRO code, with a larger active space: we selected 10 active orbitals (three b_1, three b_2 and four a_2), which can represent in principle the complete (valence) π system of this molecule. Local CAS-SCF/SZ calculation with 8 active space orbitals (two b_1, two b_2 and four a_2) were done using CASDI code. The justification of the choice of the later active space is discussed in the next secton.

3 Results and Conclusion

The energy differences (KJ/mol) between the different states, with 4 active orbitals computed by using different methods, are shown in Tables 1 and 2. For each type of calculation, the energy zero has been taken as the energy of the ground state $A_2(1)$ in the D_{2d} geometry.

In Table 3 the difference between the results of the D_{2d} geometry, obtained with the averaged and optimized geometries (at CAS-SCF TZP level), are reported. From a comparison with the corresponding results of Table 1, it is clear that the effect of replacing the optimized D_{2d} geometry by the averaged one is extremely small (about 0.8 KJ/mol at most).

748 W. Helal et al.

Table 3. Energy differences (KJ/mol) between the states of the spiro cation, computed at the optimized and the averaged D_{2d} geometries, using TZP basis set

CAS-SCF		
	D_{2d}(opt)	D_{2d}(opt) - D_{2d}(av)
$A_2(1)$	-0.112	-0.112
$A_2(2)$	9.697	0.017
B_1	44.378	-0.803
B_2	44.378	-0.803

The reaction coordinates of the spiro cation calculated at the (7/4) CAS-SCF/TZP for the ground and the first three excited states are shown in Figure 2 (top). A smooth adiabatic two-well curve was obtained for the ground state, while a parabolic curve is obtained for the first excited state. These two lower states have an A_2 symmetry and correspond actually to the averaged two states of A_2 ($A_2(1)$and $A_2(2)$). The second and third excited states are degenerate at the D_{2d} geometry and correspond to the B_1 and B_2 symmeties. In the electron transfer process, an electron is excited at any equilibium C_{2v} geometry, from the ground to the first excited state. This transition is governed by Frank-Condon principle. After geometrical rearrangement to D_{2d} geometry the electron will make transition to the ground state followed by a geometrical relaxation to the other side of the molecule.

In Figure 2 (bottom), the reaction coordinates of the ground and first three excited states of the spiro cation calculated with MRCI(SD)/TZP are shown. The global behaviour of CAS-SCF and MRCI are similar, although the well depth is lower at MRCI level. On the other hand, the energy of the excited states of B symmetry tends to be higher at MRCI level.

It can be seen from Table 2 that the effect of dynamical correlation is very important in order to get quantitative results on this mixed-valence system. This is particularly true as far as the well depth is concerned, since its value is reduced by about 20% at C_MRCI level. A much smaller reduction is shown at uncontracted MRCI level. Energy differences between the two non-crossing states are considerably less affected by dynamical correlation.

In order to improve these results, we were interested in consediring the whole π valence system of the molecular cation. The results obtained with the 10 active orbitals show a different physical content, since some of the π orbitals are replaced by orbitals having a σ character. This is a comon problem with CAS-SCF algorithms based on canonical orbitals, and was one of the reasons that pushed our group to the developement of the local CAS-SCF algorithm [12], [13].

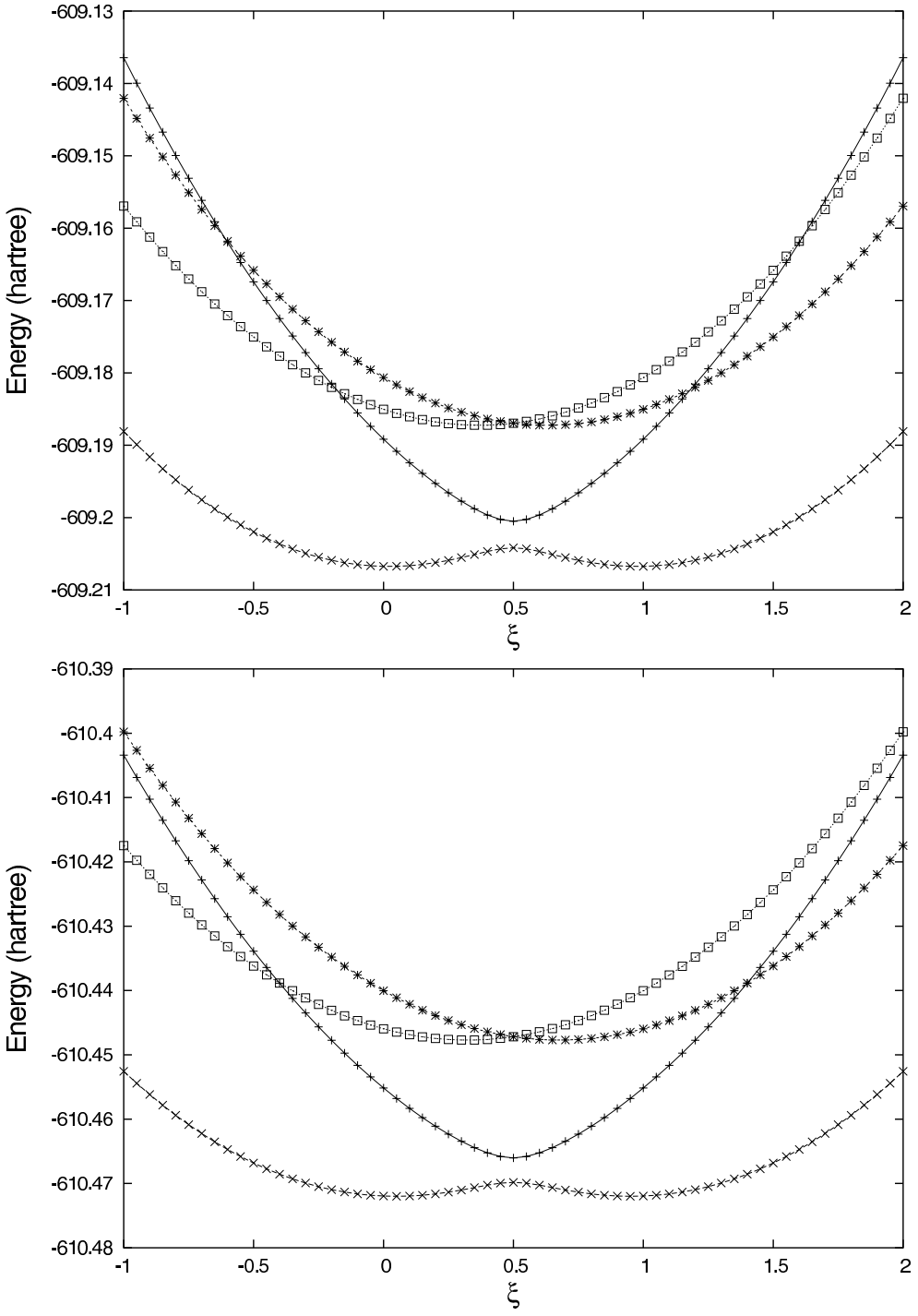

Fig. 2. Potential energy curves, in a.u., of the spiro cation for the ground and the first three excited states, as a function of the mixing parameter ξ: CAS-SCF/TZP (top), C_MRCI/TZP (bottom). ($\times$) $A_2(1)$, ($+$) $A_2(2)$, ($*$) B_1, and ($\Box$) B_2.

Table 4. Energy differences (KJ/mol) between the different states of the spiro cation, computed at Localized (7/8) CAS-SCF using SZ basis set. For each method, the energy zero has been taken as the energy of the ground state $A_2(1)$ in the D_{2d} geometry.

Localized CAS-SCF:	SZ
D_{2d}	
$A_2(1)$	0.000
$A_2(2)$	8.147
B_1	69.673
B_2	69.673
C_{2v}	
$A_2(1)$	-4.011
$A_2(2)$	44.775
B_1	75.360
B_2	96.261

This directed us to perform Local CAS-SCF calculation. We used an active space composed of $2b_1$, $2b_2$ and $4a_2$ orbitals. This corresponds to the π systems of the eight carbon atoms located on the external cycles. The C-N distance has a very small dependence on the geometry rearrangement described by the reaction coordinate $Q(\xi)$. This justifies the exclusion of the two nitrogen π orbitals (one b_1 and one b_2 orbitals) from the active space.

The energies of the different states of the two geometries for the 8 orbitals active space using lacal CAS-SCF are presented in table 4. With this active space, the depth of the two equivalent minima is strongly reduced, being 4.1 KJ/mol with the smallest basis set. This value should be compared with 8.3 KJ/mol, obtained with the 4 orbitals active space. The difference between the two A_2 states at D_{2d} is also reduced, but to a smaller extent: it passes from 9.0 KJ/mol with the (7/4) active space to 8.1 KJ/mol with the (7/8) space.

As a more general conclusion, it can be said that the use of large active space seems to be necessary for an accurate description of the small energy differences found in these types of molecules. However, the control of the nature of the active space is an extremely difficult task in canonical CAS-SCF, and the use of large active space is often problematic. For this reason, we believe that the use of local orbitals in a CAS-SCF context can be a very powerful tool for the treatment of mixed-valence systems.

References

1. Joachim, C., Gimzewski, J. K., Aviram, A.: Electronics using hybrid-molecular and mono-molecular devices. Nature. **408** (2000) 541–548
2. Launay, J.-P.: Long-distance intervalence electron transfer. Chem. Soc. Rev. **30** (2001) 386–397
3. Dehareng, D., Dive, G., Moradpour, A.: Ab Initio Study of Organic Mixed Valency. Int. J. Quantum Chem. **76** (2000) 552–573
4. Aviram, A., Ratner, M. A.: Molecular rectifiers. Chem. Phys. Lett. **29** (1974) 277–283
5. Aviram, A.: Molecules for Memory, Logic, and Amplification. J. Am. Chem. Soc. **110** (1988) 5687–5692
6. Farazdel, A., Dupuis, M., Clementi, E., Aviram, A.: Electric Field Induced Intramolecular Electron Transfer in Spiro π Electron Systems and Their Suitability as Molecular Electronic Devices. A Theoretical Study. J. Am. Chem. Soc. **112** (1990) 4206–4214
7. Sanz J. F., Calzado C. J., Marquez, A.: DFT *versus* CI Determination of the Electron-Transfer Matrix Element in some Case Examples. Int. J. Quantum Chem. **76** (2000) 458–463
8. R. D. Amos, A. Bernhardsson, A. Berning, P. Celani, D. L. Cooper, M. J. O. Deegan, A. J. Dobbyn, F. Eckert, C. Hampel, G. Hertzer, P. J. Knowels, T. Korona, R. Lindh, A. W Lloyd, S. J. McNicholas, F. R. Manby, W. Meyer, M. E. Mura, A. Nicklass, P. Palmieri, R. Pitzer, G. Raunhut, M. Schütz, U. Schumann, H. Stoll, A. J. Stone, R. Tarroni, Thorsteinsson, and H.-J. Werner. MOLPRO Version 2002.6
9. Andersson, K., Barysz, M., Bernhardsson, A., Blomberg, M. R .A., Carissan, Y., Cooper, D. L., Fulscher, M. P., Gagliardi, L., de Graaf, C., Hess, B. A., Hagberg, D., Karlstrom, G., Lindh, R., Malmqvist, P.-A., Nakajima, T., Neogrady P., Olsen, J., Raab, J., Roos, B. O., Ryde, U., Schimmelpfennig, B., Schutz, M., Seijo, L., Serrano-Andres, L., Siegbahn, P. E. M., Stalring, J., Thorsteinsson, T., Veryazov, V., Widmark, P.-O. MOLCAS Version 6.0, Lund Universiy, Sweeden, 2004
10. Widmark, P.-O., Malmqvist, P.-A., Roos, B.: Density matrix averaged atomic natural orbital (ANO) basis sets for correlated molecular wave functions. I. First row atoms. Theoret. Chem. Acta. **77** (1991) 291–306
11. Maynau, D., Ben-Amor, N., Pitarch-Ruiz, J.: CASDI Program, University of Toulouse, Toulouse, France, 1999
12. Maynau, D., Evangelisti, S., Guihéry, N., Calzado, C. J., Malrieu, J.-P.: Direct generation of local orbitals for multireference treatemnt and subsequent uses for the calculaton of the correlation energy. J. Chem. Phys. **116** (2002) 10060–10068
13. Angeli, C., Evangelisti, S., Cimiraglia, R., Maynau, D.: A novel perturbation-based complete active space–self-consistent-field algorithm: Application to the direct calculation of localized orbitals. J. Chem. Phys. **117** (2002) 10525–10533

THE JOURNAL OF CHEMICAL PHYSICS **128**, 174102 (2008)

Can the second order multireference perturbation theory be considered a reliable tool to study mixed-valence compounds?

Mariachiara Pastore,[1] Wissam Helal,[2] Stefano Evangelisti,[2] Thierry Leininger,[2] Jean-Paul Malrieu,[2] Daniel Maynau,[2] Celestino Angeli,[1,a)] and Renzo Cimiraglia[1]
[1]*Dipartimento di Chimica, Università di Ferrara, Via Borsari 46, I-44100 Ferrara, Italy*
[2]*Laboratoire de Chimie et Physique Quantiques, UMR 5626, Université de Toulouse et CNRS, 118 Route de Narbonne, F-31062 Toulouse, France*

(Received 15 February 2008; accepted 26 March 2008; published online 2 May 2008)

In this paper, the problem of the calculation of the electronic structure of mixed-valence compounds is addressed in the frame of multireference perturbation theory (MRPT). Using a simple mixed-valence compound (the 5,5′ (4*H*,4*H*′)-spirobi[ciclopenta[c]pyrrole] 2,2′,6,6′ tetrahydro cation), and the *n*-electron valence state perturbation theory (NEVPT2) and CASPT2 approaches, it is shown that the ground state (GS) energy curve presents an unphysical "well" for nuclear coordinates close to the symmetric case, where a maximum is expected. For NEVPT, the correct shape of the energy curve is retrieved by applying the MPRT at the (computationally expensive) third order. This behavior is rationalized using a simple model (the ionized GS of two weakly interacting identical systems, each neutral system being described by two electrons in two orbitals), showing that the unphysical well is due to the canonical orbital energies which at the symmetric (delocalized) conformation lead to a sudden modification of the denominators in the perturbation expansion. In this model, the bias introduced in the second order correction to the energy is almost entirely removed going to the third order. With the results of the model in mind, one can predict that all MRPT methods in which the zero order Hamiltonian is based on canonical orbital energies are prone to present unreasonable energy profiles close to the symmetric situation. However, the model allows a strategy to be devised which can give a correct behavior even at the second order, by simply averaging the orbital energies of the two charge-localized electronic states. Such a strategy is adopted in a NEVPT2 scheme obtaining a good agreement with the third order results based on the canonical orbital energies. The answer to the question reported in the title (is this theoretical approach a reliable tool for a correct description of these systems?) is therefore positive, but care must be exercised, either in defining the orbital energies or by resorting to the third order using for them the standard definition. © *2008 American Institute of Physics*. [DOI: 10.1063/1.2911699]

I. INTRODUCTION

Due to the ubiquitousness of electron transfer (ET) reactions in inorganic, organic, biological, and physical chemical systems, a large attention has been devoted, in particular in the past decades, to the study of the control and the comprehension of such processes.[1] In the domain of the intramolecular ET, mixed-valence (MV) compounds play a relevant rôle as simple model systems suitable for understanding the adiabatic ET phenomena.[2–7] Furthermore, MV compounds are extensively investigated, both experimentally and theoretically, for their appealing optical and magnetic properties as well as for their possible application in molecular electronics and photonics.[8] The simplest MV compound is composed of two moieties (hereafter indicated with A and B), linked either directly or via a bridge, where an intervalence electron transfer (IV-ET) occurs between the two redox sites being in different oxidation states. The electronic coupling between the two ideally noninteracting systems, where the electron (hole) is localized either on the left or on the right moiety, governs the communication between the two subunits, determining the general properties of the system. Such interaction is expressed by the Hamiltonian matrix element $\hat{\mathcal{H}}_{ab}=\langle\Psi_a|\hat{\mathcal{H}}|\Psi_b\rangle$, where Ψ_a and Ψ_b are the diabatic states, one with the electron/hole localized on the (left) subunit A and the other on the (right) subunit B. According to the usual classification,[9] the MV systems can be divided into three classes: Class I with the redox centers strongly localized (complete valence trapping); class II, where a partial delocalization is observed, arising from a weak electronic interaction (valence trapping); and, finally, class III, for which the strong electronic coupling gives rise to a complete delocalized system with a single minimum for the ground state (GS) (delocalized valency). The class II compounds and, in particular, the borderline compounds between class II and class III have attracted great interest in recent years. The appealing feature of these IV systems is, indeed, the appearance, in the near-infrared (NIR), of a characteristic absorption band (termed IV or CT band), associated with the optical excitation from the minimum of the GS to the lowest excited state. The analysis of this band, based on Hush's theory,[10,11] allows the important model parameters to be extracted, for instance,

a)Author to whom correspondence should be addressed. Electronic mail: anc@unife.it.

the electronic coupling $\hat{\mathcal{H}}_{ab}$ and the reorganization energy λ. While the properties of the inorganic MV compounds have been largely studied and well understood,[7,12–18] less attention has been paid to the purely organic MV systems, although, recently, a number of experimental and theoretical studies have been published.[19–29]

The theoretical study of these systems presents difficulties: The effect of the dynamical correlation has to be evaluated, improving the qualitative minimal description given by the simple mixing of the quasidegenerate determinants accounting for the two charge distributions. These difficulties are related to the intrinsic multireference (MR) nature of the ground and the first excited state wavefunctions of these systems and to their dimension, which makes impractical the use of too expensive computational approaches. MR perturbation theory (MRPT), among the other MR methods, is a good candidate due to the reliability shown in many MR applications and due to the scaling properties of the computational cost with respect to the dimensions of the system. This paper addresses the problem of the definition of an efficient computational strategy, in the frame of MRPT methods, for the description of MV compounds. To this aim, a small MV organic molecule has been studied and use has been made of a simple model for which analytic solutions are possible.

Due to its relatively small size, which allows calculations of high accuracy to be carried out, some of the previously published theoretical studies[21,30–33] were addressed to the spectroscopic investigation of a model $\pi-\sigma-\pi$ spiro compound (5,5′(4*H*,4*H*′)-spirobi[ciclopenta[c]pyrrole] 2,2′,6,6′ tetrahydrocation, termed "spiro" in the following). Recently, a MRCI study (CASSCF, CASCI and MRCI(SD)) on this system has been published,[33] (paper I in the following) where the spectroscopic features and the potential energy surface (PES) of the ground and the three lowest excited states were computed, in the framework of a simplified monodimensional two-state model.

As an extension of this MRCI study and prompted by the challenge of future applications to larger molecules, we have started an *ab initio* highly correlated characterization of the spiromonocation based on second and third order MR perturbation calculations. Making use of the *n*-electron valence state perturbation theory (NEVPT) approach,[34–38] developed in our group and already successfully applied to many interesting test cases,[39–46] we aim to set up an efficient and accurate methodology that can be possibly extended to actual MV compounds.

The present contribution is organized as follows: Sec. II presents the definition of the computational details; Sec. III shows that MRPT treatments [such as, for instance, NEVPT2 and CASPT2 (Ref. 47)] with a standard definition of the molecular orbitals (MOs) and of their energies are inadequate for the MV systems, leading to an unphysical description of the electronic energy curve as a function of the reaction coordinate. In the same section, it is shown that the application of the perturbation approach to the third order in the energy is able to restore the correct shape of the energy profile. The origin of such a behavior is illustrated in Sec. IV, by resorting to a simple Marcus-like two-state model comprising only three electrons in four orbitals. By using this model, a strategy based on the use of the canonical orbitals of a state-averaged calculation and with state-averaged orbital energies is proposed with the aim to overcome the failure of the second order perturbation treatment based on state-specific canonical orbitals and energies. This strategy is adopted in actual calculations on spiro in Sec. V, confirming its validity. Finally, Sec. VI reports some conclusive remarks.

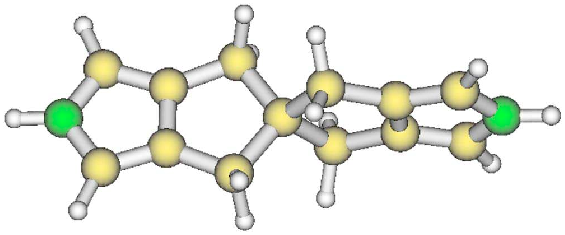

FIG. 1. (Color online) The spiro molecule.

II. COMPUTATIONAL DETAILS

The $\pi-\sigma-\pi$ spiro molecule (reported in Fig. 1) consists of two pyrrolic units (π systems), lying on two perpendicular planes, connected by a spirocicloalkane rigid σ bridge. The symmetry of the neutral molecule is D_{2d}, with the C_2 axis (the z axis) passing through the two N atoms; if an electron is removed from the system, the positive charge tends to localize on the left or on the right pyrrolic unit, distorting the symmetry and giving rise to two equivalent C_{2v} minima. These are separated by a symmetrical D_{2d} saddle point at the crossing seam, corresponding to the situation of a complete delocalization of the positive charge over the whole molecule.

Although some arguments about the equilibrium geometry of the spiro cation in either its left/right localized or delocalized structures have been provided and C_1 and C_2 symmetries have been, respectively, suggested,[21] here, as in Refs. 30, 32, and 33, we adopt the C_{2v} point group for the two minima with the localized charge and the D_{2d} symmetry for the structure at the saddle point. However, since the CASSCF wavefunctions were computed using the MOLCAS package,[48] which can only deal with Abelian point groups, the calculations for the non-Abelian D_{2d} group were carried out in the reduced C_{2v} subgroup.

As discussed in paper I, the ET process was studied by defining an *ad hoc* approximate reaction coordinate, obtained by the linear mixing of the Cartesian coordinates of the two C_{2v} geometries (left/right localized charge),

$$\mathbf{Q}(\xi) = \left(\tfrac{1}{2} - \xi\right)\mathbf{Q}_A + \left(\tfrac{1}{2} + \xi\right)\mathbf{Q}_B, \tag{1}$$

where the mixing parameter ξ was varied, in steps of 0.05, from −1.50 to +1.50 and $\mathbf{Q}_A$ and $\mathbf{Q}_B$ are vectors collecting the coordinates of the two optimized C_{2v} geometries. So, along this reaction coordinate, the two equivalent minima are found for ξ=−0.50 ($\mathbf{Q}_A$, charge localized on the left A pyrrolic unity) and ξ=0.50 ($\mathbf{Q}_B$, charge localized on the right B unit), whereas an "averaged" D_{2d} geometry is obtained at the crossing seam point (ξ=0.0). A detailed discussion about the

TABLE I. Spirocation: NEVPT2(can), NEVPT3(can), and CASPT2(can) energies (kJ/mol) of the ground state, $^2A_2(1)$, at ξ=0.0 and of the first excited state, $^2A_2(2)$, at ξ=0.0 and ξ=−0.5. All the energies are computed with respect to the energy of the GS at ξ=−0.5. For the sake of clarity, the energy splitting (ΔE, kJ/mol) between the two states at ξ=0.0 is also reported. For the CASPT2 results the level shift was varied from 0.0 to 0.2 hartree.

					CASPT2(can)		
States	CAS	SC-NEVPT2(can)	PC-NEVPT2(can)	SC-NEVPT3(can)	L.S. 0.0	L.S. 0.1	L.S. 0.2
ξ=−0.5							
$^2A_2(2)$	56.690	51.442	51.441	51.539	50.001	50.043	50.151
ξ=0.0							
$^2A_2(1)$	8.328	−5.117	−5.330	3.765	−5.790	−5.724	−5.503
$^2A_2(1)$	17.371	4.726	4.505	12.983	4.017	4.087	4.314
ΔE (ξ=0.0)							
$^2A_2(2)$	9.043	9.843	9.835	9.218	9.807	9.811	9.817

accuracy of such approximation can be found in paper I.

For the calculation of the reaction coordinate, we use the geometries optimized in paper I at the restricted open shell Hartree–Fock (ROHF) level with a triple zeta plus polarization (TZP) atomic natural orbital (ANO) basis set.[49]

The "π system" of the spiro cation consists of 11 π electrons and 10 π orbitals, so, at the single determinant level, in the C_{2v} point group, the electronic configuration is given by (σ-core) $(1b_1)^2(2b_1)^2(1b_2)^2(2b_2)^2(1a_2)^2(2a_2)^1$. The two states involved in the ET process belong to the A_2 symmetry (they are denoted as $^2A_2(1)$ and $^2A_2(2)$ in the following), corresponding to the ground and to the first excited state of the cation. State-averaged CASSCF calculations were performed for the two $^2A_2$ states, using the minimal active space, defined by three electrons in the two a_2 orbitals.

Following the previous work, the calculations were carried out with a basis sets of ANO-L (Ref. 49) type, and, in the light of the exploratory character of the present investigation (aimed essentially at the definition of an effective computational MRPT strategy), the smallest basis was used, with the contraction scheme C,N[2s1p] and H[1s]. Larger basis sets, for which a meaningful comparison with other theoretical approaches is more appropriate, are used in a forthcoming work.[50] Then, for all the NEVPT2 and CASPT2 calculations, the 1s orbitals were kept frozen.

All the energy differences are computed with respect to the energy of the GS of the cation at the C_{2v} geometry and in order to keep a coherent description, for this energy the value at ξ=+0.5 (ξ=−0.5) is always used, corresponding to that of the optimized geometry $\mathbf{Q}_A$ ($\mathbf{Q}_B$), even though it might not be the actual minimum of the curve.

III. RESULTS OF SECOND AND THIRD ORDER STANDARD MRPTs

This section is devoted to the discussion of the results obtained with a standard perturbation approach [hereafter indicated as NEVPT(can) and CASPT2(can)], which requires the use of state-specific canonical MOs and orbital energies. Therefore, the zero order wavefunctions were defined performing a state-averaged CASSCF calculation on the two $^2A_2$ states, followed by two distinct single-root CASCI calculations, in order to build the canonical orbitals and to compute the orbital energies for each state.

The computed CASSCF, NEVPT2(can), CASPT2(can), and NEVPT3(can) energy differences are collected in Table I. As is apparent from the energy profiles reported in Fig. 2, and from the computed values of the energy barriers in Table I, a nonphysical description of the two adiabatic PESs, in proximity of the symmetrical saddle point is obtained with both the NEVPT2 and CASPT2 approaches.

In particular, an increasing overestimation of the correlation energy, starting at ξ=−0.15 and culminating at ξ=0, is observed, with the consequent loss of the barrier and the appearance of a well in the avoided-crossing region. Indeed, both NEVPT2(can) and CASPT2(can) calculations, irrespective of whether a level shift is used or not in the latter case (thereby excluding an intruder state problem), yield for the $^2A_2(1)$ state the D_{2d} nuclear configuration ≃5 kJ/mol below the C_{2v} minimum. As shown in Fig. 2, the SC-NEVPT2(can) and the CASPT2(can) curves are almost parallel along the reaction coordinate and the computed energy differences col-

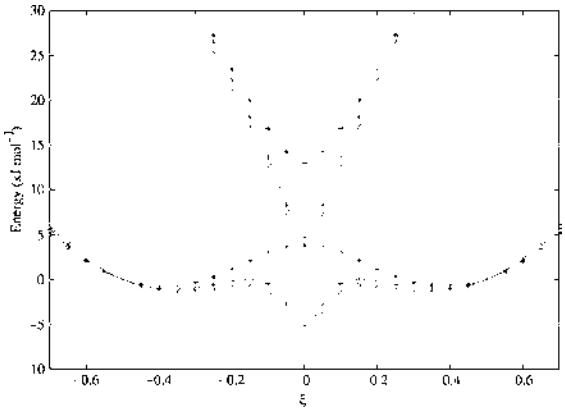

FIG. 2. SC-NEVPT2(can), SC-NEVPT3(can), and CASPT2(can) (no level shift) PES of the $^2A_2(1)$ and $^2A_2(2)$ states of the spiro cation. All the curves are shifted in order to have the two C_{2v} minima at zero energy. Full lines and "+" points, NEVPT2(can) energies; dashed lines and "×" points, CASPT2(can) energies; dotted lines and "*" points, NEVPT3(can) energies.

lected in Table I are in very good accordance. The energy splitting at the D_{2d} geometry amounts roughly to 9.8 kJ/mol, very close to that computed at CASSCF level (≃9 kJ/mol). As is apparent, proceeding up to the third order is essential to restore the correct behavior of the two PESs, with the expected double-well profile for the GS and with the smooth parabolic curve for the first excited state. The SC-NEVPT3 (Ref. 38) calculation is rather expensive on this system and one can reasonably expect the PC-NEVPT3 and CASPT3 results to agree with the SC-NEVPT3. The energy barrier computed at SC-NEVPT3(can) level is 3.765 kJ/mol, whereas a value of 8.328 kJ/mol is obtained from the CASSCF calculation. Finally, it is interesting to notice that the splitting of the two states seems to be unaffected by the wrong second order description, being essentially the same at the CASSCF, second and third order PT levels. In the following section, this general failure of the MRPT2 treatment making use of a partially monoelectronic zero order Hamiltonian and of state-specific canonical orbitals and orbital energies, together with the benefit brought by the third order correction, will be demonstrated and discussed, for a simple Marcus-like two-state model.

IV. A SIMPLE MODEL FOR MRPT ON MIXED-VALENCE SYSTEMS

Let us consider a model system A, with two electrons and two orbitals, a and a^* (a lower in energy than a^*). In a perturbation scheme, using the Møller–Plesset[51] partition of the Hamiltonian, the zero order wavefunction is the determinant $\|a\bar{a}\|$ and only one perturber ($\|a^*\bar{a}^*\|$) must be considered (if the orbitals are supposed to be optimized, the single excitations are excluded due to Brillouin's theorem[52]). The first order correction to the wavefunction is

$$\Psi^{(1)} = -\frac{\langle aa|a^*a^*\rangle}{2(\varepsilon^{\mathrm{A}}_{a^*} - \varepsilon^{\mathrm{A}}_{a})}\|a^*\bar{a}^*\|, \tag{2}$$

and the second and third order corrections to the energy are

$$E^{(2)}_{\mathrm{A}} = -\frac{|\langle aa|a^*a^*\rangle|^2}{2(\varepsilon^{\mathrm{A}}_{a^*} - \varepsilon^{\mathrm{A}}_{a})}, \tag{3}$$

$$E^{(3)}_{\mathrm{A}} = \langle\Psi^{(1)}|\mathcal{V}|\Psi^{(1)}\rangle - E^{(1)}\langle\Psi^{(1)}|\Psi^{(1)}\rangle = \frac{|\langle aa|a^*a^*\rangle|^2}{4(\varepsilon^{\mathrm{A}}_{a^*} - \varepsilon^{\mathrm{A}}_{a})^2}[E(\|a^*\bar{a}^*\|) - E(\|a\bar{a}\|)] + E^{(2)}_{\mathrm{A}}, \tag{4}$$

where $\mathcal{V}$ is the perturbation operator ($\hat{\mathcal{H}}=\hat{\mathcal{H}}_0+\mathcal{V}$),

$$\varepsilon^{\mathrm{A}}_{a} = \langle a|h|a\rangle + \langle aa|aa\rangle, \tag{5}$$

$$\varepsilon^{\mathrm{A}}_{a^*} = \langle a^*|h|a^*\rangle + 2\langle a^*a|a^*a\rangle - \langle a^*a|aa^*\rangle, \tag{6}$$

are the orbital energies of the a and a^* orbitals (the superscript A has been added to stress that the orbital energies refer to the A system treated alone) and

$$E(K) = \langle K|\hat{\mathcal{H}}|K\rangle \tag{7}$$

is the energy of determinant K.

Consider now a second system B, equal to A, and the supersystem $(\mathrm{A}\cdots\mathrm{B})^+$, where A and B are weakly interacting. The MOs of the AB system can be considered localized and they are very close to the orbitals of A and B: They are therefore indicated in the following with a, a^*, b and b^*. The GS zero order wavefunction for the supersystem has a MR nature, being a linear combination of the two quasidegenerate determinants $\|ab\bar{b}\|$ and $\|a\bar{a}b\|$ (describing the $\mathrm{A}^+\cdots\mathrm{B}$ and $\mathrm{A}\cdots\mathrm{B}^+$ charge distributions, respectively),

$$\Psi^{(0)} = c_1\|ab\bar{b}\| + c_2\|a\bar{a}b\|. \tag{8}$$

We suppose a small modification of the geometry passing from A (B) to A^+ (B^+). The weak coupling between the two systems A and B is described by an effective Hamiltonian of the form,

$$\mathbf{H} = \begin{vmatrix} k_1\left(\frac{1}{2}-\xi\right)^2 & k_2 \\ k_2 & k_1\left(\frac{1}{2}+\xi\right)^2 \end{vmatrix}, \tag{9}$$

where ξ is a "reaction coordinate:" With $\xi=-0.5$ the system is described by $\mathrm{A}^+\cdots\mathrm{B}$ while with $\xi=0.5$ the system is $\mathrm{A}\cdots\mathrm{B}^+$. The values of k_1 and k_2 are such that c_1 remains close to 1 for $\xi<-\delta$ and is close to 0 for $\delta<\xi$, with $0<\delta\ll 1$.

In order to compute the second order correction to the energy, one has to use in this case a MRPT scheme. In order to keep the approach simple, the Møller–Plesset barycentric[53] (MPB) partition of the Hamiltonian is here considered. The orbital energies of the $(\mathrm{A}\cdots\mathrm{B})^+$ system are computed using the formula[54]

$$\varepsilon_i = \langle i|h|i\rangle + \sum_k n_k\left[\langle ik|ik\rangle - \frac{1}{2}\langle ik|ki\rangle\right], \tag{10}$$

where n_k is the natural occupation of orbital k ($n_a=1+|c_2|^2$, $n_b=1+|c_1|^2$, and $n_{a^*}=n_{b^*}=0$). In the MPB partition, the zero order energy of the GS is

$$E^{(0)} = (1+|c_2|^2)\varepsilon_a + (1+|c_1|^2)\varepsilon_b. \tag{11}$$

In the following, we use the approximation to consider zero the bielectronic integrals in which one electronic distribution (of electron 1 or 2) is the product of orbitals one on A and the other on B. With this approximation, the orbital energies are

$$\varepsilon_a = \langle a|h|a\rangle + \frac{1+|c_2|^2}{2}\langle aa|aa\rangle + (1+|c_1|^2)\langle ab|ab\rangle, \tag{12}$$

$$\varepsilon_b = \langle b|h|b\rangle + \frac{1+|c_1|^2}{2}\langle bb|bb\rangle + (1+|c_2|^2)\langle ab|ab\rangle, \tag{13}$$

$$\varepsilon_{a^*} = \langle a^*|h|a^*\rangle + (1+|c_2|^2)\langle aa^*|aa^*\rangle - \frac{1+|c_2|^2}{2}\langle aa^*|a^*a\rangle + (1+|c_1|^2)\langle a^*b|a^*b\rangle, \tag{14}$$

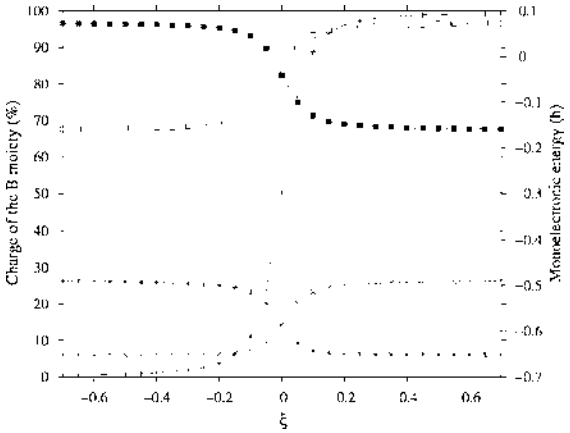

FIG. 3. Spirocation: Variation of the charge of the B moiety (in%) and of the orbital energies (in hartree) of two core and two virtual representative orbitals along the reaction coordinate ξ. Charge of the B moiety, full line and "+" symbols; energy of a core and a virtual π orbital localized on A, "×" and open square symbols, respectively; energy of a core and a virtual π orbital localized on B, "*" and black square symbols, respectively.

$$\varepsilon_{b^*} = \langle b^*|h|b^*\rangle + (1+|c_1|^2)\langle bb^*|bb^*\rangle - \frac{1+|c_1|^2}{2}\langle bb^*|b^*b\rangle + (1+|c_2|^2)\langle b^*a|b^*a\rangle. \quad (15)$$

The dependence of these orbital energies on ξ (through the dependence of c_1 and c_2 on ξ) agrees with the one found in the NEVPT calculations reported in the previous section, as is apparent from Fig. 3, where the orbital energies used in the NEVPT2 calculation for four representative inactive orbitals are reported as a function of ξ. The dependence of the charge of the B moiety (equivalent to $|c_2|^2$ in the model) as a function of ξ is also reported for the sake of clarity.

For the calculation of the second order perturbation correction to the energy, the single excitations are considered to give negligible contributions: Local single excitations on the two systems can be disposed of if the orbitals are supposed to be optimized (contracted singles would yield strictly zero according to the generalized Brillouin theorem[55]) and intersystem excitations are supposed to have a small contribution due to the weak interaction between the two systems. Therefore, only the two doubly excited perturbers, $\|ab^*\bar{b}^*\|$ and $\|a^*\bar{a}^*b\|$ (with zero order energy $\varepsilon_a+2\varepsilon_{b^*}$ and $\varepsilon_b+2\varepsilon_{a^*}$, respectively), must be treated, obtaining for the second order correction to the energy,

$$E^{(2)} = -|c_1|^2\frac{|\langle bb|b^*b^*\rangle|^2}{2\varepsilon_{b^*}-(1+|c_1|^2)\varepsilon_b-|c_2|^2\varepsilon_a} - |c_2|^2\frac{|\langle aa|a^*a^*\rangle|^2}{2\varepsilon_{a^*}-(1+|c_2|^2)\varepsilon_a-|c_1|^2\varepsilon_b}, \quad (16)$$

and for the first order correction to the wavefunction

$$\Psi^{(1)} = -c_1\frac{\langle bb|b^*b^*\rangle}{2(\varepsilon_{b^*}-\varepsilon_b)}\|ab^*\bar{b}^*\| - c_2\frac{\langle aa|a^*a^*\rangle}{2(\varepsilon_{a^*}-\varepsilon_a)}\|a^*\bar{a}^*b\|. \quad (17)$$

Given that the two systems A^+ and B (or A and B^+) are weakly interacting and that the ionized system is devoid of correlation energy, the correct $E^{(2)}$ is close (equal in the case of vanishing interaction) to the one computed in Eq. (3) for all $-0.5\leqslant\xi\leqslant0.5$.

One easily notes that for $\xi=-0.5$ and $\xi=0.5$ ($c_1\simeq1$, $c_2\simeq0$ and $c_1\simeq0$, $c_2\simeq1$, respectively), Eq. (16) correctly reduces to Eq. (3), apart from the small integrals $\langle ab|ab\rangle$ and $\langle a^*b|a^*b\rangle$.

Consider now the case $\xi=0$: Using the equalities $|c_1|^2=|c_2|^2$, $\varepsilon_{a^*}=\varepsilon_{b^*}$ and $\varepsilon_a=\varepsilon_b$ and noting that $\langle aa|a^*a^*\rangle=\langle bb|b^*b^*\rangle$, one has

$$E^{(2)} = -\frac{|\langle aa|a^*a^*\rangle|^2}{2(\varepsilon_{a^*}-\varepsilon_a)} \quad (18)$$

and

$$\Psi^{(1)} = -\frac{\langle aa|a^*a^*\rangle}{2(\varepsilon_{a^*}-\varepsilon_a)}[c_1\|ab^*\bar{b}^*\| + c_2\|a^*\bar{a}^*b\|], \quad (19)$$

where

$$\varepsilon_a = \langle a|h|a\rangle + 0.75\langle aa|aa\rangle + 1.5\langle ab|ab\rangle, \quad (20)$$

$$\varepsilon_{a^*} = \langle a^*|h|a^*\rangle + 1.5\langle a^*a|a^*a\rangle - 0.75\langle a^*a|aa^*\rangle + 1.5\langle a^*b|a^*b\rangle. \quad (21)$$

Expressions (20) and (21) for the orbital energies are different from those reported in Eqs. (5) and (6), even disregarding the small integrals $\langle ab|ab\rangle$ and $\langle a^*b|a^*b\rangle$. The denominator in Eq. (18) is smaller than the one in Eq. (3) (the onsite repulsion integrals $\langle aa|aa\rangle$ and $\langle a^*a|a^*a\rangle$ being large and positive) and the correlation energy is therefore larger in module.

The model here discussed is described only with active and virtual orbitals. The inclusion of core orbitals complicates the derivation of the equations and is not fully described here. In short, one can show that for $\xi=0$ the perturbers obtained by a promotion of two core electrons into the active space ($V(-2)$ or $2h$ class) are associated with a denominator larger than the correct one and therefore their contribution to the correlation energy is too small. The same happens for the promotion of one core electron into the active space accompanied by an excitation inside the active space ($V(+1)'$ or $1h$ class). In the cases where both the core and the virtual orbitals are involved in the excitation process ($V(0)$ or $2h-2p$, $V(+1)$ or $1h-2p$, $V(-1)$ or $2h-1p$, and $V(0)'$ or $1h-1p$ classes), the analysis is more complex and there is a competition between the effect of the virtual orbital energies (which tend to give too small denominators) and the one of the core orbital energies (which, on the contrary, tend to give too large denominators).

One has to note that even if this result has been derived within the MPB partition, a similar behavior is expected also for partitions of the Hamiltonian based, at least partially, on a one electron definition of $\hat{\mathcal{H}}_0$ with the orbitals localized on the two subunits, as happens for NEVPT2 and CASPT2 with state-specific canonical orbitals.

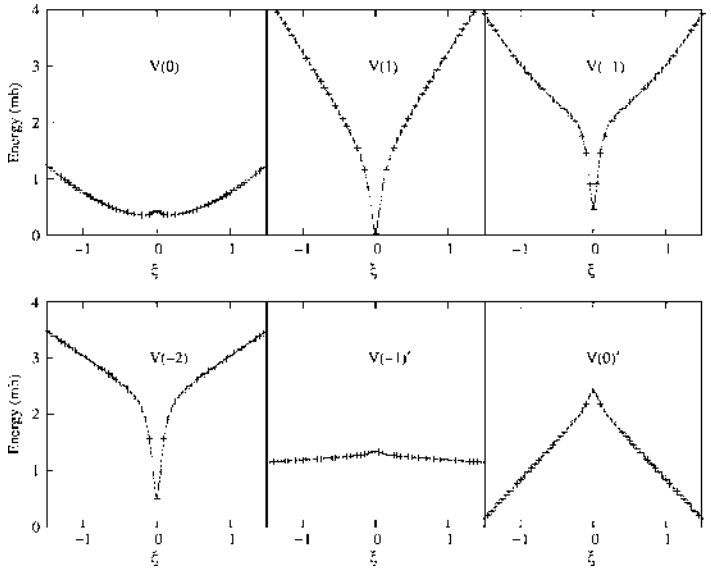

FIG. 4. Spirocation: Contribution of the different classes to the NEVPT second order correction to the energy (in millihartree) as a function of the reaction coordinate ξ. The $V(2)$ and $V(+1)'$ classes give vanishing contribution. In order to make the comparison between the different classes easier, the energy reported in figure is $E^{(2)}+E_{\text{shift}}$, where E_{shift} (in hartree) is different for each class: $V(0)\rightarrow E_{\text{shift}}=0.6480$ hartree, $V(1)\rightarrow E_{\text{shift}}=0.0185$ hartree, $V(-1)\rightarrow E_{\text{shift}}=0.0730$ hartree, $V(-2)\rightarrow E_{\text{shift}}=0.0115$ hartree, $V(-1)'\rightarrow E_{\text{shift}}=0.0030$ hartree, and $V(0)'\rightarrow E_{\text{shift}}=0.3000$ hartree. Moreover the same energy scale is adopted for all plots.

The analogy between the model system and the NEVPT2 description of the spiro molecule is confirmed by the curves shown in Fig. 4 where the NEVPT2 correlation energy for each excitation class is reported as a function of ξ. In order to have a prompt comparison of the behavior of the different NEVPT2 classes, the origin of the energy scale is different for each class and all plots have the same energy range (for more details, see caption of Fig. 4). As expected the $V(-2)$ class (two active electrons promoted to the virtual space) shows a sharp profile with too large a correlation energy close to $\xi=0$. All the other classes, apart from the $V(-1)'$ class, involve both core and virtual orbitals and the effect of the virtual orbital energies is dominant for the $V(1)$ and $V(-1)$ classes, while for the $V(0)'$ the effect of the core orbital energies slightly prevails. The two effects almost compensate each other in the case of the $V(0)$ class. The behavior of the $V(-1)'$ class is peculiar: Given that in this case only virtual inactive orbitals are involved in the excitation process, from the model system one can expect for this class a behavior similar to the one observed for the $V(-2)$ class, while the NEVPT2 curve shows an opposite shape. One must, however, note that, in the same energy scale of the other classes, the contribution of this class is almost constant and that the deviation from the correct behavior is negligible. The curve of the total CASSCF+NEVPT2 energy, described in Sec. III and reported in Fig. 2, indicates that the effect of the virtual orbital energies (too large a correlation energy for $\xi=0$) is dominant.

As for the third order correction to the energy, the full derivation of its expression is rather tedious, even considering only active and virtual orbitals. In this case, one can, however, easily verify that for $\xi=-0.5$ and $\xi=0.5$ the correct behavior is obtained. For $\xi=0$, one has

$$E^{(3)}=\frac{|\langle aa|a^*a^*\rangle|^2}{4(\varepsilon_{a^*}-\varepsilon_a)^2}[E(\|a^*\bar{a}^*b\|)-E(\Psi^{(0)})]+E^{(2)}, \tag{22}$$

where use has been made of the relations $E(\|a^*\bar{a}^*b\|)=E(\|ab^*\bar{b}^*\|)$ and $\langle\|a^*\bar{a}^*b\|\|\mathcal{V}\|\|ab^*\bar{b}^*\|\rangle=0$. Introducing the new quantities

$$\Delta\varepsilon=2(\varepsilon^{\text{A}}_{a^*}-\varepsilon^{\text{A}}_a) \tag{23}$$

and

$$\Delta=\Delta\varepsilon-2(\varepsilon_{a^*}-\varepsilon_a), \tag{24}$$

one can expand $E^{(2)}$ and $E^{(3)}$ in McLaurin series with respect to $\Delta/\Delta\varepsilon$ (which is expected to be $\ll 1$) obtaining to the first order,

$$E^{(2)}\simeq E^{(2)}_{\text{A}}\left(1+\frac{\Delta}{\Delta\varepsilon}\right), \tag{25}$$

$$\begin{aligned}E^{(3)}&\simeq\frac{|\langle aa|a^*a^*\rangle|^2}{(\Delta\varepsilon)^2}[E(\|a^*\bar{a}^*b\|)-E(\Psi^{(0)})]\left(1+2\frac{\Delta}{\Delta\varepsilon}\right)\\&\quad+E^{(2)}_{\text{A}}\left(1+\frac{\Delta}{\Delta\varepsilon}\right)\\&\simeq E^{(3)}_{\text{A}}+E^{(2)}_{\text{A}}\left(1-2\frac{[E(\|a^*\bar{a}^*b\|)-E(\Psi^{(0)})]}{\Delta\varepsilon}\right)\frac{\Delta}{\Delta\varepsilon},\end{aligned} \tag{26}$$

where the relation $E(\|a^*\bar{a}^*b\|)-E(\Psi^{(0)})\simeq E(\|a^*\bar{a}\|)-E(\|a\bar{a}\|)$ has been used (the equality holds if A and B are noninteracting). Therefore, neither $E^{(2)}$ nor $E^{(3)}$ show the correct behav-

ior (which is $E_A^{(2)}$ and $E_A^{(3)}$, respectively) at the first order in $\Delta/\Delta\varepsilon$, but the sum of the two corrections

$$E^{(2)}+E^{(3)} \simeq E_A^{(2)}+E_A^{(3)} + 2E_A^{(2)}\left(1-\frac{[E(\|a^*\bar{a}^*b\|)-E(\Psi^{(0)})]}{\Delta\varepsilon}\right)\frac{\Delta}{\Delta\varepsilon} \quad (27)$$

has the correct expression if $E(\|a^*\bar{a}^*b\|)-E(\Psi^{(0)})=\Delta\varepsilon$. Even though such equality does not hold rigorously, the two terms can be supposed to be close, the first representing the energy difference between $\|a^*\bar{a}^*b\|$ and $\Psi^{(0)}$ computed with the full Hamiltonian, the second the same energy difference, but using the zero order Hamiltonian.

This simple model allows the full rationalization of the results reported in Sec. III: The energy curve corrected to the second order using MRPTs in which the zero order Hamiltonian depends (at least partially) on the orbital energies shows an unphysical behavior with a well around the symmetric situation $\xi=0$. Both NEVPT2 and CASPT2 are subject to this error but such behavior is expected to be common to practically all MRPTs (with a possible exception of the ones based on Epstein–Nesbet partition of the Hamiltonian[53]). For NEVPT2, in which $\hat{\mathcal{H}}_0$ contains the orbital energies only for the inactive (core and virtual) orbitals, the problem can be alleviated by enlarging the active space (that is increasing $\Delta\varepsilon$). For CASPT2 this strategy is destined to fail, because of the monoelectronic nature of $\hat{\mathcal{H}}_0$ in all orbital spaces. The irregularity is almost completely removed if the perturbation approach is applied up to the third order, thus restoring a regular curve.

One has to note that this result implies a serious problem in the perspective of the use of MRPT for the study of actual MV systems, for which the application of the third order approach with reasonable active spaces is too expensive. To this aim, the model here exposed suggests a practical strategy for limiting the calculation to the second order: Indeed, if Eqs. (12)–(15) are made independent of c_1 and c_2, the second order energy remains constant for all ξ and the unphysical well is removed. This can be achieved, for instance, by using $|c_1|^2=|c_2|^2=0.5$, or equivalently by taking, for each orbital energy, the average of the two values computed at ξ and $-\xi$. An important remark must be, however, done: In this scheme the irregular behavior is removed by forgoing the computation of the "correct" second order approximation to the correlation energy (for $\xi=-0.5$ and $\xi=0.5$ $E^{(2)}\neq E_A^{(2)}$) with a view to obtaining a homogeneous estimate of it at all internuclear distances. The second order corrected energy curve computed in this way coincides with the one obtained from Eq. (16) for $\xi=0$, while it is lower than the one of Eq. (16) for the other values of ξ. In actual calculations, the average of a given quantity at two different geometries poses practical problems. The same result can be obtained computing, for each nuclear geometry, the orbital energies which are averaged between those pertaining to the GS and to the first excited state of the same symmetry, for which the zero order description of the wavefunction is

TABLE II. Spirocation: NEVPT2(av) energies (kJ/mol) of the GS, $^2A_2(1)$, at $\xi=0.0$ and of the first excited state, $^2A_2(2)$, at $\xi=0.0$ and $\xi=-0.5$. All the energies are computed with respect to the energy of the GS at $\xi=-0.5$. For the sake of clarity, the energy splitting (ΔE, kJ/mol) between the two states at $\xi=0.0$ is also reported.

States	SC-NEVPT2(av)	PC-NEVPT2(av)
$\xi=-0.05$		
$^2A_2(2)$	50.892	50.786
$\xi=0.0$		
$^2A_2(1)$	3.892	3.890
$^2A_2(2)$	13.697	13.687
ΔE ($\xi=0.0$)		
$^2A_2(2)$	9.805	9.797

$$\Psi_{exc}^{(0)}=c_2\|ab\bar{b}\|-c_1\|a\bar{a}b\|. \quad (28)$$

This strategy can be easily implemented and its application in the case of the spiro compound is reported in the next section.

We note that the use of state-averaged orbital energies has been previously proposed in MRPT, as, for instance, in Ref. 56 where various electronic states are treated together in a quasidegenerate perturbation theory approach. In such a case, the orbital energies used in the definition of the state independent one-particle zero order Hamiltonian are based on a state-averaged one-particle density matrix in order to have a balanced description of the various states. Here, instead, state-specific MRPT approaches are studied (each state is considered individually) and the state-averaged orbital energies are introduced in order to have a balanced treatment of a given state at different internuclear geometries.

V. THE USE OF STATE-AVERAGED ORBITALS

In the present section, we shall discuss the results obtained on the spiro cation by the application of the above proposed computational strategy, relying on a second order NEVPT treatment based on "charge-averaged" orbital energies (NEVPT2(av)). In order to avoid strong variations of the orbitals along the reaction coordinate (a strong dependence on the charge distribution is expected in particular for the virtual orbitals), the orbitals are obtained by diagonalizing the state-averaged Fock operator (state-averaged canonical orbitals). The energy differences, displayed in Table II, clearly demonstrate the benefit resulting from the application of such computational procedure.

Indeed, as expected on the basis of the considerations reported in the previous section on the simple model, this alternative strategy is able to completely remove the nonphysical well observed in a standard MRPT2 computation, restoring the correct energy profile of the two adiabatic states. The energy barrier for the thermal ET is computed to be around 3.9 kJ/mol, in agreement with the value of ≃3.7 obtained at SC-NEVPT3 level (see Table I). Then, from the comparison between the values in Tables I and II, it can be noticed that the energy splitting at $\xi=0$, as already pointed out in Sec. III, is practically insensitive to the wrong behavior of the standard second order curves, being ≃9.8 kJ/mol

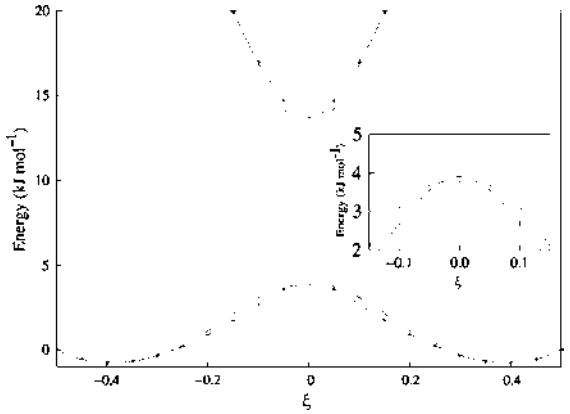

FIG. 5. SC-NEVPT2(av) and SC-NEVPT3(can) PES of the $^2A_2(1)$ and $^2A_2(2)$ states of the spiro cation. All the curves are shifted in order to have the two C_{2v} minima at zero energy. In the inset, a close-up of the GS barrier maximum is reported. Full lines and "+" points, NEVPT2(av) energies; dashed lines and "×" points, NEVPT3(can) energies.

both in the NEVPT2(can) and NEVPT2(av) computations. The energy difference between the $^2A_2(2)$ at the C_{2v} geometry and the $^2A_2(1)$ at ξ=0 amounts roughly to 51 kJ/mol, exactly as computed at SC-NEVPT3(can) level (Table I). In order to judge on the merits of this charge-averaged approach, in Fig. 5, we have reported the SC-NEVPT2(av) potential energy curves plotted together with those obtained from the standard SC-NEVPT3(can) computation.

In agreement with the considerations reported in Sec. IV for the third order correction to the energy in the model system, from Fig. 5 one notes that the irregular behavior is not completely removed going to the third order, since a very slight leftover of the wrong second order description still remains (see the close-up inset of Fig. 5). On the contrary, two perfectly smooth curves are attained when the alternative and computationally less demanding second order strategy is applied.

VI. CONCLUSIONS

In this paper, the ability of state-specific second order MRPTs to correctly describe the lowest electronic states of MV compounds has been discussed using the small-size spiro compound for actual calculations and a very simple model system for the interpretation of the results. It has been shown that MRPTs with a definition of the zero order Hamiltonian based (at least partially) on canonical orbital energies are prone to present an unphysical behavior in proximity of the symmetric (delocalized) nuclear geometry. The description can be improved by going to the third order correction in the energy or, remaining at the second order level in the energy, by using a partition of the Hamiltonian in which $\hat{\mathcal{H}}_0$ is based on state-averaged orbital energies. In the latter case, the energy curves show a correct behavior, but the price to pay is that in the model system this strategy gives an incorrect value of the second order approximation of the correlation energy for the two conformations with localization of the electronic charge.

In summary, since for the description of MV systems, basically, what is important is the determination of energy differences (the height of the barrier for the thermal ET or the excitation energy for the optically induced ET) rather than the absolute energies of the states, the NEVPT2(av) method here proposed appears to be a practical and effective solution to overcome the failure of the standard MRPT approach. To test the reliability as well as the generality of this approach, work is in progress in our groups on the spiro compounds with larger basis sets and on more meaningful MV systems.

ACKNOWLEDGMENTS

This work has been financed by the University of Ferrara, by the Italian MIUR through its PRIN grant and by the European Community through the COST action D37. Computational facilities provided by CALMIP (Toulouse) are gratefully acknowledged.

[1] M. Bixon and J. Jortner, *Electron Transfer: From Isolated Molecules to Biomolecules*, Advances in Chemical Physics, Vols. 106 and 107 (Wiley, New York, 1999).
[2] C. Creutz, Prog. Inorg. Chem. **30**, 1 (1983).
[3] N. Sutin, Prog. Inorg. Chem. **30**, 441 (1983).
[4] R. J. Crutchley, Adv. Inorg. Chem. **41**, 273 (1994).
[5] P. F. Barbara, T. J. Meyer, and M. A. Ratner, J. Phys. Chem. **100**, 13148 (1996).
[6] S. F. Nelsen, R. F. Ismagilov, and D. A. Trieber, Science **278**, 846 (1997).
[7] J.-P. Launay, Chem. Soc. Rev. **30**, 386 (2001).
[8] C. Joachim, J. K. Jimzewski, and A. Aviram, Nature (London) **408**, 541 (2000).
[9] M. Robin and P. Day, Adv. Inorg. Chem. Radiochem. **10**, 247 (1967).
[10] P. H. Cribb, S. Nordholm, N. S. Hush, Chem. Phys. **29**, 43 (1978).
[11] N. S. Hush, Coord. Chem. Rev. **64**, 135 (1985).
[12] K. D. Demadis, C. M. Hartshorn, and T. J. Meyer, Chem. Rev. (Washington, D.C.) **101**, 2655 (2001).
[13] B. S. Brunschwig, C. Creutz, and N. Sutin, Chem. Soc. Rev. **31**, 168 (2002).
[14] C. J. Calzado and J. F. Sanz, J. Am. Chem. Soc. **120**, 1051 (1998).
[15] S. F. Nelsen, Chem.-Eur. J. **6**, 581 (2000).
[16] Y. Carissan, J.-L. Heully, F. Alary, and J.-P. Daudey, Inorg. Chem. **43**, 1411 (2004).
[17] D. M. D'Alessandro and R. Keene, Chem. Soc. Rev. **35**, 424 (2006).
[18] M. H. Chisholm and N. J. Patmore, Acc. Chem. Res. **40**, 19 (2007).
[19] K. Lahil, A. Moradpour, C. Bowlas, F. Menou, P. Cassoux, J. Bonvoisin, J.-P. Launay, G. Dive, and D. Dehareng, J. Am. Chem. Soc. **117**, 9995 (1995).
[20] C. Lambert, W. Gaschler, E. Schmälzlin, K. Meerholz, and C. Bräuchle, J. Chem. Soc., Perkin Trans. 2 **3**, 577 (1999).
[21] D. Dehareng, G. Dive, and A. Moradpour, Int. J. Quantum Chem. **76**, 552 (2000).
[22] M. Malagoli and J. L. Brédas, Chem. Phys. Lett. **327**, 13 (2000).
[23] R. C. Johnson and J. P. Hupp, J. Am. Chem. Soc. **123**, 2053 (2001).
[24] V. Coropceanu, M. Malagoli, J. M. André, and J. L. Brédas, J. Chem. Phys. **115**, 10409 (2001).
[25] V. Coropceanu, M. Malagoli, J. M. André, and J. L. Brédas, J. Am. Chem. Soc. **124**, 10519 (2002).
[26] C. Lambert and G. Nöll, Chem.-Eur. J. **8**, 3467 (2002).
[27] C. Lambert, S. Amthor, and J. Schelter, J. Phys. Chem. A **108**, 6474 (2004).
[28] A. V. Szeghalmi, M. Erdmann, V. Engel, M. Schmitt, S. Amthor, V. Kriegisch, G. Nöll, R. Stahl, C. Lambert, D. Leusser, D. Stalke, M. Zabel, and J. Popp, J. Am. Chem. Soc. **126**, 7834 (2004).
[29] S. F. Nelsen, A. E. Kondradsson, and J. P. Telo, J. Am. Chem. Soc. **127**, 920 (2005).
[30] A, Farazdel, M. Dupuis, E. Clementi, and A. Aviram, J. Am. Chem. Soc. **112**, 4206 (1990).

[31] J. F. Sanz, C. J. Calzado, and A. Márquez, Int. J. Quantum Chem. **76**, 458 (2000).
[32] W. Helal, B. Bories, S. Evangelisti, T. Leininger, and D. Maynau, Lect. Notes Comput. Sci. **3980**, 744 (2006).
[33] W. Helal, S. Evangelisti, T. Leininger, and D. Maynau, "*Ab initio* multireference study of an organic mixed-valence spiro molecular system," J. Comput. Chem. (in press).
[34] C. Angeli, R. Cimiraglia, S. Evangelisti, T. Leininger, and J.-P. Malrieu, J. Chem. Phys. **114**, 10252 (2001).
[35] C. Angeli, R. Cimiraglia, and J.-P. Malrieu, Chem. Phys. Lett. **350**, 297 (2001).
[36] C. Angeli, R. Cimiraglia, and J.-P. Malrieu, J. Chem. Phys. **117**, 9138 (2002).
[37] C. Angeli, S. Borini, M. Cestari, and R. Cimiraglia, J. Chem. Phys. **121**, 4043 (2004).
[38] C. Angeli, B. Bories, A. Cavallini, and R. Cimiraglia, J. Chem. Phys. **124**, 054108 (2006).
[39] C. Angeli, S. Borini, and R. Cimiraglia, Theor. Chem. Acc. **111**, 352 (2004).
[40] C. Angeli, S. Borini, L. Ferrighi, and R. Cimiraglia, J. Chem. Phys. **122**, 114304 (2005).
[41] C. Angeli, S. Borini, A. Cavallini, M. Cestari, R. Cimiraglia, L. Ferrighi, and M. Sparta, Int. J. Quantum Chem. **106**, 686 (2006).
[42] M. Pastore, C. Angeli, and R. Cimiraglia, Chem. Phys. Lett. **422**, 522 (2006).
[43] M. Pastore, C. Angeli, and R. Cimiraglia, Chem. Phys. Lett. **426**, 445 (2006).
[44] C. Angeli, M. Pastore, and R. Cimiraglia, Theor. Chem. Acc. **117**, 743 (2007).
[45] M. Pastore, C. Angeli, and R. Cimiraglia, Theor. Chem. Acc. **118**, 35 (2007).
[46] C. Angeli, A. Cavallini, and R. Cimiraglia, J. Chem. Phys. **127**, 074306 (2007).
[47] K. Andersson, P. Malmqvist, B. O. Roos, A. J. Sadlej, and K. Wolinski, J. Phys. Chem. **94**, 5483 (1990).
[48] M. Andersson, A. Barysz, M. Bernhardsson *et al.*, MOLCAS 5.4, 2002.
[49] P.-O. Widmark, P. Ä. Malmqvist, and B. O. Roos, Theor. Chim. Acta **77**, 291 (1990).
[50] M. Pastore, W. Helal, S. Evangelisti, T. Leininger, J.-P. Malrieu, D. Maynau, C. Angeli, and R. Cimiraglia, "Application of a 'charge-averaged' second order multireference perturbation theory strategy to the study of a model mixed-valence compound," J. Chem. Theory Comput. (submitted).
[51] C. Møller and M. S. Plesset, Phys. Rev. **46**, 618 (1934).
[52] L. Brillouin, Actualités scientifiques et Industrielles **71** (1933); **159** (1934).
[53] B. Huron, J. P. Malrieu, and P. Rancurel, J. Chem. Phys. **58**, 5745 (1973).
[54] C. Angeli, R. Cimiraglia, and J. P. Malrieu, Chem. Phys. Lett. **317**, 472 (2000).
[55] B. Levy and G. Berthier, Int. J. Quantum Chem. **2**, 307 (1968).
[56] H. Nakano, J. Chem. Phys. **99**, 7983 (1993).

Journal of Molecular Structure: THEOCHEM 896 (2009) 12–17

Contents lists available at ScienceDirect

Journal of Molecular Structure: THEOCHEM

journal homepage: www.elsevier.com/locate/theochem

Application of a "charge-averaged" second order multireference perturbation theory strategy to the study of a model Mixed-Valence compound

Mariachiara Pastore [a,*], Wissam Helal [b], Celestino Angeli [a], Stefano Evangelisti [b], Thierry Leininger [b], Renzo Cimiraglia [a]

[a] Dipartimento di Chimica, Università di Ferrara, Via Borsari 46, I-44100 Ferrara, Italy
[b] Laboratoire de Chimie et Physique Quantiques, UMR 5626, Université Paul Sabatier et CNRS, 118 Route de Narbonne, F-31062 Toulouse, France

ARTICLE INFO

Article history:
Received 29 July 2008
Received in revised form 22 October 2008
Accepted 26 October 2008
Available online 11 November 2008

Keywords:
Multireference perturbation theory
NEVPT
Mixed-Valence systems
Electronic transfer

ABSTRACT

A new proposed second order Multireference Perturbation Theory (MRPT) approach (termed NEVPT2(av)), based upon the use of state-averaged canonical molecular orbitals instead of the state-specific canonical ones, is applied to the study of a model Mixed-Valence compound. Such strategy has already been shown, on the basis of some preliminary calculations reported in a previous paper, to be able to overcome the inadequacy of a standard second order MRPT treatment for such MV systems. In order to test the validity and the firmness of the NEVPT2(av) methodology, an investigation is carried out, using basis sets of various size and two different active spaces. The reliability of the method is fully confirmed by the good agreement achieved with the results of highly-correlated Multireference Configuration Interaction (MRCI) computations recently published.

1. Introduction

The pivotal rôle played by the Electron Transfer (ET) processes in a great deal of chemical–physical and biological phenomena, accounts for the extensive research efforts addressed to the understanding of its mechanisms. The experimental and theoretical investigation of Mixed-Valence (MV) compounds, has received a great attention over the last years, particularly in the field of the inorganic binuclear MV complexes, such as the well-known Creutz–Taube ion [1]. Nevertheless, more recently, an increasing attention has been paid to the purely organic MV systems (see, for instance, the extensive work on the triarylamine-based MV systems by Lambert and Nöll [2]), since their Inter Valence Charge Transfer (IV-CT) band is, generally, not affected by the overlap with other low-lying transitions, contrary to what may occur for inorganic compounds due to appearance of the $d \rightarrow d$ metal to ligand (MLCT) or ligand to metal (LMCT) charge transfer excitations.

The rate of the ET process, and hence the properties of the system, are influenced by various parameters, such as, for instance, the nature of the redox centers as well as the properties and the length of the bridge and they are essentially governed by the electronic coupling between the two diabatic (charge/hole-localized) states. The extent of this interaction is expressed by the matrix elements $\mathscr{H}_{ab} = \langle \Psi_a | \hat{\mathscr{H}} | \Psi_b \rangle$, where Ψ_a and Ψ_b are the above mentioned localized states. According to the magnitude of $\mathscr{H}_{ab}$, the MV systems are commonly classified into three classes [3]. In the case of class II and class III compounds (from moderate to strong electronic coupling), the analysis of the IV-CT band, either based on the semiclassical Hush theory [4,5] or on a more rigorous quantum mechanical approach [6], provides a direct way to estimate $\mathscr{H}_{ab}$, and the reorganization energy, λ. The extent of the electronic coupling can also be obtained experimentally by means of Electron Spin Resonance (ESR), Nuclear Magnetic Resonance (NMR) Spectroscopy as well as Photoelectron Spectroscopy measures (see Refs. [7,8] for a more detailed overview). Nevertheless, since the obtaining of a reliable experimental measure of $\mathscr{H}_{ab}$ is often not possible, particularly for strongly coupled systems, where the ET rates are much faster than the typical time scale of the above cited experimental techniques and, additionally, the significant vibronic coupling makes the Hush theory no longer applicable, the development of accurate and efficient computational strategies represents a crucial issue in the study of MV systems. Moreover, the accurate theoretical prediction of the electronic coupling would represent a powerful tool for the design of new "spacers", allowing the specific modulation of the properties of the ET process (e.g. long or short distance ET).

In the framework of the widely used two-state one-mode model and in the simple case of symmetry-equivalent donor and acceptor groups, the electronic coupling $\mathscr{H}_{ab}$ is defined as half the energy splitting (ΔE) between the two adiabatic potential surfaces at the crossing seam, and it can be computed using different methodologies and approaches [2,9–23].

* Corresponding author.
E-mail address: pstmch@unife.it (M. Pastore).

0166-1280/$ - see front matter © 2008 Elsevier B.V. All rights reserved.
doi:10.1016/j.theochem.2008.10.042

With the exception of some recent semiempirical Austin Model 1 (AM1) computations [2,19], the most frequently applied methods, to study the ET process, are based on Density Functional [12] and Time-Dependent Density Functional Theories (TD-DFT) [16,17]. However, as shown in different applications [17,24], some doubts have been raised concerning the applicability of the DFT approach to the study of the electron transfer in MV compounds, since the computed electronic coupling has been shown to be systematically underestimated by 20–30% in comparison to the results of more refined *ab initio* calculations.

In the present contribution, as a conclusion of a research project [22,23,25] addressed to the theoretical description of the ET process in a model organic MV system [9], we investigate the application of a recently proposed [25] computational strategy, based upon second order Multireference Perturbation Theory (MRPT). The model MV system under consideration is a $\pi-\sigma-\pi$ spiro compound (5,5′(4H,4H′)-spirobi[cyclopenta[c]pyrrole]2,2′,6,6 ′tetrahydro cation, termed "spiro" in the following), which, due to its relatively small size, is particularly suitable to validate the application of highly-correlated theoretical approaches. In Ref. [23] (hereafter referred to as paper I), the spiro monocation was studied at Multireference Configuration Interaction (MRCI) level [Complete Active Space–Self Consistent Field (CASSCF), Complete Active Space–Configuration Interaction (CASCI), and Multireference Configuration Interaction Singles and Doubles (MRCI(SD))] by using different basis sets and computational approaches (canonical *vs*. localized orbitals). Then, the variational study of paper I was extended, making use of the *n*-electron valence state perturbation theory (NEVPT) approach, [26–31] in Ref. [25] (paper II), where the general problems connected with a standard MRPT treatment of MV systems are addressed. In fact, as we shall discuss later (Section 2), a second order MRPT approach, in which a monoelectronic zero order Hamiltonian is employed, provides an unphysical description of the ET process if canonical orbitals are used, basically due to a sudden change of the orbital energy differences along the reaction path. In order to overcome this failure and avoid the computationally demanding third order calculations, a practical and efficient strategy (termed NEVPT2(av) [25]) was proposed, relying on the use of state-averaged canonical orbitals. Here, our aim is to extend the preliminary NEVPT2(av) calculations reported in paper II, resorting to the use of different active spaces and basis sets; the reliability and the computational efficiency of the NEVPT2(av) strategy will be judged with respect to the results obtained from the MRCI calculations of paper I as well as to other theoretical results available in the literature. Furthermore, when possible, a direct comparison with the third order NEVPT results will also be proposed.

The paper is organized as follows: Section 2 summarizes the main findings and results of paper II [25]; the computational details are illustrated in Section 3; Section 4 is, then, devoted to the discussion and to the analysis of the results and, finally, some conclusive remarks are reported in Section 5.

2. Failure of standard MRPT: the NEVPT2(av) strategy

In the present section we shall briefly recall the main points discussed in paper II, pertaining to the failure of a standard MRPT approach to describe the ET process in MV systems. To this aim, a simple MRPT model based upon a two-states three electrons–four orbitals system was introduced in paper II [25].

The model consists in a supersystem $(A\cdots B)$, whose two subunits A and B, supposed to be weakly interacting, are composed of two electrons and two orbitals a (b) and a^* (b^*), where a (b) has a lower energy than a^* (b^*); the small interaction between A and B allows the orbitals of the supersystem to be regarded as essentially localized and very close to those of the isolated moieties. The ionized system $(A\cdots B)^+$ can suitably represent a symmetrical MV system, whose ground state zero order wavefunction is a linear combination of the two quasi-degenerate determinants $||ab\bar{b}||$ and $||a\bar{a}b||$, corresponding to the $A^+\cdots B$ and $A\cdots B^+$ charge distributions respectively:

$$\Psi^{(0)} = c_1||ab\bar{b}|| + c_2||a\bar{a}b||. \tag{1}$$

The small coupling between A and B is given by the following effective Hamiltonian

$$\mathbf{H} = \begin{vmatrix} k_1\left(\frac{1}{2}-\xi\right)^2 & k_2 \\ k_2 & k_1\left(\frac{1}{2}+\xi\right)^2 \end{vmatrix} \tag{2}$$

with ξ being a suitable "reaction coordinate" (*vide infra*), where the value $\xi = -0.5$ (or $\xi = 0.5$), corresponds to the charge-localized situation with $c_1 \simeq 1$ and $c_2 \simeq 0$ (or $c_2 \simeq 1$ and $c_1 \simeq 0$) and where $\xi = 0.0$ corresponds to the situation of the charge supposed to be equally shared by the two units with $|c_1|^2 = |c_2|^2$.

In order to obtain the second order correction to the energy, in the Møller–Plesset barycentric partition of the Hamiltonian [32], one has to consider only the doubly excited determinants $||ab^*\bar{b}^*||$ and $||a^*\bar{a}^*b||$, since the single excitations are expected to give an unimportant contribution [25]. So, $E^{(2)}$ becomes

$$E^{(2)} = -|c_1|^2\frac{|\langle bb|b^*b^*\rangle|^2}{2\varepsilon_{b^*} - (1+|c_1|^2)\varepsilon_b - |c_2|^2\varepsilon_a} - |c_2|^2\frac{|\langle aa|a^*a^*\rangle|^2}{2\varepsilon_{a^*} - (1+|c_2|^2)\varepsilon_a - |c_1|^2\varepsilon_b} \tag{3}$$

with the monoelectronic energies having the form

$$\varepsilon_a = \langle a|h|a\rangle + \frac{1+|c_2|^2}{2}\langle aa|aa\rangle + (1+|c_1|^2)\langle ab|ab\rangle \tag{4}$$

$$\varepsilon_b = \langle b|h|b\rangle + \frac{1+|c_1|^2}{2}\langle bb|bb\rangle + (1+|c_2|^2)\langle ab|ab\rangle \tag{5}$$

$$\varepsilon_{a^*} = \langle a^*|h|a^*\rangle + (1+|c_2|^2)\langle aa^*|aa^*\rangle - \frac{1+|c_2|^2}{2}\langle aa^*|a^*a\rangle + (1+|c_1|^2)\langle a^*b|a^*b\rangle \tag{6}$$

$$\varepsilon_{b^*} = \langle b^*|h|b^*\rangle + (1+|c_1|^2)\langle bb^*|bb^*\rangle - \frac{1+|c_1|^2}{2}\langle bb^*|b^*b\rangle + (1+|c_2|^2)\langle b^*a|b^*a\rangle \tag{7}$$

For the sake of clarity we recall that, in this simplified model, for the definition of the monoelectronic energies, the form reported in Ref. [33] was used and the bielectronic integrals with one electronic distribution given by the product of orbitals one on A and the other on B are neglected.

Since the two subsystems A^+ and B (or A and B^+) are supposed to be weakly interacting and given that the ionized system need not be correlated, the second order approximation to the energy, $E^{(2)}$, is expected to be very close (equal at the non-interaction limit) to that of the isolated system A (or B), which, in the Møller–Plesset [34] partition of the Hamiltonian, has the well-known form:

$$E_A^{(2)} = -\frac{|\langle aa|a^*a^*\rangle|^2}{2(\varepsilon_{a^*}^A - \varepsilon_a^A)} \tag{8}$$

with orbital energies

$$\varepsilon_a^A = \langle a|h|a\rangle + \langle aa|aa\rangle \tag{9}$$

$$\varepsilon_{a^*}^A = \langle a^*|h|a^*\rangle + 2\langle a^*a|a^*a\rangle - \langle a^*a|aa^*\rangle \tag{10}$$

Note that the superscript A indicates that the energies are those of the isolated system A.

It can be proved that, in the two localized minima ($\xi = -0.5$ and $\xi = +0.5$) as well as in the delocalized saddle point ($\xi = 0.0$ with $|c_1|^2 = |c_2|^2$ and $\varepsilon_{a^*} = \varepsilon_{b^*}$ and $\varepsilon_a = \varepsilon_b$), the value of $E^{(2)}$ for the whole $(A\cdots B)^+$ system (Eq. 3) is formally equal to that given in Eq. 8. Nevertheless, while in $\xi = -0.5$ ($\xi = +0.5$), $E^{(2)}$ almost equals the correct correlation energy $E_A^{(2)}$, in $\xi = 0.0$ the monoelectronic energies are

$$\varepsilon_a = \langle a|h|a\rangle + 0.75\langle aa|aa\rangle + 1.5\langle ab|ab\rangle \quad (11)$$

$$\varepsilon_{a^*} = \langle a^*|h|a^*\rangle + 1.5\langle a^*a|a^*a\rangle - 0.75\langle a^*a|aa^*\rangle + 1.5\langle a^*b|a^*b\rangle \quad (12)$$

which are different, even if the integrals $\langle ab|ab\rangle$ and $\langle a^*b|a^*b\rangle$ are neglected, from those displayed in Eqs. 9 and 10. The denominator in Eq. 3 turns out to be smaller than that in Eq. 8 and hence the second order energy turns out to be larger in module than the correct one.

Then, leaving out the detailed derivation of the third order correction to the energy, which can be found in paper II [25], we shall only recall here that, although $E^{(3)}$ shows an incorrect behavior, the sum of $E^{(2)}$ and $E^{(3)}$ is almost equal to the correct value given by $E_A^{(2)} + E_A^{(3)}$. Therefore, going to the third order correction in the energy can be a strategy, at least for the cases in which at the second order the irregularity is not too pronounced, to restore a regular curve.

This model is able to fully rationalize the unphysical "well" observed in proximity of the avoided-crossing point in the NEVPT2 and CASPT2 calculations as well as the almost correct behavior shown by the NEVPT3 results (see Fig. 1). But, in the perspective of applying MRPT methods to real MV systems with a good quality basis set and reasonably large active spaces, the strategy to perform a third order calculation appears as too expensive a solution. In paper II we have proposed and tested a practical and alternative second order strategy, termed NEVPT2(av), in which the monoelectronic energies are made independent of the coefficients c_1 and c_2, just computing for all ξ the average value between the energies of the ground state and those of the first excited state of the same symmetry. Practically, this "charge-averaged" MRPT2 approach, relies on the use of state-averaged canonical molecular orbitals, obtained by diagonalization of the state-averaged Fock operator. These findings are illustrated in Fig. 1, where a comparison between the standard (full lines) NEVPT2 and NEVPT3 energy profiles and those computed at NEVPT2(av) level (dashed lines) is shown. The curves have been obtained using a double zeta (DZ) basis set and an active space including the full valence π space of the cation (see next section for more details).

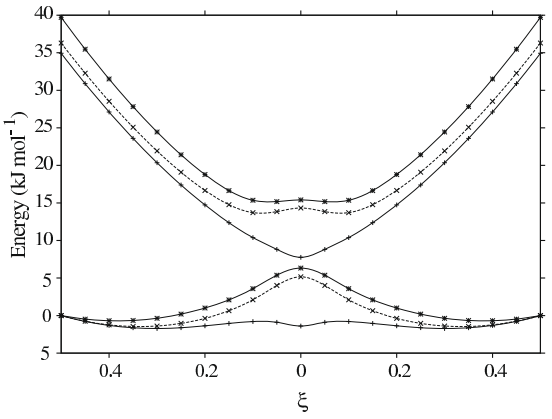

Fig. 1. SC-NEVPT2(can), SC-NEVPT3(can) (full lines with "+" and "∗" points, respectively) and SC-NEVPT2(av) (dashed lines with "×" points) energy profiles of the ground, $^2A_2(1)$, and of the first excited state, $^2A_2(2)$, of the spiro monocation. All the PES have been shifted in order to have the two C_{2v} minima at zero energy (see text for computational details).

Finally, we recall that in the NEVPT2(av) strategy, one has to give up the correct absolute value of the second order energy (notice that in this approach for $\xi = -0.5$ and $\xi = +0.5$ $E^{(2)} \neq E_A^{(2)}$), the trade-off being a coherent evaluation of the energy along the "reaction path". This allows to get an accurate estimate of all those energy differences, such as the extent of the barrier, the energy splitting at the crossing seam as well as the excitation energy for the optically-activated ET, which are the key parameters in the study of the ET processes. Some further remarks may be addressed to the question of how general such "charge-averaged" MRPT2 approach can be. Actually, the strategy of using a zero order wavefunction as the result of an average procedure along the whole reaction path between the two charge distributions can be, in principle, extended to non-symmetrical MV systems, to MV compounds containing transition metals and also to strongly-coupled systems. About the last point, it should be noted that the incorrect description of the region around the saddle point is basically related to the weak coupling between the two subunits, that brings about a sudden change in the monoelectronic energy differences as the nuclear configuration approaches the symmetrical delocalized conformation. Thus, even though the NEVPT2(av) method is well applicable to more strongly-coupled compounds, in these kinds of systems the application of a standard MRPT2 approach is expected to be less problematic due to the more gradual change of the nature of the wavefunction when passing from one charge distribution to the other.

3. Computational details

The spiro molecule, whose structure is reported in Fig. 2, is composed of two pyrrolic units, lying on two orthogonal planes which are connected by a spirocycloalkane rigid bridge. As in the previous studies [23,25], we adopt the D_{2d} geometry, suggested by Faradzel et al. [9], for the neutral molecule (with the C_2 axis passing through the N atoms) and the C_{2v} symmetry for the two charge-localized equivalent minima, arising from the ionization of the system. These minima are separated by a symmetrical D_{2d} saddle point at the crossing seam, in which the positive charge is delocalized, equally shared by the two π systems of the molecule.

However, since the MOLCAS package [35], used to compute the CASSCF wavefunctions, can only deal with Abelian point groups, the calculations for the non-Abelian D_{2d} group were performed in the reduced C_{2v} symmetry.

The electron transfer process was studied along an *ad hoc* approximate reaction path, defined by the linear mixing of the cartesian coordinates of the two optimized C_{2v} geometries [23]:

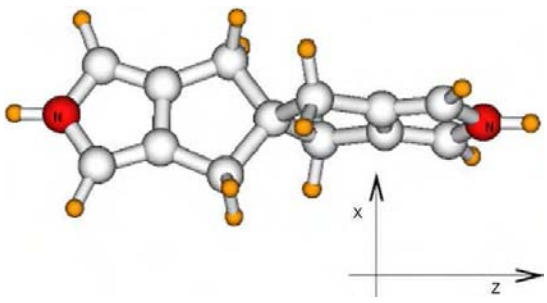

Fig. 2. The spiro molecule. The orientation used in the present calculations is such that the *z* axis (the C_2 axis) passes along the N atoms.

$$\mathbf{Q}(\xi) = \left(\frac{1}{2} - \xi\right)\mathbf{Q}_A + \left(\frac{1}{2} + \xi\right)\mathbf{Q}_B \quad (13)$$

where the mixing parameter ξ was varied, in steps of 0.05, from −1.50 to +1.50 and $\mathbf{Q}_A$ and $\mathbf{Q}_B$ are vectors collecting the coordinates of the two optimized C_{2v} geometries. Therefore, the two equivalent minima are in $\xi = -0.50$ ($\mathbf{Q}_A$, charge on the left A moiety) and $\xi = +0.50$ ($\mathbf{Q}_B$, charge on the right B moiety). An "averaged" D_{2d} geometry, which was, however, found to be very close to the optimized one (see paper I [23]), is obtained at the crossing seam point ($\xi = 0.0$).

For the calculation of the reaction path, we have used the geometries optimized in paper I at the Restricted Open Shell Hartree-Fock (ROHF) level with a triple zeta plus Polarization (TZP) ANO basis set [36].

Following the previous works, the calculations were carried out with basis sets of Atomic Natural Orbitals (ANO-L) [36] type. Different contractions levels were adopted: C,N[2*s*1*p*] and H[1*s*] (SZ); C,N[3*s*2*p*] and H[2*s*] (DZ); C,N[3*s*2*p*1*d*] and H[2*s*1*p*] (DZP) and, finally, C,N[4*s*3*p*1*d*] and H[3*s*1*p*] (TZP).

The "π system" of the spiro cation, composed of the π systems localized on the two pyrrolic rings, comprises 11 π electrons and 10 π orbitals and, at the single determinant level and in the C_{2v} point group, the electronic configuration is given by $(\sigma\text{-core})(1b_1)^2(2b_1)^2(1b_2)^2(2b_2)^2(1a_2)^2(2a_2)^1$. Therefore, the ground and the first excited states, involved in the ET process, are two states of A_2 symmetry, denoted as $^2A_2(1)$ and $^2A_2(2)$ in the following. State-averaged CASSCF calculations were carried out for the two $^2A_2$ states, using the MOLCAS5.4 package [35]; two different active spaces were employed: CAS(11/10), comprising the whole π system of the molecule, obtained distributing eleven active electrons into ten active orbitals and a smaller space, composed of seven electrons and four orbitals, CAS(7/4). The explicit composition, in the C_{2v} point group, of the active spaces used, is reported in Table 1. We recall that two variants of NEVPT2, differing in the number of correction functions used in the perturbative expansion, have been implemented [27,28], namely the "strongly contracted" (SC-NEVPT2) and the "partially contracted" (PC-NEVPT2), with the latter being the more accurate one. Although the NEVPT3 method was also implemented both in the SC [31] and PC [29] schemes, since the third order correction on this system is rather a demanding calculation, we limited the computation to the simpler SC-NEVPT3 approach; however, according to our experience, a similar behavior is to be expected of the PC-NEVPT3 method. For both active spaces and with the SZ and DZ basis sets (89 and 163 basis functions, respectively), we performed standard second and third order calculations, NEVPT2(can) and NEVPT3(can), as well as "state-averaged" second order computations, NEVPT2(av); then, for the larger basis sets, DZP and TZP (280 and 354 basis functions, respectively), we limited ourselves only to the second order computations, NEVPT2(can) and NEVPT2(av). In all the perturbative calculations, the 1s orbitals of N and C were kept frozen.

Finally, all the energy differences, reported in the next section, were computed with respect to the energy of the ground state of the cation at the C_{2v} geometry with $\xi = +0.5$ ($\xi = -0.5$), corresponding to that of the optimized geometry $\mathbf{Q}_A$ ($\mathbf{Q}_B$), although it might not be the actual minimum of the curve.

Table 1
Active spaces composition.

Active space	Composition[a]
CAS(7/4)	$12b_1$, $12b_2$, 3–$4a_2$
CAS(11/10)	11–$13b_1$, 11–$13b_2$, 3–$6a_2$

[a] At the SCF level, in the C_{2v} point group, the ground state electronic configuration of the neutral system is $(25a_1)^2(12b_1)^2(12b_2)^2(4a_2)^2$.

4. Results and discussion

Tables 2 and 3 display the CASSCF and NEVPT excitation energies obtained with the four basis sets and the two active spaces, CAS(7/4) and CAS(11/10), respectively. Table 4, instead, collects the MRCI results published in paper I [23] and here used as benchmark values to judge on the quality of those obtained at NEVPT2(av) and NEVPT3(can) levels; the comparison is made more meaningful by the use of the same basis sets (ANO-L [36] with SZ and DZ contractions) and of the same active space, CAS(7/4). The MRCI results reported here have been obtained at CAS + SD level using both an internally-contracted [37] (C-CAS + SD) and an uncontracted (CAS + SD) approach; finally, the subscript "can" indicates that canonical molecular orbitals were used. We have reported the excitation energies (kJ/mol) from the ground state, $^2A_2(1)$, at its energy minimum, taken as the value at $\xi = -0.5$, to the first excited state, $^2A_2(2)$, both at the C_{2v} ($\xi = -0.5$) and D_{2d} ($\xi = 0.0$) points; the height of the barrier for the thermal ET and the energy splitting ΔE at the crossing seam were also computed.

4.1. The energy barrier

As expected on the basis of the considerations reported in Section 2, since in the NEVPT2 scheme the dependence of $\hat{\mathscr{H}}_0$ on the orbital energies is limited to the inactive (core and virtual) orbitals, the strategy of enlarging the active space alleviates the problem around the symmetric D_{2d} geometry in the standard PT2 treatment. Therefore, we notice that, with the minimal basis set, the barrier goes from a slightly negative value, ≃−2.5 kJ/mol, with the CAS(7/4) to a slightly positive value, ≃3 kJ/mol, with the largest active space; we recall that the corresponding value, computed with the minimal CAS(3/2) space and reported in paper II, amounts about to −5 kJ/mol. Such little benefit is, however, made completely fruitless when the dimension of the basis is increased and, even with the DZ basis set, a negative energy barrier is again obtained with the CAS(11/10) (see Table 3). To clarify this behavior,

Table 2
Spiro cation-CAS(7/4): NEVPT2(can), NEVPT3(can), NEVPT2(av) energies (kJ/mol) of the ground state, $^2A_2(1)$, at $\xi = 0.0$ and of the first excited state, $^2A_2(2)$, at $\xi = 0.0$ and $\xi = -0.5$. All the energies are computed with respect to the energy of the ground state at $\xi = -0.5$. For the sake of clarity the energy splitting (ΔE kJ/mol) between the two states at $\xi = 0.0$ is also reported.

	States	CASSCF	NEVPT(can)			NEVPT2(av)	
			SC-PT2	PC-PT2	SC-PT3	SC-PT2	PC-PT2
	SZ basis set						
$\xi = -0.5$	$^2A_2(2)$	56.69	51.50	51.49	51.32	49.63	49.50
$\xi = 0.0$	$^2A_2(1)$	8.33	−2.15	−2.89	5.03	4.98	4.76
	$^2A_2(2)$	17.37	7.56	6.79	14.23	14.67	14.42
ΔE		9.04	9.71	9.68	9.20	9.70	9.66
	DZ basis set						
$\xi = -0.5$	$^2A_2(2)$	45.82	38.82	38.71	42.94	40.53	40.36
$\xi = 0.0$	$^2A_2(1)$	5.64	−7.82	−8.57	8.33	4.68	4.45
	$^2A_2(2)$	15.63	2.69	1.91	18.33	15.04	15.03
ΔE		9.99	10.52	10.47	10.00	10.36	10.58
	DZP basis set						
$\xi = -0.5$	$^2A_2(2)$	46.38	36.47	36.34		38.00	37.73
$\xi = 0.0$	$^2A_2(1)$	6.53	−11.70	−12.53		4.96	4.85
	$^2A_2(2)$	16.19	−1.31	−2.19		15.33	15.44
ΔE		9.66	10.38	10.33		10.36	10.59
	TZP basis set						
$\xi = -0.5$	$^2A_2(2)$	46.14	36.43	36.33		38.72	38.44
$\xi = 0.0$	$^2A_2(1)$	6.75	−11.54	−12.39		6.50	6.42
	$^2A_2(2)$	16.38	−1.23	−2.17		17.15	16.99
ΔE		9.63	10.31	10.23		10.66	10.57

Table 3
Spiro cation-CAS(11/10): NEVPT2(can), NEVPT3(can), NEVPT2(av) energies (kJ/mol) of the ground state, $^2A_2(1)$, at $\xi = 0.0$ and of the first excited state, $^2A_2(2)$, at $\xi = 0.0$ and $\xi = -0.5$. All the energies are computed with respect to the energy of the ground state at $\xi = -0.5$. For the sake of clarity the energy splitting (ΔE kJ/mol) between the two states at $\xi = 0.0$ is also reported.

	States	CASSCF	NEVPT(can)			NEVPT2(av)	
			SC-PT2	PC-PT2	SC-PT3	SC-PT2	PC-PT2
	SZ basis set						
$\xi = -0.5$	$^2A_2(2)$	55.51	47.34	47.13	48.34	46.93	46.76
$\xi = 0.0$	$^2A_2(1)$	7.99	3.13	3.01	5.33	5.62	5.49
	$^2A_2(2)$	15.40	11.41	11.39	13.52	13.88	13.86
ΔE		7.41	8.28	8.38	8.19	8.27	8.37
	DZ basis set						
$\xi = -0.5$	$^2A_2(2)$	47.61	34.93	34.49	39.71	36.29	35.73
$\xi = 0.0$	$^2A_2(1)$	6.92	−1.40	−3.21	6.33	5.17	4.02
	$^2A_2(2)$	15.45	7.75	5.89	15.40	14.33	13.13
ΔE		8.53	9.15	9.10	9.07	9.16	9.11
	DZP basis set						
$\xi = -0.5$	$^2A_2(2)$	47.10	32.99	32.54		34.10	33.60
$\xi = 0.0$	$^2A_2(1)$	7.04	−4.96	−6.92		5.18	4.22
	$^2A_2(2)$	15.55	4.21	2.17		14.45	13.40
ΔE		8.51	9.18	9.10		9.27	9.18
	TZP basis set						
$\xi = -0.5$	$^2A_2(2)$	46.66	33.21	32.81		36.90	36.47
$\xi = 0.0$	$^2A_2(1)$	7.17	−4.85	−6.61		7.16	6.34
	$^2A_2(2)$	15.62	4.24	2.40		16.39	15.48
ΔE		8.45	9.09	9.01		9.22	9.15

Table 4
Spiro cation-CAS(7/4): CAS + SD_{can} and C-CAS + SD_{can} energies (kJ/mol) of the ground state, $^2A_2(1)$, at $\xi = 0.0$ and of the first excited state, $^2A_2(2)$, at $\xi = 0.0$ and $\xi = -0.5$. The values have been obtained from the values reported in paper I, taking as the zero energy that of the ground state $^2A_2(1)$ at $\xi = -0.5$. See paper I for further details.

	States	CAS + SD_{can}	C-CAS + SD_{can}
	SZ basis set		
$\xi = -0.5$	$^2A_2(2)$	53.80	53.76
$\xi = 0.0$	$^2A_2(1)$	6.48	6.68
	$^2A_2(2)$	15.72	16.01
ΔE		9.25	9.32
	DZ basis set		
$\xi = -0.5$	$^2A_2(2)$	43.86	44.00
$\xi = 0.0$	$^2A_2(1)$	4.41	4.67
	$^2A_2(2)$	14.60	14.96
ΔE		10.19	10.29

it is worthwhile to point out that going from the minimal SZ basis to the DZ one produces a reduction in the energy gap between the occupied orbitals, which are shifted to higher energies, and the virtual orbitals, whose energies are, instead, brought down. This effect makes the system more sensitive to the change of the energy differences in proximity of the symmetric D_{2d} point, undoing, therefore, the slight improvement obtained by the enlargement of the CAS dimensions. Such phenomenon, although still present, is certainly less pronounced going from the DZ to DZP and then to the TZP basis sets. Moreover, as proved in paper II and shown by a first comparison between the results in Tables 2 and 3 and those in Table 4, the third order computation is unable to completely restore the correct shape of the curve. Indeed, one can appreciate that, while a good accordance between the NEVPT3(can) and NEVPT2(av) results is obtained when the NEVPT2(can) barrier is just slightly negative (see CAS(7/4)/SZ and CAS(11/10) values in Tables 2 and 3), the third order correction tends to overestimate the depth of the well when the NEVPT2(can) gives considerably wrong results. Indeed, with CAS(7/4) and DZ basis set, where the NEVPT2(can) predicts the D_{2d} point to be about 8 kJ/mol below the C_{2v} minimum, the energy barrier is estimated to be about 8 kJ/mol at NEVPT3(can) level, whereas a value amounting to $\simeq$ 4.5 kJ/mol is obtained with the NEVPT2(av) approach; such value is corroborated by the MRCI results of paper I, which estimate the height of the barrier to be about 4.5 kJ/mol (see the DZ values reported in Table 4). These considerations, apart from the expensiveness of the third order calculations, that makes this strategy not efficiently applicable to large-sized MV systems, confirm the NEVPT2(av) technique as a valuable and efficient approach to study the ET process in this class of compounds. The reliability and the firmness of the new proposed perturbative strategy is further assessed by the good accordance shown by the results obtained with the two different active spaces employed: the height of the barrier is computed to be in the range 4–5 kJ/mol with the three smallest basis sets and to be $\simeq$ 6 kJ/mol with the TZP basis. These values are in reasonable accordance with the results of the more correlated MRCI calculations (Table 4): here, with the CAS(7/4), the barrier is computed, both at the internally-contracted [37] (C-CAS + SD) and uncontracted CAS + SD level, to be about 6.5 kJ/mol (SZ) and 4.5 kJ/mol (DZ).

4.2. The energy splitting

As already argued in paper II and supported by the results in Tables 2 and 3, the energy splitting ΔE at the crossing seam, being twice the value of the electronic coupling $\mathscr{H}_{ab}$, is essentially not affected by the wrong behavior of the standard PT2 approach. One can indeed notice a remarkable agreement between the values provided by the NEVPT2(can) calculations and those attained at NEVPT3(can) and NEVPT2(av) levels. A small effect of the dynamical correlation is also evident, since a reasonable estimate of this parameter is already obtained at CASSCF level. Moreover, as also found in paper I at MRCI level, this energy difference shows practically no dependence on the basis set dimension (with the exception of a small underestimation with the minimal basis) since a value of $\simeq$ 9 kJ/mol is computed with the CAS(11/10) and $\simeq$ 10 kJ/mol with the CAS(7/4). These values for ΔE are in noticeable accordance with those computed in paper I and reported in Table 4, where the splitting, with the larger basis set, is calculated to be 10.2 and 10.3 kJ/mol at uncontracted CAS + SD and internally contracted C-CAS + SD levels respectively. Furthermore, very similar values were also obtained in the previous calculations by Sanz et al. [12]: the splitting was computed to be 9.5 (DFT), 11.0 (UHF) and 11.9 kJ/mol (DDCI). Then, a simple way to get a first estimate of the energy splitting between the two adiabatic surfaces at the crossing seam is to apply Koopmans' theorem [38,39]. Since, within a single-determinant approximation, the two electronic configurations corresponding to the ground state of the monocation and to its first excited state can be obtained from two appropriate ionization processes from the closed-shell configuration, ΔE can be approximated by the difference in the RHF energies of the HOMO and HOMO-1 orbitals of the neutral system at the symmetrical geometry. The values computed using such a rough approach provide results in good agreement with those obtained at higher levels of calculations: the splitting is indeed calculated to be 9.98 (SZ), 10.76 (DZ), 10.50 (DZP) and 10.24 kJ/mol (TZP).

4.3. Excitation energy to the $^2A_2(2)$ state

The other key parameter in the study of the ET process is the excitation energy corresponding to the optically-induced ET, namely the vertical excitation energy from the ground state at its charge-localized minimum to the first excited state. We recall that in the simple Hush's approach [4,5], for MV systems characterized by a weak electronic coupling, this quantity equals the

reorganization energy λ. As is apparent from the results in Tables 2 and 3, this energy difference appears to be much more sensitive to the correlation energy, as well as to the dimension of the basis set, than the above discussed ΔE. Overall, a small and progressive reduction can be observed going from the minimal basis to the largest one; while this reduction is sizable when passing from SZ to DZ (slightly less than 10 kJ/mol), it tends to become negligible proceeding up to the DZP and TZP basis sets. The same trend was found in paper I at MRCI level and, as shown in Table 4, the excitation energy of the $^2A_2(2)$ state, at the C_{2v} minimum, decreases by $\simeq$ 10 kJ/mol when increasing the basis set dimension. Furthermore, one can notice that also the enlargement of the active space results in a similar small lowering in the energy, anyway not exceeding 4 kJ/mol. Finally, referring to the results obtained with the same active space and basis sets (CAS(7/4)/SZ, DZ), a good accordance, up to within 5 kJ/mol, was achieved between the MRCI computations of paper I and the present NEVPT3(can) and NEVPT2(av) results.

5. Conclusions

In the present contribution we have tested the application of an alternative second order MRPT strategy, NEVPT2(av), elsewhere presented [25], to the study of the ET process in a model MV spiro compound. The NEVPT2(av) has proved to be a reliable and efficient strategy to study these kinds of systems, for which a standard MRPT2 approach is completely inadequate and at least a third order correction is needed. Although the energy splitting of the two adiabatic states at the crossing seam is essentially correct in spite of the unphysical description obtained from a standard PT2 treatment, the "charge-averaged" approach, presented here, is essential to correctly estimate the energy barrier for the thermal ET and the excitation energy for the optically-activated ET. The coherent trend shown by the results computed with different active spaces and basis sets as well as the good agreement obtained with the highly-correlated MRCI results [23] show the applicability and the firmness of this computational approach and pave the way for its future application to actual MV compounds of larger size.

Acknowledgement

This work was financed by the University of Ferrara, by the Italian MIUR through its PRIN funds, by the European Community through the COST action D37 and by CNRS through the French-Italian cooperation project PICS 4263.

References

[1] C. Creutz, H. Taube, J. Am. Chem. Soc. 91 (1969) 3988.
[2] C. Lambert, G. Nöll, J. Am. Chem. Soc. 121 (1999) 8434.
[3] M. Robin, P. Day, Adv. Inorg. Chem. Radiochem. 10 (1967) 247.
[4] N.S. Hush, Prog. Inorg. Chem. 8 (1967) 391.
[5] N.S. Hush, Coord. Chem. Rev. 64 (1985) 135.
[6] B.S. Brunschwig, C. Creutz, N. Sutin, Chem. Soc. Rev. 31 (2002) 168.
[7] V. Coropceanu, N.E. Gruhn, S. Barlow, C. Lambert, T.G.B.J.C. Durivage, G. Nöll, S.R. Marder, J.-L. Brédas, J. Am. Chem. Soc. 126 (2004) 2727.
[8] D.M. D'Alessandro, F.R. Keene, Chem. Soc. Rev. 35 (2006) 424.
[9] A. Farazdel, M. Dupuis, E. Clementi, A. Aviram, J. Am. Chem. Soc. 112 (1990) 4206.
[10] M.D. Newton, Chem. Rev. 91 (1991) 767.
[11] J.F. Sanz, J.-P. Malrieu, J. Phys. Chem. 97 (1992) 99.
[12] J.F. Sanz, C.J. Calzado, A. Márquez, Int. J. Quantum Chem. 76 (2000) 458.
[13] D. Dehareng, G. Dive, A. Moradpour, Int. J. Quantum Chem. 76 (2000) 552.
[14] M. Malagoli, J.L. Brédas, Chem. Phys. Lett. 327 (2000) 13.
[15] R.C. Johnson, J.P. Hupp, J. Am. Chem. Soc. 123 (2001) 2053.
[16] V. Coropceanu, M. Malagoli, J.M. André, J.L. Brédas, J. Chem. Phys. 115 (2001) 10409.
[17] V. Coropceanu, M. Malagoli, J.M. André, J.L. Brédas, J. Am. Chem. Soc. 124 (2002) 10519.
[18] C. Lambert, G. Nöll, Chem. Eur. J. 8 (2002) 3467.
[19] C. Lambert, S. Amthor, J. Schelter, J. Chem. Phys. A 108 (2004) 6474.
[20] A.V. Szeghalmi, M. Erdmann, V. Engel, M. Schmitt, S. Amthor, V. Kriegisch, G. Nöll, R. Stahl, C. Lambert, D. Leusser, D. Stalke, M. Zabel, J. Popp, J. Am. Chem. Soc. 126 (2004) 7834.
[21] S.F. Nelsen, A.E. Kondradsson, J.P. Telo, J. Am. Chem. Soc. 127 (2005) 920.
[22] W. Helal, B. Bories, S. Evangelisti, T. Leninger, D. Maynau, Lect. Notes Comp. Sci. 3980 (2006) 744.
[23] W. Helal, S. Evangelisti, T. Leninger, D. Maynau, J. Comp. Chem. 30 (2009) 83.
[24] C. Calzado, J.-P. Malrieu, Chem. Phys. Lett. 317 (2000) 404.
[25] M. Pastore, W. Helal, C. Angeli, R. Cimiraglia, S. Evangelisti, T. Leninger, D. Maynau, J.P. Malrieu, J. Chem. Phys. 128 (2008) 174102.
[26] C. Angeli, R. Cimiraglia, S. Evangelisti, T. Leininger, J.-P. Malrieu, J. Chem. Phys. 114 (2001) 10252.
[27] C. Angeli, R. Cimiraglia, J.-P. Malrieu, Chem. Phys. Lett. 350 (2001) 297.
[28] C. Angeli, R. Cimiraglia, J.-P. Malrieu, J. Chem. Phys. 117 (2002) 9138.
[29] C. Angeli, M. Pastore, R. Cimiraglia, Theor. Chem. Acc. 117 (2007) 743.
[30] C. Angeli, S. Borini, M. Cestari, R. Cimiraglia, J. Chem. Phys. 121 (2004) 4043.
[31] C. Angeli, B. Bories, A. Cavallini, R. Cimiraglia, J. Chem. Phys. 124 (2006) 054108.
[32] B. Huron, J.P. Malrieu, P. Rancurel, J. Chem. Phys. 58 (1973) 5745.
[33] C. Angeli, R. Cimiraglia, J.-P. Malrieu, Chem. Phys. Lett. 317 (2000) 462.
[34] C. Møller, M.S. Plesset, Phys. Rev. 46 (1934) 618.
[35] M. Andersson, A. Barysz, M. Bernhardsson, R.A. Blomberg, D.L. Cooper, M.P. Fülscher, C. de Graaf, B.A. Hess, G. Karlström, R. Lindh, P.-Å. Malmqvist, T. Nakajima, P. Neogrády, J. Olsen, B.O. Roos, B. Schimmelpfennig, M. Schütz, L. Seijo, L. Serrano-Andrés, P.E.M. Siegbahn, J.S.T. Thorsteinsson, V. Veryazov, P.-O. Widmark, Molcas5.4 (2002).
[36] P.-O. Widmark, P. Malmqvist, B.O. Roos, Theor. Chim. Acta 77 (1990) 291–306.
[37] H.-J. Werner, P.J. Knowles, J. Chem. Phys. 89 (1988) 5803.
[38] T. Koopmans, Physica 1 (1933) 104.
[39] C. Angeli, J. Chem. Edu. 75 (1998) 1494.

8.2 Other results of calculations on Spiro using CAS(7/4), CAS(7/8) and CAS(11/10) active spaces with different basis sets

This section contains tables with results of calculations on Spiro that were not reported in sections §4.4.4, 4.4.5, and 4.4.6.

Table 8.1: *Absolute energies, in a.u., of the different states of Spiro cation, at D_{2d} geometry ($\xi = 0.00$) and C_{2v} geometry ($\xi = 0.50$), for different methods using SZ basis set and CAS(7/4): CAS_{can}, C-$CAS+SD_{can}$, $CAS_{loc-guess}$, $CAS_{loc-opt}$, $CAS+S_{loc}$ and $CAS+SD_{loc}$*
.

Geometry	State	CAS_{can}	C-$CAS+SD_{can}$	$CAS_{loc-guess}$	$CAS_{loc-opt}$	$CAS+S_{loc}$	$CAS+SD_{loc}$
D_{2d}	1^2A_2	-607.818761	-608.393342	-607.797952	-607.818309	-607.869516	-608.497676
	2^2A_2	-607.815317	-608.389791	-607.797670	-607.814868	-607.866445	-608.494212
	$^2B_1$	-607.801717	-608.372785	-607.671072	-607.800878	-607.836126	-608.477425
	$^2B_2$	-607.801717	-608.372785	-607.671072	-607.800878	-607.836126	-608.477425
C_{2v}	1^2A_2	-607.821933	-608.395887	-607.802639	-607.821582	-607.871438	-608.500290
	2^2A_2	-607.800341	-608.375411	-607.781109	-607.799783	-607.852817	-608.479630
	$^2B_1$	-607.798706	-608.370591	-607.662968	-607.797982	-607.837476	-608.474939
	$^2B_2$	-607.793353	-608.363373	-607.667020	-607.792019	-607.825980	-608.467912

Table 8.2: *Energies, in kJ/mol, of the different states of Spiro cation, at D_{2d} geometry ($\xi = 0.00$) and C_{2v} geometry ($\xi = 0.50$), for different methods using SZ basis set and CAS(7/4): CAS_{can}, C-$CAS+SD_{can}$, $CAS_{loc-guess}$, $CAS_{loc-opt}$, $CAS+S_{loc}$ and $CAS+SD_{loc}$. For each method, the reference energy has been taken as the energy of the ground state 1^2A_2 in the D_{2d} geometry.*

Geometry	State	CAS_{can}	C-$CAS+SD_{can}$	$CAS_{loc-guess}$	$CAS_{loc-opt}$	$CAS+S_{loc}$	$CAS+SD_{loc}$
D_{2d}	1^2A_2	0.000	0.000	0.000	0.000	0.000	0.000
	2^2A_2	9.043	9.323	0.743	9.035	8.063	9.096
	$^2B_1$	44.748	53.972	333.126	45.766	87.666	53.170
	$^2B_2$	44.748	53.972	333.126	45.766	87.666	53.170
C_{2v}	1^2A_2	-8.328	-6.684	-12.305	-8.593	-5.048	-6.862
	2^2A_2	48.362	47.076	44.223	48.638	43.842	47.380
	$^2B_1$	52.655	59.732	354.402	53.369	84.120	59.698
	$^2B_2$	66.710	78.682	343.763	69.024	114.303	78.146

Table 8.3: *Absolute energies, in a.u., of the different states of Spiro cation, at D_{2d} geometry ($\xi = 0.00$) and C_{2v} geometry ($\xi = 0.50$), for different methods using DZ basis set and CAS(7/4): CAS_{can}, C-$CAS+SD_{can}$, $CAS_{loc-guess}$, $CAS_{loc-opt}$, $CAS+S_{loc}$ and $CAS+SD_{loc}$.*

Geometry	State	CAS_{can}	C-$CAS+SD_{can}$	$CAS_{loc-guess}$	$CAS_{loc-opt}$	$CAS+S_{loc}$	$CAS+SD_{loc}$
D_{2d}	1^2A_2	-608.847468	-609.677281	-608.823693	-608.846770	-608.908804	-609.831383
	2^2A_2	-608.843664	-609.673361	-608.822858	-608.842997	-608.905484	-609.827600
	$^2B_1$	-608.827797	-609.653514	-608.678618	-608.826895	-608.864884	-609.808070
	$^2B_2$	-608.827797	-609.653514	-608.678618	-608.826895	-608.864884	-609.808070
C_{2v}	1^2A_2	-608.849617	-609.679059	-608.827720	-608.849094	-608.910002	-609.831383
	2^2A_2	-608.832163	-609.662305	-608.809405	-608.831314	-608.895001	-609.827600
	$^2B_1$	-608.825787	-609.652346	-608.671799	-608.825116	-608.864240	-609.806682
	$^2B_2$	-608.820946	-609.645710	-608.675835	-608.819818	-608.856267	-609.800375

Table 8.4: *Energies, in kJ/mol, of the different states of Spiro cation, at D_{2d} geometry ($\xi = 0.00$) and C_{2v} geometry ($\xi = 0.50$), for different methods using DZ basis set and CAS(7/4): CAS_{can}, C-$CAS+SD_{can}$, $CAS_{loc-guess}$, $CAS_{loc-opt}$, $CAS+S_{loc}$ and $CAS+SD_{loc}$. For each method, the reference energy has been taken as the energy of the ground state 1^2A_2 in the D_{2d} geometry.*

Geometry	State	CAS_{can}	C-$CAS+SD_{can}$	$CAS_{loc-guess}$	$CAS_{loc-opt}$	$CAS+S_{loc}$	$CAS+SD_{loc}$
D_{2d}	1^2A_2	0.000	0.000	0.000	0.000	0.000	0.000
	2^2A_2	9.987	10.290	2.191	9.908	8.717	9.933
	$^2B_1$	51.646	62.400	380.894	52.182	115.312	61.209
	$^2B_2$	51.646	62.400	380.894	52.182	115.312	61.209
C_{2v}	1^2A_2	-5.640	-4.669	-10.573	-6.102	-3.148	-4.914
	2^2A_2	40.185	39.319	37.513	40.581	36.239	39.546
	$^2B_1$	56.923	65.467	398.796	56.854	117.002	63.289
	$^2B_2$	69.636	82.888	388.201	70.764	137.934	79.849

Table 8.5: *Absolute energies, in a.u., of the different states of Spiro cation, at D_{2d} geometry ($\xi = 0.00$) and C_{2v} geometry ($\xi = 0.50$), for different methods using DZP basis set and CAS(7/4): CAS_{can}, C-$CAS+SD_{can}$, $CAS_{loc-guess}$, $CAS_{loc-opt}$ and $CAS+S_{loc}$.*

Geometry	State	CAS_{can}	C-$CAS+SD_{can}$	$CAS_{loc-guess}$	$CAS_{loc-opt}$	$CAS+S_{loc}$
D_{2d}	1^2A_2	-609.167882	-610.379384	-609.143392	-609.167230	-609.235470
	2^2A_2	-609.164201	-610.375546	-609.142561	-609.163559	-609.232250
	$^2B_1$	-609.150163	-610.356006	-608.997896	-609.149207	-609.190771
	$^2B_2$	-609.150163	-610.356006	-608.997896	-609.149207	-609.190771
C_{2v}	1^2A_2	-609.170368	-610.381363	-609.147787	-609.169873	-609.237064
	2^2A_2	-609.152703	-610.364514	-609.129080	-609.151899	-609.221655
	$^2B_1$	-609.148152	-610.354651	-608.991080	-609.147436	-609.190290
	$^2B_2$	-609.143726	-610.348659	-608.995482	-609.142483	-609.182367

Table 8.6: *Absolute energies, in a.u., of the different states of Spiro cation, at D_{2d} geometry ($\xi = 0.00$) and C_{2v} geometry ($\xi = 0.50$), for different methods using TZP basis set and CAS(7/4): CAS_{can}, C-CAS+SD_{can}, $CAS_{loc-guess}$, $CAS_{loc-opt}$ and CAS+S_{loc}.*

Geometry	State	CAS_{can}	C-CAS+SD_{can}	$CAS_{loc-guess}$	$CAS_{loc-opt}$	CAS+S_{loc}
D_{2d}	1^2A_2	-609.204169	-610.469834	-609.179038	-609.203517	-609.272375
	2^2A_2	-609.200503	-610.466026	-609.178224	-609.199858	-609.269179
	$^2B_1$	-609.186961	-610.447186	-609.033755	-609.186003	-609.227881
	$^2B_2$	-609.186961	-610.447186	-609.033755	-609.186003	-609.227881
C_{2v}	1^2A_2	-609.206742	-610.471959	-609.183498	-609.206246	-609.273645
	2^2A_2	-609.189167	-610.455161	-609.164928	-609.188353	-609.258637
	$^2B_1$	-609.185037	-610.445951	-609.027117	-609.184303	-609.227503
	$^2B_2$	-609.180657	-610.440031	-609.031408	-609.179398	-609.219805

Table 8.7: *Absolute energies, in a.u., of the different states of Spiro cation, at D_{2d} geometry ($\xi = 0.00$) and C_{2v} geometry ($\xi = 0.50$), for different methods using SZ basis set and CAS(7/8): CAS_{can}, $CAS_{loc-guess}$, $CAS_{loc-opt}$ and $CAS+S_{loc}$.*

Geometry	State	CAS_{can}	$CAS_{loc-guess}$	$CAS_{loc-opt}$	$CAS+S_{loc}$
D_{2d}	1^2A_2	-607.896162	-607.868004	-607.895906	-608.053959
	2^2A_2	-607.893114	-607.867715	-607.892719	-608.050856
	$^2B_1$	-607.880496	-607.764338	-607.878741	-608.027384
	$^2B_2$	-607.880496	-607.764338	-607.878741	-608.027384
C_{2v}	1^2A_2	-607.898402	-607.872386	-607.898151	-608.055489
	2^2A_2	-607.878749	-607.851241	-607.878331	-608.036908
	$^2B_1$	-607.876468	-607.754224	-607.874897	-608.025225
	$^2B_2$	-607.872620	-607.762092	-607.870870	-608.017268

Table 8.8: *Absolute energies, in a.u., of the different states of Spiro cation, at D_{2d} geometry ($\xi = 0.00$) and C_{2v} geometry ($\xi = 0.50$), for different methods using DZ basis set and CAS(7/8): CAS_{can}, $CAS_{loc-guess}$, $CAS_{loc-opt}$ and $CAS+S_{loc}$.*

Geometry	State	CAS_{can}	$CAS_{loc-guess}$	$CAS_{loc-opt}$	$CAS+S_{loc}$
D_{2d}	1^2A_2	-608.924267	-608.890171	-608.922241	-609.116863
	2^2A_2	-608.920814	-608.889352	-608.918704	-609.113530
	$^2B_1$	-608.906532	-608.766935	-608.902327	-609.082477
	$^2B_2$	-608.906532	-608.766935	-608.902327	-609.082477
C_{2v}	1^2A_2	-608.925970	-608.894409	-608.924055	-609.117670
	2^2A_2	-608.909564	-608.875541	-608.907331	-609.103002
	$^2B_1$	-608.903388	-608.757849	-608.899181	-609.081180
	$^2B_2$	-608.900451	-608.766314	-608.896408	-609.074203

Table 8.9: *Absolute energies, in a.u., of the different states of Spiro cation, at D_{2d} geometry ($\xi = 0.00$) and C_{2v} geometry ($\xi = 0.50$), for different methods using DZP basis set and CAS(7/8): CAS_{can}, $CAS_{loc-guess}$.*

Geometry	State	CAS_{can}	$CAS_{loc-guess}$
D_{2d}	1^2A_2	-609.240349	-609.204067
	2^2A_2	-609.236983	-609.203249
	$^2B_1$	-609.225609	-609.079248
	$^2B_2$	-609.225609	-609.079248
C_{2v}	1^2A_2	-609.242000	-609.208595
	2^2A_2	-609.225970	-609.189452
	$^2B_1$	-609.222506	-609.070262
	$^2B_2$	-609.219803	-609.078825

Table 8.10: *Energies, in kJ/mol, of the different states of Spiro cation, at D_{2d} geometry ($\xi = 0.00$) and C_{2v} geometry ($\xi = 0.50$), for different methods using DZP basis set and CAS(7/8): CAS_{can}, $CAS_{loc-guess}$. For each method, the reference energy has been taken as the energy of the ground state 1^2A_2 in the D_{2d} geometry.*

Geometry	State	CAS_{can}	$CAS_{loc-guess}$
D_{2d}	1^2A_2	0.000	0.000
	2^2A_2	8.838	2.146
	$^2B_1$	38.699	327.710
	$^2B_2$	38.699	327.710
C_{2v}	1^2A_2	-4.597	-11.888
	2^2A_2	37.752	38.370
	$^2B_1$	46.848	351.303
	$^2B_2$	53.943	328.821

Table 8.11: *Absolute energies, in a.u., of the different states of Spiro cation, at D_{2d} geometry ($\xi = 0.00$) and C_{2v} geometry ($\xi = 0.50$), for different methods using TZP basis set and CAS(7/8): CAS_{can}, $CAS_{loc-guess}$.*

Geometry	State	CAS_{can}	$CAS_{loc-guess}$
D_{2d}	1^2A_2	-609.276308	-609.239205
	2^2A_2	-609.272967	-609.238404
	$^2B_1$	-609.262128	-609.114573
	$^2B_2$	-609.262128	-609.114573
C_{2v}	1^2A_2	-609.278140	-609.243785
	2^2A_2	-609.262124	-609.224807
	$^2B_1$	-609.259162	-609.105805
	$^2B_2$	-609.256415	-609.114177

Table 8.12: *Energies, in kJ/mol, of the different states of Spiro cation, at D_{2d} geometry ($\xi = 0.00$) and C_{2v} geometry ($\xi = 0.50$), for different methods using TZP basis set and CAS(7/8): CAS_{can}, $CAS_{loc-guess}$. For each method, the reference energy has been taken as the energy of the ground state 1^2A_2 in the D_{2d} geometry.*

Geometry	State	CAS_{can}	$CAS_{loc-guess}$
D_{2d}	1^2A_2	0.000	0.000
	2^2A_2	8.771	2.102
	$^2B_1$	37.230	327.220
	$^2B_2$	37.230	327.220
C_{2v}	1^2A_2	-4.811	-12.024
	2^2A_2	37.241	37.803
	$^2B_1$	45.016	350.242
	$^2B_2$	52.230	328.262

Table 8.13: *Absolute energies, in a.u., of the different states of Spiro cation, at D_{2d} geometry ($\xi = 0.00$) and C_{2v} geometry ($\xi = 0.50$), for different methods using SZ basis set and CAS(11/10): CAS_{can}, $CAS_{loc-guess}$, $CAS_{loc-opt-frz}$, $CAS{+}S_{loc-frz}$, $CAS{+}SD_{loc-frz}$, $CAS_{loc-opt}$ and $CAS{+}S_{loc}$.*

Geometry	State	CAS_{can}	$CAS_{loc-guess}$	$CAS_{loc-opt-frz}$	$CAS{+}S_{loc-frz}$	$CAS{+}SD_{loc-frz}$	$CAS_{loc-opt}$	$CAS{+}S_{loc}$
D_{2d}	1^2A_2	-607.927553	-607.904904	-607.906994	-607.907657	-607.911957	-607.927377	-608.122487
	2^2A_2	-607.924731	-607.904674	-607.906705	-607.907366	-607.911666	-607.924459	-608.119512
	$^2B_1$	-607.922151	-607.868391	-607.868301	-607.868533	-607.872690	-607.921760	-608.098607
	$^2B_2$	-607.922151	-607.868391	-607.868301	-607.868533	-607.872690	-607.921760	-608.098607
C_{2v}	1^2A_2	-607.930596	-607.909555	-607.911612	-607.912262	-607.916525	-607.930432	-608.124202
	2^2A_2	-607.909452	-607.887786	-607.889829	-607.890498	-607.894846	-607.909159	-608.105313
	$^2B_1$	-607.920306	-607.866066	-607.865955	-607.866182	-607.870326	-607.919913	-608.096481
	$^2B_2$	-607.911870	-607.858301	-607.858249	-607.858482	-607.862662	-607.911473	-608.088329

Table 8.14: *Absolute energyies, in a.u., of the different states of Spiro cation, at D_{2d} geometry ($\xi = 0.00$) and C_{2v} geometry ($\xi = 0.50$), for different methods using DZ basis set and CAS(11/10): CAS_{can}, $CAS_{loc-guess}$, $CAS_{loc-opt-frz}$ and CAS+$S_{loc-frz}$.*

Geometry	State	CAS_{can}	$CAS_{loc-guess}$	$CAS_{loc-opt-frz}$	CAS+$S_{loc-frz}$
D_{2d}	1^2A_2	-608.949720	-608.920412	-608.933790	-608.961700
	2^2A_2	-608.946471	-608.919673	-608.932728	-608.960792
	$^2B_1$	-608.945129	-608.877160	-608.900009	-608.918742
	$^2B_2$	-608.945129	-608.877160	-608.900009	-608.918742
C_{2v}	1^2A_2	-608.952356	-608.924844	-608.938174	-608.965738
	2^2A_2	-608.934223	-608.905620	-608.918663	-608.947133
	$^2B_1$	-608.944212	-608.876286	-608.899291	-608.918170
	$^2B_2$	-608.936647	-608.868315	-608.891066	-608.909598

Table 8.15: *Energies, in kJ/mol, of the different states of Spiro cation, at D_{2d} geometry ($\xi = 0.00$) and C_{2v} geometry ($\xi = 0.50$), for different methods using DZ basis set and CAS(11/10): CAS_{can}, $CAS_{loc-guess}$, $CAS_{loc-opt-frz}$ and CAS+$S_{loc-frz}$. For each method, the reference energy has been taken as the energy of the ground state 1^2A_2 in the D_{2d} geometry.*

Geometry	State	CAS_{can}	$CAS_{loc-guess}$	$CAS_{loc-opt-frz}$	CAS+$S_{loc-frz}$
D_{2d}	1^2A_2	0.000	0.000	0.000	0.000
	2^2A_2	8.530	1.942	2.789	2.646
	$^2B_1$	12.053	113.560	88.691	113.048
	$^2B_2$	12.053	113.560	88.691	113.048
C_{2v}	1^2A_2	-6.920	-11.637	-11.510	-10.339
	2^2A_2	40.688	38.838	39.717	38.508
	$^2B_1$	14.462	115.853	90.577	114.550
	$^2B_2$	34.323	136.782	112.173	137.055

Table 8.16: *Absolute energies, in a.u., of the different states of Spiro cation, at D_{2d} geometry ($\xi = 0.00$) and C_{2v} geometry ($\xi = 0.50$), for different methods using DZP basis set and CAS(11/10): CAS_{can}, $CAS_{loc-guess}$, $CAS_{loc-opt-frz}$ and $CAS{+}S_{loc-frz}$.*

Geometry	State	CAS_{can}	$CAS_{loc-guess}$	$CAS_{loc-opt-frz}$	$CAS{+}S_{loc-frz}$
D_{2d}	1^2A_2	-609.264132	-609.232001	-609.248080	-609.289570
	2^2A_2	-609.260890	-609.231250	-609.246991	-609.288535
	$^2B_1$	-609.260282	-609.187822	-609.215069	-609.245289
	$^2B_2$	-609.260282	-609.187822	-609.215069	-609.245289
C_{2v}	1^2A_2	-609.266811	-609.236705	-609.252487	-609.293326
	2^2A_2	-609.248871	-609.217235	-609.233177	-609.275283
	$^2B_1$	-609.259409	-609.187109	-609.214613	-609.244809
	$^2B_2$	-609.252066	-609.179120	-609.206164	-609.236269

Table 8.17: *Energies, in kJ/mol, of the different states of Spiro cation, at D_{2d} geometry ($\xi = 0.00$) and C_{2v} geometry ($\xi = 0.50$), for different methods using DZP basis set and CAS(11/10): CAS_{can}, $CAS_{loc-guess}$, $CAS_{loc-opt-frz}$ and $CAS{+}S_{loc-frz}$. For each method, the reference energy has been taken as the energy of the ground state 1^2A_2 in the D_{2d} geometry.*

Geometry	State	CAS_{can}	$CAS_{loc-guess}$	$CAS_{loc-opt-frz}$	$CAS{+}S_{loc-frz}$
D_{2d}	1^2A_2	0.000	0.000	0.000	0.000
	2^2A_2	8.512	1.973	2.859	2.719
	$^2B_1$	10.107	115.992	86.671	116.260
	$^2B_2$	10.107	115.992	86.671	116.260
C_{2v}	1^2A_2	-7.035	-12.349	-11.570	-9.862
	2^2A_2	40.067	38.770	39.130	37.511
	$^2B_1$	12.400	117.865	87.868	117.519
	$^2B_2$	31.679	138.841	110.050	139.942

Table 8.18: *Absolute energies, in a.u., of the different states of Spiro cation, at D_{2d} geometry ($\xi = 0.00$) and C_{2v} geometry ($\xi = 0.50$), for different methods using TZP basis set and CAS(11/10): CAS_{can}, $CAS_{loc-guess}$, $CAS_{loc-opt-frz}$ and CAS+$S_{loc-frz}$.*

Geometry	State	CAS_{can}	$CAS_{loc-guess}$	$CAS_{loc-opt-frz}$	CAS+$S_{loc-frz}$
D_{2d}	1^2A_2	-609.300202	-609.267049	-609.283464	-609.325118
	2^2A_2	-609.296984	-609.266311	-609.282391	-609.324095
	$^2B_1$	-609.296505	-609.222845	-609.250216	-609.280657
	$^2B_2$	-609.296505	-609.222845	-609.250216	-609.280657
C_{2v}	1^2A_2	-609.286089	-609.271803	-609.287912	-609.328940
	2^2A_2	-609.267317	-609.252492	-609.268793	-609.311055
	$^2B_1$	-609.256452	-609.222245	-609.249812	-609.280224
	$^2B_2$	-609.249049	-609.214265	-609.241513	-609.271856

Bibliography

[1] Plank, M., *Ann. Physik.*, 1901, **4**, 553.

[2] Einstein, A., *Ann. Physik.*, 1905, **17**, 132.

[3] Bohr, N., *Phil. Mag.*, 1913, **26**(1), 476.

[4] Compton, H. A., *Phys. Rev.*, 1923, **22**, 409.

[5] Bohr, N., *Z. Phys.*, 1923, **13**, 117.

[6] de Broglie, L., *Phil. Mag.*, 1924, **47**, 446.

[7] de Broglie, L., *Ann. Physik.*, 1925, **3**, 22.

[8] Heisenberg, W., *Z. Phys.*, 1925, **33**, 879.

[9] Born, M; Jordan, P., *Z. Phys.*, 1925, **34**, 858.

[10] Born, M; Heisenberg, W.; Jordan, P., *Z. Phys.*, 1926, **35**, 557.

[11] Schrödinger, E., *Ann. Physik.*, 1926, **79**, 361.

[12] Schrödinger, E., *Ann. Physik.*, 1926, **79**, 489.

[13] Schrödinger, E., *Ann. Physik.*, 1926, **79**, 734.

[14] Schrödinger, E., *Ann. Physik.*, 1926, **80**, 437.

[15] Schrödinger, E., *Ann. Physik.*, 1926, **81**, 109.

[16] Schrödinger, E., *Phys. Rev.*, 1926, **28**, 1049.

[17] Dirac, P. A. M., *Proc. Roy. Soc.*, 1927, **A114**, 243.

[18] Jordan, P,; Klein, O., *Z. Phys.*, 1927, **45**, 751.

[19] Jordan, P,; Wigner, E., *Z. Phys.*, 1928, **47**, 631.

[20] Feynman, R. P., *Rev. Mod. Phys.*, 1948, **20**, 367.

[21] Feynman, R. P.; Hibbs, A. R., *Quantum Mechanics and Path Integrals*, McGraw-Hill, 1965.

[22] Heitler, W. London, F., *Z. Phys.*, 1927, **44**, 455.

[23] Slater, J. C., *Phys. Rev.*, 1931, **37**, 481.

[24] Slater, J. C., *Phys. Rev.*, 1931, **38**, 1109.

[25] Pauling, L., *J. Am. Chem. Soc.*, 1931, **53**, 1367, 3225.

[26] Lennard-Jones, J. E., *Trans. Faraday Soc.*, 1929, **25**, 668.

[27] Hund, F., *Z. Phys.*, 1931, **73**, 1, 565.

[28] Hund, F., *Z. Phys.*, 1932, **74**, 429.

[29] Mulliken, R. S., *Phys. Rev.*, 1932, **40**, 55.

[30] Mulliken, R. S., *Phys. Rev.*, 1932, **41**, 49, 751.

[31] Mulliken, R. S., *Phys. Rev.*, 1933, **43**, 279.

[32] Mulliken, R. S., *J. Chem. Phys.*, 1933, **1**, 492.

[33] Van Vleck, J. H., Sherman, A., *Rev. Mod. Phys.*, 1935, **7**, 167.

[34] Richards, W. G.; Horsley, J. A., *Ab Initio Molecular Orbital Calculations for Chemists*, Clarendon Press, Oxford, 1970.

[35] Schaefer III, H. F., *The Electronic Structure of Atoms and Molecules, a Survey of Rigorous Quantum Mechanical Results*, Addison-Wesley, 1972.

[36] Cook, D. B., *Ab Initio Valence Calculations in Chemistry*, John Wiley and Sons, New York, 1974.

[37] Schaefer, H. F., Ed., *Methods of Electronic Structure Theory*, Plenum, New York, 1977.

[38] Schaefer, H. F., Ed., *Applications of Electronic Structure Theory*, Plenum, New York, 1977.

[39] Dykstra, C. E., Ed., *Advanced Theories and Computational Approaches to the Electronic Structure of Molecules*, Reidel, Dordrecht, 1984.

[40] Bartlett, R. J., Ed., *Comparison of Ab Initio Quantum Chemistry with Experiment for Small Molecules, the State of the Art*, Reidel, Dordrecht, 1985.

[41] Hehre, W. J.; Radom, L.; Schleyer, P. v. R.; Pople, J. A., *Ab Initio Molecular Orbital Theory*, John Wiley and Sons, New York, 1986.

[42] Lawley, K. P., Ed., *Adv. Chem. Phys.: Ab Initio Methods in Quantum Chemistry, Part I*, 1987, **67**, John Wiley and Sons, Chichester.

[43] Lawley, K. P., Ed., *Adv. Chem. Phys.: Ab Initio Methods in Quantum Chemistry, Part II*, 1987, **69**, John Wiley and Sons, Chichester.

[44] Simons, J., *J. Phys. Chem.*, 1991, **95**, 1017.

[45] Yarkony, D. R., Ed., *Modern Electronic Structure Theory*, World Scientific, 1995.

[46] Helgaker, T.; Jørgensen, P.; Olsen, J., *Molecular Electronic-Structure Theory*, John Wiley, 2000.

[47] Krauss, M., *Compendium of* ab initio *Calculations of Molecular Energies and Properties, Nat. Bur. Stand. (USA)*, 1967, Tech. Note 438.

[48] Allen, L. C., *Ann. Rev. Phys. Chem.*, 1969, **20**, 315.

[49] Richards, W. G.; Walker, T. E. H.; Hinkley, R. K., *A Bibliography of Ab Initio Molecular Wavefunctions*, Clarendon Press, Oxford, 1971; Richards, W. G.; Walker, T. E. H.; Farnell, L.; Scott, P. R., *Supplement for 1970–1973*, 1974; Richards, W. G.; Scott, P. R.; Colbourn, E. A., Marchington, A. F., *Supplement for 1974–1977*, 1978; Richards, W. G.; Scott, P. R.; Sackwild, V., Robins, S. A., *Supplement for 1978–1980*, 1981.

[50] Mulliken, R. S.; Ermler, W. C., *Diatomic Molecules* Academic Press, 1977.

[51] Mulliken, R. S.; Ermler, W. C., *Polyatomic Molecules* Academic Press, 1981.

[52] Ohno, K.; Morokuma, K., *Quantum Chemistry Literature Data Base*, Elsevier, New York, 1982.

[53] Segal, G. A., Ed., *Semiempirical Methods of Electronic-Structure Calculation, Part A: Techniques*, Plenum, New York, 1977.

[54] Segal, G. A., Ed., *Semiempirical Methods of Electronic-Structure Calculation, Part B: Applications*, Plenum, New York, 1977.

[55] Sadley, J., *Semi-Empirical methods of Quantum Chemistry*, John Wiley, 1985.

[56] Zerner, M. C., *Rev. Comput. Chem.*, 1991, **2**, 313.

[57] Parr, R. G.,; Yang, W., *Density Functional Theory*, Oxford University Press, 1989.

[58] Zeigler, T., *Chem. Rev.*, 1991, **91**, 651.

[59] Bartolotti, L. J.; Flurchick, K., *Rev. Comput. Chem.*, 1996, **7**, 187.

[60] St-Amant, A., *Rev. Comput. Chem.*, 1996, **7**, 217.

[61] Seminario, J. M., Ed., *Recent Developments and Applications of Modern Density Functional Theory*, Elsevier, 1996.

[62] Baerends, E. J.; Gritsenko, O. V., *J. Phys. Chem.*, 1997, **101**, 5383.

[63] Koch, W.; Holthausen, M. C., *A Chemist's Guide to Density Functional Theory*, 2nd. ed., WILEY-VCH

[64] Metropolis, N.; Ulam, S., *J. Am. Stat. Assoc.*, 1949 **44**, 335.

[65] Anderson, J. B., *J.Chem, Phys.* 1975, **64**, 149.

[66] Hasting, W. K., *Biometrika*, 1970, **57**, 97.

[67] Reynolds P. J.; Ceperley, D., *J. Chem. Phys.* 1982, **77**, 5593.

[68] Dirac, P. A. M., *The Principles of Quantum Mechanics*, 4th ed., Oxford University Press, 1958.

[69] Lindeberg, J; Öhrn, Y., *Propagators in Quantum Chemistry*, Academic Press, New York, 1973.

[70] Avery, J., *Creation and Annihilation Operators*, McGraw-Hill, New York, 1976.

[71] Jørgensen, P.; Simons, J., *Second Quantization-Based Methods in Quantum Chemistry*, Academic Press, New York, 1981.

[72] Pitzer, K. S., *Acc. Chem. Res.*, 1979, **12**, 271.

[73] Pyykkö, P.; Desclaux, J. P., *Acc. Chem. Res.*, 1979, **12**, 276.

[74] Pyykkö, P., *Chem. Rev.*, 1988, **88**, 563.

[75] Born, M.; Oppenheimer, J. R., *Ann. Physik.*, 1927, **84**, 457.

[76] Born, M.; Haung, K., *Dynamical Theory of Crystal Lattices*, Oxford University Press, Oxford, 1954.

[77] Born M.,; Fock, V. A., *Z. Phys.*, 1928, **51**, 165.

[78] Kato, T., *J. Phys. Soc. of Japan*, 1950, **5**, 435.

[79] Handy, N. C.; Lee, A. M., *Chem. Phys. Lett.*, 1996, **252**, 425.

[80] Kolos, W.; Wolniewicz, L., *J. Chem. Phys.*, 1964, **41**, 3663.

[81] Sutcliffe, B. T., *Adv. Quantum Chem.*, 1997, **28**, 65.

[82] Yarkony, D. R., *J. Phys. Chem.*, 1996, **100**, 18612.

[83] Newton, M. D., *Chem. Rev.*, 1991, **91**, 767.

[84] Baer, M.; Ng, C.-Y., *Adv. Chem. Phys.*, 1992, **82**, John Wiley and Sons: New York.

[85] Pauli, W., *Z. Phys.*, 1925, **31**, 765.

[86] Slater, J. C., *Phys. Rev.*, 1929, **34**, 1293.

[87] Slater, J. C., *Phys. Rev.*, 1930, **35**, 210.

[88] Roothaan, C. C. J., *Rev. Mod. Phys.*, 1951, **23**, 69.

[89] Hall, G. G., *Proc. Roy. Soc.*, (London), 1951, **A205**, 541.

[90] Hartree, D. R., *Proc. Cambridge. Phil. Soc.*, 1928, **24**, 89.

[91] Fock, V., *Z. Phys.*, 1930, **61**, 126.

[92] Koopmans, T., *Physica*, 1933, **1**, 104.

[93] Berthier, G., *J. Chem. Phys.*, 1954, **51**, 363.

[94] Pople, J. A.; Nesbet, R. K., *J. Chem. Phys.*, 1954, **22**, 571.

[95] Roothaan, C. C. J., *Rev. Mod. Phys.*, 1960, **32**, 179.

[96] Pople, J. A.; Binkley, J. S.; Seeger, R., *Int. J. Quantum Chem. Quantum Chem. Symp.*, 1976, **10**, 1.

[97] Bartlett, R. J.; Purvis, G. D., *Int. J. Quantum Chem.*, 1978, **14**, 561.

[98] Brillouin, L., *Actualités Sci. Ind.* 1933, No. **71**.

[99] Brillouin, L., *Actualités Sci. Ind.* 1934, No. **159**.

[100] Löwdin, P.-O., *Adv. Chem. Phys.*, 1959, **2**, 207.

[101] Goddard III, W. A., *J. Chem. Phys.*, 1968, **48**, 5337.

[102] Hunt, W. J.; Hey, P. J.; Goddard, W. A., *J. Chem. Phys.*, 1972, **57**, 738.

[103] Hey, P. J.; Hunt, W. J.; Goddard, W. A., *J. Am. Chem. Soc.*, 1972, **94**, 8293.

[104] Goddard, W. A.; Dunning, T. H.; Hunt, W. J.; Hey, P. J., *Acc. Chem. Res.*, 1973, **6**, 368.

[105] Goddard, W. A.; Harding, L.B., *Ann. Rev. Phys. Chem.*, 1978, **29**, 363.

[106] Bartlett, R. J., *Ann. Rev. Phys. Chem.*, 1981, **32**, 359.

[107] Wilson, S., *Chem. Rev.*, 1980, **80**, 263.

[108] Hurley, A. C., *Electron Correlation in Small Molecules*, Academic Press, New York, 1976.

[109] Wilson, S., *Electron Correlation in Molecules*, Clarendon Press, Oxford, 1984.

[110] Wilson, S., Ed., *Methods in Computational Chemistry, Vol. 1: Electron Correlation in Atoms and Molecules*, Plenum Press, New York, 1987.

[111] Raghavachari, K., *Ann. Rev. Phys. Chem.*, 1991, **42**, 615.

[112] Raghavachari, K.; Anderson, J. B., *J. Phys. Chem.*, 1996, **100**, 12960.

[113] Sinanoğlu, O., *Adv. Chem. Phys.*, 1964, **6**, 358.

[114] Mok, D. K. W.; Neumann, R.; Handy, N. C., *J. Phys. Chem.*, 1996, **100**, 6225.

[115] Hylleraas, E. A., *Z. Phys.*, 1928, **48**, 467.

[116] Weinbaum, S., *J. Chem. Phys.*, 1933, **1**, 593.

[117] Boys, S. F., *Proc. R. Soc. London*, 1950, **A200**, 542.

[118] Boys, S. F., *Proc. R. Soc. London*, 1950, **A201**, 125.

[119] Boys, S. F., *Philos. Trans. R. Soc. London*, 1952, **A245**, 139.

[120] Boys, S. F., *Proc. R. Soc. London*, 1953, **A217**, 136.

[121] Boys, S. F., *Proc. R. Soc. London*, 1953, **A217**, 235.

[122] Parr, R. G.; Craig, D. P,; Ross, I. G., *J. Chem. Phys.*, 1950, **18**, 1561.

[123] Handy, N, C., *Chem. Phys. Lett.*, 1980, **74**, 280.

[124] Saxe, P.; Schaefer, H. F.; Handy, N. C., *Chem. Phys. Lett.*, 1981, **79**, 202.

[125] Harrison, R. J.; Handy, N. C., *Chem. Phys. Lett.*, 1983, **95**, 386.

[126] Handy, N, C., *Faraday Symp. Chem. Soc.*, 1984, **19**, 17.

[127] Bartlett, R. J.; Sekino, H.; Purvis III, G. D., *Chem. Phys. Lett.*, 1983, **98**, 66.

[128] Brown, F. B.; Shavitt, I.; Shepard, R., *Chem. Phys. Lett.*, 1984, **105**, 363.

[129] Bauschlicher, C. W.; Langhoff, S. R.; Taylor, P. R.; Partridge, H., *Chem. Phys. Lett.*, 1985, **126**, 436.

[130] Bauschlicher, C. W.; Taylor, P. R., *J. Chem. Phys.*, 1986, **85**, 2779.

[131] Bauschlicher, C. W.; Taylor, P. R., *J. Chem. Phys.*, 1986, **85**, 6510.

[132] Bauschlicher, C. W.; Langhoff, S. R., *Chem. Phys. Lett.*, 1987, **135**, 67.

[133] Bauschlicher, C. W.; Langhoff, S. R., *Comments At. Mol. Phys.*, 1989, **23**, 1.

[134] Bauschlicher, C. W.; Langhoff, S. R.; Taylor, P. R., *Adv. Chem. Phys.*, 1990, **77**, 103.

[135] van Mourik, T.; van Lenthe, J. H., *J. Chem. Phys.*, 1995, **102**, 7479.

[136] Knowles, P. J.; Handy, N. C., *Chem. Phys. Lett.*, 1984, **111**, 315.

[137] Olsen, J.; Roos, B. O.; Jørgensen, P.; Jensen, H. J. A., *J. Chem. Phys.*, 1988, **89**, 2185.

[138] Knowles, P. J., *Chem. Phys. Lett.*, 1989, **155**, 513.

[139] Knowles, P. J.; Handy, N. C., *J. Chem. Phys.*, 1989, **91**, 2396.

[140] Olsen, J.; Jørgensen, P.; Simons, J., *Chem. Phys. Lett.*, 1990, **169**, 463.

[141] Mitrushenkov, A., *Chem. Phys. Lett.*, 1994, **217**, 559.

[142] Mitrushenkov, A.; Dmitriev, Y. Y., *Chem. Phys. Lett.*, 1995, **235**, 410.

[143] Bendazzoli, G. L.; Evangelisti, S., *J. Chem. Phys.*, 1993, **98**, 3141.

[144] Ansaloni, R.; Bendazzoli, G. L.; Evangelisti, S.; Rossi, E., *Comput. Phys. Comm.*, 2000, **128**, 496.

[145] Roos, B. O., *Chem. Phys. Lett.*, 1972, **15**, 153.

[146] Paldus, J., *J. Chem. Phys.*, 1974, **61**, 5321.

[147] Shavitt, I., *Int. J. Quantum Chem.*, 1977, **S11**, 131.

[148] Shavitt, I., *Int. J. Quantum Chem.*, 1978, **S12**, 5.

[149] Siegbahn, P. E. M., *Chem. Phys.*, 1977, **25**, 197.

[150] Helgaker, T.; Jørgensen, P.; Olsen, J., *J. Chem. Phys.*, 1997, **106**, 6430.

[151] Møller, C; Plesset, M. S., *Phys. Rev.*, 1934, **46** , 618.

[152] Cízek, J., *J. Chem. Phys.*, 1966, **45**, 4256.

[153] Cízek, J., *Adv. Chem. Phys.*, 1969, **14**, 35.

[154] Cízek, J.; Paldus, J., *Int. J. Quantum Chem.*, 1971, **5**, 359.

[155] Siegbahn, P. E. M.; Heiberg, A.; Roos, B. O., Levy, B., *Phys. Scripta*, 1980, **21**, 323.

[156] Roos, B. O., Taylor, P. R.; Siegbahn, P. E. M., *Chem. Phys.*, 1980, **48**, 157.

[157] Siegbahn, P. E. M.; Almlöf, J.; Heiberg, A.; Roos, B. O., *J. Chem. Phys.*, 1981, **74**, 2384.

[158] Roos, B. O., *Adv. Chem. Phys.*, 1987, **69**, 399.

[159] Werner, H.-J.; Knowles, P. J. *J. Chem. Phys.*, 1988, **89**, 5803.

[160] Knowles, P. J.; Werner, H.-J., *Chem. Phys. Lett.* 1988, **145**, 514.

[161] Bauschlisher, C. W.; Langhoff, S. R.; Taylor, P. R., *Adv. Chem. Phys.*, 1990, **77**, 103.

[162] Roos, B. O.; Anderson, K.; Fülsher, M. P.; Malmqvist, P.-Å.; Serrano-Andres, L.; Pierloot, K.; Merchan, M., *Adv. Chem. Phys.*, 1996, **93**, 216.

[163] Angeli, C.; Cimiraglia, R.; Evangelisti, S.; Leininger, T.; Malrieu, J.-P. *J. Chem. Phys.*, 2001, **114**, 10252.

[164] Angeli, C.; Cimiraglia, R.; Malrieu, J.-P. *J. Chem. Phys.*, 2002, **117**, 9138.

[165] Angeli, C.; Borini, S.; Cestari, M.; Cimiraglia, R. *J. Chem. Phys.*, 2004, **121**, 4043.

[166] Angeli, C.; Bories, B.; Cavallini, A.; Cimiraglia, R. *J. Chem. Phys.*, 2006, **124**, 054108.

[167] Davidson, E. R., *J. Phys. Chem.*, 1996, **100**, 6161.

[168] Chaban, G.; Gordon, M. S.; Nguyen, K. A., *J. Phys. Chem.*, 1997, **101**, 4283.

[169] Lewis, G. N., *J. Am. Chem. Soc.*, 1916, **38**, 762.

[170] Van Vleck, J. M., *J. Chem. Phys.*, 1933, **1**, 177.

[171] Van Vleck, J. M., *J. Chem. Phys.*,1933, **1**, 219.

[172] Boys, S. F., *Rev. Mod. Phys.*, 1960, **32**, 296.

[173] Foster, J. M.; Boys, S. F., *Rev. Mod. Phys.*, 1960, **32**, 300.

[174] Edmiston, C.; Ruendenberg, K., *Rev. Mod. Phys.*, 1963, **35**, 457.

[175] Weinstein, H.; Paunez, R., *Adv. At. Mol. Phys.*, 1971, **7**, 97.

[176] Goedecker, S., *Rev. Mod. Phys.*, 1999, **71**, 1085.

[177] J. Pipek and P. G. Mezey, *J. Chem. Phys.*, 1989, **90**, 4916.

[178] Ayala, P. Y.; Scuseria, G. E. *J. Chem. Phys.*, 1999, **110**, 3660.

[179] Hampel, C.; Werner, H. J. *J. Chem. Phys.*, 1996, **104**, 6286.

[180] Scuseria, G. E.; Ayala, P. Y. *J. Chem. Phys.*, 1999, **111**, 8330.

[181] Guihéry, N.; Malrieu, J.-P.; Evangelisti, S.; Maynau, D. *Chem. Phys. Lett.*, 2001, **349**, 555.

[182] Maynau, D.; Evangelisti, S.; Guihéry, N.; Calzado, C. J.; Malrieu, J.-P. *J. Chem. Phys.*, 2002, **116**, 10060.

[183] Angeli, C.; Evangelisti, S.; Cimiraglia, R.; Maynau, D. *J. Chem. Phys.*, 2002, **117**, 10525.

[184] Angeli, C.; Calzado, C. J.; Cimiraglia, R.; Evangelisti, S.; Guihéry, N.; Malrieu, J.-P.; Maynau, D. *J. Comp. Meth. Sci. Eng.*, 2002, **3**, 1.

[185] Angeli, C.; Calzado, C. J.; Cimiraglia, R.; Evangelisti, S.; Guihéry, N.; Malrieu, J.-P.; Maynau, D.; Pitarch-Ruiz, J. V.; Sparta, M. *Mol. Phys.*, 2003, **101**, 1389.

[186] Daudey, J. P. *Chem. Phys. Lett.*, 1974, **24**, 574.

[187] Rubio, J.; Povill, A.; Malrieu, J.-P.; Reinhardt, P. *J. Chem. Phys.* 1997, **107**, 10044.

[188] Ruedenberg, K.; Cheung, L. M.; Elbert, S. T. *Int. J. Quantum Chem.*, 1979, **16**, 1069.

[189] Levy, B.; Berthier, G. *Int. J. Quantum Chem.*, 1968, **2**, 307.

[190] Pitarch-Ruiz, J.; Evangelisti, S.; Maynau, D. *Chem. Phys. Lett.*, 2003, **372**, 22.

[191] Pitarch-Ruiz, J.; Evangelisti, S.; Maynau, D. *Int. J. Quantum. Chem.*, 2004, **97**, 688.

[192] Pitarch-Ruiz, J.; Evangelisti, S.; Maynau, D. *Int. J. Quantum. Chem.*, 2005, **101**, 325.

[193] Pitarch-Ruiz, J.; Calzado, C. J.; Evangelisti, S.; Maynau, D. *Int. J. Quantum. Chem.*, 2006, **106**, 609.

[194] Calzado, C. J.; Evangelisti, S.; Maynau, D. *J. Phys. Chem.*, 2003, **107**, 7581.

[195] Suaud, N; Pastor, G. M.; Evangelisti, S.; Maynau, D. *Chem. Phys. Lett.*, 2003, **378**, 503.

[196] Pitarch-Ruiz, J.; Evangelisti, S.; Maynau, D. *J. Mol. Struct. (Theochem)*, 2004, **681**, 203.

[197] Pitarch-Ruiz, J.; Evangelisti, S.; Maynau, D. *J. Chem. Theory Comput.*, 2005, **1**, 1079.

[198] Calzado, C. J.; Evangelisti, S.; Maynau, D. *J. Mol. Struct. (Theochem)*, 2003, **621**, 51.

[199] Evangelisti, S.; Guihéry, N.; Leininger, T.; Malrieu, J.-P.; Maynau, D.; Pitarch-Ruiz, J. V.; Suaud, N; Angeli, C.; Cimiraglia, R.; Calzado, C. J. *J. Mol. Struct. (Theochem)*, 2004, **709**, 1.

[200] Borini, S.; Maynau, D.; Evangelisti, S. *J. Comput. Chem.*, 2005, **26**, 1042.

[201] Junquera-Hernández, J. M.; Pitarch-Ruiz, J.; Sánchez-Marín, J.; Maynau, D.; Evangelisti, S. *J. Comput. Chem.*, 2005, **26**, 1254.

[202] Leininger, T.; Angeli, C.; Evangelisti, S.; Cimiraglia, R.; Maynau, D. *Chem. Phys. Lett.*, 2003, **371**, 49.

[203] Hohenberg, P.; Kohn, W. *Phys. Rev. B*, 1964, **136**, 864.

[204] Kohn, W.; Sham, L. J. *Phys. Rev. A*, 1965, **140**, 1133.

[205] Slater, J. C., *Phys. Rev.*, 1930, **36**, 57.

[206] Boys, S. F., *Proc. Roy. Soc. London*, 1950, **A200**, 542.

[207] Widmark, P.-O.; Malmqvist, P.-Å.; Roos, B., *Theor. Chim. Acta* 1990, **77**, 291.

[208] Almlöf, J.; Taylor, P. R., *J. Chem. Phys.*, 1992, **90**, 551.

[209] Almlöf, J.; Taylor, P. R., *Adv. Quantum Chem.*, 1991, **22**, 301.

[210] Marcus, R. A., *Rev. Mod. Phys.*, 1993, **65**, 599.

[211] Barbara, P. F.; Meyer, T. J.; Ratner, M. A. *J. Phys. Chem.*, 1996, **100**, 13148.

[212] *Chem. Rev.*, 1992, **92**, issue 3, pp. 365–490. This issue is devoted to ET processes.

[213] Bixon, M.; Jortner, J. (eds), *Adv. Chem. Phys.: Electron transfer: from Iosolated molecules to biomolecules*. 1999, **106-107**, John Wiley and Sons, New York.

[214] Balzani, V. (ed), *Electron transfer in chemistry*. 2001, vols 1-5, Wiley-VCH, Weinheim.

[215] Moser, C. C.; Keske, J. M.; Warncke, K.; Farid, R. S.; Dutton, P. L., *Nature*, 1992, **355**, 796.

[216] Willner, I.; Willner, B., *Top. Curr. Chem.*, 1991, **159**, 153.

[217] Wasielewski, M. R., *Chem. Rev.*, 1992, **92**, 435.

[218] Closs, G. L.; Miller, J. R., *Science*, 1988, **240**, 440.

[219] Paddon-Row, M. N., *Acc. Chem. Res.*, 1994, **27**, 18.

[220] Tolbert, L. M.; Zhao, X.; Ding, Y.; Bottomley, L. A., *J. Am. Chem. Soc.*, 1995, **117**, 12891.

[221] Jiang, B.; Yang, S. W.; Bailey, S. L.; Hermans, L. G.; Niver, R. A.; Bolcar, M. A.; Jones, W. E., *Coord. Chem. Rev.*, 1998, **171**, 365.

[222] Tour, J. M.; Kozaki, M.; Seminario, J. M., *J. Am. Chem. Soc.*, 1998, **120**, 8486.

[223] Davies, W. B.; Svec, W. A.; Ratner, M. A.; Wasielewski, M. R., *Nature*, 1998, **396**, 60.

[224] Creager, S.; Yu, C. J.; Bamdad, C.; O'Connor, S.; MacLean, T.; Lam, E.; Chong, Y.; Olsen, G. T.; Luo, J.; Gozin, M.; Kayyem, J. F. J., *Am. Chem. Soc.*, 1999, **121**, 1059.

[225] Joachim, C.; Gimzewski, J. K.; Aviram, A., *Nature*, 2000, **408**, 541.

[226] Fraysse, S.; Coudret, C.; Launay, J.-P., *Eur. J. Inorg. Chem.*, 2000, **1** 1581.

[227] Barigelletti, F.; Flamigni, L., *Chem. Soc. Rev.*, 2000, **29**, 1.

[228] Lukas, A. S.; Bushard, P. J.; Wasielewski, M. R., *J. Am. Chem. Soc.*, 2001, **123**, 2440.

[229] Braun-Sand, S. B.; Wiest, O., *J. Phys. Chem. B*, 2003, **107**, 9624.

[230] Creutz, C.; Taube, H., *J. Am. Chem. Soc.*, 1969, **91**, 3988.

[231] Creutz, C., *Prog. Inorg. Chem.*, 1983, **30**, 1.

[232] Richardson, D. E.; Taube, H., *Coord. Chem. Rev.*, 1984, **60**, 107.

[233] Marcus, R. A., *J. Chem. Phys.*, 1956, **24**, 979.

[234] Marcus, R. A., *J. Chem. Phys.*, 1965, **43**, 679.

[235] Hush, N. S., *Trans. Faraday. Soc.*, 1961, **57**, 155.

[236] Hush, N. S., *Elecrochim. Acta*, 1968, **13**, 1005.

[237] Hush, N. S., *Coord. Chem. Rev.*, 1985, **64**, 135.

[238] Robin, M.; Day, P., *Adv. Inorg. Radiochem.*, 1967, **10**, 247.

[239] Nelsen, S. F., *Chem. Eur. J.*, 2000, **6**, 581.

[240] Demadis, K. D.; Hartshorn, C. M.; Meyer, T. J., *Chem. Rev.*, 2001, **101**, 2655.

[241] Brunschwig, B. S.; Creutz, C.; Sutin, N., *Chem. Soc. Rev.*, 2002, **31**, 168.

[242] D'Alessandro, D. M.; Keene, R., *Chem. Soc. Rev.*, 2006, **35**, 424.

[243] Marcus, R. A.; Sutin, N., *Biochim. Biophys. Acta*, 1985, **811**, 265.

[244] Sutin, N., *Prog. Inorg. Chem.*, 1983, **30**, 441.

[245] Creutz, C.; Newton, M. D.; Sutin, N., *J. Photochem. Photobiol. A*, 1994, **82**, 47.

[246] Dolin, S. P.; German, E. D.; Dogonadze, R. R., *J. Chem. Soc., Faraday Trans. 2*, 1977, **73**, 648.

[247] Kestner, N. R.; Logan, J.; Jortner, J., *J. Phys. Chem.*, 1974, **78**, 2148.

[248] Piepho, S. B.; Krausz, E. R.; Schatz, P. N., *J. Am. Chem. Soc.*, 1978, **100**, 2996.

[249] Wong, K. Y.; Schatz, P. N., *Prog. Inorg. Chem.*, 1981, **28**, 369.

[250] Brunschwig, B. S.; Logan, J.; Newton, M. D.; Sutin, N., *J. Am. Chem. Soc.*, 1980, **102**, 5798.

[251] Ferretti, A.; Lami, A.; Ondrechen M. J.; Villani, G., *J. Phys. Chem.*, 1995, **99**, 10484.

[252] Newton, M. D.; Sutin, N., *Annu. Rev. Phys. Chem.*, 1984, **35**, 437.

[253] Mikkelsen, K. V.; Ratner, M. A., *Chem. Rev.*, 1987, **87**, 113.

[254] Root, L. J.; Ondrechen, M. J., *Chem. Phys. Lett.*, 1982, **93**, 421.

[255] Ko, J.; Ondrechen, M. J., *J. Am. Chem. Soc.*, 1985, **107**, 6161.

[256] Borshch, S. A.; Kotov, I. N.; Bersuker, I. B., *Chem. Phys. Lett.*, 1982, **89**, 381.

[257] Fernández, E.; Blancafort, L.; Olivucci, M.; Robb, M., *J. Am. Chem. Soc.*, 2000, **122**, 7528.

[258] Blancafort, L.; Fernández, E.; Olivucci, M.; Robb, M., *J. Am. Chem. Soc.*, 2001, **123**, 722.

[259] Lambert, C.; Nöll, G.; Schelter, J., *Nat. Mater.*, 2002, **1**, 69.

[260] Lambert, C.; Amthor, S.; Schelter, J., *J. Phys. Chem. A*, 2004, **108**, 6474.

[261] Hush, N. S.; Reimers, J. R., *Coord. Chem. Rev.*, 1998, **177**, 37.

[262] Hush, N. S.; Reimers, J. R., *Chem. Rev.*, 2000, **100**, 775.

[263] Nelsen, S. F.; Newton, M. D., *J. Phys. Chem. A.*, 2000, **104**, 10023.

[264] Curtiss, L. A.; Naleway, C. A.; Miller, J. R., *J. Phys. Chem.*, 1995, **99**, 1182.

[265] Braga M.; Larsson, S., *Chem. Phys. Lett.*, 1993 **213**, 217.

[266] Cave, R. J.; Baxter, D. V.; GoddardIII, W. A.; Baldeschwieler, J. D., *J. Chem. Phys.*, 1987, **87**, 926.

[267] Liang C.; Newton, M. D., *J. Phys. Chem.*, 1993 **97**, 3199.

[268] Sanz, J. F.; Malrieu, J. P., *J. Phys. Chem.*, 1993, **97**, 99.

[269] von Barth, U., *Phys. Rev. A*, 1979, **20**, 1693.

[270] Hush, N. S.; Reimers, J. R., *Chem. Phys.*, 1996, **208**, 177.

[271] Cave R. J.; Newton, M. D., *Chem. Phys. Lett.*, 1996, **249**, 15.

[272] Cave R. J.; Newton, M. D., *J. Chem. Phys.*, 1997, **106**, 9213.

[273] Crutchley, R. J., *Adv. Inorg. Chem.*, 1994, **41**, 273, and references cited therein.

[274] Brunschwig, B. S.; Sutin, *Coord. Chem. Rev.*, 1999, **187**, 233, and references cited therein.

[275] Launay, J.-P.; Coudret, C., in *Electron Transfer in Chemistry* Vol. 5, ed. De Silva, A. P. and Balzani, V., Wiley-VCH, Weinheim, 2001, ch. 1, and references cited therein.

[276] Launay, J.-P., *Chem. Soc. Rev.*, 2001, **30**, 386.

[277] Kaim, W.; Klein, A.; Glöcke, M., *Acc. Chem. Res.*, 2000, **33**, 755

[278] Flores-Torres, S.; Hutchinson, G. R.; Soltzberg, L. J.; Abruna, H. D., *J. Am. Chem. Soc.*, 2006, **128**, 1513.

[279] Wolpher, H.; Huang, P.; Borgström, M.; Bergquist, J.; Styring, S.; Sun, L.; Åkermark, B., *Catal. Today*, 2004, **98**, 529.

[280] Kar, S.; Chanda, N.; Mobin, S. M.; Datta, A.; Urbanos, F. A.; Puranik, V. G.; Jimenez- Aparicio, R.; Lahiri, G. K., *Inorg. Chem.*, 2004, **43**, 4911.

[281] Maurer, J.; Winter, R. F.; Sarkar, B.; Zalis, S. J., *Solid State Electrochem.*, 2005, **9**, 738.

[282] Fabrizi de Biani, F.; Dei, A.; Sangregorio, C.; Sorace, L., *Dalton Trans.*, 2005, 3868.

[283] Newell, M.; D., I. J.; Easun, T. L.; Vickers, S. J.; Adams, H., *Inorg. Chem.*, 2006, **45**, 821.

[284] Reimers, J. R.; Cai, Z.-L.; Hush, N. S., *Chem. Phys.*, 2005, **319**, 39.

[285] Endicott, J. F.; Chen, Y.-J.; Xie, P., *Coord. Chem. Rev.*, 2005, **249**, 343.

[286] Distefano, A. J.; Wishart, J. F.; Isied, S. S., *Coord. Chem. Rev.*, 2005, **249**, 507.

[287] Bailey, S. E.; Zink, J. I.; Nelsen, S., *J. Am. Chem. Soc.*, 2003, **125**, 5939.

[288] Bolvin, H., *Inorg. Chem.*, 2007, **46**, 417.

[289] Carissan, Y; Heully, J.-L.; Alary, F., Daudey, J.-P. *Inorg. Chem.*, 2004, **43**, 1411.

[290] Nelsen, S. F.; Tran, H. Q.; Nagy, M. A., *J. Am. Chem. Soc.*, 1998, **120**, 298.

[291] Jozefiak, T. H.; Miller, L. L., *J. Am. Chem. Soc.*, 1987, **109**, 6560.

[292] Rak, S. F.; Miller, L. L., *J. Am. Chem. Soc.*, 1992, **114**, 1388.

[293] Risko, C.; Barlow, S.; Coropceanu, V.; Halik, M.; Brédas, J.-L.; Marder, S. R., *Chem. Commun.*, 2003, 194.

[294] Nelsen, S. F.; Konradsson, A. E.; Weaver, M. N.; Telo, J. P., *J. Am. Chem. Soc.*, 2003, **125**, 12493.

[295] Nelsen, S. F.; Weaver, M. N.; Zink, J. I., *J. Am. Chem. Soc.*, 2005, **127**, 10611.

[296] Bonvoisin, J.; Launay, J.-P.; Rovira, C.; Veciana, J., *Angew. Chem., Int. Ed. Engl.*, 1994, **33**, 2106.

[297] Sedó, J.; Ruiz, D.; Vidal-Gancedo, J.; Rovira, C.; Bonvoisin, J.; Launay, J.-P.; Veciana, J., *Synth. Met.*, 1997, **85**, 1651.

[298] Nelsen, S. F.; Chang, H.; Wolff, J. J.; Adamus, J., *J. Am. Chem. Soc.*, 1993, **115**, 12276.

[299] Nelsen, S. F.; Ismagilov, R. F.; Powell, D. R., *J. Am. Chem. Soc.*, 1996, **118**, 6313.

[300] Rosokha, S. V.; Sun, D.-L.; Kochi, J. K., *J. Phys. Chem. A*, 2002, **106**, 2283.

[301] Lindeman, S. V.; Rosokha, S. V.; Sun, D.; Kochi, J. K., *J. Am. Chem. Soc.*, 2002, **124**, 843.

[302] Nelsen, S. F.; Tran, H. Q., *J. Phys. Chem. A*, 1999, **103**, 8139.

[303] Bonvoisin, J.; Launay, J.-P.; Van der Auweraer, M.; De Schryver, F. C., *J. Phys. Chem.*, 1994, **98**, 5052.

[304] Stickley, K. R.; Blackstock, S. C., *Tetrahedron Lett.*, 1995, **36**, 1585.

[305] Lambert, C.; Nöll, G.; Schälzlin, E.; Meerholz, K.; Bräuchle, C., *Chem. Eur. J.*, 1998, **4**, 2129.

[306] Lambert, C.; Nöll, G., *Angew. Chem., Int. Ed.*, 1998, **37**, 2107.

[307] Lambert, C.; Nöll, G., *J. Am. Chem. Soc.*, 1999, **121**, 8434.

[308] Lambert, C.; Nöll, G.; Hampel, F., *J. Phys. Chem. A*, 2001, **105**, 7751.

[309] Coropceanu, V.; Malagoli, M.; André, J. M.; Brédas, J. L., *J. Chem. Phys.*, 2001, **115**, 10409.

[310] Lambert, C.; Nöll, G., *Chem. Eur. J.*, 2002, **8**, 3467.

[311] Coropceanu, V.; Malagoli, M.; André, J. M.; Brédas, J. L., *J. Am. Chem. Soc.*, 2002, **124**, 10519.

[312] Yano, M.; Ishida, Y.; Aoyama, K.; Tatsumi, M.; Sato, K.; Shiomi, D.; Ichimura, A.; Takui, T., *Synth. Met.*, 2003, **137**, 1275.

[313] Coropceanu, V.; Lambert, C.; Nöll, G.; Brédas, J. L., *Chem. Phys. Lett.*, 2003, **373**, 153.

[314] Low, P. J.; Paterson, M. A. J.; Puschmann, H.; Goeta, A. E.; Howard, J. A. K.; Lambert, C.; Cherryman, J. C.; Tackley, D. R.; Leeming, S.; Brown, B., *Chem. Eur. J.*, 2004, **10**, 83.

[315] Coropceanu, V.; Gruhn, N. E.; Barlow, S.; Lambert, C.; Durivage, J. C.; Bill, T. G.; Nöll, G.; Marder, S. R.; Brédas, J. L., *J. Am. Chem. Soc.*, 2004, **126**, 2727.

[316] Lambert, C.; Risko, C.; Coropceanu, V.; Schelter, J.; Amthor, S.; Gruhn, N. E.; Durivage, J. C.; Brédas, J. L., *J. Am. Chem. Soc.*, 2005, **127**, 8508.

[317] Barlow, S.; Risko, C.; Chung, S. J.; Tucker, N. M.; Coropceanu, V.; Jones, S. C.; Levi, Z.; Brédas, J. L.; Marder, S. R., *J. Am. Chem. Soc.*, 2005, **127**, 16900.

[318] Heckman, A.; Amthor, S.; Lambert, C., *Chem. Com.*, 2006, 2959.

[319] Dapperheld, S.; Steckhan, E.; Grosse-Brinkhaus, K.-H.; Esch, T., *Chem. Ber.*, 1991, **124**, 2557.

[320] Kido, J.; Kimura, M.; Nagai, K., *Science*, 1995, **267**, 1332.

[321] Bulovic, V.; Gu, G.; Burrows, P. E.; Forrest, S. R.; Thompson, M. E., *Nature*, 1996, **380**, 29.

[322] Kato, S.; Jaffe, R. L.; Komornicki, A.; Morokuma, K. *J. Chem. Phys.*, 1983, **78**, 4567.

[323] Aviram, A.; Ratner, M. A., *Chem. Phys. Lett.*, 1974, **29**, 277.

[324] Aviram, A., *J. Am. Chem. Soc.*, 1988, **110**, 5687.

[325] Farazdel, A.; Dupuis, M.; Clementi, E.; Aviram, A., *J. Am. Chem. Soc.*, 1990, **112**, 4206.

[326] Hush, N. S.; Wong, A. T.; Bacskay, G. B.; Reimers, J. R., *J. Am. Chem. Soc.*, 1990, **112**, 4192.

[327] Tour, J. M.; Wu, R.; Schumm, J. S., *J. Am. Chem. Soc.*, 1990, **112**, 5662.

[328] Tour, J. M.; Wu, R.; Schumm, J. S., *J. Am. Chem. Soc.*, 1991, **113**, 7064.

[329] Aviram, A., *Int. J. Quantum Chem.*, 1992, **42**, 1615.

[330] Dehareng, D.; Dive, G.; Moradpour, A., *Int. J. Quantum Chem.*, 2000, **76**, 552.

[331] Sanz, J. F.; Calzado, C. J.; Marquez, A., *Int. J. Quantum Chem.*, 2000, **76**, 458.

[332] Helal, W.; Evangelisti, S.; Leininger, T.; Maynau, D., *J. Comput. Chem.*, 2008, **30**, 83.

[333] Bauschlicher, C. W.; Langhoff, S. R. *J. Chem. Phys.*, 1988, **89**, 4246.

[334] Helal, W.; Bories, B.; Evangelisti, S.; Leininger, T.; Maynau, D., in *Lecture Notes in Computer Science (LNCS 3980)*, Gavrilova, M. et al. (Eds.), **I**, 744, Springer-Verlag, 2006.

[335] Pastore, M.; Helal, W.; Evangelisti, S.; Leininger, T.; Malrieu, J.-P.; Maynau, D.; Angeli C.; Cimiraglia, R., *J. Chem. Phys.*, 2008, **128** 174102.

[336] Pastore, M.; Helal, W.; Angeli C.; Evangelisti, S.; Leininger, T.; D.; Cimiraglia, R., *J. Mol. Struct. (Theochem)*, 2009, **896**, 12.

[337] Helal, W.; Monari, A.; Evangelisti, S.; Leininger, T., *J. Phys. Chem. A*, 2009, **113**, 5240.

Abstract

The electronic structure and the intramolecular charge transfer properties of a selected number of mixed valence compounds were investigated at multireference *ab-initio* level, using both canonical and localized molecular orbitals.

The chemical compounds studied are: a spiro π-σ-π molecular cation: 5,5_(4H,4H_)-spirobi[cyclopenta[c]pyrrole]2,2',6,6'tetrahydro cation (the "Spiro" molecule in the following); a series of cationic linear chains composed of beryllium atoms: Be_N, (with N = 6, ..., 12); and two bis-Triaryl amines molecules: namely N,N,N',N'-Tetra(4-methoxyphenyl)-1,4-phenylenediamine cation, and bis{4-[N,N-di(4-methoxyphenyl)amino]phenyl}butadiyne cation. The theoretical models and computational methods used in this work are: CAS-SCF, CAS+S, CAS+SD (MRCI), and CAS+SD using localized orbitals. Different basis sets contractions were used.

For Spiro cation, The potential energy surfaces of the adiabatic ground and the lowest three excited electronic states have been computed, within a two-state model, and a double-well potential has been obtained for the ground electronic state. We have demonstrated a low coupling interaction between the two redox moieties of this molecular cation by following the charge localization/delocalization in the valence _ system through the reaction coordinate of the intramolecular charge transfer. The effect of dynamical correlation, using either localized or canonical orbitals, was found to be crucial for a quantitative
description of the electronic structure and some important electron transfer parameters of this model mixed-valence system.

The results of the linear beryllium chains show a consistent gradual shift between different classes of mixed-valence compounds as the number of beryllium atoms increases, from class-III strong coupling toward class-II valence trapped. Indeed, in the largest cases (N > 10), the cationic chains were found to be closer to class I, where the coupling vanishes. The intramolecular electron transfer parameters V_{ab}, E_a, and E_{opt} were calculated for each atomic chain. It is shown that the decrease of V_{ab} with increasing N follows an exponential pattern.

Résumé

La structure électronique et les propriétés de transfert de charge intramoléculaire de certains composés à valence mixte ont été étudiés au niveau *ab-initio* multi-référence, en utilisant des orbitales moléculaires canoniques et localisées.

Les composés chimiques étudiés sont : un cation de spiro π-σ-π : 5,5'(4H,4H')-spirobi-[cyclopenta[c]pyrrole]2,2',6,6'tetrahydro cation, ("Spiro" dans le texte suivant); une série des chaînes cationiques linéaires composées d'atomes de béryllium : Be_N, (avec N = 6, ..., 12); et deux molécules bis-triarylamines : N,N,N',N'-Tetra(4-méthoxyphényl)-1,4phénylènediamine cation, et bis{4–[N,N-di(4-méthoxyphnyl)amino]phényl}butadiyne cation. Les modèles théoriques et les méthodes de calcul utilisées dans ce travail sont les suivants : CAS-SCF, CAS+S, CAS+SD (MRCI), et CAS+SD en utilisant des orbitales localisées. Des différents bases contractées ont été utilisés.

Les surfaces d'énergie potentielles adiabatiques de l'état électronique fondamentale et les trois états excités les plus bas du cation de Spiro, ont été calculés, au sein d'un modèle à deux états, et un potentiel de double-puits a été obtenu pour l'état électronique fondamental. En suivant la localisation/délocalisation de charge dans le système π de valence du Spiro à travers la coordonnée de réaction du transfert de charge intramoléculaire, nous avons montré un faible couplage électronique entre les deux moitiés d'oxydoréduction de ce cation moléculaire. L'effet de la corrélation dynamique, en utilisant des orbitales localisées ou canoniques, a été jugé cruciale pour une description quantitative de la structure électronique et les autres paramètres importantes de transfert d'électron de ce système modèle à valence mixte.

Les résultats des chaînes linéaires de béryllium montrent une évolution progressive de classe III (couplage électronique fort) envers classe II (couplage électronique faible) en fonction de nombre d'atomes de béryllium. En effet, dans les cas où (N > 10), les chaînes cationiques ont été trouvés se rapprocher de la classe I, où le couplage disparaît. Les paramètres de transfert d'électrons intramoléculaire V_{ab}, E_a, et E_{opt} ont été calculés pour chaque chaîne atomique. Il à été montré que la baisse des valeurs de V_{ab} avec l'augmentation de N suit une courbe exponentielle.